

# **The Mechanistic Action and Performance of Metal Deactivators for Polyolefins**

**Sajid Hussain**

**PhD 2021**

**The Mechanistic Action and Performance of Metal Deactivators  
for Polyolefins**

**Sajid Hussain**

**A thesis submitted in partial fulfilment of the requirements of  
Manchester Metropolitan University  
for the degree of Doctor of Philosophy**

**Department of Natural Sciences  
Faculty of Science and Engineering  
Manchester Metropolitan University  
in collaboration with Addivant UK Ltd**

**2021**

## DEDICATION

WHERE WOULD I BE WITHOUT OTHERS ?

NO ONE IS MASTER OF THEIR OWN SUCCESS

I DEDICATE THIS WORK TO MY LATE TWO BROTHERS AND ONE SISTER  
I AM EVER GRATEFUL TO MY GOD, MOTHER, WIFE, FOR THEIR LARGESSE

TO, MY DIRECTOR OF STUDIES DR MICHELE EDGE, I OWE THE MOST  
FOR HER GUIDANCE THAT SHAPED ME INTO THE CHEMIST, I AM TODAY  
TO MY SUPERVISOR DR CHRISTOPHER LIAUW, MY FIRM FOR FINANCIAL  
SUPPORT

THANK YOU, PROFESSOR NORMAN ALLEN, FOR YOUR SUPPORT, YOUR  
CARING, YOUR LOVE

## COPYRIGHT

Attention is drawn to the fact that the copyright of all materials contained within this thesis rests  
with its author.

This copy of the thesis has been supplied on condition that anyone who consults it is  
understood to recognise that its copyright rests with its author and that no quotation from  
the thesis and no information derived from it may be published without the prior, express written  
permission of the author.

This thesis may be made available for consultation within the Manchester Metropolitan University  
Library and may be photocopied or lent to other libraries for the purposes of consultation.

Signed (Director of studies)	<i>Dr Michele Edge</i>	Date: Jun, 2021
Signed (author)	<i>Sajid Hussain</i>	Date: Jun, 2021

## Declaration

The work described in this thesis was carried out in the School of Science and Environment, Faculty of Science and Engineering, Manchester Metropolitan University, England, United Kingdom, between January 2015 and Jun 2021. All of this work is my own unless specifically stated otherwise. No part of this work has previously been submitted for a degree at this or any other university

## Acknowledgements

*Thank you, [Dr Michele Edge](#) and [Professor Norman Allen](#), for believing in me. Due to a long layoff in the field, I lacked confidence in my ability to go with polymer science when I arrived at MMU. You mentored me expertly by adapting your style to suit my changing needs. By initially guiding me closely, providing perspective in hard times, encouraging me constantly, and later feeding me with difficult but achievable problems that developed my abilities, you helped forge me into the scientist I am today. You are an excellent teacher and a Supervisor. Also, thank you for encouraging me to pursue excellence in polymer testing and analysis. I must also thank the Addivant UK Ltd for financial support for this project. Dr Christopher Liauw, thank you for your support and training in the polymer lab and your excellent feedback and instruction during writing. Dr Paul Warren, thank you for your help with various organic characterisation methods, NMR software, and instrumental training.*

## Abstract

The main action of metal deactivators is to slow down or reduce the metal-catalysed oxidation of polymers. Although metal ions may be introduced inadvertently to polymers (e.g. by metal polymerisation catalyst residues, fillers, pigments), major problems arise when polymers are used as an insulating material for the manufacture of power cables and copper wires, because copper is a pro-oxidant metal. Over 20 novel metal deactivators have been synthesised and their structures verified by IR, NMR and LC-MS. The molecules have been designed in a systematic manner, to introduce various chelating structures (derivatives of: hydrazine monohydrate; tris-amines; hydrazones; dilauryl dithioprionate; propanehydrazide; triazines) and antioxidant structures (sterically hindered phenols, furans, pyrazolones), with a view to improving the roles of the individual and combined functionalities. The performance of these novel structures has been evaluated in LDPE, oxidised during circulation mode extrusion, using MFI, YI and FTIR spectroscopy. Nearly all the structures have an ability to complex  $\text{Cu}^{2+}$  and demonstrate wide ranging performance. Inhibition of oxidative degradation by these antioxidant-metal deactivators is complex and arises from a subtle balance of antioxidant and metal deactivator functions. The work highlights the importance of the complex interplay between different routes to degradation and their inhibition. Here the concentration profile of peroxy radicals and peroxides that leads to the carbonyls (aldehyde, ketone, ester) that dominate the degradation profile of polymers such as LDPE. The best performance of antioxidant-metal deactivator structures is presented by molecules that optimise metal coordination at multiple sites with proximity to an effective peroxy and alkoxy radical scavenger (i.e. primary antioxidants, particularly hindered phenols). These principles may be used to tailor antioxidant-metal deactivator ligands to metal redox systems (e.g.  $\text{Fe}^{2+}/\text{Fe}^{3+}$ ) and so improve the performance of metal deactivators in a range of commercial applications.

## Acronyms/Abbreviations

**ALKANOX® 240:** Tris (2, 4-di-tert-butylphenyl) phosphite  
**Anox® 20:** (Tetrakis(methylene(3,5-di-tert-butyl-4-hydroxyhydrocinnamate) methane)  
**AO:** Antioxidants  
**CaSt:** Calcium Stearate  
**CB-D:** Chain-breaking donor  
**CB-A:** Chain-breaking acceptor  
**NAUGARD® DLTDP:** Dilauryl thiodipropionate (**SONGNOX® DLTDP** Antioxidant)  
**NAUGARD® DSTDP:** Distearyl thiodipropionate (**SONGNOX® DSTDP** Antioxidant)  
**NAUGARD® 412S:** Pentaerythritol tetrakis(3-laurylthiopropionate) (**SONGNOX® 4120** Antioxidant)  
**EDTA:** Ethylenediaminetetraacetic acid  
**FTIR:** Fourier transforms infrared  
**GC-MS:** Gas chromatography mass spectrometry  
**HALS:** Hindered amine light stabilisers  
**HDPE:** High-density polyethylene  
**HD:** Hydroperoxide decomposer  
**InH:** Phenols  
**In•:** Phenoxy radical  
**LC-MS:** Liquid column-Mass spectrometry  
**LLDPE:** Linear low-density polyethylene  
**LDPE:** low-density polyethylene  
**LOWILITE® 94:** Poly[[6-[[[1,1,3,3-tetramethylbutyl)amino]-1,3,5-triazine-2,4-diyl]][(2,2,6,6-tetramethyl-4-piperidyl)imino]hexamethylene[[2,2,6,6-tetramethyl-4-piperidyl)imino]]  
**LOWINOX®1790:**1,3,5-tris(4-tert.-butyl-3-hydroxy-2,6-dimethylbenzyl)-1,3,5-triazine-2,4,6-(1H,3H,5H) trione  
**LOWINOX®MD24:** 3-(3,5-Ditert-butyl-4-hydroxyphenyl)-N'-[3-(3,5-ditert-butyl-4 hydroxyphenyl) propanoyl] propanehydrazide  
**MDPE:** Medium density polyethylene  
**MD:** Metal deactivator  
**MFI:** Melt Flow Index  
**MFR:** Melt Flow Ratio  
**M<sup>n+1</sup>:** Metal ions  
**MW:** Molecular weight  
**NMR:** Nuclear Magnetic Resonance  
**Naugard® XL-1:**2,2'-oxalyldiamidobis[ethyl 3-(3,5-di-tert-butyl-4-hydroxyphenyl)propionate]  
**OIT:** Oxidative induction time  
**-oxy radicals:** Alkoxy and peroxy radicals  
**PE:** Polyethylene  
**PP:** polypropylene  
**PO:** Polyolefin  
**R•:** Alkyl radicals  
**RO•:** Alkoxy radicals  
**ROO•:** Peroxy radicals  
**ROOH:** Hydroperoxide  
**SONGNOX 1680:** Tris (2, 4-di-tert-butylphenyl) phosphite  
**SONGNOX® 1010:** Pentaerythritol tetrakis (3-(3, 5--di-tert-butyl-4hydroxyphenyl) propionate  
**SUMILIZER GA-80:** 3, 9-Bis [2-[3-(3-tert-butyl-4-hydroxy-5-methylphenyl) propionyloxy]-1, 1-dimethylethyl] - 2, 4, 8, 10-tetraoxaspiro, undecane  
**UHMWPE:** Ultra high molecular weight polyethylene  
**ULDPE:** Ultra low-density polyethylene  
**ULMWPE:** Ultra low molecular weight polyethylene  
**UV:** Ultraviolet  
**VLDPE:** Very low-density polyethylene  
**YI:** Yellowness Index  
**ZnSt:** Zinc Stearate

## Background

Applications during service-life that bring polymers into contact with metals and metal ions require the incorporation of organic metal deactivators in the polymer matrix. The main action of metal deactivators (MD) is to slow down or reduce the metal-catalysed oxidation of polymers<sup>1</sup>. Although metal ions may be introduced to polymers indirectly, for example when metal polymerisation catalyst, certain types of fillers, fibres and pigments are introduced to different types of polymers. The major problems arise when polymers are used as an insulating material for the manufacture of power cables and copper wires because copper is a pro-oxidant metal due to the arrangement of electrons in its outer *d* orbital. Polymers degrade through interaction with molecular oxygen by an autocatalytic free-radical process. This process generates polymer peroxides and hydroperoxides as intermediates in the chain reaction. Copper plays a catalytic role in the initiation of free-radical production by decomposition of hydroperoxides, which leads to further polymer oxidation. The existence of an ionic process and a redox system alters the mechanism of polymer oxidation substantially.

To extend the lifetime of polymers it is necessary to add antioxidants, which act as chain-breaking donors (CB-D) or chain-breaking acceptor (CB-A) of radicals, so terminating chain reactions. In direct contact with metals, the performance of processing and service-life antioxidants is inadequate so metal deactivators (MD) are required as adjuncts.

The metal deactivators are usually multi-functional chelating compounds with ligands containing atoms such as nitrogen (N), oxygen (O), sulphur (S) and phosphorous (P) that can co-ordinate metal ions and prevent their participation in the catalytic decomposition of peroxides: for example, phosphites, hindered phenols, and nitrogen-based additives such as aromatic triazoles, substituted thiadiazoles and azoles<sup>2</sup>. Other potential chelating agents are not used in polymers because they impart unwanted colour or have proven environmental toxicity (e.g. EDTA). In many cases, the multi-functional nature of the MDs is provided by integral structures that serve as CB-D or CB-A type antioxidants. It is therefore very difficult to decouple the relative activities and relevance of the two functions. For example, the commercial metal deactivator Naugard XL-1 contains a hindered phenol moiety that also functions as a chain-breaking donor (CB-D) antioxidant<sup>3</sup>. Furthermore, antioxidants

themselves (phosphites, phenols, thiols) may complex metal ions to a degree; resulting in competition with their primary CB-D and chain-breaking acceptor (CB-A) roles. It might be expected that an efficient metal deactivator reduces the diffusion rates of metal ions within the bulk polymer matrix by effective complexation. However, studies on N,N'-diphenyloxamide, a typical copper deactivator, have shown that this chelating agent has little effect on the diffusion rates of metal ions within the polymer matrix and that, in the early stages of polymer degradation, reactions at the metal surface are the critical inhibition process, rather than bulk phase scavenging of metal ions. The active species appear to be low molecular weight metal (copper) species formed at the polymer/copper interface<sup>4</sup>. Other studies also show that the processing window (temperature range) for the polymer plays a vital role in the performance of metal deactivator<sup>5</sup>. This suggests that the complex formation constant, for a MD with specific metal ions, is important when determining the complex stability throughout a range of processing temperatures and during service-life exposure. Despite the important role of metal deactivators in commercial applications, there is little evidence of systematic studies having been undertaken in the published literature. For this reason, a series of novel metal deactivators have been synthesized with variable antioxidant and metal chelation functionalities.

## Aims and Objectives

The aim of this project is to improve understanding of the mechanisms by which metal deactivators operate and to formulate novel metal deactivator stabiliser packages and delivery mechanisms, in the presence of antioxidant stabilisers.

The objectives will then be to:

- I. Select a range of commercially available metal deactivators and antioxidants (and other polymer additives, e.g. lubricants/acid scavengers such as calcium stearate) and evaluate their ability to complex metal ions (specifically copper), using spectroscopic methods (FTIR, NMR).
- II. Synthesize a range of metal deactivators 'assembled' in a systematic manner, to introduce various chelating (derivatives of hydrazine monohydrate; tris-amines; hydrazones; dilauryl dithiopronate; propanehydrazide; triazines) and antioxidant (sterically hindered phenols) groups with a view to improving the roles of the individual and combined functionalities. Verify the structure of these novel metal deactivators by IR, NMR, LC-MS and evaluate their ability to complex metal ions (specifically copper), using spectroscopic methods (FTIR, NMR).
- III. Incorporate selected commercial and novel (synthesized) metal deactivators and antioxidants in a representative polyolefin (e.g. HDPE, LDPE, LLDPE, PEX, PP) to assess performance properties (using industry adopted test methods of MFI and YI).

## List of Figures

**Figure 1-1** Types of hydroperoxides resulting from degradation of Polyolefins

**Figure 1-2:** Heat ageing of polypropylene in air and in contact with aluminium, lead, nickel and copper<sup>71</sup>

**Figure 1-3**  $\pi$ -donor interaction between a sulfur 3p orbital and metal d orbital

**Figure 1-4** Repulsive interaction between thiolate sulfur 3p orbital and metal d-orbital that stimulate the oxidation and nucleophilic attack by the sulfur atom

**Figure 1-5:** Chelation stability as a function of chelating ring structure for selected transition metal ions

**Figure 2-1** Thermo Scientific HAAKE MiniCTW laboratory extruder setups

**Figure 2-2** PerkinElmer UATR Spectrum Two spectrometer

**Figure 2-3** Ray-Ran<sup>®</sup> Melt Flow Indexer

**Figure 2-4** CIE-L\*a\*b\* colour space

**Figure 2-5** GretagMacbeth Spectroeye Colorimeter

**Figure 3.1** MFI values relative to LDPE, for Commercial-Series formulations in LDPE extruded without and with CuCl (s.d = 0.01 g/10 min)

**Figure 3-2** Yellowness ( $\Delta b^*$ ) values relative to LDPE, for Commercial-Series formulations in LDPE extruded without and with CuCl (s.d = 0.04)

**Figure 3-3:** FTIR spectra (1800-1500  $\text{cm}^{-1}$ ) of LDPE and, CaSt and Alkanox 240 in LDPE extruded for 0, 5 and 10 minutes without and with CuCl

**Figure 3-4:** FTIR absorption intensities of carbonyl and unsaturated species in LDPE and, CaSt and Alkanox 240 in LDPE; extruded for 0, 5 and 10 minutes without and with CuCl

**Figure 3-5:** FTIR spectra (1800-1500  $\text{cm}^{-1}$ ) of Anox 20, Naugard XL-1 and Lowinox MD24 in LDPE extruded for 0, 5 and 10 minutes without and with CuCl

**Figure 3-6:** FTIR absorption intensities of carbonyl and unsaturated species Anox 20, XL1 and MD24 extruded for 0, 5 and 10 minutes without and with CuCl

**Figure 3-7** FTIR spectra of Cu-LOWINOX<sup>®</sup>MD24 and its copper complex

**Figure 3-8** FTIR spectra of Cu-NAUGARD<sup>®</sup>XL-1 and its copper complex

**Figure 3-9** MFI of S-Series formulations in LDPE extruded for 0, 5 and 10 minutes without CuCl (s.d = 0.01 g/10 min)

**Figure 3-10** MFI of S-Series formulations in LDPE extruded for 0, 5 and 10 minutes with CuCl (s.d = 0.01 g/10 min)

**Figure 3-11** Yellowing ( $\Delta b^*$ ) of S-Series formulations in LDPE extruded for 0, 5 and 10 minutes without CuCl (s.d = 0.04)

**Figure 3-12** Yellowness ( $\Delta b^*$ ) of S-Series formulations in LDPE extruded for 0, 5 and 10 minutes with CuCl (s.d = 0.04)

**Figure 3-13:** FTIR spectra (1800-1500  $\text{cm}^{-1}$ ) of S0, S1 and S2 in LDPE extruded for 0, 5 and 10 minutes without and with CuCl

**Figure 3-14:** FTIR absorption intensities of carbonyl and unsaturated species for S0, S1 and S2 in LDPE extruded for 0, 5 and 10 minutes without and with CuCl

**Figure 3-15:** FTIR spectra (1800-1500  $\text{cm}^{-1}$ ) of S3, S4 and S5 in LDPE extruded for 0, 5 and 10 minutes without and with CuCl

**Figure 3-16:** FTIR absorption intensities of carbonyl and unsaturated species for S3, S4 and S5 in LDPE extruded for 0, 5 and 10 minutes without and with CuCl

**Figure 3-17:** FTIR spectra (1800-1500  $\text{cm}^{-1}$ ) of S6, S7 and S8 in LDPE extruded for 0, 5 and 10 minutes without and with CuCl

**Figure 3-18:** FTIR absorption intensities of carbonyl and unsaturated species for S6, S7 and S8 in LDPE extruded for 0, 5 and 10 minutes without and with CuCl

**Figure 3-19** FTIR spectra of free ligand S0 and its copper complex

**Figure 3-20** FTIR spectra of free ligand S1 and its copper complex

**Figure 3-21** FTIR spectra of free ligand S2 and its copper complex

**Figure 3-22** FTIR spectra of free ligands S3/S4/S5 and their copper complex

**Figure 3-23** FTIR spectra of free ligand S6 and its copper complex

**Figure 3-24** FTIR spectra of free ligand S7 and its copper complex

**Figure 3-25** FTIR spectra of free ligand S8 and its copper complex

**Figure 3-26** Effect of methoxy group on Melt Flow Index of LDPE+ L1, LDPE+L2, LDPE+L3 and LDPE+ L1A, LDPE+L2A, LDPE+L3A formulations in the presence and absence of CuCl (s.d = 0.01 g/10 min)

**Figure 3-27** Yellowness ( $\Delta b^*$ ) for LDPE+ L1, LDPE+L2, LDPE+L3 and LDPE+ L1A, LDPE+L2A, LDPE+L3A formulations in the presence and absence of CuCl (s.d = 0.04)

**Figure 3-28:** FTIR spectra (1800-1500  $\text{cm}^{-1}$ ) of L1, L2 and L3 in LDPE extruded for 0, 5 and 10 minutes without and with CuCl

**Figure 3-29:** FTIR absorption intensities of carbonyl and unsaturated species for L1, L2 and L3 in LDPE extruded for 0, 5 and 10 minutes without and with CuCl

**Figure 3-30:** FTIR spectra (1800-1500  $\text{cm}^{-1}$ ) of L1A, L2A and L3A in LDPE extruded for 0, 5 and 10 minutes without and with CuCl

**Figure 3-31:** FTIR absorption intensities of carbonyl and unsaturated species for L1A, L2A and L3A in LDPE extruded for 0, 5 and 10 minutes without and with CuCl

**Figure 3-32** FTIR spectra of free ligands L1, L2, L3, L1A, L2A, L3A and their copper complex

**Figure 3-33** MFI (s.d = 0.01 g/10 min) and Yellowness ( $\Delta b^*$ ) (s.d = 0.04) for T-Series antioxidant-metal deactivators in LDPE in the absence and presence of CuCl extruded for 0, 5 and 10 minutes.

**Figure 3-34:** FTIR spectra (1800-1500  $\text{cm}^{-1}$ ) of T0, T1 and T2 in LDPE extruded for 0, 5 and 10 minutes without and with CuCl

**Figure 3-35:** FTIR absorption intensities of carbonyl and unsaturated species for T0, T1 and T2 in LDPE extruded for 0, 5 and 10 minutes without and with CuCl

**Figure 3-36:** FTIR spectra (1800-1500  $\text{cm}^{-1}$ ) of T2, T3 and T4 in LDPE extruded for 0, 5 and 10 minutes without and with CuCl

**Figure 3-37:** FTIR absorption intensities of carbonyl and unsaturated species for T2, T3 and T4 in LDPE extruded for 0, 5 and 10 minutes without and with CuCl

**Figure 3-38** FTIR spectra of free ligand T0 and its complex with copper

**Figure 3-39** FTIR spectra of free ligand T1 and its complex with copper

**Figure 3-40** FTIR spectra of free ligand T3 and its complex with copper

**Figure 3-41** FTIR spectra of free ligand T3 and its complex with copper

**Figure 3-42** Melt flow index (MFI) (s.d = 0.01 g/10 min) and Yellowness ( $\Delta b^*$ ) (s.d = 0.04) for LDPE+MD1A, LDPE +MD1B and LDPE+MD1C formulations in the absence and presence of CuCl during circulation mode extrusion for 0, 5 and 10 minutes.

**Figure 3-43:** FTIR spectra (1800-1500  $\text{cm}^{-1}$ ) of MD1, MD1B and MD1C in LDPE extruded for 0, 5 and 10 minutes without and with CuCl

**Figure 3-44:** FTIR absorption intensities of carbonyl and unsaturated species for MD1, MD1B and MD1C in LDPE extruded for 0, 5 and 10 minutes without and with CuCl

**Figure 3-45:** FTIR spectra (1800-1500  $\text{cm}^{-1}$ ) of MD0, MD2A and MD2B in LDPE extruded for 0, 5 and 10 minutes without and with CuCl

**Figure 3-46:** FTIR absorption intensities of carbonyl and unsaturated species for MD0, MD2A and MD2B in LDPE extruded for 0, 5 and 10 minutes without and with CuCl

**Figure 3-47:** FTIR spectra MD4, MD7 and MD7A extruded for 0, 5 and 10 minutes without and with CuCl in carbonyl region

**Figure 3-48:** FTIR absorption intensities of carbonyl and unsaturated species for MD4, MD7 and MD7A in LDPE extruded for 0, 5 and 10 minutes without and with CuCl

**Figure 3-49** FTIR spectra of free ligand MD1 and its complex with copper

**Figure 3-50** FTIR spectra of free ligand MD1B and its complex with copper

**Figure 3-51** FTIR spectra of free ligand MD1C and its complex with copper

**Figure 3-52** FTIR spectra of free ligand MD0 and its copper complex

**Figure 3-53** FTIR spectra of Cu-MD2A and Cu-MD2B complex

**Figure 3-54** FTIR spectra of Cu-MD7 and Cu-MD7A complex

**Figure 3-55** MFI of novel antioxidant-metal deactivators in LDPE in the absence of copper (I) chloride

**Figure 3-56** MFI of novel antioxidant-metal deactivators in LDPE in the presence of copper (I) chloride

**Figure 3-57**  $\Delta b^*$  of novel antioxidant-metal deactivators in LDPE in the absence of copper (I) chloride

**Figure 3-58**  $\Delta b^*$  of novel antioxidant-metal deactivators in LDPE in the presence of copper (I) chloride

**Figure 3-59** MFI values for LDPE subjected to multi-pass and circulation mode extrusion (s.d = 0.01 g/10 min)

## List of Schemes

**Scheme 1-1** The initiation reaction leading to the formation of alkyl radicals. The reactions are based on the interaction of oxygen with the active sites and unsaturation along the polymeric chain.

**Scheme 1-2** The key chemical reactions that happen during different stages of the auto-oxidative degradation cycle in polyolefin (Symbols: R; polymeric chain or a chain fragment).

**Scheme 1-3** Formation of  $\alpha$ -methylated carboxylic acids from the primary alkyl radical in propagation stage of degradation of PP

**Scheme 1-4** Reactions of alkoxy radicals in a polyolefin matrix generating a range of carbonyl species of molecular nature

**Scheme 1-5** Intramolecular hydrogen atom transfer in peroxy radical

**Scheme 1-6** Intramolecular hydrogen abstraction by peroxy radicals in the polyethylene chain formation of  $\alpha$ - $\gamma$ -di-hydroperoxide and  $\alpha$ , $\gamma$ -keto-hydroperoxide

**Scheme 1-7** Formation of hydro-peroxides and di-hydro-peroxides in PP matrix

**Scheme 1-8** Homolytic and Hetrolytic decomposition of Hydro-peroxides

**Scheme 1-9** Reaction of a formed aldehyde with primary hydroperoxide

**Scheme 1-10** Formation of ester through an ionic reaction

**Scheme 1-11** Formation of methyl and end chain ketones by  $\beta$ -scission at the methyl branch and main polymeric chain C-C bond in a tertiary alkoxy radicals formed by the decomposition of an isolated hydro-peroxide.

**Scheme 1-12** Formation of ketones from the alkoxy radicals (1<sup>st</sup> approach).

**Scheme 1-13** Formation of methyl ketone and diketones from the alkoxy radical, formed by di-hydrogen-peroxides on alternating and consecutive position along a polymeric chain (2<sup>nd</sup> approach).

**Scheme 1-14.** Homologue series of ketones and aldehydes through chain scission of primary and secondary alkoxy radicals.

**Scheme 1-15:** Reaction of metal dithiocarbamate with hydroperoxides<sup>83, 84</sup>.

**Scheme 1-16:** Photosensitisation by metal compound (M is ground state metal; M\* is excited state metal; RH is ground state polymer and RH\* is the excited state polymer).

**Scheme 1-17** Interaction between chain-breaking antioxidant and peroxy radical

**Scheme 1-18** Sterically hindered phenols inhibitors

**Scheme 1-19** Hypothetical chelating effect (the host and guest binding process)

**Scheme 1-20** Hypothetical chelating effect (the affinity of a host and guest is complementarity)

**Scheme 2-1** General mechanism of Schiff base reactions.

**Scheme 3-1** Formation of volatiles from chain-ends during LDPE oxidation

**Scheme 3-2** Cage reactions of peroxy and alkoxy radicals in LDPE

**Scheme 3-3** Equations and Redox Couple for the copper catalysed decomposition of peroxide

**Scheme 3-4** Phenolic antioxidant redox couple in the absence (a) and presence (b) of copper

**Scheme 3-5** Oxidation of  $\text{Cu}^+$  by peroxide and complexation of  $\text{Cu}^{2+}$  by a metal deactivator

**Scheme 3-6** Quinonoid transformation product of a hindered phenol

**Scheme 3-7** Proposed mechanism of action of phosphite in the destruction of conjugation in LDPE

**Scheme 3-8** Coordination of copper with unsaturated carbonyls

**Scheme 3-9** Removal of peroxy radicals by hydrogen atom transfer (HAT) from a hindered phenol

**Scheme 3-10** Regeneration of  $\text{Cu}^+$  by redox reaction with hindered phenol

**Scheme 3-11** Structures of copper complexes of LOWINOX<sup>®</sup>MD24 and NAUGARD<sup>®</sup>XL-1

**Scheme 3-12** Amide-Iminol tautomerism

**Scheme 3-13** Reaction of ester, aldehydes, ketones and carboxylic acids by the additive SO

## List of Tables

**Table 1-1:** Effective temperatures for stabilizers and their stabilisation action

**Table 1-2**  $\beta$  values for  $\text{Cu}^{+2}$  and  $\text{Ni}^{+2}$  with ammonia and ethyleneamine

**Table 3-1** Assignment of FTIR absorptions of oxidised species in LDPE

## Table of Contents

Chapter 1: Introduction to Polymer Degradation .....	1
1.1 General Aspects of Polymer Degradation .....	1
1.2 Chemistry of thermo-oxidative degradation of polyolefins.....	2
1.2.1 Influence of alkoxy and peroxy radicals .....	5
1.2.2 Intramolecular hydrogen transfer in peroxy, alkoxy, and alkyl radicals .....	6
1.2.3 Hydroperoxides as primary products of Polyolefin oxidation.....	7
1.2.4 The role of hydroperoxides and their products in thermo-oxidative degradation.....	8
1.3 Effect of metallic compounds on the degradation of polymers .....	15
1.3.1 The action of Metallic Compounds as Accelerators.....	16
1.3.2 The action of metallic compounds as retarders.....	17
1.4 Antioxidants .....	19
1.4.1 Capacity, strength, and efficiency of antioxidants .....	20
1.4.2 Kinetic classification of antioxidants .....	22
1.4.3 Primary antioxidants (Free-radical scavengers) .....	23
1.4.4 Phenolic antioxidants .....	23
1.5 Metal deactivators .....	32
1.5.1 The coordination chemistry of how metal deactivators .....	33
1.5.2 Copper chelation .....	39
1.5.3 Copper Index .....	40
1.5.4 Maximum chelation stability (Stability Constant) .....	41
1.5.5 Volume of Space.....	43
1.6 Development of Metal Deactivators .....	44
1.7 Justification for the research.....	47
Chapter 2: Experimental .....	49
2.1 Materials and Analytical Methods .....	49
2.2 Synthesis of Antioxidant-Metal Deactivators (AO/MDs) .....	55
2.2.1 Rationale for synthesis .....	55
2.2.2 Synthesis of S-Series AO/MDs .....	55
2.2.3 Synthesis of L-Series AO/MDs .....	61
2.2.4 Synthesis of T-Series AO/MDs.....	66
3,3'-thiodi(propanehydrazide) [T0] .....	66
2.2.5 Synthesis of MD-Series AO/MDs .....	69

Chapter 3: Results and Discussion .....	72
3.1 Commercial Stabilizer Performance.....	75
3.1.1 MFI and Yellowness Index (Commercial Series).....	75
3.1.2 FTIR Analysis of Commercial-Series Antioxidants and Metal Deactivators in LDPE.....	79
3.1.3 FTIR spectra of Commercial-Series antioxidants and metal deactivators and their copper complexes.....	86
3.2 Novel Stabilizer Performance (S-Series).....	90
3.2.1 MFI and Yellowness Index (S-Series).....	91
3.2.2 FTIR Analysis of S-Series Antioxidants and Metal Deactivators in LDPE .....	94
3.2.3 FTIR spectra of S-Series antioxidants and metal deactivators and their copper complexes ..	104
3.3 Novel Stabilizer Performance (L-Series).....	113
3.3.1 MFI and Yellowness Index (L-Series) .....	113
3.3.2 FTIR Analysis of L-Series Antioxidants and Metal Deactivators in LDPE .....	116
3.3.3 FTIR spectra of L-Series antioxidants and metal deactivators and their copper complexes ..	121
3.4 Novel Stabilizer Performance (T-Series).....	122
3.4.1 MFI and Yellowness Index (T-Series).....	122
3.4.2 FTIR Analysis of T-Series Antioxidants and Metal Deactivators in LDPE .....	124
3.4.3 FTIR spectra of T-Series antioxidants and metal deactivators and their copper complexes ..	129
3.5 Novel Stabilizer Performance (MD-Series).....	133
3.5.1 MFI and Yellowness Index (MD-Series).....	134
3.5.2 FTIR Analysis of MD-Series Antioxidants and Metal Deactivators in LDPE .....	135
3.5.3 FTIR spectra of MD-Series antioxidants and metal deactivators and their copper complexes	142
Chapter 4: Conclusion and Further work .....	158
4.1 Conclusions .....	158
4.2 Further Work.....	161
References.....	164
Appendix .....	170

# Chapter 1: Introduction to Polymer Degradation

## 1.1 General Aspects of Polymer Degradation

In a wider sense, the term “degradation of polymers” encompasses all changes in chemical structure and physical properties of polymers due to external chemical or physical stresses that lead to materials with characteristics different from those of the starting material. According to their chemical structure, organic polymers are susceptible to the deleterious effects of their environment. This includes attack by chemical agents (for example, active oxygen humidity and atmospheric pollutants such as active nitrogen species) and physical stresses (e.g. heat, mechanical forces, radiation, etc). During the lifetime of all polymers, the pertinent stages leading to deterioration are separated as melt degradation (during processing) and service-life degradation.<sup>1-5</sup>

Polymer degradation processes arise from the effects of structural inhomogeneities introduced during polymerisation and processing which include unsaturation, oxygenated structures and non-polymeric dopants, such as different metallic impurities or photoactive pigments. The concentration of active impurities (catalysts or sensitizers) increases during the polymer lifetime.<sup>6</sup>

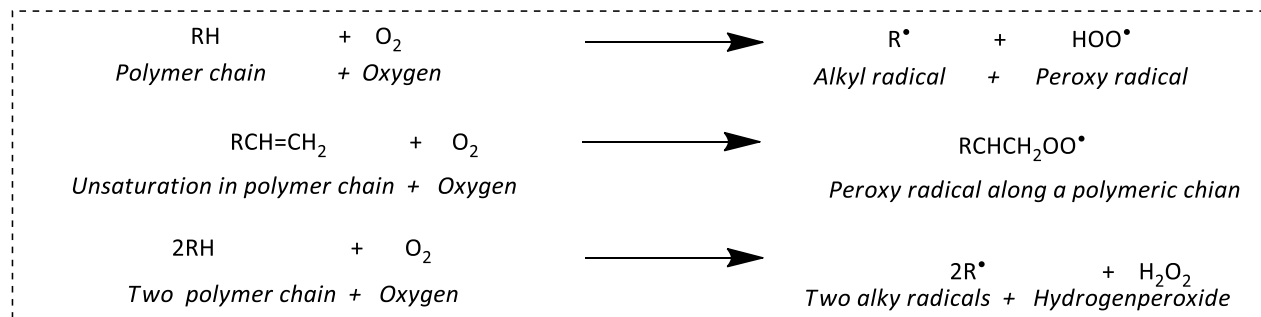
During the past two decades, the field of polymer degradation and stabilization has become a subject of central importance in polymer science and technology. Dielectrics and insulators are prevalent in our daily life yet there are few papers which deal with compatibility between metallic wires and their polymeric insulating materials<sup>7</sup>. Despite the many years of research on the degradation chemistry of polyolefins, what is known of the phenomenon is still not resolved. It is understood that synthetic and natural organic materials readily undergo reactions with oxygen<sup>8</sup> and the process of oxidation is of vital interest here if the organic material is a polymer. The difficulty lies in the fact that variations in chemical and physical properties of polymers occur at very low conversion rate with passage of time. For example, when a linear polymer having 10000 monomer units in its backbone goes through an oxidation process then a conversion rate of 100 ppm is enough to reduce the molecular weight of the polymer up to half of the total molecular weight. At any stage if the polymer oxidizes, it loses its mechanical properties, e.g., tensile strength, toughness, modulus, elongation, and rougher surface appearance and discoloration may result, affected by polymer structure, molecular weight and morphology<sup>8-50</sup>.

## 1.2 Chemistry of thermo-oxidative degradation of polyolefins

The interaction between olefins and molecular oxygen is not only a subject of widespread industrial importance but is one of the most well-known chemical processes<sup>51</sup>. Polyolefins are sensitive to oxidative degradation, and this process speeds up the deterioration of their physical properties. Oxidative degradation of polyolefins involves very complex mechanisms, proceeding through various simultaneous and successive chemical reactions. Degradative influences under practical conditions are impurities, additives, oxygen, light, temperature, and humidity<sup>52</sup>. Polyolefins undergo continuous degradation throughout their life cycle. The number of agents that can trigger degradation are numerous and so are the subsequent pathways. Although, thermo-oxidative degradation predominates the processing stages and service life in high-temperature applications, e.g. in automobiles, various other degradation pathways, e.g. photodegradation and mechanical scission, etc., are simultaneously in operation at any given stage in the life cycle of the polymer. The complicated chemistry that could arise from such a situation has been tackled by the assumption that, except for the initiation stages, the overall chemistry of various types of degradation process is not too different. A mechanistic or kinetic model therefore, with some adjustments to account for the initiation stages, can be used to explain this. The current section focuses on thermo-oxidative degradation and degradation in the presence of metal ions of polyolefins. In polyolefins, thermo-oxidative degradation begins when the polymer is exposed to oxygen and this is exacerbated at high temperatures.

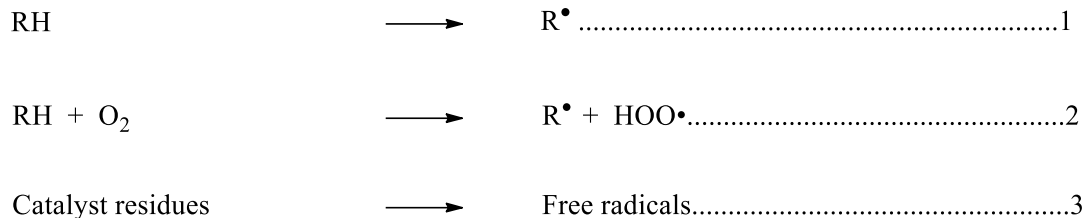
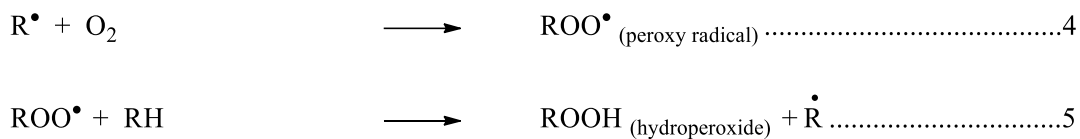
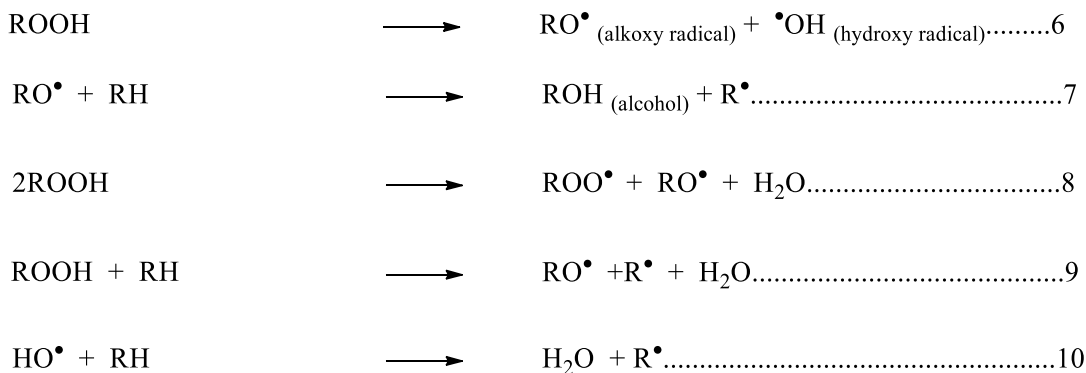
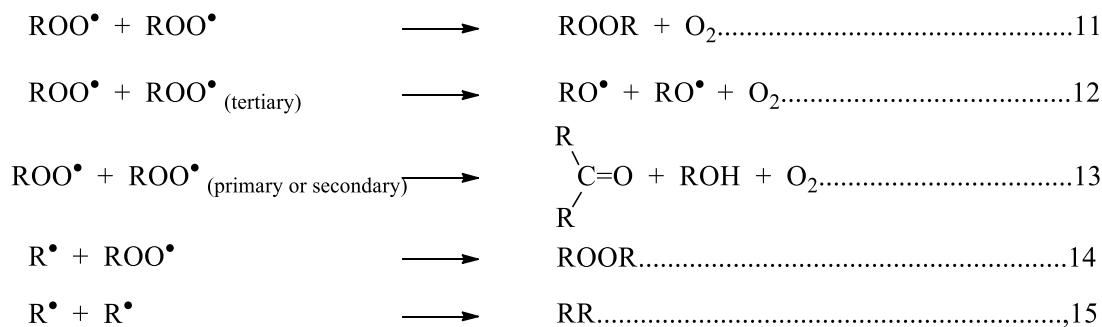
Oxidative degradation of organic materials is one of the most widely studied chemical processes. The earliest investigations that began as early as the first half of the 19<sup>th</sup> century revealed the significant role of oxygen and hydrogen peroxide in oxidation in general. Later, various types of hydroperoxides were detected among the primary intermediate products of oxidation in a hydrocarbon-based system in multiple studies. The hydroperoxides were explained to be formed by free radical chain mechanisms, which led to the proposed auto-oxidative degradation cycle. The auto-oxidative degradation cycle describes interactions that involve continuous genesis, reaction and decomposition of the hydroperoxides. Derived from the low molecular weight liquid and gaseous state systems, the scope of the auto-oxidative free radical mechanism of polyolefin

degradation was in reality too limited to cover all aspects of oxidation in a polymer undergoing a complex life-cycle (**Scheme 1-1**)<sup>53</sup>.



**Scheme 1-1** The initiation reaction leading to the formation of alkyl radicals. The reactions are based on the interaction of oxygen with the active sites and unsaturation along the polymeric chain.

However, because it is hard to draw a physical boundary between the various stages of this process, for the sake of simplicity, the cycle is typically divided into initiation, propagation, and termination stages (**Scheme 1-2**). Here specific steps are susceptible to factors such as heat, ultraviolet and ionizing radiation exposure<sup>39, 54, 55</sup>.

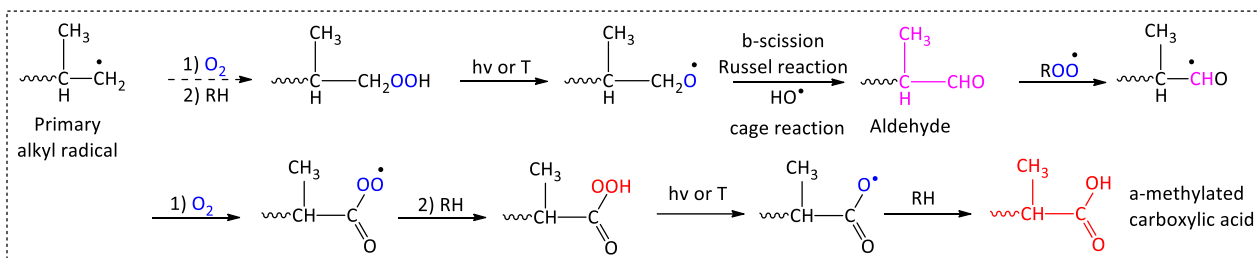
**Initiation:****Propagation:****Branching:****Termination:**

**Scheme 1-2** The key chemical reactions that happen during different stages of the auto-oxidative degradation cycle in polyolefin (Symbols: R; polymeric chain or a chain fragment).

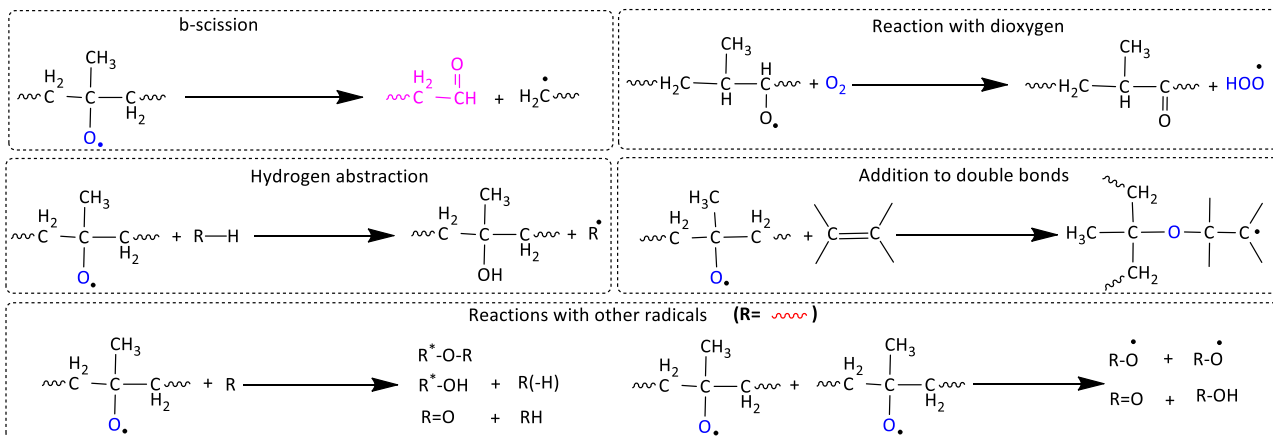
### 1.2.1 Influence of alkoxy and peroxy radicals

The influence of Peroxyl radicals in various reactions, e.g., hydrogen abstraction, isomerization, decay, and addition to a double bond is an important aspect of the radical chain degradation. Starting with alkyl radicals, the precursors of most of the other radicals, once formed, alkyl radicals are attacked by oxygen forming alkoxy ( $\text{RO}^\bullet$ ) and peroxy radicals ( $\text{ROO}^\bullet$ ). Peroxy radicals, chemically unstable, are reduced into hydroperoxides after abstracting hydrogen from vulnerable/ reactive sites along the polymeric chain. Hydroperoxides, relatively stable chemical species, are formed through a reaction that not only carries an auto-acceleratory character but is also slow enough to be used as the rate-determining reaction for the propagation phase of thermo-oxidative degradation in polyolefins.

Alkoxy radicals can be formed in two ways either by direct oxidation of alkyl radicals or through decomposition of hydro-peroxides (**Scheme 1-3**) undergo various reaction, e.g.  $\beta$ -scission, hydrogen abstraction, addition to a double bond, reaction with di-radical of oxygen, generating carbonyl species of molecular nature, e.g. ketones, aldehydes and acids as shown in **Scheme 1-4**<sup>34, 56</sup>.



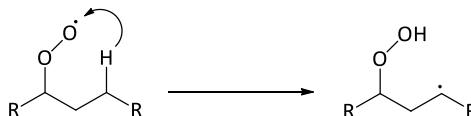
**Scheme 1-3** Formation of  $\alpha$ -methylated carboxylic acids from the primary alkyl radical in propagation stage of degradation of PP



**Scheme 1-4** Reactions of alkoxy radicals in a polyolefin matrix generating a range of carbonyl species of molecular nature

## 1.2.2 Intramolecular hydrogen transfer in peroxy, alkoxy, and alkyl radicals

- ❖ **Peroxy Radicals:** If a hydrogen atom is abstracted by peroxy radical from another molecule then it is called intermolecular hydrogen transfer and if hydrogen atom is abstracted by peroxy radical from the same molecule then it is termed as intramolecular hydrogen transfer. Such type of reaction is very important in the oxidation of carbon-chain polymers<sup>57, 58</sup>.



- ❖ **Alkoxy radicals:** Alkoxy radicals are very active and with sufficiently long alkyl substituents react with intramolecular hydrogen atom transfer, as in the example:



- ❖ **Alkyl radicals:** Alkyl radical isomerisation go with a free-valence transfer from one carbon atom to another in a polymer chain.



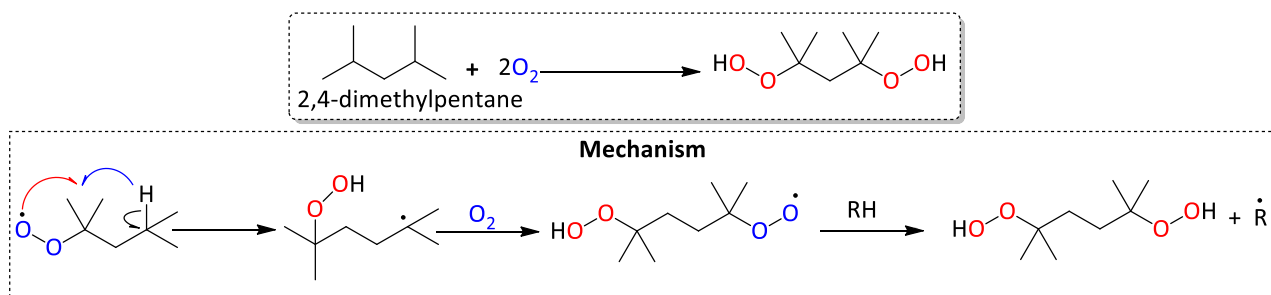
This arises during the chain cracking and radiolysis of hydrocarbons<sup>58, 59</sup>, radical polymerisation and oligomerisation of monomers<sup>58, 60</sup>, thermal and thermo-oxidative destruction of polymers and oxidation of hydrocarbon at low dioxygen pressure.

### 1.2.3 Hydroperoxides as primary products of Polyolefin oxidation

As said previously, a key intermediate in the oxidation of polymers is hydroperoxide (ROOH), which is an effective electron acceptor. It is proven that hydroperoxides are produced as a primary molecular product during the oxidation of aliphatic and alkyl aromatic hydrocarbons under mild conditions, in which the formed hydroperoxide is a stable product. The concentration of ROOH produced during oxidation was found to be nearly equal to the amount of consumed dioxygen. The structure of the oxidized hydrocarbon is most important as the yield of the formed hydroperoxide depends on it. Tertiary hydroperoxides are the most stable and are expected to be present in hydrocarbon oxidation in high yield<sup>58</sup>.

During the oxidation of branched alkanes, dihydroperoxides are also produced. This study was first conducted by Rust, who observed that during the oxidation of 2,4-dimethylpentane at 388 K, dihydroperoxide was found to be the main product and the yield of dihydroperoxide depends on the common position of two tertiary C-H bonds. These primary products of hydrocarbon oxidation are the result of peroxy radical isomerisation. The peroxy radical of a hydrocarbon can abstract hydrogen of another hydrocarbon. When peroxy radical attacks its own C-H bond, the reaction is called intramolecular hydrogen atom abstraction. In addition to this bimolecular abstraction, the final product, dihydroperoxide are formed (**Scheme 1-5**).

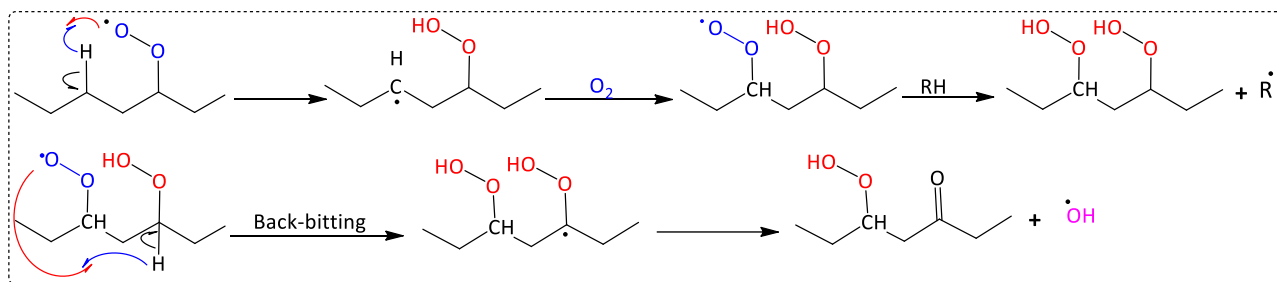
The effect of intramolecular chain propagation was first observed by **Rust** in the oxidation of 2,4-dimethylpentane<sup>61</sup>.



Scheme 1-5 Intramolecular hydrogen atom transfer in peroxy radical

A hydrogen atom is abstracted by peroxy radicals during the oxidation of polyolefins at the propagation stage and it can either an intermolecular abstraction or intramolecular abstraction. The

peroxy radicals attack at the  $\beta$ -position via intramolecular abstraction. It was observed that approximately 30% of intramolecular hydrogen atom abstraction was thought to occur. The significant concentrations of  $\alpha,\gamma$ -di-hydroperoxides is obtained during the intramolecular hydrogen abstraction of peroxy in the presence of molecular oxygen (**Scheme 1-6**)<sup>62</sup>.



**Scheme 1-6** Intramolecular hydrogen abstraction by peroxy radicals in the polyethylene chain formation of  $\alpha,\gamma$ -di-hydroperoxide and  $\alpha,\gamma$ -keto-hydroperoxide

There are various types of hydroperoxides that are produced during the degradation of polyolefins. Thus, primary, secondary and tertiary hydroperoxides can be obtained, however, secondary hydroperoxides are usually most abundant in polyethylene. The chemical structures of possible hydroperoxides formed during the degradation process are shown in **Figure 1-1**.

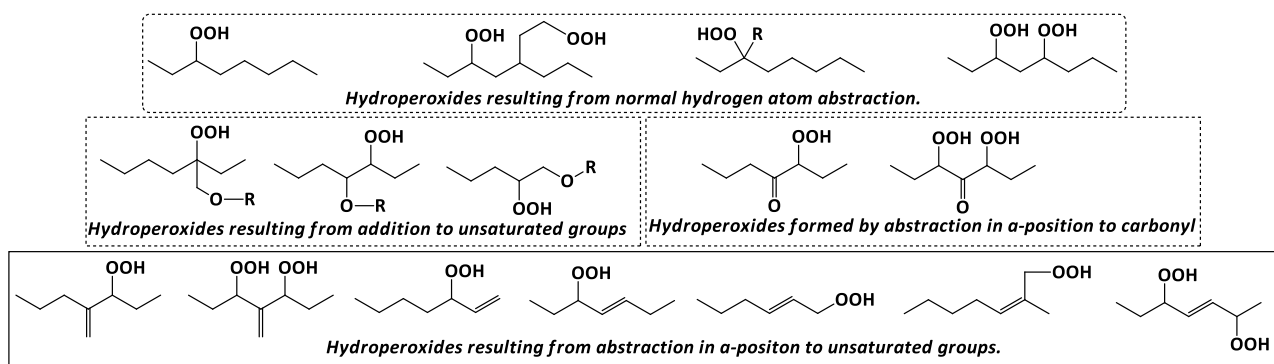
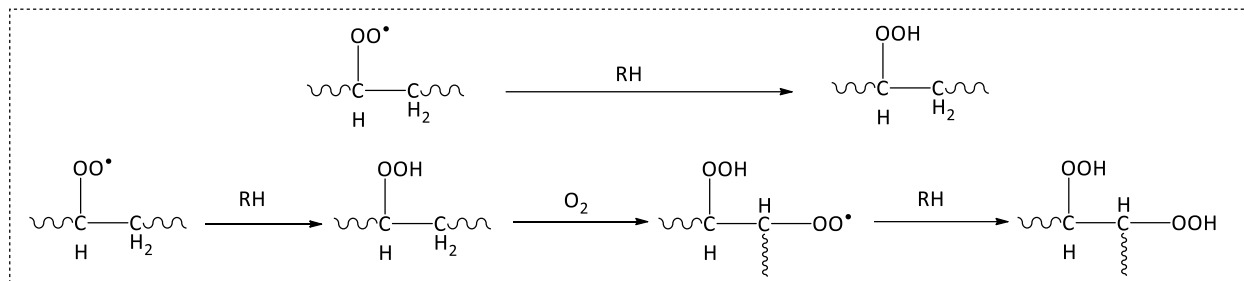


**Figure 1-1** Types of hydroperoxides resulting from degradation of Polyolefins

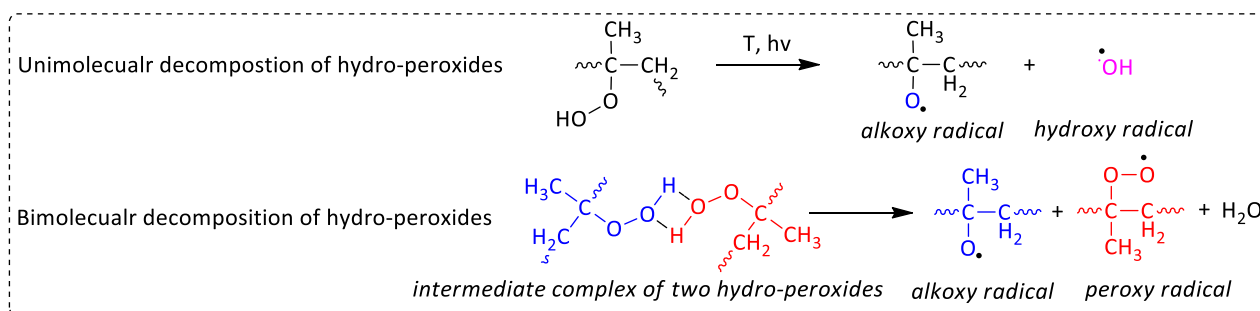
#### 1.2.4 The role of hydroperoxides and their products in thermo-oxidative degradation

As stated previously, hydroperoxides are formed by isomerisation or reduction of peroxy radicals. Formation of hydro-peroxides is a relatively slow reaction during degradation, and due to their less reactive nature than the alkoxy and peroxy radicals, they are available for a long time to contribute to various chemical reactions. The key role of hydro-peroxides in thermo-oxidative degradation of

polyolefins is associated with their decomposition and the chemistry that is initiated by the decomposition products (**Scheme 1-7**).



*Scheme 1-7 Formation of hydro-peroxides and di-hydro-peroxides in polymer matrix*

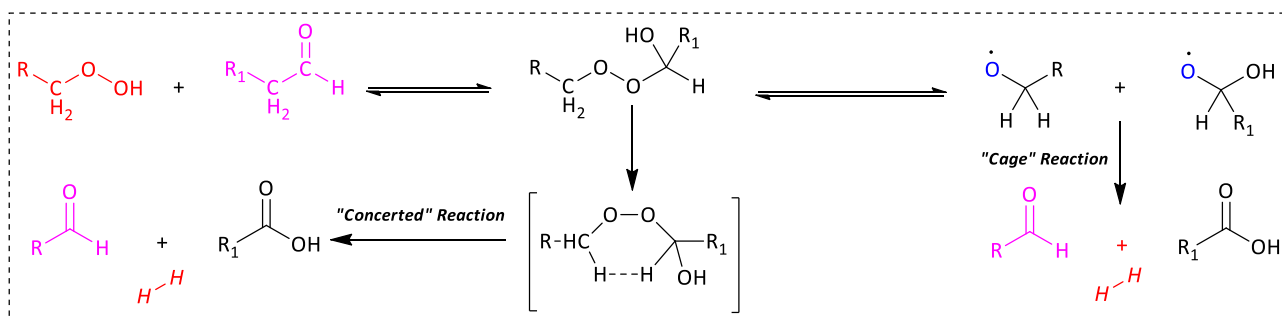


*Scheme 1-8 Homolytic and Heterolytic decomposition of Hydro-peroxides*

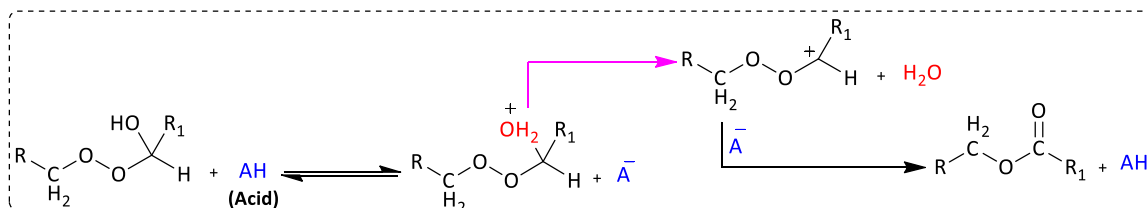
Heterolytic decomposition of hydro-peroxides (**Scheme 1-8**) in polyolefins is a bi-molecular reaction of inter and intramolecular nature. In solid-state polyolefins, the homolytic breakdown of hydroperoxide is negligible during thermo-oxidative degradation. At high melt viscosities and for semi-crystalline materials, the mobility of any isolated species in the polymer is limited by cage effects. In this scenario, the immediate products of the thermo-oxidative degradation are involved further reactions. Such reactions can be either inter and intramolecular in nature and the range of potential reactions is wide. **Gugumus** used this theory to propose alternative pathways for the formation of ketones and aldehydes in PP<sup>56, 62, 63</sup> which include the following reactions:

### 1.2.4.1 Hydroperoxides as intermediates

Alcohol and carbonyl compounds (aldehyde and ketone) are produced from the breakdown of hydroperoxides in the presence of free radical and heat. The primary hydroperoxides are unstable and decompose into aldehyde, acid, and dihydrogen through the contact with a formed aldehyde (**Scheme 1-9**).

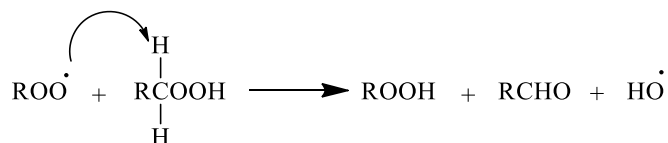


**Scheme 1-9** Reaction of a formed aldehyde with primary hydroperoxide



**Scheme 1-10** Formation of ester through an ionic reaction

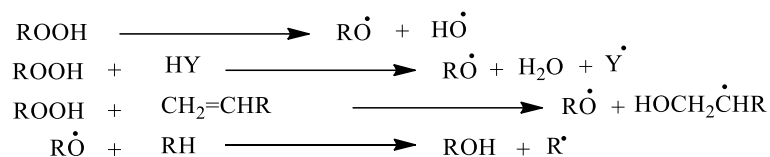
The aldehyde formed during the oxidation process act as an active intermediate and, therefore, the breakdown of the hydroperoxide occurs autocatalytically. Ester is also formed in parallel, clearly by the ionic reaction which is explained in **Scheme 1-10**. An Aldehyde is formed when peroxy radical of the oxidized hydrocarbon attacks at  $\alpha$ -C-H bond which is considered a weak bond in hydroperoxides.



In overall reaction, the primary hydroperoxide is decomposed into aldehyde, carbonic acid, ester, and dihydrogen and secondary hydroperoxides are disintegrated into alcohols and ketones.

### 1.2.4.2 Formation of Alcohols

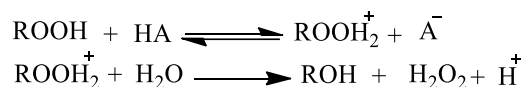
The oxidation of polyolefins into alcohol is an exothermic process and heat of oxidation depends on the structure of oxidised group. The homolytic splitting of the O-O bond of hydroperoxides produces alcohols as shown in the chemical equation below.



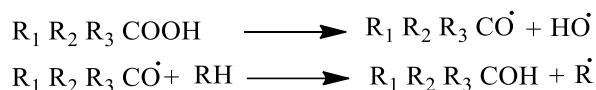
In parallel, alcohols are also shaped by the disproportionation of peroxy radicals<sup>64</sup>.



In addition, hydroperoxides are hydrolysed with the catalytic action of acid formed in the oxidized hydrocarbon while tertiary hydro-peroxide is converted into hydroperoxide and alcohol.<sup>65, 66</sup>



The hydrocarbon with a tertiary C-H bond is oxidized to stable tertiary hydro-peroxide which decomposes homolytically into alcohol<sup>67</sup>.

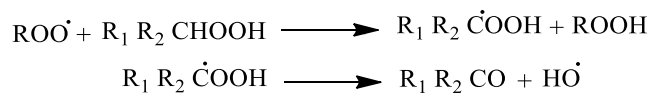


Along with this process, the alkoxy radicals are shaped by the recombination of the tertiary peroxy radical.

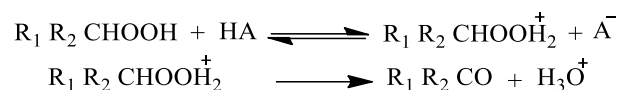


### 1.2.4.3 Formation of Ketones

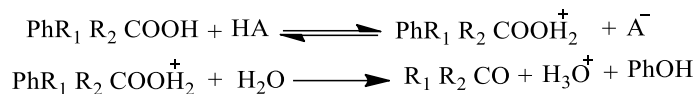
Ketones are formed in oxidized hydrocarbons when secondary hydroperoxides are attacked by peroxy radicals followed by the splitting of the O-O bond<sup>67</sup>.



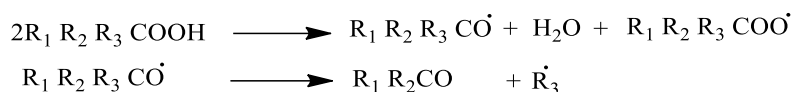
Secondary hydro-peroxide also give carbonyl compounds in presence of acids catalyst<sup>65, 66</sup>.



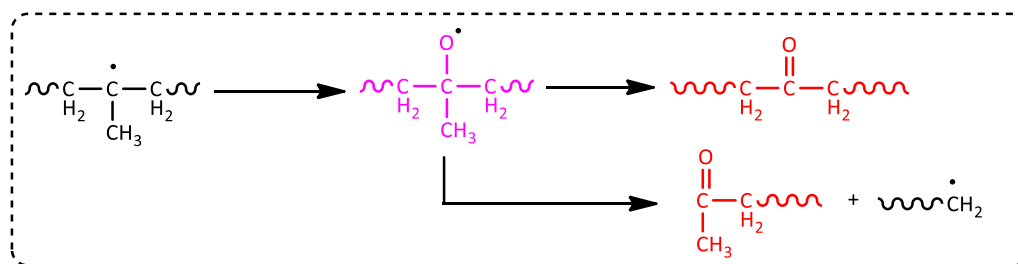
Acid catalyses the tertiary  $\alpha$ -aryl hydroperoxides and produces phenol and ketone<sup>65, 68</sup>.



Alkoxy and peroxy radicals are produced by splitting of tertiary hydro-peroxide and alkoxy radical breakdown into ketone and the alkyl radical<sup>69</sup>.

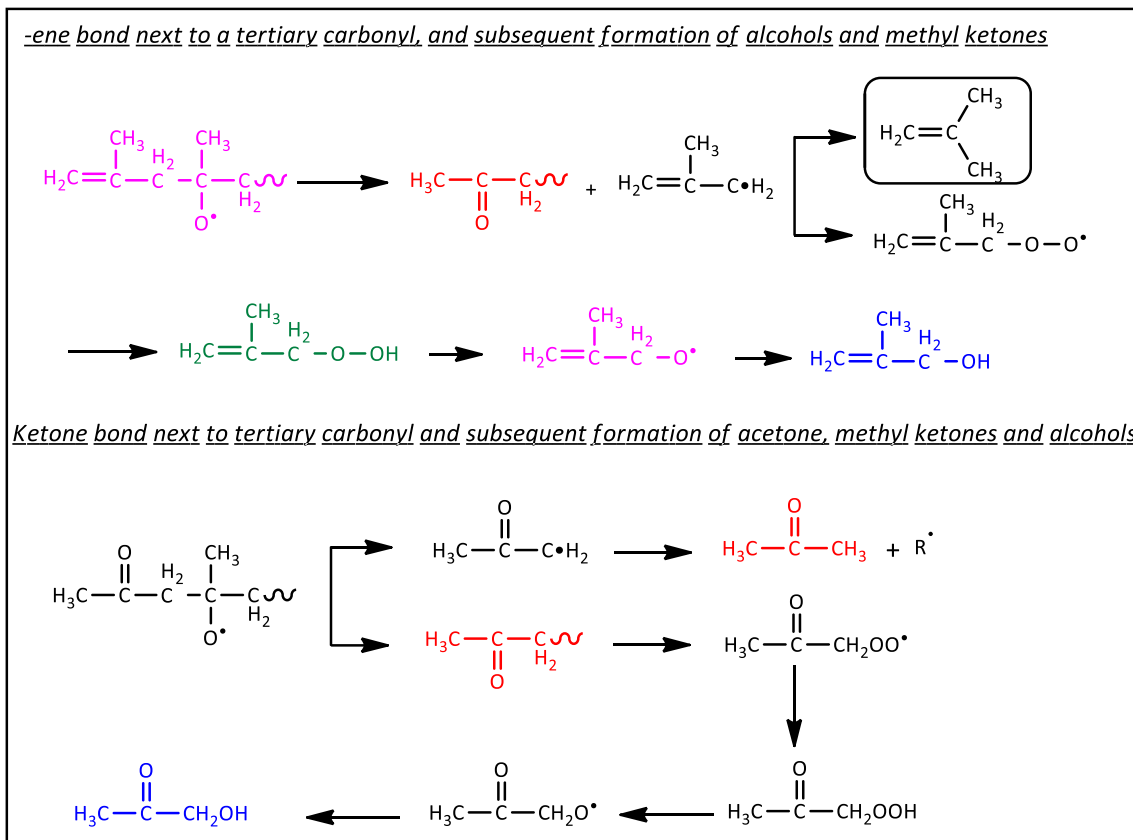


Tertiary alkoxy radicals are the main source of ketones production in polypropylene. The first possibility is the formation of ketones from the alkoxy radicals generated by the breakdown of isolated hydro-peroxides in a polymeric chain. The alkoxy radicals thus formed can cut along the methyl branch or polymer main chain generating main-chain ketone and methyl ketone respectively. The production of methyl ketones is facilitated by the presence of unsaturation in the proximity of the alkoxy radical in a polymeric chain (**Scheme 1-11**).

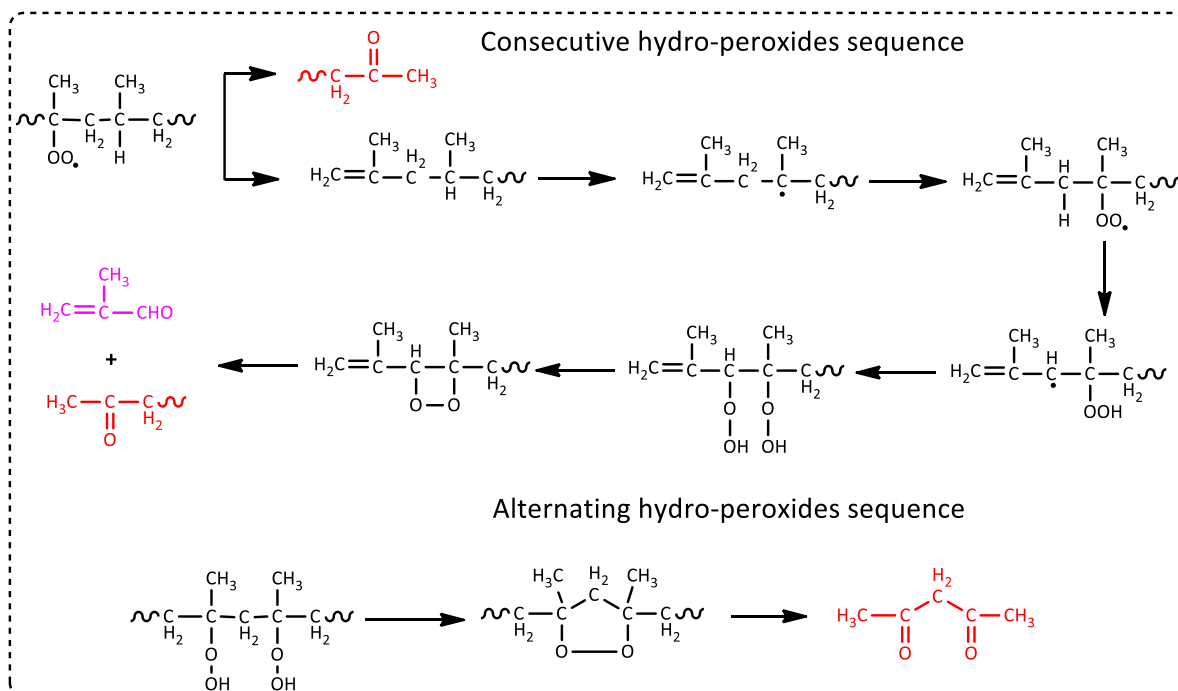


**Scheme 1-11** Formation of methyl and end chain ketones by  $\beta$ -scission at the methyl branch and main polymeric chain C-C bond in a tertiary alkoxy radicals formed by the decomposition of an isolated hydro-peroxide.

The second option is that dihydro-peroxides and hydro-peroxides at alternating carbons in polymeric chain lead to the formation of diketones, while those on the consecutive carbons produce methyl ketones and methyl acrolein. Alcohols and acids are also formed during this process as a by-product (**Scheme 1-12**).



**Scheme 1-12** Formation of ketones from the alkoxy radicals (1<sup>st</sup> approach).



**Scheme 1-13** Formation of methyl ketone and diketones from the alkoxy radical, formed by di-hydrogen-peroxides on alternating and consecutive position along a polymeric chain (2<sup>nd</sup> approach).

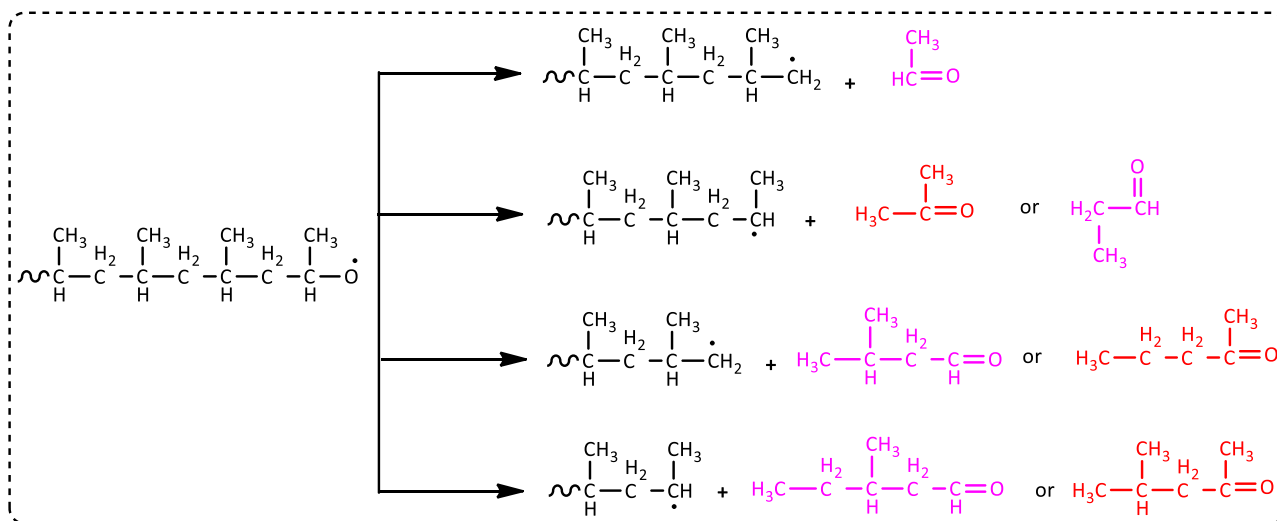
Formation of ketones in PP degradation act as precursors for various further reactions. For example methyl ketone act as precursors of acetone, methanol, methane, and carbon mono and dioxide <sup>49, 70</sup>. While the tertiary alkoxy radicals, secondary alkoxy radicals also involved in the formation of ketones, while the primary alkoxy radicals are mainly known for their role in the formation of aldehydes and  $\alpha$ -methylated carboxylic acids <sup>50, 70-72</sup>.

#### 1.2.4.4 Formation of Aldehydes

Starting with alkyl radicals, the precursors of most of the other radicals, once formed, alkyl radicals are attacked by oxygen forming alkoxy ( $RO^\bullet$ ) and peroxy radicals ( $ROO^\bullet$ ).

Alkoxy radicals can be formed in two ways either by direct oxidation of alkyl radicals or through decomposition of hydro-peroxides (**Scheme 1-3**) undergo various reaction, e.g.  $\beta$ -scission, hydrogen abstraction, addition to a double bond, reaction with di-radical of oxygen-generating a range of carbonyl species of molecular nature, e.g. ketones, aldehydes and acids as shown in **Scheme 1-4**<sup>34, 56</sup>.

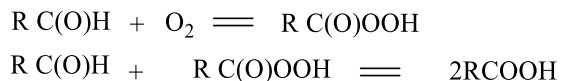
Unlike ketones, aldehydes are shaped by  $\beta$ -scission of primary and secondary alkoxy radicals<sup>47, 70</sup>. The yield of aldehydes during degradation is also limited by their further oxidation into  $\alpha$ -methylated carboxylic acids as shown in **Scheme 1-14**.



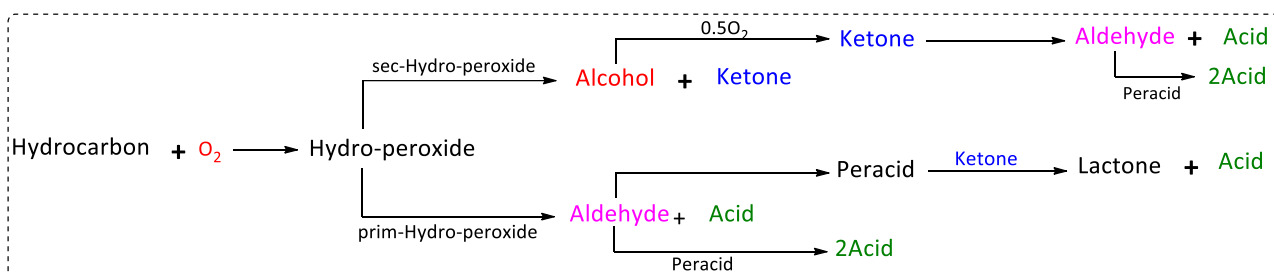
**Scheme 1-14.** Homologue series of ketones and aldehydes through chain scission of primary and secondary alkoxy radicals.

### 1.2.4.5 Acids

The oxidation of aldehydes produces carboxylic acids.



The oxidation of aliphatic and alkyl aromatic hydrocarbons contains the following stages<sup>58</sup>:



### 1.3 Effect of metallic compounds on the degradation of polymers

Transition metal ions play a special and much important role in the peroxidation of polymers. Among transition metals, copper metal and copper ions cannot be controlled easily due to their electronic arrangement in d orbitals. Copper power cables and electrical wires insulated with polyolefins are affected due to its pro-oxidant nature. **Figure 1-2** shows the effect of a range of trace metals on the failure time of polypropylene.

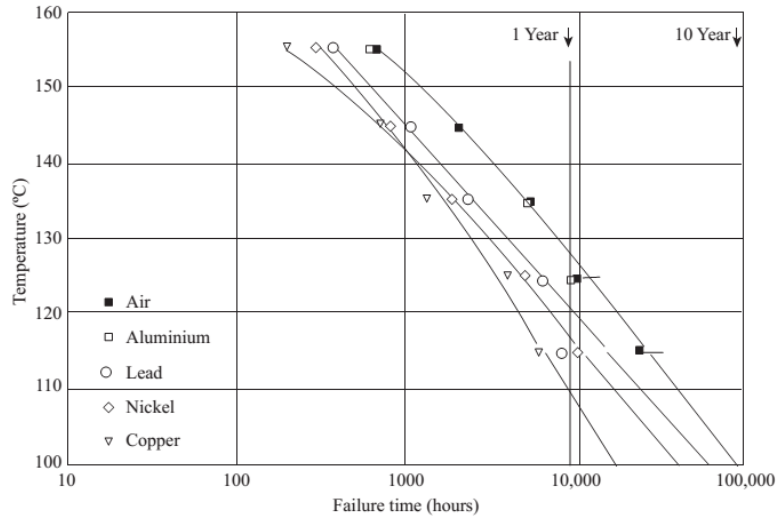
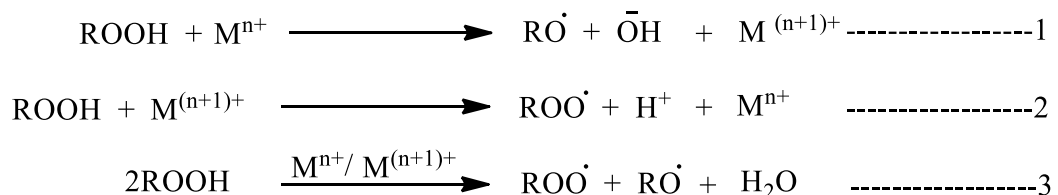


Figure 1-2: Heat ageing of polypropylene in air and in contact with aluminium, lead, nickel and copper<sup>74</sup>

But some research studies show that by adding an excess amount of copper from 60 ppm to 2000 ppm can suppress peroxidation of hydrocarbons<sup>75-79</sup>. This might be by complexing the peroxy radicals and interrupting the chain process<sup>78</sup>. Hydrocarbon peroxidation is accelerated by the amount of copper less than 100 ppb<sup>80</sup>. Therefore, it is very difficult to anticipate systematically the effect of particular metallic compounds on the degradation of the polymer. The effect of metallic compounds on various types of polymer is different. Some act as accelerators of degradation for one polymer but not for another. Although the role of metallic compounds in the degradation of polymers is very complicated, the metallic compounds may be classified into accelerators and retarders.

### 1.3.1 The action of Metallic Compounds as Accelerators

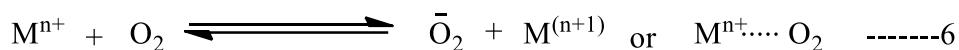
The breakdown of hydroperoxides into free radicals is promoted by different types of accelerators (Reaction 1-3)<sup>81, 82</sup>.



There is also a direct reaction between metallic compound and substrate polymer in the early stages of the degradation which may result in free radicals (Reaction 4 and 5).



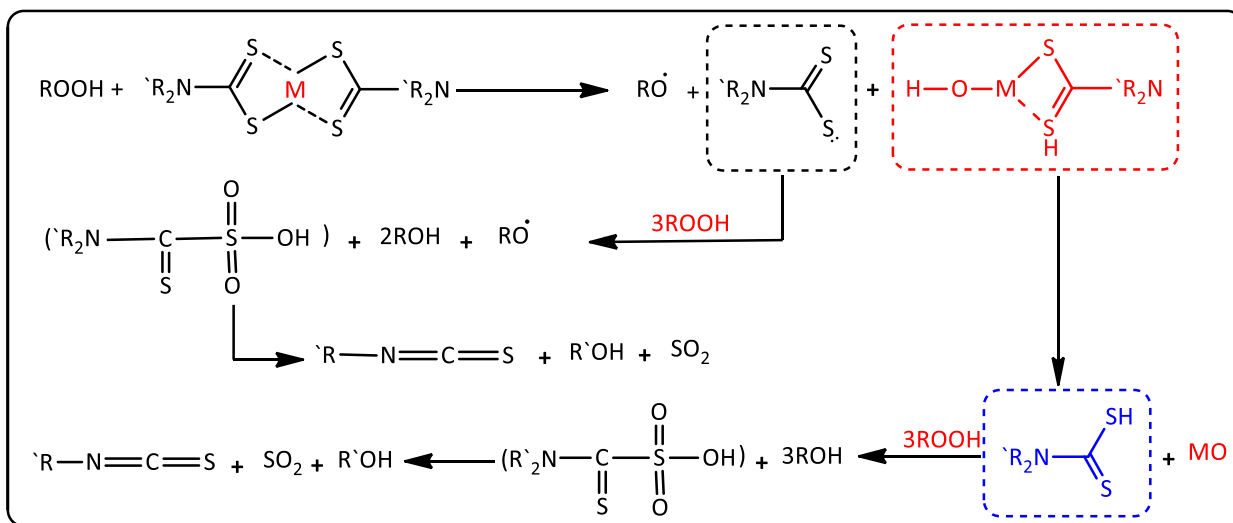
When oxygen interacts with metallic ion it may lead to a charge transfer complex or active oxygen, and these active species can react with polymer (Reaction 6-8).



An energy source such as light can excite the metallic compound as a result, active radicals are produced which may attack the substrate (**Scheme 1-16**).

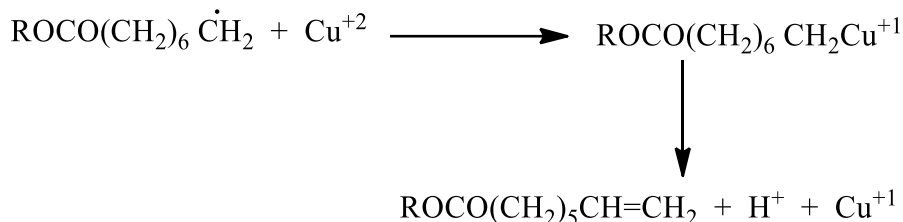
### 1.3.2 The action of metallic compounds as retarders

Hydroperoxides are decomposed by the metallic compounds into harmless components. A typical hydroperoxide decomposer, metal (Ni)alkyl-di-thiocarbamate, decomposes hydroperoxides as given in **Scheme 1-15**.

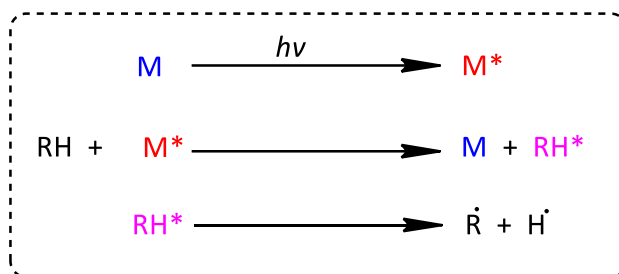


**Scheme 1-15:** Reaction of metal dithiocarbamate with hydroperoxides<sup>83, 84</sup>.

The direct reaction of free radicals with metallic compounds inhibits continuing chain growth in polymers. For example, the photo-stabilising effect of  $\text{Cu}^{+2}$  was proposed by Rasti and Scott<sup>85</sup> as given below the chemical equation.



Ultraviolet radiation is also an issue. A metallic compound can absorb UV light which is harmful to the polymer or may prevent penetration of UV radiation (**Scheme 1-16**).



**Scheme 1-16:** Photosensitisation by metal compound ( $M$  is ground state metal;  $M^*$  is excited state metal;  $RH$  is ground state polymer and  $RH^*$  is the excited state polymer).

Several researchers have studied the effect of metallic catalysts on the oxidative degradation of various polymers. Yasina, *et al.* studied the role of iron in the thermo-oxidative degradation of polypropylene<sup>86, 87</sup>. They reported that the amount of degradation products increased 300% when 0.005 to 0.03 weight %  $\text{FeCl}_2$  was added to the system. The  $\text{FeCl}_2$  had no effect on the polymer under vacuum conditions.

It is of interest to investigate the kinetic parameters which can play an important role in the degradation of polymer materials promoted by metal/polymer contact. The main sources of chemical degradation of polymers are the catalytic decomposition of peroxides, the direct reaction of a metallic compound with an organic molecule, the action of oxygen, transfer of energy during photolysis; the largest effect is obtained when two of them are combined. Thus, the main goal of this project is the thermal stability assessment of PE, which is an insulating material in electrical cable

manufacturer. The essential problem of the long-term operation of electrical wires and cables is the durability, the measure of material chemical resistance.

The alloying components that are contained in metallic conductors are permanently in direct contact with polymer insulation. The chemical resistance of polyethylene coating being quite different from one material to the other, the integrity of the cover determines the service life of electrical wires and cables. The rate of free radical generation in the polymer matrix depends on the practical circumstances and also on the molecular structure of the polymer. When the external surface of the insulation is continuously subjected to the attack of oxygen, humidity, and sunlight, the inner area that is in direct contact with the metal will be influenced. When oxygen diffuses from the environment to the outer polymer layers causes the formation of peroxides and these peroxides are considered to be the starting intermediates for the propagation stage of oxidation. It may be assumed that the different metals would show the different catalytic effect on polymer alteration. The peculiarity of each metal/polymer system consists of the specific kinetic parameters that illustrate the capability to accelerate thermal degradation in the polymer.

Aluminium is the least reactive metal but unfortunately, copper, which is the basic metal in electrical conductor production, shows an induction time which is six times higher than aluminum. The parameters that define the oxidation induction period, halftime of degradation and total oxidation time place the catalytic activity of metals in the following order<sup>88</sup>:



## 1.4 Antioxidants

Antioxidants (AO) are chemical compounds having the ability to prevent polymer during thermal and photooxidation processes or slow down the oxidation of polymer matrix during natural aging. Generally, an antioxidant can protect against free radicals thus terminating the chain reaction in the polymer matrix.

Antioxidants are divided into primary and secondary categories and each category has a specific function in polymer stabilization.

- **Primary** – used to protect the finished product. This type of stabilization ensures performance over the life of the finished good. Primary antioxidants prevent oxidation via chain-terminating reactions. They have reactive -OH or -NH groups (hindered phenols and secondary aromatic amines). Inhibition starts with the transfer of a proton to the free radical species and thus stable radicals are formed which are unable to abstract a proton from the polymer chain.
- **Secondary** – used as a processing stabilizer, frequently referred to as hydroperoxide decomposers, they act to change hydro-peroxides into nonradical, nonreactive, and thermally stable products. An effective way to protect the polymer during processing, especially when the polymer undergoes multiple heat histories. Typical chemistries employed include phosphites or thioesters.

**Table 1-1:** Effective temperatures for stabilizers and their stabilisation action

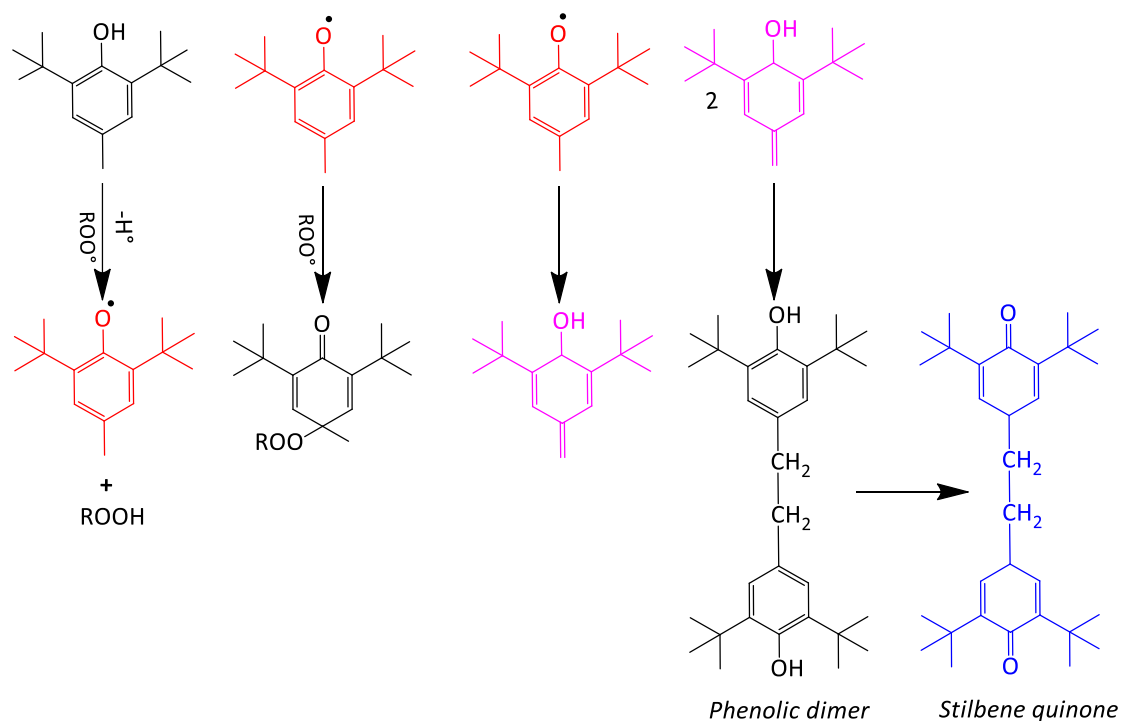
<b>Antioxidants</b>	<b>Long-term thermal stability</b>				<b>Processing stability</b>		
<i>Hindered phenols</i>							
<i>Thio-synergists</i>					No	Melt	Processing
<i>Lactones</i>	No long	term	Thermal	stability			
<i>Hydroxylamine</i>	No long	term	Thermal	stability			
<i>Organic-phosphites</i>	No long	term	Thermal	stability			
<i>Hindered amines</i>					No	Melt	Processing
<b>Temperature (°C)</b>	<b>0</b>	<b>50</b>	<b>100</b>	<b>150</b>	<b>200</b>	<b>250</b>	<b>300</b>

It can be seen from **Table 1-1** that from active-temperature zones of different antioxidants, a single antioxidant is usually not enough for adequate stabilisation, that actually encompasses an extended temperature range. The chemistry of only phenolic antioxidants will be discussed in detail in this study with a little explanation of other primary and secondary antioxidants here.

#### 1.4.1 Capacity, strength, and efficiency of antioxidants

Inhibitors have the ability to slow down oxidation by breaking chains or by decomposing hydroperoxide and the inhibitory action of an antioxidant stops when it is completely used up. The age of an antioxidant depends on its mechanism of action, the nature of reactions, and the side reactions taking place inside the polymer matrix. The action of the antioxidant in each system can practically be studied in terms of inhibitory capacity. The capacity of a chain-breaking antioxidant

can be measured by the *inhibition stoichiometric coefficient*<sup>89</sup>. The interaction between a chain-breaking antioxidant and a peroxy radical is given in **Scheme 1-17**.



**Scheme 1-17** Interaction between chain-breaking antioxidant and peroxy radical

According to the above interaction of antioxidant and peroxy radical, the inhibitory capacity of antioxidants is equal to the inhibition stoichiometric coefficient  $f=1-2$ . The capacity of antioxidants depends on the side reactions in which it is inefficiently used up. In this case, there is an inversely link between inhibitory capacity and the intensity of side reactions. For example, an antioxidant **A** is decomposing hydroperoxide in a chemical reaction then its inhibitory capacity can be written as:

$$n_{ROOH}/n_A$$

that is, the number of hydroperoxide molecules decomposed per antioxidant molecule. The degree of inhibition of any antioxidant can be calculated by the ratio  $v_0/v$ , where  $v$  and  $v_0$  are the rates of oxidation in the presence and absence of the inhibitor, respectively. The oxidation rate of any antioxidant can be a nonzero value ( $v^\infty$ ) when the antioxidant is present in excess. On the other

hand, an antioxidant can join chain initiation by reacting with molecular oxygen and hydroperoxide. Now, the strength of the antioxidant can be defined as its ultimate inhibitory capacity stated through the ratio;

$$\frac{v_0}{v_\infty} \quad \text{where } v_\infty = v \text{ at } [InH] \rightarrow \infty$$

When, with respect to chain propagation, if inactive radical is formed from antioxidant then the chain length  $\nu \rightarrow 0$  and oxidation rate will be  $\nu \rightarrow \nu_\infty = \nu_i$  with increasing  $[InH]_0$ . So, stronger the inhibitor lower will be the value of  $\nu_i/\nu_\infty$  and vice versa.

The concentration of an antioxidant and rate of oxidation are inversely related to each other and the activity of antioxidant can be described as per unit concentration, as a retarding agent. An antioxidant can terminate chain, but the chain can also be terminated due to peroxy radical so the activity of introduced antioxidant can be written by the mathematical equation;

$$F = \frac{v_0}{v} \left(1 - \frac{\nu^2}{\nu_0^2}\right)$$

The efficiency of the introduced inhibitor will be, the ratio  $F/[In H]$ . This ratio does not depend on the antioxidant concentration if the latter terminates the chains and intermediate radical  $In^\bullet$  does not propagate through the chains<sup>73, 89</sup>.

#### 1.4.2 Kinetic classification of antioxidants

Oxygen is one of the most essential components for living, it also acts as a double-edged sword. Molecular oxygen acts as a free radical and can become part of potentially damaging molecules commonly called "free radicals." Oxidation is a chemical reaction in which an electron is transferred from electron-rich to electron-deficient. The electron-deficient molecule is called an oxidizer or oxidizing agent, e.g. heavy metals due to the presence of vacant d-orbital behave as potent oxidizing agents<sup>90</sup>.

Oxidation of polyolefins occurs by the chain mechanism via alternating reactions of alkyl and peroxy radicals. The collected hydroperoxides are unstable species and decompose into radicals, thereby

increasing the rate of oxidation. The oxidation of polyolefins may be slow down or prevented by one of the following three ways<sup>90</sup>:

- *Breaking the chains perpetuated by the acceptor reaction with peroxy radicals.*
- *Breaking the chains by the reaction of an acceptor with alkyl radicals.*
- *Oxidation due to hydroperoxides can be retarded by the addition of additives capable to decompose hydroperoxide without the formation of free radicals.*

Generally, antioxidants can be divided into two groups according to their protection mechanism:

- *Kinetic chain-breaking antioxidants (chain terminators, chain scavengers). These antioxidants are also called primary or phenolic antioxidants can scavenge some or even all generated low molecular radicals such as  $R^\bullet$ ,  $RO^\bullet$ ,  $ROO^\bullet$ ,  $HO^\bullet$ , etc. and polymeric radicals like  $P^\bullet$ ,  $PO^\bullet$ ,  $POO^\bullet$  by chain-breaking electron donor mechanism;*
- *Hydroperoxide decomposing antioxidants. These compounds react with hydroperoxides and decompose hydroperoxy groups ( $HOO-$ ) present in a polymer without forming free radicals: sulfides, phosphites, arsenites, thiophosphates, carbamates, and some metal complexes. Reactions with hydroperoxides can be either stoichiometric (typical of, for example, sulfides and phosphites) or catalytic (typical of chelate metal complexes)<sup>73</sup>.*

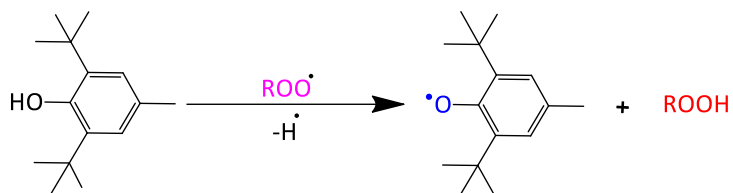
#### **1.4.3 Primary antioxidants (Free-radical scavengers)**

Primary antioxidants (chain-breaking antioxidants) have the ability to interfere with free radicals generated during the propagation stage of the auto-oxidative degradation cycle and convert alkyl, alkoxy and peroxy radicals into hydro-peroxides. These antioxidants prevent polymer degradation by donating labile hydrogen atoms that neutralize or quench the free radical. Chain breaking antioxidants cover different classes of compounds that can retard the oxidative degradation of polymers during their service time. The hydro-peroxides are less reactive as compared to alkyl, alkoxy and peroxy radicals and are decomposed by the secondary antioxidants in another event of stabilisation. Primary antioxidants fall into three categories, hindered phenols, hindered amines and thiobis-phenols but further divided into chain-breaking electron acceptors (CB-A) and chain-breaking electron donors (CB-D) categories.

#### **1.4.4 Phenolic antioxidants**

Phenolic antioxidants are primary antioxidants and are classified chemically depending upon the number of Phenolic groups in the molecule. Phenolic antioxidants act as a H-donors and are most widely used in polyolefins. The phenol section during this reaction is converted into phenoxyl radical

due to H-abstraction, which stabilises itself through internal delocalisation of electrons, and hence is capable of additional stabilisation.

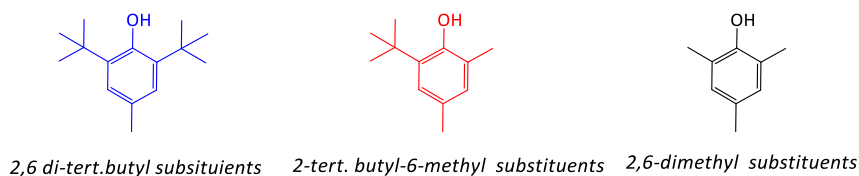


**Scheme 1-18** Sterically hindered phenols inhibitors

The peroxy radicals are converted into hydro-peroxides by accepting abstracted hydrogen atom from the phenolic unit. The hydro-peroxides are comparatively less reactive as compared to alkyl, alkoxy and peroxy radicals and cause a decrease in the rate of degradation.

#### 1.4.4.1 Structures of hindered phenols

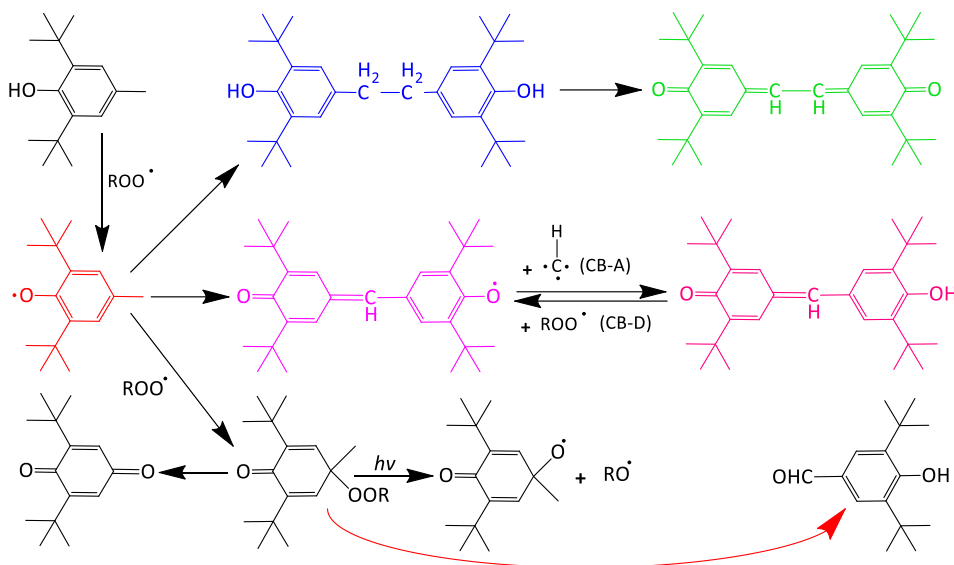
The chemical structure of a hindered phenols plays a key role in the stabilisation. Fully hindered phenols are better than partially hindered, while the unhindered phenols are the least efficient due to the higher chances of hydrogen bonding between the O-H bond and hydrogen on the ortho and para position of the aromatic ring and this the reason, unhindered phenols are hardly ever used as stabilisers<sup>91</sup>. The biggest and important factor which is governing antioxidant efficiency is the steric hindrance of the substituents in the 2,6-position of phenolic moiety<sup>92</sup>. There is a temperature limit below which phenoxyl radicals do not abstract hydrogen from the polymer backbone due to hindrance. The efficiency of sterically hindered phenolic antioxidants used, during service life of polymers at temperatures > 120 –150 °C decreases in the order, 2,6 di-tert.butyl > 2-tert. butyl-6-methyl > 2,6-dimethyl groups as substituents as shown below<sup>93</sup>:



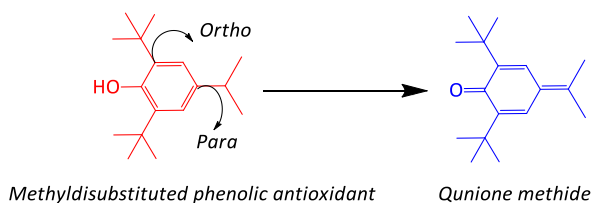
#### 1.4.4.2 Mechanism of action and classification of phenolic antioxidants

Hindered phenols may differ from each other depending upon the group attached to the para position as described here.

- ❖ *Butylated hydroxytoluene (BHT), also known as dibutylhydroxytoluene, is a fat soluble synthetic organic compound, chemically a derivative of phenol is used in foods, polymers, etc. due to its antioxidant properties. The oxidative transformation products of BHT are written below by chemical reaction<sup>92, 94</sup>.*

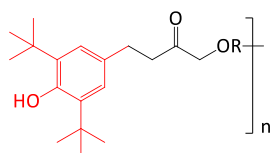


- ❖ *Methyl disubstituted phenolic antioxidant bears a methyl or a mono/disubstituted methyl group at the para position:*



*After giving the proton from the phenolic unit, these antioxidants transform into stable quinone methides. These quinone methide show less contribution towards the integral stability of the polymer.*

- ❖ *Propionate substituted phenolic antioxidants are very effective group of antioxidants with a residue of propionic acid derivatives with general formula  $-CH_2-CH_2-CO_2R$  at the para position.*

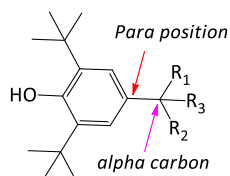


*The quinone methides formed by propionate substituted phenolic antioxidant is reactive and easily disposed to isomerise to derivatives of 4-hydroxycinnamic acid. Intramolecular rearrangement takes*

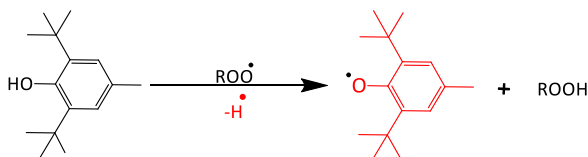
place to regenerate the hindered phenolic functionality, consuming peroxy radicals resulting in stabilisation of polymer after the primary consumption of phenol.



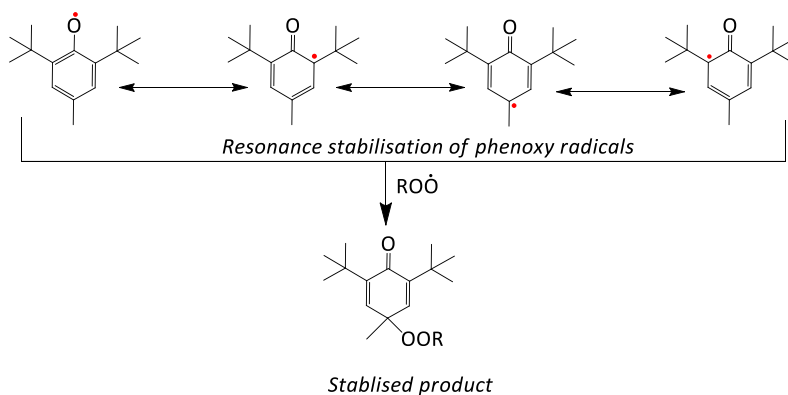
- ❖ Phenolic antioxidants with no hydrogen atom on the  $\alpha$ -carbon of para substituent do not form quinone methides because of a missing hydrogen atom at  $\alpha$ -carbon atom and hence resistant to discolouration as shown below.



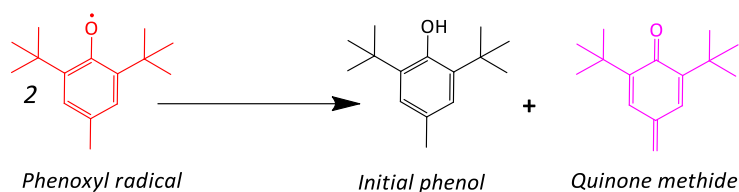
Sterically Hindered phenols act by scavenging alkoxy and peroxy Radicals through H-atom transfer from the -OH group to form hydroperoxides and phenoxy radicals. The reaction mechanism is given below:



The further reactions of phenoxy radicals are an integral part of the stabilisation mechanism of phenolic antioxidants. The phenoxy radical is stabilized by electron delocalisation or resonance as shown below:

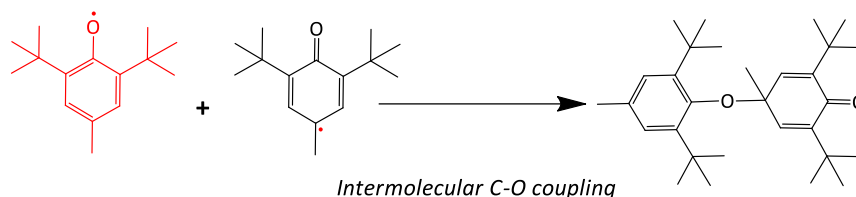


The disproportionation reaction of phenoxyl with at least one H-atom on the C-atom ( $\alpha$  position) vicinal to the phenyl group in 4-position generates the initial phenol (reformation) and a quinone methide as given here:

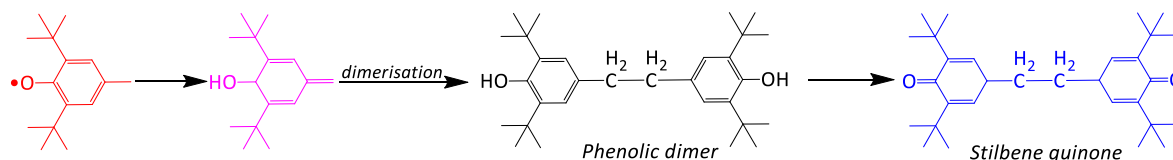


*Disproportionation of phenoxyl radical*

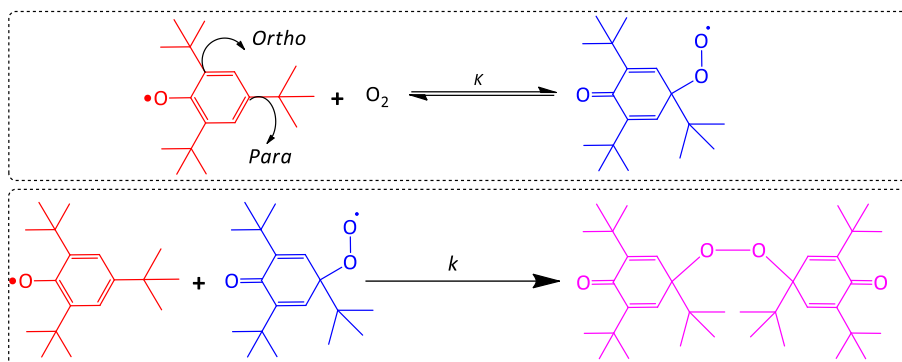
Intermolecular C-O coupling between a phenoxyl radical and cyclohexadienonyl radical may occur when substituents at ortho position are small and there is no H-atom on the C-atom ( $\alpha$  position) vicinal to the phenyl group in 4-position as shown in structure below:



Phenolic dimers are also expected due to interaction between two cyclohexadienonyl radicals and is called C-C coupling as:



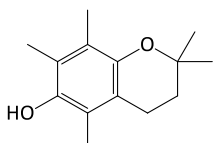
The phenoxyl radicals can react with molecular oxygen and the  $O_2$  molecule attaches itself at the para position in a similar way as alky radical because the electron density at ortho and para position is maximum. Therefore, the formation of quinolide peroxide occurs in two steps, e.g. 2,4,6-tris(1,1-dimethylethyl)phenoxyl radical as written below<sup>95</sup>:



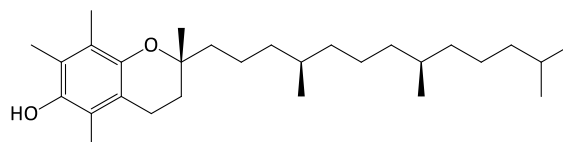
#### 1.4.4.3 Activity and efficiency of phenolic antioxidants

All synthetic hindered phenolic antioxidants are based on BHT-like units to a core (BHT is an abbreviation for 2,6-di-tert-butyl-4-methylphenol). There are different reasons behind the activity and efficiency of hindered phenolic antioxidants and knowledge of these reasons can be applied to understand and synthesise a better antioxidant. These factors are discussed here.

- A. **The aliphatic tail:** *The long tail (-C<sub>16</sub>H<sub>33</sub>) attached to α-tocopherol plays an important role and this effect of the long aliphatic tail on the efficiency was first examined by K.D. Breese et al<sup>96</sup>.*



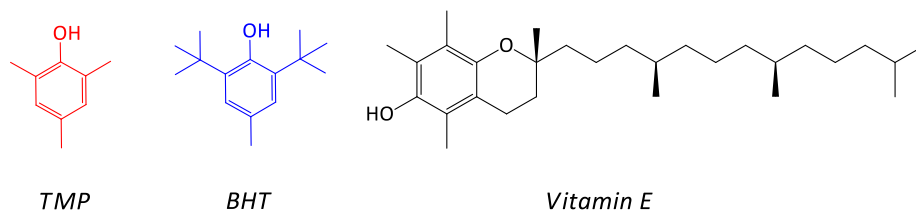
2,2,5,7,8-Pentamethyl-6-chromanol (PMHC)



vitamin E

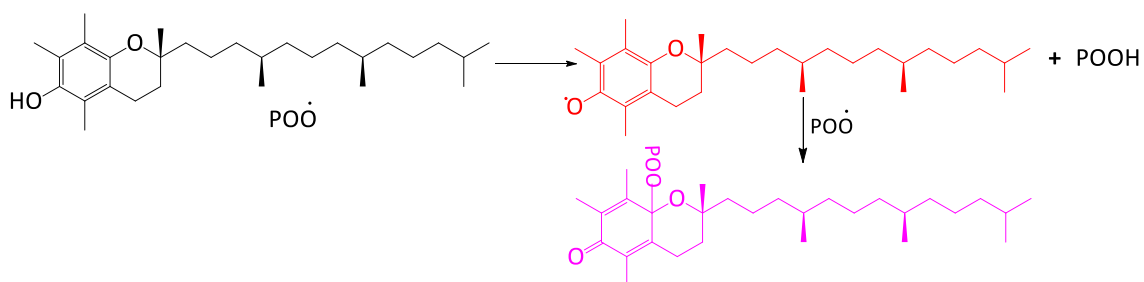
*The efficiency of α-tocopherol and 2,2,5,7,8-pentamethyl-6-chromanol (PMHC) is similar. There is one methyl group in PMHC instead of long chain hydrocarbon tail and it was found somewhat more efficient than α-tocopherol at concentration up to about 100 μM of hindered phenol groups. Higher concentrations of α-tocopherol shows more efficiency than PMHC. This increase in efficiency is thought to be due to the presence of long aliphatic tail and this long chain increases the solubility of α-tocopherol. Burton and Ingold<sup>97</sup> reported that the PMHC and α-tocopherol were equally reactive towards peroxy radicals it was concluded that the long phytol tail does not contribute towards the high antioxidant activity of α-tocopherol.*

- B. Ortho substitution effects:** It has been observed that the ortho-methyl substituted phenolic antioxidants are more efficient process stabiliser and ortho-butyl substitution shows long term stabilisation for polymers at all temperature range. For example, tri-methyl phenol (TMP) has two methyl group at the position ortho to the active -OH group,  $\alpha$ -tocopherol has two methyl group at ortho-position and BHT has two tertiary butyl groups<sup>98</sup>.



It is reported that TMP is a worse stabiliser even having two methyl groups at the ortho position. The reason behind this failure is the volatility of TMP at high temperatures because of its lower molecular weight and size<sup>96</sup>.

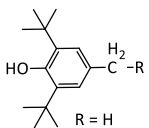
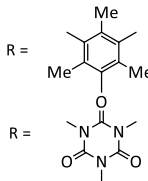
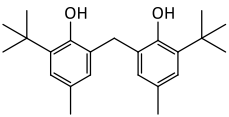
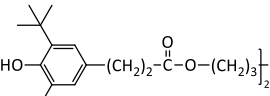
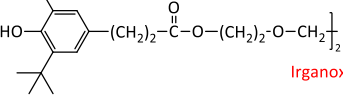
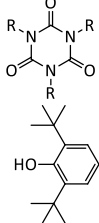
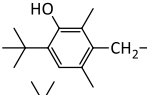
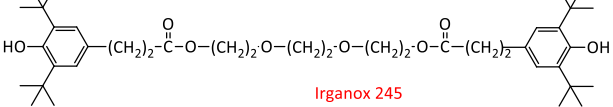
- C. Effect of the -OH group:** When H-atom is abstracted from the phenolic unit then the next interesting geometric parameter for this system is the bond length between the active oxygen atom and its neighbour carbon which is located in phenyl ring. The shortening of the interatomic distances  $HO-C_{Phenyl}$  is observed about  $0.05\text{\AA}$  after the formation of the radical on the oxygen atom. The presence of the unpaired electron on the oxygen atom is responsible for the decrease in charge on oxygen<sup>99</sup>. Another factor is the bond dissociation energy which produces two fragments after breaking O-H link in this case;
- $$AO-H \rightarrow AO\cdot + H$$

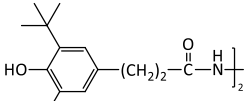
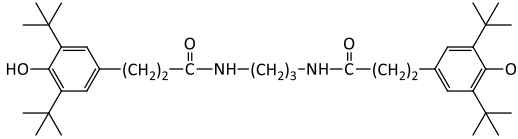
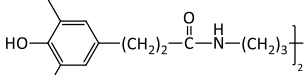
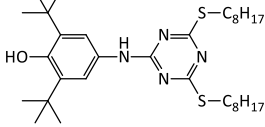


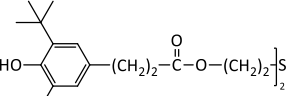
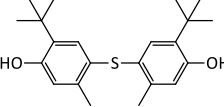
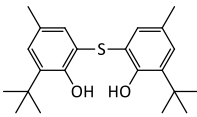
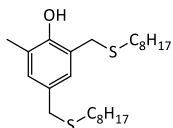
The bond dissociation energy plays an important role in determining the efficacy of an antioxidant. In this context, we can say that weaker the OH bond, the faster will be the reaction with the free radicals<sup>100</sup>.

### 1.4.4.4 Commercially available phenolic antioxidants

A range of commercially available phenolic antioxidants are listed below, along with their physical properties.

Phenolic Antioxidants	Commercial or common name	MW	Molecular formula	MP
 R = H R = -CH <sub>2</sub> CO <sub>2</sub> C <sub>18</sub> H <sub>37</sub> R = -CH <sub>2</sub> CO <sub>2</sub> C <sub>8</sub> H <sub>17</sub> R = -(CH <sub>2</sub> CO <sub>2</sub> CH <sub>2</sub> ) <sub>4</sub> C	<b>Butylated hydroxytoluene (BHT)</b>  <b>Topanol O</b> <b>Irganox 1076</b> <b>Irganox 1135</b> <b>Irganox 1010</b> <b>Irganox 1330, Ethanox 330</b>	 220.35 g/mol 531 g/mol 362.554 g/mol 1178 g/mol 775 g/mol	 C <sub>15</sub> H <sub>24</sub> O C <sub>35</sub> H <sub>62</sub> O <sub>3</sub> C <sub>23</sub> H <sub>38</sub> O <sub>3</sub> C <sub>73</sub> H <sub>108</sub> O <sub>12</sub> C <sub>54</sub> H <sub>78</sub> O <sub>3</sub>	 70 °C 50-50 °C 110-125 °C 241-247 °C
 R =	<b>Irganox 3114, Goodrite 3114</b>	784 g/mol	C <sub>48</sub> H <sub>69</sub> N <sub>3</sub> O <sub>6</sub>	218-223 °C
	<b>Irganox 2246</b>	340.50 g/mol	C <sub>23</sub> H <sub>32</sub> O <sub>2</sub>	130 °C
 (CH <sub>2</sub> ) <sub>2</sub> -C(=O)-O-(CH <sub>2</sub> ) <sub>3</sub>	<b>Irganox 259</b>	638.92 g/mol	C <sub>40</sub> H <sub>62</sub> O <sub>6</sub>	104-108 °C
 (CH <sub>2</sub> ) <sub>2</sub> -C(=O)-O-(CH <sub>2</sub> ) <sub>2</sub> -O-CH <sub>2</sub>	<b>Irganox 245, Songnox®2450</b>	587 g/mol	C <sub>40</sub> H <sub>62</sub> O <sub>8</sub>	76-80 °C
 R (CH <sub>2</sub> ) <sub>2</sub> -C(=O)-O-(CH <sub>2</sub> ) <sub>2</sub> -	<b>Irganox 3125, Goodrite 3125</b>	1042.35 g/mol	C <sub>60</sub> H <sub>87</sub> N <sub>3</sub> O <sub>12</sub>	N/A
 =R	<b>Irganox 170, Cyanox 1790</b>	699.92 g/mol	C <sub>42</sub> H <sub>57</sub> N <sub>3</sub> O <sub>6</sub>	159-162 °C
 (CH <sub>2</sub> ) <sub>2</sub> -C(=O)-O-(CH <sub>2</sub> ) <sub>2</sub> -O-(CH <sub>2</sub> ) <sub>2</sub> -O-(CH <sub>2</sub> ) <sub>2</sub> -O-C(=O)-(CH <sub>2</sub> ) <sub>2</sub> -	<b>Irganox 245</b>	586.76 g/mol	C <sub>34</sub> H <sub>50</sub> O <sub>8</sub>	76-79 °C

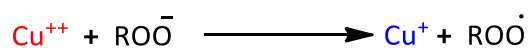
Multi-functional Phenolic Antioxidants	Common name	MW	Molecular formula	MP
	Irganox MD 1024	552.788 g/mol	C <sub>34</sub> H <sub>52</sub> N <sub>2</sub> O <sub>4</sub>	221-232 °C
	Irganox 1019	594.86 g/mol	C <sub>37</sub> H <sub>58</sub> N <sub>2</sub> O <sub>4</sub>	Not known
	Irganox 1098	637 g/mol	C <sub>40</sub> H <sub>64</sub> N <sub>2</sub> O <sub>4</sub>	156-162 °C
	Irganox 565	588.954 g/mol	C <sub>35</sub> H <sub>56</sub> N <sub>4</sub> OS <sub>2</sub>	156-162 °C

Thio-Phenolic Antioxidants	Commercial/common name	MW	Molecular formula	MP
	Irganox 1035, Songnox® 1035	643 g/mol	C <sub>38</sub> H <sub>58</sub> O <sub>6</sub> S	65 °C
	Irganox 415, Lowinox TBM-6	358.54 g/mol	C <sub>22</sub> H <sub>30</sub> O <sub>2</sub> S	160-165 °C
	Irganox 1081, Lowinox TBM-6	358.54 g/mol	C <sub>22</sub> H <sub>30</sub> O <sub>2</sub> S	81-86 °C
	Irganox 1520,	425 g/mol	C <sub>25</sub> H <sub>44</sub> OS <sub>2</sub>	

## 1.5 Metal deactivators

Metal deactivators are the compounds that work by chelating dissolved trace metals or metal ions in material things to reduce the catalytic process at its source. In other words, an atom or group of atoms which has the ability to chelate or exchange sites with metal ions and prevent it from reacting with other components of the system. Normally these compounds have chelation sites containing nitrogen, oxygen, phosphorus and sulphur.

Copper and many of its compounds are powerful pro-oxidant catalysts in polyethylene. For example, cupric chloride, cupric oleate, cupric oxide, cupric sulphide, cuprous oxide and metallic copper can act as pro-oxidant in polyethylene. Metallic copper can promote degenerative chain branching in polymer, but the catalytic states lie between cuprous and cupric. Cupric is reduced to cuprous but not to the metallic state. It is assumed that during the earlier stages of autoxidation of pure hydrocarbons at low temperatures, no compound capable of reducing divalent copper which exists in the system and the catalytic power of copper does not play any role in the polymer. The addition of an antioxidant able the copper to function as a catalyst. When autoxidation is in full progress after the destruction of the antioxidant, oxidation products, such as aldehydes, are formed which are capable of reducing cupric copper. It has been suggested that peroxides may also cause reduction according to the following equation.

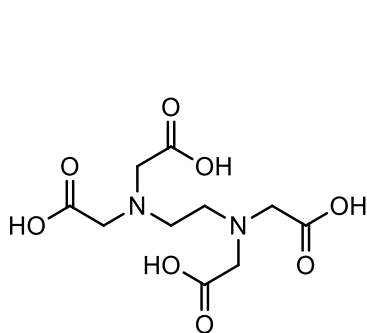


But this reaction is likely to be negligible in the presence of an efficient antioxidant. The harmful effect of copper can be counteracted by the addition of enough antioxidants in the system, as shown below in the mechanism of copper catalysis<sup>101</sup>.

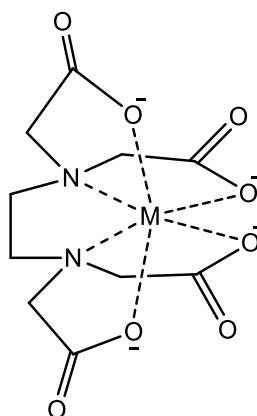


### 1.5.1 The coordination chemistry of how metal deactivators are thought to work

A metal deactivator has multiple donor atoms which are covalently connected by atoms that surround the complexed metal ion with several rings and deactivate it. The ability of a metal deactivator depends on the number of donor sites and is termed as polydentency. The metal deactivators are normally polyfunctional chelating compounds with ligands containing atoms such as N, O, S and P that have lone pair of electrons. They donate the lone pair to the central metal atom or ion forming a coordinate covalent bond. Metal deactivator generally forms a ring structure around the central metal ion. Some metal deactivators are called Flexi-dentate because they can use any number of chelation sites to capture metal atom or ion. For example, EDTA is a Flexi-dentate chelating agent and coordinates to metal ions through six chelation sites and prevents the metals from reacting as shown below.



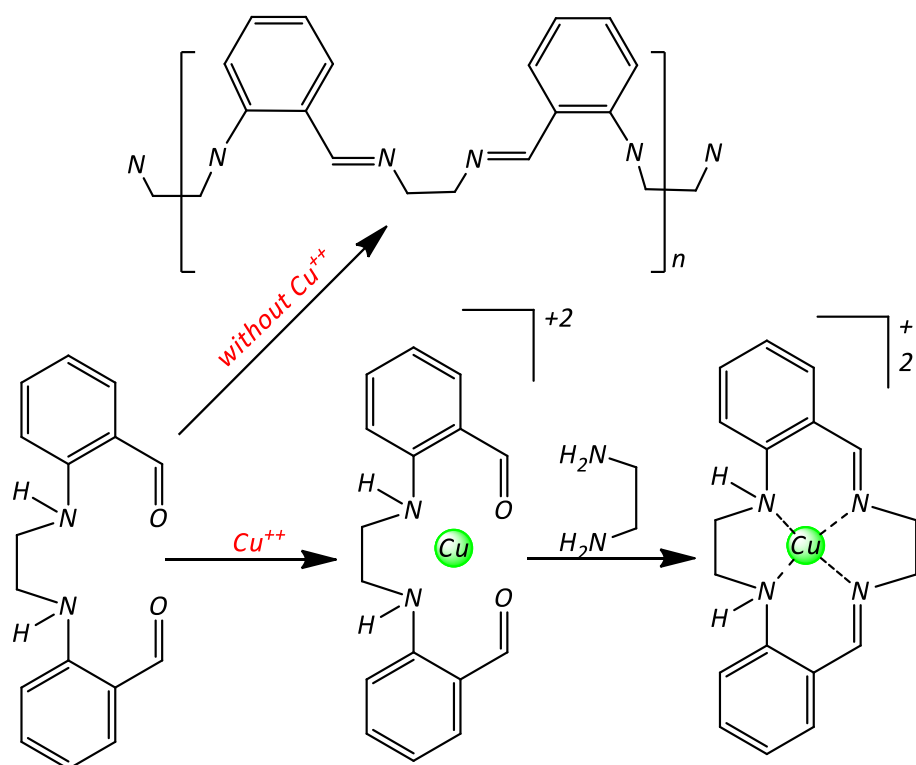
EDTA



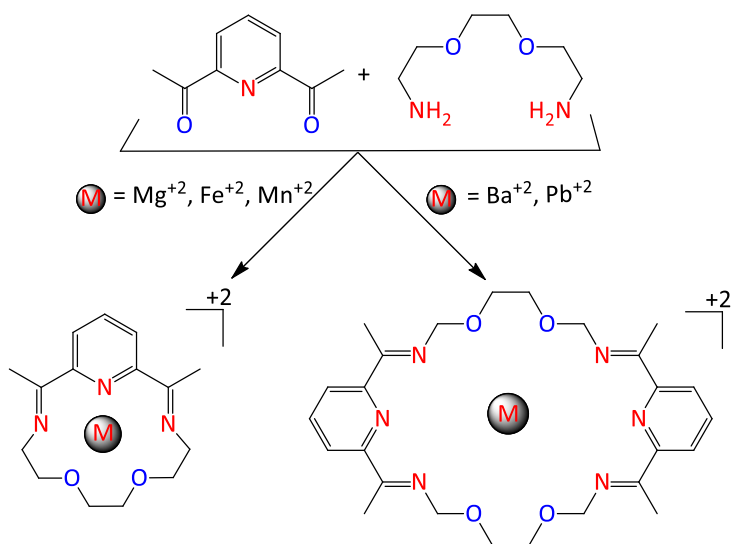
EDTA hexadentate complex with metal atom

#### 1.5.1.1 Ligand template Synthesis

When Schiff-base reaction occurs in the presence of a metal ion. Metal ion binds itself with the oxygen atom of carboxylic or aldehyde groups and then set the path for amines to react and form the macrocycle. The temple effect is governed by the kinetic factor which involves the actual formation of ligands about the metal centre, in essence, the ligand would not form in the absence of the templating metal. The synthesis of macrocycle hinges upon the use of a metal-directed template method for bringing the constituent components of cyclic ligand together. In the absence of a metal ion, typically first-row transition metals or  $d^{10}$  metals, cyclisation does not occur. As a result, a polymer or oligomers is produced as given below in a chemical equation.



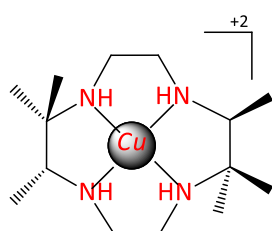
The most important in this case is the size of cations used because they set the structured pathway in the Schiff-base system. The size of cations can influence the formation of macrocyclic products during a chemical reaction as given in the chemical reaction below.



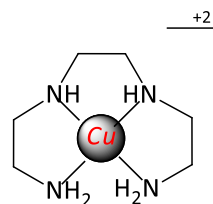
### 1.5.1.2 Preorganisation and complementarity

The relationship between a chelating agent and a metal atom or ion sometimes called host-guest in a complex and this complex shows good stability. The host in these complexes is a chelating agent (large ring with different chelation sites) that bind the metal atom or ion by using different chelating atoms having lone pairs. These molecules gain stability through macrocyclic effects. There is an additional effect through which a chelation agent chelates metal atom or ion and this effect is the organisation of binding sites in space and in this case, energy is not expended to wrap the guest.

The macrocyclic effect was first studied by Cabbiness and Margerum in 1969 by using copper (II) complex. In both molecules, there are four chelation sites but the copper chelation 1 is about 104 times more stable than copper chelation 2 due to an additional preorganisation of macrocycle as shown below<sup>102, 103</sup>.



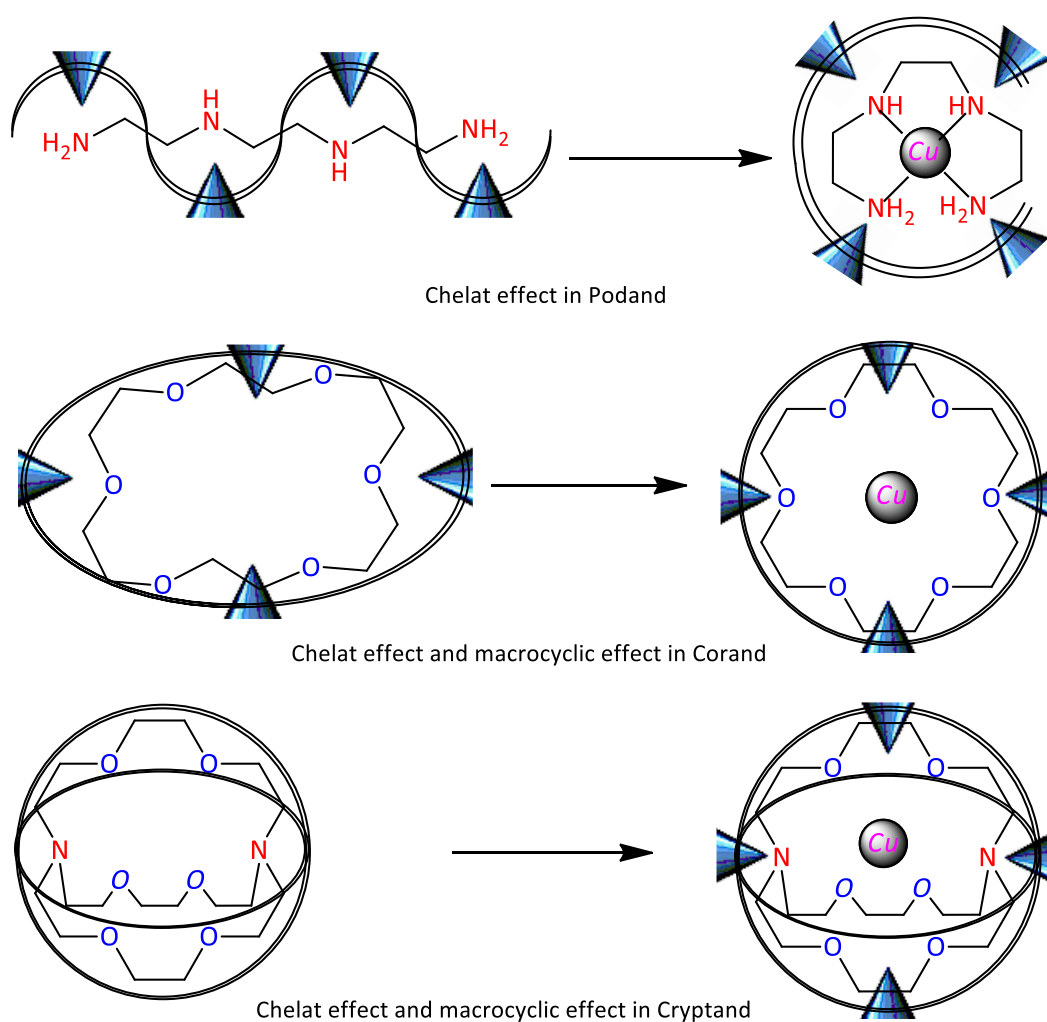
*Copper chelation 1*



*Copper chelation 2*

The host and guest binding process go through two sets of stages. In the first stage, the host undergoes conformational readjustment, and this is known as the activation stage. In the activation stage host molecule arrange its binding sites to bind metal atom or ion in a proper way and same time it minimises the unfavourable interaction between the donor atoms with lone pair. During the conformational readjustment, energy is never paid back because the Cu guest is captured by host for a lifetime in the host-guest complex. On the other side, during rearrangements binding between host and guest is energetically favourable. The overall free energy of complexation can be calculated by the taking difference between unfavourable reorganisation energy and favourable binding energy. The host-guest complex is destabilised when reorganisation energy is large and if the host is preorganised then this rearrangement energy is small, and the system becomes stable. When the

preorganised host is in a rigid system then it will be difficult for the host to go through a complexation transition state so its guest binding ability may reduce. But in a mobile system, the host can adjust itself according to surrounding conditions and in this situation complexation and decomplexation can occur simultaneously. The effect of preorganisation is enhanced by the solvation because the unbound host is stabilised more effectively by solvation than after its gripping on guest (metal atom or ion) and at this step after grabbing the guest, it presents small surface area to the surrounding medium. The chelating effect is shown in a hypothetical scheme (**Scheme 1-19**)

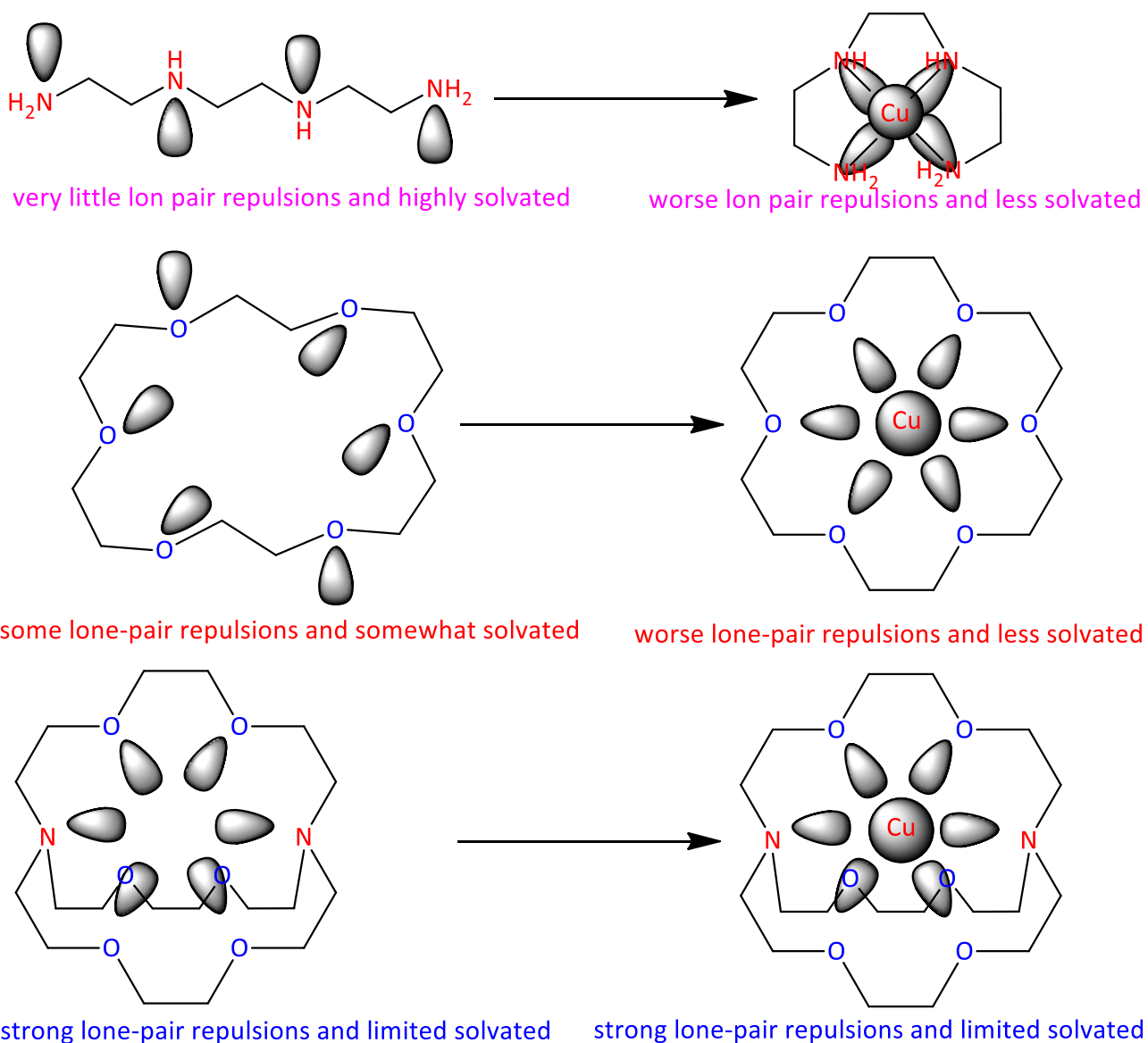


**Scheme 1-19** Hypothetical chelating effect (the host and guest binding process)

The second effect to understand is the affinity of a host and guest complementarity. According to Donald Cramp, the complementarity can be stated as “To complex, hosts must have binding sites

which cooperatively contact and attract binding sites of guests without generating nonbonded repulsions”.

The correct electronic characters such as polarity, H-bond, hardness, softness and donor/acceptor ability are must for a host to grab guest atom. Hydrogen bond donor ability must match with the acceptor and the host binding site must have space and this space must be directed towards the guest as shown in **Scheme 1-20**<sup>102</sup>.



**Scheme 1-20** Hypothetical chelating effect (the affinity of a host and guest is complementarity)

### 1.5.1.3 Thiolates-Metal bonding

Thiolates ligands have one sigma ( $\sigma$ ) donor orbital and two lone-pair orbitals, which are principally sulfur  $3p$  in character. One of these lone pair orbitals has the correct symmetry for  $\pi$  interactions with metal  $d$  orbitals and can act as  $\pi$  donor ligand<sup>104</sup> as shown in **Figure 1-3**.

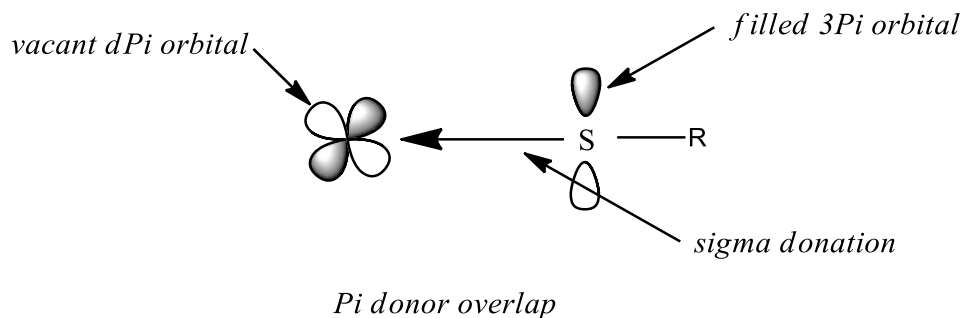


**Figure 1-3**  $\pi$ -donor interaction between a sulfur  $3p$  orbital and metal  $d$  orbital

If the metal  $d$  orbital is formally unoccupied, the thiolate ligand may serve as a four-electron donor ( $2\sigma + 2\pi$ ). The collaboration between metal and thiolate is important to stabilise metal centres in high oxidation state<sup>105</sup> or co-ordinatively unsaturated complexes<sup>106</sup>. When the  $d\pi$  orbitals of metal are occupied then  $d\pi$   $\pi$  interactions occur between the lone pair of sulfur and filled metal orbitals. Sulfur atom donates 4 electrons to the metal atom and gives rise to a highly occupied molecular orbital (HOMO) and this orbital is sulfur  $3p$  in character or antibonding. The interaction between metal-filled  $d$ -orbitals and thiolate sulfur lone pair of electron ends up with generating thiyl radicals. This can happen by the reaction with electrophiles as shown in **Figure 1-4**<sup>107</sup>.

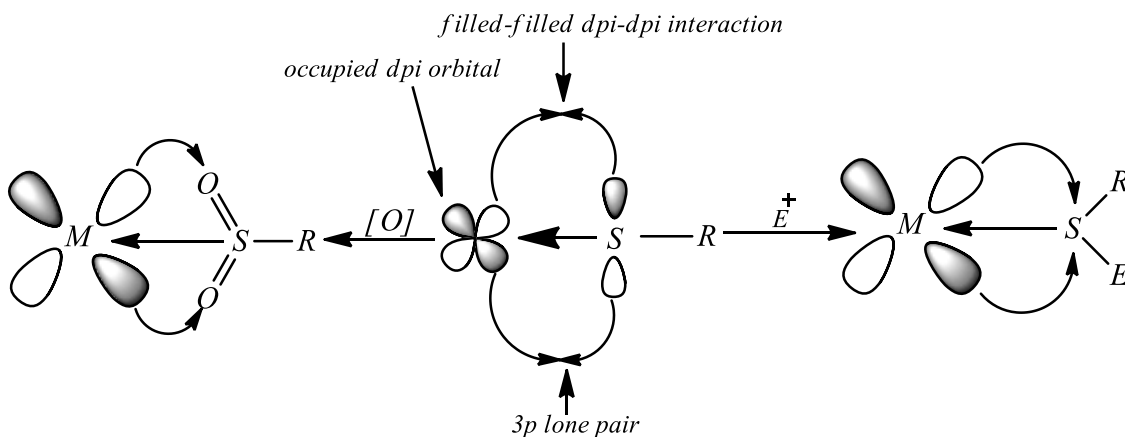
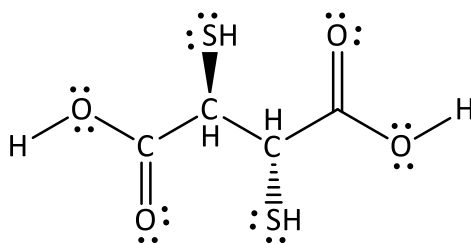


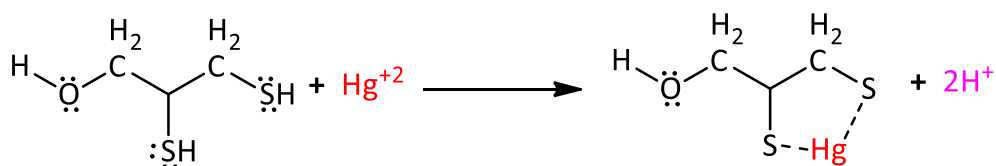
**Figure 1-4** Repulsive interaction between thiolate sulfur  $3p$  orbital and metal  $d$ -orbital that stimulate the oxidation and nucleophilic attack by the sulfur atom

If we look at dimercaptosuccinic acid in which all the oxygen and sulfur atoms have lone pairs of electrons and these lone pair can be used to coordinate to a metal center, so there are six possible donor atoms. Geometrically, only two of these atoms can be coordinated to metal at once. The most common binding mode involves the coordination of one sulfur atom and one oxygen atom, forming a five-member ring with the metal as shown in the chemical structure below.



*Dimercaptosuccinic acid*

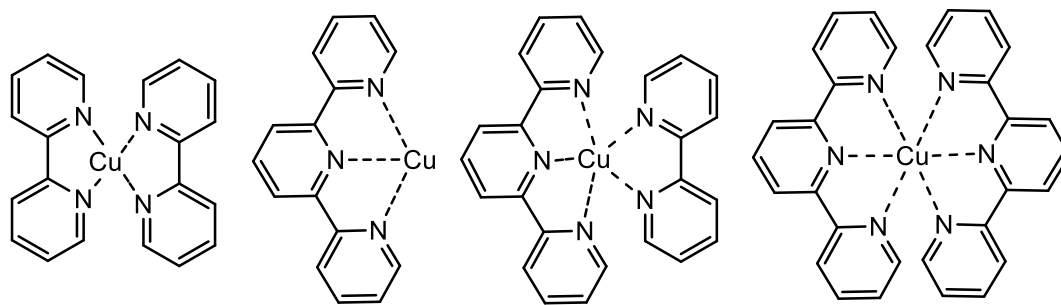
Another example is dimercaprol (2,3-dimercapto-1-propanol) is an effective chelating agent for heavy metals such as arsenic, mercury, antimony, and gold. These heavy metals form a strong bond to the sulfur atoms in dimercaprol as shown in the chemical equation below.



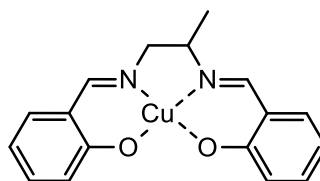
### 1.5.2 Copper chelation

The question of coordination number in copper (II) complexes is far from simple. The CSD (Cambridge Structural Database) contains about 4649 copper (II) complexes with coordination number four, 6501 shows that coordination number is five and 4513 claims that copper (II) has coordination number six. Based on this structural data, copper (II) exhibits coordination number five. It is notable that a slight expansion ( $0.1 \text{ \AA}$ ) in the coordination sphere of the copper(II) reveals additional interactions tending towards a six-coordinate geometry and that a significant number of

these “five-coordinate” complexes display a longer sixth interaction in a position that approximately describes an octahedral arrangement of donors. The favoured coordination number is six, although this depends on the asymmetry of the ligand. The compound symmetrical Schiff’s base or imine which is formed by condensation of salicylaldehyde and alkylene diamine forms a tetradentate ligand complex with metal compounds. For example, 2,2':6',2''-terpyridine and bipyridine and, N, N'-disalicylidene 1,2-propane diamine, deactivating copper as shown in the chemical structures below<sup>108</sup>.



2,2':6',2''-terpyridine and bipyridine with copper



N, N'-disalicylidene 1,2-propane diamine with Cu

### 1.5.3 Copper Index

The values of oxidation rates for Aluminium is 222 ru.g<sup>-1</sup>.min<sup>-1</sup>, for Iron 347 ru.g<sup>-1</sup>.min<sup>-1</sup>, and 854 ru.g<sup>-1</sup>.min<sup>-1</sup> for copper. These values represent an important difference between the thermal degradation catalytically induced by metals. The kinetic parameters that assess the progress in any chemical process, the thermal degradation of polymers in contact with metals can be alternatively characterised by a copper index. The copper index can be simply defined as the ratio between a certain property of any metal with respect to the value for copper. In the polymer matrix, the low

values of the copper index can be justified by the presence of the different antioxidants<sup>88, 109</sup>, which efficiently prevent oxidation in the first thermal degradation stages of polyolefin.

The surface interaction between copper and a polymer accelerates the thermal degradation of the organic phase at different rates. The most reactive metal, among all the other metals, is copper which induces degradation with the shortest oxidation induction time and the highest oxidation rate. On the opposite side, aluminium presents remarkable inertia relative to other studied metals (Mo, Ti, Zn, Pb, Fe). The catalytic effect of metals on the propagation of accelerated ageing reveals the unlike behaviour of different types of polyethylene<sup>7, 110</sup>.

#### 1.5.4 Maximum chelation stability (Stability Constant)

The ability of a metal deactivator to deactivate metal ion depends on the number of atoms in the backbone of each chelation ring. Maximum chelation stability occurs when ring backbones contain five or six atoms. Chelation rings with less than five atoms can experience ring strain, while chelation rings with more than six become less stable because of reduced ring closure. If a metal deactivator has a bulky side chain branching near the donor site, the level of deactivation will be reduced. As a result, the side chain can hinder the close approach of the metal ion. The chelation stability of 3 rings (trien), 2 ring (dien) and 1 ring (en) system are shown in the graph given below<sup>111</sup>.

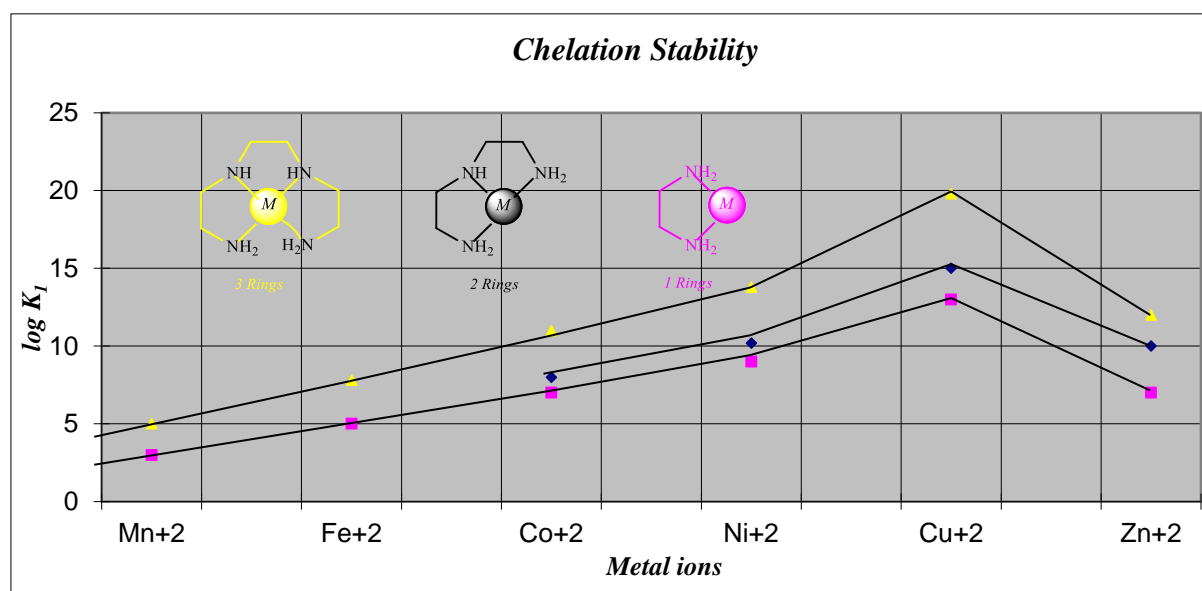


Figure 1-5: Chelation stability as a function of chelating ring structure for selected transition metal ions

The chelation ability of metal deactivators depends upon the value of  $\beta$  (stability constant or equilibrium constant). The higher the value of  $\beta$ , the higher will be the stability of metal deactivators complexes, for example, the metal deactivators with higher  $\beta$  values form more stable complexes than do an equivalent number of related monodentate ligands (**Table 1-2**) in case of copper and nickel ions<sup>112</sup>.

**Table 1-2**  $\beta$  values for  $\text{Cu}^{+2}$  and  $\text{Ni}^{+2}$  with ammonia and ethyleneamine

<b>Metal Ion</b>	<b>Ligand</b>	<b>Complex</b>	<b>Log <math>\beta</math></b>
$\text{Cu}^{+2}$	$\text{NH}_3$	$[\text{Cu}(\text{NH}_3)_4]^{+2}$	12.6
$\text{Cu}^{+2}$	<i>en</i>	$[\text{Cu}(\text{en})_2]^{+2}$	20.6
$\text{Ni}^{+2}$	$\text{NH}_3$	$[\text{Ni}(\text{NH}_3)_6]^{+2}$	8.7
$\text{Ni}^{+2}$	<i>en</i>	$[\text{Ni}(\text{en})_3]^{+2}$	18.0

The individual ligands are displaced stepwise and an equilibrium expression can be written for every step, but the final deduction is made through an overall expression for the overall ligand displacement reaction. Like equilibrium constants, stability constants are dependent on the temperature change and vary with change in temperature. The overall stability constants are given by the symbol  $\beta$  with a suffix to indicate the number of ligands involved as shown below.



$$\beta_1 = \frac{[ML]}{[M][L]}$$



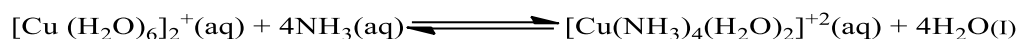
$$\beta_2 = \frac{[ML_2]}{[M][L]^2}$$



$$\beta_n = \frac{[ML_n]}{[M][L]^n}$$

Where the  $\beta_1$  to  $\beta_n$  values are overall stability constants

For example,



$$\begin{aligned} \text{Stability Constant} &= \frac{[\text{Cu}(\text{NH}_3)_4(\text{H}_2\text{O})_2]^{+2}(\text{aq})}{[\text{Cu}(\text{H}_2\text{O})_6]^{+2}(\text{aq})[\text{NH}_3(\text{aq})]^4} \\ &= 1 \times 10^{12} \text{ mole}^{-4} \text{ dm}^{12} \text{ at } 298\text{K} \end{aligned}$$

The value is often expressed as its logarithm,  $\log \beta$ , making the numbers easier to handle.

### 1.5.5 Volume of Space

The electronic property of metals is influenced by the addition of ligands. If the ligands are negatively charged, then there is a decrease in positive charge on complex which influences the stability constant. The presence of interactions among ligands is another factor. For example, a small ligand such as the  $\text{F}^-$  and six  $\text{F}^-$  donor-atom can fit around an ion such as  $\text{Co}^{+3}$  to give  $[\text{CoF}_6]^{-3}$ . If we replace six  $\text{F}^-$  by six  $\text{Cl}^-$  around the  $\text{Co}^{+3}$  then the complex like  $[\text{CoCl}_6]^{-3}$  is not possible but  $[\text{CoCl}_4]^{-2}$  is obtained. The first coordination sphere around the metal ion depends on the size and shape of the ligands because size and shape decide the number of atoms that can fit into the volume of space around the metal atom. This is called steric interactions between the ligands which limit the co-ordination number of the complex<sup>103</sup>.

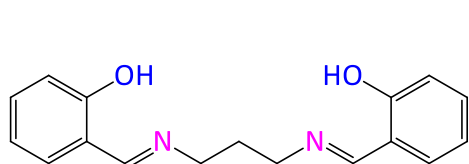
## 1.6 Development of Metal Deactivators

The development of chelating agents has been reported mostly in the patent literature. The main reason behind this work has been a need for metal (copper) deactivation primarily in fuels, lubricants, and polymers (polypropylene insulation for copper wiring). The first commercial metal deactivators were developed in 1939<sup>113</sup> for fuels but were found to be not adequately operative for copper wire insulation<sup>114</sup>.

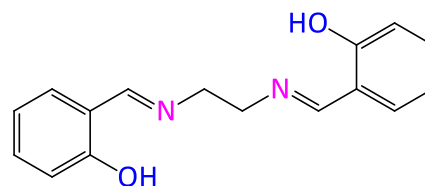
Metal deactivators can be categorised by chemical structure into six broad classes: Schiff's bases (imines), hydrazides, oxalyl amides (oxamides), oxalo-hydrazides, heterocycles, Mannich bases.

### 1.6.1 Schiff's bases (Imines)

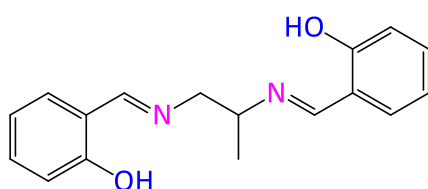
The condensation of an aldehyde or ketone with a primary amine gives Schiff's base (imine). The oldest known fuel metal deactivator, *N,N'*-disalicylidene alkylene diamine is a symmetrical Schiff's base and is synthesised by condensation of salicylaldehyde and alkylene diamine<sup>115-120</sup>.



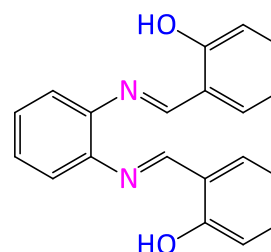
*N,N'*-Bis(salicylidene)-1,3-propanediamine



*N,N'*-Bis(salicylidene)ethylenediamine



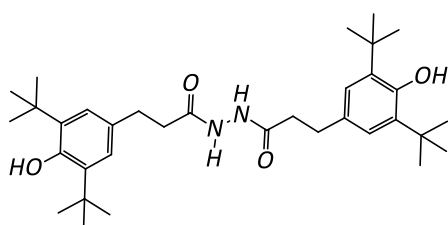
*N,N'*-disalicylidene-1,2-propane diamine



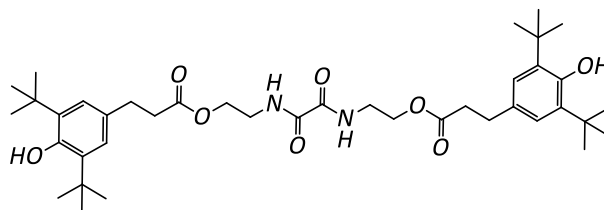
*N,N'*-Bis(salicylidene)-1,2-phenylenediamine

### 1.6.2 Hydrazides

Hydrazides are acylated derivatives of hydrazine. They were developed to provide metal chelation in polypropylene insulation used in electrical (copper) wiring. The first hydrazide metal deactivator was synthesised by grouping hydrazide and Schiff's base<sup>121</sup>. *N,N'*-Dihydrazides of a single hydrazine unit were synthesised later<sup>122-124</sup>. The chemical structure of commercially available metal deactivators is given below.



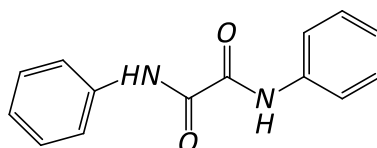
LOWINOX®MD24



NAUGARD®XL-1

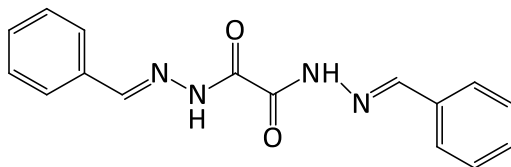
### 1.6.3 Oxalyl amides (Oxamides)

At nearly the same time that the first hydrazide metal deactivator was being developed, oxalyl amides were also proposed as metal deactivators for polypropylene insulation used in copper wiring<sup>125, 126</sup>. One of the earliest and simplest structures of oxalyl amide is given below.



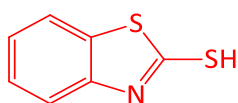
### 1.6.4 Oxalo-Hydrazides

After modification of the previous two classes of metal deactivators, oxalo-hydrazides were synthesised for polypropylene used in copper wire insulation. The oxalo-hydrazides are formed by the condensation of the appropriate aldehyde or ketone with oxalyl dihydrazide. The dibenzyl additives have also been proposed as metal deactivators for polypropylene used in the copper wire in the 1970<sup>114</sup>.

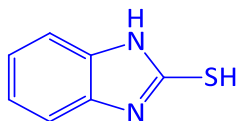


### 1.6.5 Heterocycles

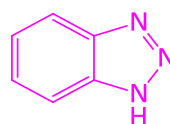
Heterocyclic compounds containing a nitrogen atom, have been used as a metal chelator for fuels, lubricants, and polypropylene wiring insulation<sup>127</sup>. These additives contain the benzotriazoles and other heterocyclic compounds as shown below in chemical structures.



2-Mercapto-1,3-benzothiazole



2-Mercaptobenzimidazole



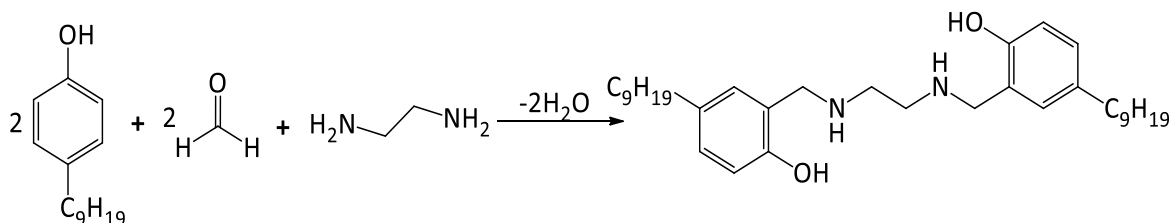
1,2,3-Benzotriazole



1,2,3-Thiadiazole

### 1.6.6 Mannich bases

Mannich bases are condensation products of carbonyl compounds (aldehydes or ketones), amines, and compounds such as activated phenols that have labile hydrogen<sup>128</sup>. The formation and likely structure of one Mannich base chelating agent is given below<sup>129</sup>.



It is thought that Mannich base metal deactivators are effective against a wider range of metals including cobalt, nickel, manganese, and iron.

## 1.7 Justification for the research

Metal deactivators (MD) important in applications where metal ions in contact with metals e.g. copper cable.

Limited understanding of the role of MD in polymers at present and their influence on stability – most of the publications simply process the MD with the polymer at look at how polymer properties change (key works by Osawa)– with no systematic investigation of how the specific structure influences this. The presence of a metal deactivator, even in excessive amounts, is usually not sufficient to completely overcome the catalytic effects of the metal. The reasons for this are not clear, and in general, the relationship between the structure of the inhibitor and the magnitude of inhibition is not well understood.

The aim of the current project was to synthesise MDs that have a systematic variation in their structure. The reason for this is that most commercial MDs such as MD1024 and XL-1 can behave as an antioxidant as well as MD and it is not clear whether both functionalities are necessary i.e. phenolic group and coordination, or just the coordination and separate phenolics (or other antioxidants) in a formulation are better. (i.e. a typical additive combination has a stearate to help processing, primary and secondary antioxidants and if required the MD). Do they work better in the same molecule or better if added separately?

To what extent can other stabilisers e.g. phenolics, phosphites coordinate metal ions or participate in any competitive exchange of metal ions?

Although many approaches have been used to synthesise the chelating agents, the goal of this study was to prepare metal deactivators and multifunctional metal deactivators containing nitrogen, oxygen and sulphur atoms without using catalysts and avoiding hazardous organic solvents. In this study, only ethanol, methanol and water were used (except halogen compounds) for protection of the environment. The vast majority of commercial metal deactivators are based oxamides and hydrazides, often coupled to sterically hindered phenols and these templates have been exploited in this study. In some cases, other commercially available polymer antioxidant structures were

modified into metal deactivators by systematic variation in their structure, in order to combine the two or more functionalities to find how the specific structure influences.

The most common synergism is that occurring between chain-breaking antioxidants (such as hindered phenols) and hydroperoxide decomposers (such as aromatic phosphites). Although the mechanism is not fully explained, one important role of phosphite stabilisers is to preserve the hindered phenol. An attempt has been made to explain the function and interaction of phosphite stabiliser with other additives present in the polymer formulations.

A new class of antioxidants known as autosynergists consist of a hindered phenolic antioxidant and a hydroperoxide decomposer in a single molecule. Irganox 1035 is an example of such an autosynergist. It is bifunctional, with two hindered phenolic substituents attached to a central sulfur atom and is used for special high-temperature applications in PE pipes and cables. This additive cannot be used in formulations containing HALS (hindered amine light stabiliser such as Chimassorb 944) because the acidity of sulphur antioxidant neutralizes HALS effectiveness as both are antagonistic. To avoid this interaction between HALS and thioesters compounds, a new additive containing both functionalities has been synthesised by replacing ester oxygen of Irganox 1035 by a nitrogen atom.

These approaches will be combined to vary the combination of antioxidant and metal deactivator functionalities both in proximity to each other and when spaced apart with alkyl chains and other groups.

## Chapter 2: Experimental

### 2.1 Materials and Analytical Methods

#### 2.1.1 Materials and Preparation

All reagents for synthesis and the copper salts (copper (I) chloride, copper (II) acetate) were purchased from Sigma-Aldrich, Alfa Aesar or Fluka. All synthetic reactions were monitored by thin-layer chromatography using pre-coated sheets of silica gel 60, 0.25 mm thick F254 Merck KGaA®).

Low density polyethylene (LDPE, MFI 1.5 g/10 min (190°C, 2.16 kg)) and commercial antioxidants (CaSt, ALKANOX®240, ANOX®20) and metal deactivators (LOWINOX®MD24, NAUGARD®XL-1) were provided by Addivant UK Ltd.

Novel AO/MDs were prepared according to the synthetic methods described in **Section 2.2** and their ability to coordinate copper assessed by reaction with copper (II) salts.

Copper (II) acetate complexes of AO/MDs were prepared by dissolving individual AO/MDs (0.55 mmol) in methanol (50 mL) to which copper (II) acetate (1.1 mmol) was added and stirred for 1–2 hours at room temperature. Filtration and washing with methanol, gave green solids, which were air dried at room temperature. Purity of the ligand and complexes was checked by TLC. **Characterisation data for the complexes is not given here but discussed in the results section, since it is directly relevant to the performance of the AO/MDs.**

The stabilisation performance of the novel AO/MDs was assessed by extrusion in circulation mode and normal mode (multi-pass). Structures and physical data of all antioxidants is given in the **Appendix (Tables A-11 to A-15)**

Formulations for circulation mode extrusion of novel AO/MDs without copper were prepared using standard *phr* (percent hundred ratio) methodology, by shaking the precisely weighed AO/MD (0.075 %w/w) and LDPE (99.925 %w/w) in a polyethylene bag to distribute additives uniformly throughout the polymer. Formulations for extrusion with copper were prepared in the same way but Copper (I) Chloride (0.100 % w/w) was added to the mixture before shaking.

Formulations for normal mode (multi-pass) extrusion, with and without copper, were prepared in the same way as for circulation mode extrusion, except that the precisely weighed additives were present in the following amounts: LDPE (99.6 %w/w), base stabiliser (0.3 %w/w) and the AO/MD (0.1 %w/w). The base stabiliser consisted of Cast (0.1 %w/w), ALKANOX®240 (0.1 %w/w) and ANOX®20 (0.1 %w/w).

The formulations (5.0 g) were then extruded in a twin-screw co-rotating extruder (Thermo Scientific HAAKE MiniCTW) as shown in **Figure 2-1**. This permitted effective extrusion where relatively small amounts of novel stabilisers had been synthesized. The extrusion of the LDPE formulations was carried out by operating the MiniCTW in two different modes at 190°C with screws co-rotating at speeds of 25 rpm, as described below:

- a) Circulation mode:** *By running the instrument in circulation mode, the required cycle time (0 min, 5 min and 10 min) can be controlled easily. At the end of the test, the bypass valve can be opened, and the sample is extruded as a strand. Single stabiliser performance was studied by circulation mode.*
- b) Normal mode:** *This technique involves repeatedly passing the polymer through an extruder and then collecting the samples after each pass (multi-pass extrusion). In order to perform a subsequent analysis, the standard polyethylene's formulations were subjected to five extrusion passes and samples were collected from pass 1, pass3 and pass 5.*



*Figure 2-1 Thermo Scientific HAAKE MiniCTW laboratory extruder setups*

### 2.1.2. Methods for Analysis of Synthesised Novel AO/MDs

IR spectra of the novel AO/MDs synthesized in this study were recorded on a Nicolet® 380 FTIR – Fourier Transform Infrared Spectrometer in ATR mode. Only the frequencies (in  $\text{cm}^{-1}$ ) characterising copper-ligand interactions and functional groups arising from the oxidative degradation of LDPE have been reported.

$^1\text{H}$  NMR and  $^{13}\text{C}$  NMR have been recorded on a JEOL® ECS-400 (400 and 100.6 MHz, respectively) using  $\text{CDCl}_3$ ,  $\text{DMSO-D}_6$  or  $\text{CD}_3\text{OD}$  as solvent. Chemical shift values are reported in ppm with TMS as internal standard ( $\text{CDCl}_3$ :  $\delta$  7.26 for  $^1\text{H}$ -NMR,  $\delta$  77.0 for  $^{13}\text{C}$ -NMR). Data are reported as follows: chemical shifts, multiplicity ( $s$  = singlet,  $t$  = triplet,  $m$  = multiplet), coupling constants (Hz).

High resolution mass spectra were measured on an Agilent Technologies® 6540 Ultra-High-Definition (UHD) Accurate-Mass equipped with a time of flight (Q-TOF) analyser and the samples were ionized by ESI techniques and introduced through a high pressure liquid chromatography (HPLC) model Agilent Technologies®.

### 2.1.3. Methods for Analysis of Extruded Formulations

To monitor functional groups changes arising from oxidative degradation of LDPE, the pelletised LDPE formulations from circulation mode (0 min, 5 min and 10 min) and normal mode extrusion (pass 1, pass 3 and pass 5) were analysed in absorbance mode using a PerkinElmer UATR Spectrum Two spectrometer as shown in **Figure 2-2**. All samples were examined, and FTIR data was recorded between 4,000 and 400  $\text{cm}^{-1}$ , resolution of  $4\text{cm}^{-1}$  and 16 scans.

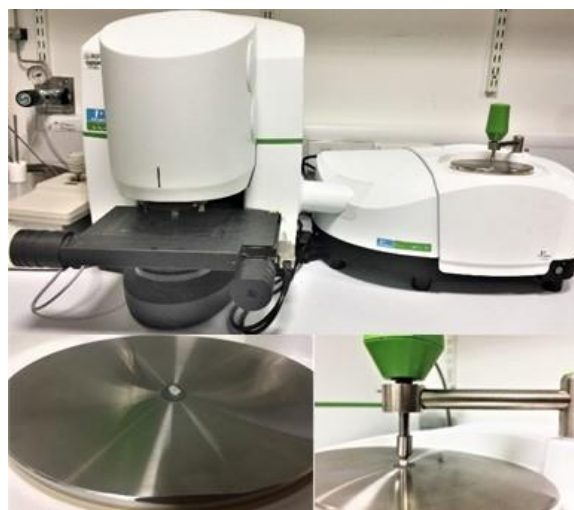


*Figure 2-2 PerkinElmer UATR Spectrum Two spectrometer*

LDPE formulation from both circulation mode (0 min, 5 min and 10 min) and normal mode extrusion (pass 1, pass 3 and pass 5) were also analysed using typical industry performance indicators of Melt Flow Index (MFI) and Yellowness Index (YI).

#### **Melt Flow Index (MFI)**

MFI is an indirect measure of the molecular weight of the polymer, so can indicate if chain-scission has taken place. This is assessed by melting the polymer and applying a standard weight to push it through a narrow capillary. MFI was measured using a Ray-Ran® *Melt Flow Indexer* capillary melt viscometer by applying a standard weight (2.16 kg) at a melt temperature of 190°C as shown in **Figure 2-3**.



*Figure 2-3 Ray-Ran® Melt Flow Indexer*

A small amount of the sample (5 grams) was placed in the cylinder (preheated at 190°C for at least 15 minutes). The material was packed inside the barrel to avoid the formation of air pockets. A piston was introduced, and a specified weight of 2.16 kg was introduced onto the piston. To measure the rate of extrusion the extrudate was cut-off at the jet, at convenient measured intervals of time (2 minutes) and was weighed accurately. This process was repeated at least three-times and the average value for three cuts was noted. MFI was expressed in grams of sample per 10 minutes of the duration of the test.

MFI values for samples extruded by circulation and normal modes are given in the **Appendix (Tables A-1 to A-10)** in addition to their graphical representation in the results and discussion (**Section 3**).

### **Yellowness Index (YI)**

The discolouration arising during the melt oxidation of LDPE polymer can be attributed to the transformation products of antioxidants (major contributor), but also arises from conjugated sequences associated with carbonyl groups in the polymer (minor contributor).

Colour in polymers is compared using Colour Index values, as defined by the Commission Internationale de l'Eclairage (CIE). An  $L^*a^*b^*$  colour space is modelled after a colour-opponent theory stating that two colours cannot be red and green at the same time or yellow and blue at the same time. The colour space is shown in **Figure 2-4** where,  $L^*$  indicates lightness,  $a^*$  is the red/green

coordinate, and b\* is the yellow/blue coordinate. Deltas for L\* ( $\Delta L^*$ ), a\* ( $\Delta a^*$ ) and b\* ( $\Delta b^*$ ) may be positive (+) or negative (-). The total difference, Delta E ( $\Delta E^*$ ), however, is always positive.

$$\Delta E^* = \sqrt{(\Delta L^*)^2 + (\Delta a^*)^2 + (\Delta b^*)^2}$$

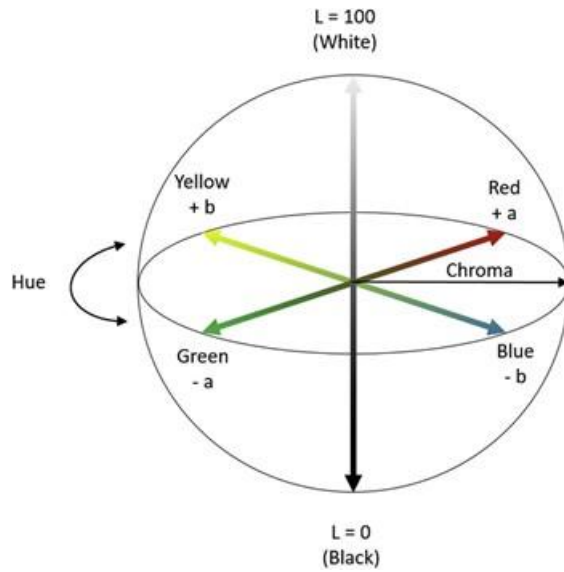


**Figure 2-4** CIE-L\*a\*b\* colour space

Colour measurements were carried out on a GretagMacbeth Spectroeye Colorimeter (Colour data Systems Ltd., Wirral, UK). In this study change in yellowness is given as  $\Delta b^*$ .



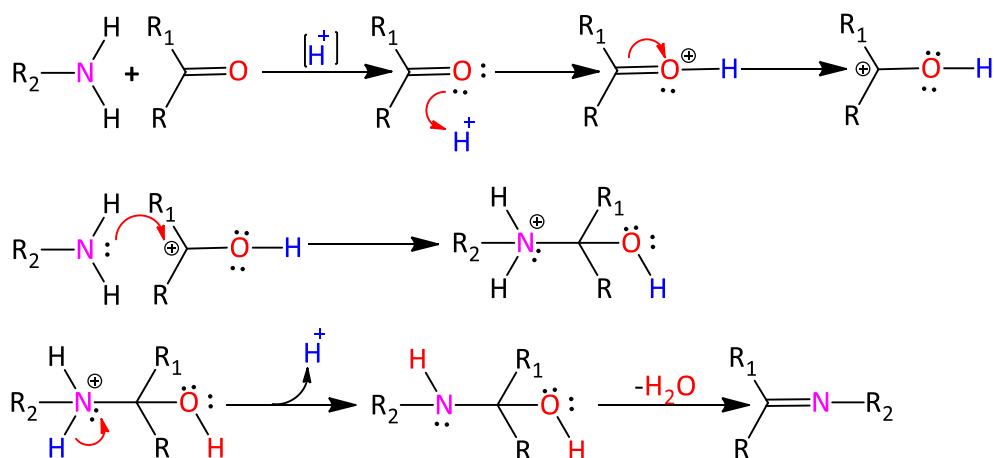
**Figure 2-5** GretagMacbeth Spectroeye Colorimeter

CIE-L\*a\*b\* values for samples extruded by circulation and normal modes are given in the **Appendix (Tables A-1 to A-10)** in addition to their graphical representation in the results and discussion (**Section 3**).

## 2.2 Synthesis of Antioxidant-Metal Deactivators (AO/MDs)

### 2.2.1 Rationale for synthesis

Following the method previously reported by Arifuzzaman *et al*<sup>130</sup>, different Schiff base reactions were employed to generate a series of antioxidant -metal deactivators (AO/MDs). Mechanistically, the synthesis of an imine (Schiff base) consists of two steps. In the first step, the amine nitrogen acts as a nucleophile and attacks the carbonyl carbon. This is closely analogous to hemiacetal and hemiketal formation. In the second step, the nitrogen is deprotonated, and C=N is formed, and a water molecule is ejected.



*Scheme 2-1* General mechanism of Schiff base reactions.

### 2.2.2 Synthesis of S-Series AO/MDs

#### 3,5-di-*tert*-butyl-4-hydroxyhydrocinnamic acid hydrazide [S0]

The synthesis of 3,5-di-*tert*-butyl-4-hydroxyhydrocinnamic acid hydrazide has already been reported in literature, by using *ethyl 3-(3,5-di-*tert*-butyl-4-hydroxyphenyl)propanoate* and hydrazine hydrate as reactants<sup>131</sup>. In this study this product was also made by using a commercial phenolic antioxidant, **Anox 20** (*pentaerythritol tetrakis(3-(3,5-di-*tert*-butyl-4-hydroxyphenyl) propionate)*).

**Anox 20** (5 g, 4.425 mmol) was dissolved in dry methanol (250 mL). To this solution hydrazine hydrate (20 ml, 40 mmol) was added at room temperature. The mixture was then refluxed for 2 hours and cooled to room temperature. Crystallisation upon addition of distilled water, followed by filtration, washing with cold methanol and drying gave **S0** (4.4 g, 88 % yield) as a white solid; m.p. 156-160 °C; FTIR (ATR) ( $\text{cm}^{-1}$ ): 1626 (C=O, hydrazide);  $^1\text{H-NMR}$  (400 MHz,  $\text{CDCl}_3$ ,  $\text{D}_2\text{O}$ )  $\delta$  (ppm) = 6.98 (s, 2H, Ar), 2.88 (t,  $J = 8.0$  Hz, 2H,  $-\text{CH}_2\text{CH}_2\text{CO}$ ), 2.42 (t,  $J = 8.0$  Hz, 2H,  $-\text{CH}_2\text{CO}$ ), 1.43 (s, 18H, tert-butyl);  $^{13}\text{C NMR}$  (100 MHz,  $\text{CDCl}_3$ ):  $\delta$  (ppm) = 173.4 (1C, C=O), 152.3 (1C, C-OH), 136.1 (2C, Ar C-C-tertbutyl), 131.1 (1C, Ar para carbon), 124.8 (2C, Ar), 37.0(1C, C-C-C=O), 34.4 (2C, C-tert-butyl), 31.4 (1C, CC=O), 30.3 (6C); ESI-MS:  $m/z$  ( $[\text{M}+\text{H}]^+$ ) = 292.22

#### **$\text{N}',\text{N}''$ -(ethane-1,2-diylidene)bis[3-(3,5-di-tert-butyl-4-hydroxyphenyl)propanehydrazide] [S1]**

The precursor compound **S0** (1 g, 3.4 mmol) was dissolved in methanol (25 mL) by heating at 60 °C. Glyoxal (0.25 mL) was introduced dropwise and the solution heated (60 °C) with constant stirring. Cooling and filtration gave **S1** (0.93g, 93% yield) as a white solid; m.p. 275-277 °C, FTIR (ATR) ( $\text{cm}^{-1}$ ): 1667 (C=O, hydrazide), 3204 (NH), 3637 (-OH);  $^1\text{H-NMR}$  (400 MHz,  $\text{DMSO-}d_6$ )  $\delta$  (ppm) = 11.65-11.45 (m, 2H, OH), 7.86-7.58 (m, 2H, HC=N), 6.92 (s, 4H, Ar), 6.73 (dd,  $J = 10.5, 2.7$  Hz, 2H, NH), 2.77 (t,  $J = 4.1$  Hz, 4H,  $\text{CH}_2\text{-CH}_2\text{C=O}$ ), 2.67 (t,  $J = 1.8$  Hz, 4H,  $-\text{CH}_2\text{C=O}$ ), 1.35 (s, 36H, tert-butyl);  $^{13}\text{C NMR}$  (100 MHz,  $\text{DMSO-}d_6$ ):  $\delta$  (ppm) = 174.3 (2C, C=O), 152.4 (2C, C-OH), 144.6 (2C, C=N), 139.6 (4C, Ar C-C-tertbutyl), 132.2 (2C, para carbon), 124.8 (4C, Ar), 36.7 (2C, C-C-C=O), 34.8 (4C, C-tertbutyl), 33.5 (2C, CC=O), 30.9 (12C, methyl); ESI-MS:  $m/z$  ( $[\text{M}+\text{H}]^+$ ), +ESI Scan(0.264 min) Frag=70.0V, 607.4218,  $\text{M}+\text{NH}^+4$  624.4485.

#### **$\text{N}',\text{N}''$ -(pentane-1,5-diylidene)bis[3-(3,5-di-tert-butyl-4-hydroxyphenyl)propanehydrazide] [S2]**

The precursor compound **S0** (1 g, 3.4 mmol) was dissolved in methanol (25 mL) and glutaraldehyde (0.35 mL) introduced dropwise on heating the solution (60°C) with constant stirring for 15 minutes. After cooling to room temperature, distilled water was added to precipitate the solid. Filtration gave **S2** (0.82g, 82% yield) as a white solid; m.p. 98-102 °C, FTIR (ATR) ( $\text{cm}^{-1}$ ): 1667 (C=O, hydrazide), 3207

(NH), 3641 (-OH); <sup>1</sup>H-NMR (400 MHz, CDCl<sub>3</sub>) δ (ppm) = 9.44 (s, 2H, NH), 7.17 (t, *J* = 5.0 Hz, 2H, C=N), 7.04 (s, 4H, Ar), 5.09 (s, 2H, -OH), 2.90 (m, 4H, -CH<sub>2</sub>-C=N), 2.49 (t, *J* = 8.0 Hz, 2H, -CH<sub>2</sub>CH<sub>2</sub>CO), 2.32 (dd, *J* = 12.4, 7.3 Hz, 4H, -CH<sub>2</sub> C=O), 1.82 (q, *J* = 7.5 Hz, 2H, -CH<sub>2</sub>CH<sub>2</sub>C=N-), 1.43 (s, 36H, tert-butyl); <sup>13</sup>C NMR (100 MHz, DMSO-D<sub>6</sub>): δ (ppm) = 175.3 (2C, C=O), 152.1 (2C, C-OH), 146.1 (2C, C=N), 135.9 (4C, Ar C-C-tertbutyl), 131.8 (2C, para carbon), 125.0 (4C, Ar), 35.1 (2C, C-C=O), 34.3 (4C, C-tertbutyl), 31.6 (2C, CCC=O), 30.4 (12C), 29.8 (2C, CC=N), 22.9 (2C, -CCC=N); ESI-MS: *m/z* ([M+H]<sup>+</sup>, +ESI Scan(0.208 min) Frag=60.0V, 649.4699

### **N'1,N'6-bis(3-(3,5-di-tert-butyl-4-hydroxyphenyl)propanoyl)adipohydrazide [S3]**

Dimethyl adipate (1ml, 6.09 mmol), was refluxed with an alcoholic solution of **S0** (3.55 g) for 1 hour. Addition of distilled water gave a white powder (92% yield); m.p. 224 °C; FTIR ATR (cm<sup>-1</sup>): 1662 (C=O, hydrazide), 3211 (NH), 3641 (-OH); <sup>1</sup>H-NMR (400 MHz, DMSO-D<sub>6</sub>) δ (ppm) = 9.71 (d, *J* = 27.5 Hz, 4H, -NH), 6.86 (s, 4H, Ar), 6.12 (s, 2H, Phenolic), 2.66 (t, 4H, *J* = 8.2 -CH<sub>2</sub>CH<sub>2</sub>CO), 2.36 (t, *J* = 8.2 Hz, 4H, -CH<sub>2</sub>CO), 2.12 (s, 4H, ethylene), 1.55 (s, 4H, ethylene), 1.30 (s, 36H, tert-butyl); <sup>13</sup>C NMR (100 MHz, DMSO-D<sub>6</sub>) δ (ppm) = 171.1 (2C, C=O), 170.9 (2C, C=O), 152.3 (2C, C-OH), 138.4 (4C, ArC-C-tertbutyl), 131.9 (2C, para carbon), 124.6 (4C, Ar), 36.1 (2C, -CCO), 34.7 (4C, C-tert-butyl), 31.9 (2C, adipic unit), 31.0 (2C, CCC=O), 30.6 (12C, tert-butyl), 25.0 (2C, adipic unit); ESI-MS: *m/z* ([M+H]<sup>+</sup>, +ESI Scan(-27.84 min) Frag=80.0V, 695.4750

### **N'1,N'8-bis(3-(3,5-di-tert-butyl-4-hydroxyphenyl)propanoyl)octanedihydrazide [S4]**

Dimethyl suberate (1ml, 5.24 mmol), was refluxed with an alcoholic solution of **S0** (3.06 g) for 1 hour. Addition of distilled water gave a white powder (90% yield); m.p. 178 °C; FTIR (ATR) (cm<sup>-1</sup>): 1667 (C=O, hydrazide), 3204 (NH), 3645 (-OH); <sup>1</sup>H-NMR (400 MHz, DMSO-D<sub>6</sub>) δ (ppm) = 9.65 (d, *J* = 25.2 Hz, 4H, NH), 6.86 (s, 4H, Ar), 5.59 (s, 2H, OH), 2.71 (t, *J* = 8.0 Hz, 4H -CH<sub>2</sub>CH<sub>2</sub>CO), 2.38 (t, *J* = 8.2 Hz, 4H, -CH<sub>2</sub>-C=O), 2.14 (t, *J* = 6.4 Hz, 4H, ethylene), 1.51 (t, *J* = 11.0 Hz, 4H, ethylene), 1.29 (s, 36H, tert-butyl), 1.17-0.98 (m, 4H, ethylene); <sup>13</sup>C-NMR (400 MHz, DMSO-D<sub>6</sub>) δ (ppm) = 171.5 (2C, C=O), δ 171.4, (2C, C=O, Suberic unit), δ 152.2 (2C, C Phenolic), δ 137.1 (4C, ArC-C-tertbutyl), δ 131.6 (2C, Ar), δ 124.5 (4C, Ar), δ 36.3 (2C, -CCO), δ 34.5 (4C, C-tert-butyl), δ 33.3 (2C, ethylene suberic), δ 31.7

(2C, C=O),  $\delta$  30.4 (12C, tert-butyl),  $\delta$  27.9 (2C, ethylene suberic),  $\delta$  25.2 (2C, ethylene suberic); ESI-MS: m/z ([M+H]<sup>+</sup>, +ESI Scan(-27.86 min) Frag=80.0V, 723.5064.

**N'1,N'10-bis(3-(3,5-di-tert-butyl-4-hydroxyphenyl)propanoyl)decanedihydrazide [S5]**

Dimethyl sebacate 1ml, 4.43 mmol), was refluxed with an alcoholic solution of **S0** (2.58) for 1 hour. Addition of distilled water gave a white powder (88% yield); m.p. 168°C; FTIR (ATR) (cm<sup>-1</sup>): 1665 (C=O, hydrazide), 3205 (NH), 3643 (-OH); <sup>1</sup>H-NMR (400 MHz, DMSO-D6)  $\delta$  (ppm) = 9.70 (d, *J* = 16.0 Hz, 4H, NH), 6.88 (s, 4H, Ar), 6.68 (s, 2H, OH), 2.66 (t, *J* = 8.0 Hz, 4H, -CH<sub>2</sub>CH<sub>2</sub>CO), 2.32 (t, *J* = 8.0 Hz, 4H, -CH<sub>2</sub>CO), 2.06 (t, *J* = 7.3 Hz, 4H, ethylene), 1.46 (t, *J* = 6.0 Hz, 4H, ethylene), 1.32 (s, 36H, tert-butyl), 1.21 (s, 8H, ethylene); <sup>13</sup>C-NMR (400 MHz, DMSO-D6)  $\delta$  (ppm) = 171.3 (2C, C=O),  $\delta$  170.9, (2C, C=O, sebacoyl Unit),  $\delta$  152.5 (2C, C Phenolic),  $\delta$  139.6 (4C, Ar-C-tertbutyl),  $\delta$  132.3 (2C, Ar),  $\delta$  124.7 (4C, Ar),  $\delta$  35.9 (2C, -CCO),  $\delta$  34.9 (4C, C-tert-butyl),  $\delta$  33.6 (2C, ethylene sebacoyl),  $\delta$  31.5 (2C, -CCCO),  $\delta$  30.9 (12C, tert-butyl),  $\delta$  29.0 (4C, ethylene sebacoyl),  $\delta$  25.6 (2C, ethylene sebacoyl); +ESI Scan(0.217 min) Frag=80.0V, 751.5375, M+Na<sup>+</sup> 773.5198.

**N,N''-(6-{2-[3-(3,5-di-tert-butyl-4-hydroxyphenyl)propanoyl]hydrazineylidene-1,6-dihydro-1,3,5-triazine-2,4-diyl})bis[3-(3,5-di-tert-butyl-4-hydroxy phenyl)propanehydrazide] [S6]**

Precursor compound **S0** (2.4 g, 8.21 mmol) and cyanuric chloride (0.5 g, 2.71 mmol) were refluxed in acetic acid (25 mL) for 15 minutes. Removal of excess of acetic acid by rotary evaporation, gave **S6** as a white solid (84% yield); m.p. 179-183 °C, FTIR (ATR) (cm<sup>-1</sup>): 1661 (C=O, hydrazide), 3255 (NH), 3643 (-OH); <sup>1</sup>H-NMR (400 MHz, CDCl<sub>3</sub>)  $\delta$  (ppm) = 9.01 (s, 3H, NHC=O), 8.69 (s, 3H, NH), 6.97 (s, 6H, Ar), 5.08 (s, 3H, -OH), 2.87 (t, *J* = 8.0 Hz, 6H, ethylene), 2.53 (t, *J* = 8.2 Hz, 6H, ethylene), 1.40 (s, 54H, tert-butyl); <sup>13</sup>C NMR (100 MHz, CDCl<sub>3</sub>):  $\delta$  (ppm) = 169.6 (3C, C=O), 167.1 (3C, Ring N-C=N), 152.3 (3C, C-OH), 136 (6C, Ar C-tert-butyl), 130.7 (3C, Ar) 124.9 (6C, Ar), 36.6 (3C, C-C=O), 34.3 (6C, C-tert), 31.5 (3C, C-C-C=O), 30.3 (18C); ESI-MS: m/z ([M+H]<sup>+</sup>, +ESI Scan(0.271 min) Frag=70.0V, 951.633.

**N',N'',N'''-{1,3,5-triazine-2,4,6-triyltris[oxy(3-methoxy-4,1-phenyl ene) (E) methanylylidene]} tris[3-(3,5-di-tert-butyl-4-hydroxyphenyl)propanehydrazide] [S7]**

Salicylic aldehyde (10 ml, 95 mmol) in acetone (10 ml) was added to NaOH (3.83 g) in water (equimolar quantities) and cyanuric chloride (5.82 g, 31.64 mmol) in acetone (50 ml) added and the solution stirred at room temperature for 2h and filtered to give **2,2',2''-[1,3,5-triazine-2,4,6-triyltris(oxy)] tribenzaldehyde** as a white solid; m.p. 164-167 °C, FTIR (ATR) (cm<sup>-1</sup>): 1687 (C=O); <sup>1</sup>H-NMR (400 MHz, CDCl<sub>3</sub>) δ (ppm) = 10.04 (s, 3H, Carbonyl), 7.88 (dd, *J* = 7.8, 1.8 Hz, 1H), 7.83 (dd, *J* = 7.6, 1.6 Hz, 2H), 7.66 (td, *J* = 7.8, 1.8 Hz, 1H), 7.60 (td, *J* = 7.8, 1.5 Hz, 2H), 7.46 (td, *J* = 7.6, 0.9 Hz, 1H), 7.39 (t, *J* = 7.3 Hz, 2H), 7.22 (d, *J* = 8.2 Hz, 1H), 7.19 (dd, *J* = 8.2, 0.9 Hz, 2H); <sup>13</sup>C NMR (100 MHz, CDCl<sub>3</sub>): δ (ppm) = 188.4 (3C, Carbonyl), 173.8 (3C, Ring N=C-N), 152.164.0 (3C, Ar C-O-), 135.6 (3C, ArC-C=C-O), 131.0 (3C, ArC=C-C=O), 128.0 (3C, ArC-C=O), 126.5 (3C, para carbon), 122.9 (3C, RingC=C-O); ESI-MS: m/z ([M+H]<sup>+</sup>, +ESI Scan(0.251 min) Frag=70.0V, 442.1037, M+Na<sup>+</sup> 464.0853

Following this **2,2',2''-[1,3,5-triazine-2,4,6-triyltris(oxy)]tribenzaldehyde** was dissolved in methanol at 60-70 °C. and **S0** was added (3 equimolar equivalents). After stirring for 2 hours, the resultant solid was filtered, washed, dried and recrystallised from ethanol to give **S7** as a light pink powder (75% yield); m.p. 155-160 °C, FTIR (ATR) (cm<sup>-1</sup>): 1670 (C=O, hydrazide), 3255 (NH), 3637 (-OH Phenolic); <sup>1</sup>H-NMR (400 MHz, CD<sub>3</sub>OD) δ (ppm) = 8.76 (s, 3H, HN), 8.10 (s, 3H, HC=N-), 7.24 (d, *J* = 7.8 Hz, 3H, Benzene C=C-C=N-), 7.20-7.14 (m, 3H, Benzene C-C=C-O-), 6.90 (s, 6H, Ar), 6.83 (d, *J* = 10.5 Hz, 3H, Benzene C=C-O-), 6.78 (t, *J* = 8.0 Hz, 3H, Benzene para C), 2.79 (t, *J* = 7.6 Hz, 6H, C-C-C=O), 2.41 (t, *J* = 7.6 Hz, 6H, C-C=O), 1.28 (s, 54H, tert-butyl); <sup>13</sup>C NMR (100 MHz, CD<sub>3</sub>OD): δ (ppm) = 170.8 (3C, C=O), 165.8 (3C, Ring N=C-N), 152.4 (RingC-OH) 149.9 (3C, Ar C-O-), 142.7 (3C, C=N), 138.7 (6C, ArC-C-tertbutyl), 132.4 (3C, ArC-C=C-O), 131.8 (3C, para carbon), 130.9 (3C, ring C=C-C=N). 124.8 (6C, Aromatic), 119.8 (3C, ring C=C-O), 118.7 (3C, benzene ring para Carbon), 117.0 (3C, Benzene ring C-C=N), 37.6 (3C, C-C=O), 34.8 (6C, C-tert-butyl), 32.2 (3C, C-C-C=O), 30.2 (18C); ESI-MS: m/z ([M+H]<sup>+</sup>, +ESI Scan(0.271 min) Frag=70.0V, 1264.7162, M+Na<sup>+</sup> 1286.6971.

**N',N'',N'''-{1,3,5-triazine-2,4,6-triyltris[oxy-2,1-phenylene(Z)methanylylidene]} tris[3-(3,5-di-tert-butyl-4-hydroxyphenyl)propanehydrazide] [S8]**

Vanillin (14.44 g, 95 mmol) in acetone (50 ml) was added to NaOH (3.83 g) in water (equimolar quantities) and cyanuric chloride (5.82 g, 31.64 mmol) in acetone (50 ml) added and the solution stirred at room temperature for 2h and filtered to give **4,4',4''-((1,3,5-triazine-2,4,6-triyl)tris(oxy))tris(3-methoxy benzaldehyde)** as a white solid; FTIR (ATR) ( $\text{cm}^{-1}$ ): 1689 (C=O);  $^1\text{H-NMR}$  (400 MHz, DMSO- $\text{D}_6$ )  $\delta$  (ppm) = 9.90 (s, 3H, Carbonyl), 7.55 (s, 3H Ar), 7.41 (d,  $J = 8.2$  Hz, 3H, Ar), 3.77 (s, 9H,  $\text{CH}_3$ );  $^{13}\text{C NMR}$  (100 MHz, DMSO- $\text{D}_6$ ):  $\delta$  (ppm) = 192.4 (3C, Carbonyl), 173.4 (3C, Cyanuric), 151.0 (3C, Vanillin -CO  $\text{CH}_3$ ), 150.0 (3C, Vanillin C-O), 145.0 (3C, Vanillin Ar C=O), 135.8 (Vanillin Ar), 124.6 (3C, Vanillin Ar), 112.6 (3C, Vanillin Ar), 56.1 (3C, methyl).

Following this **4,4',4''-((1,3,5-triazine-2,4,6-triyl)tris(oxy))tris(3-methoxy benzaldehyde)** was dissolved in methanol at 60-70 °C. and **S0** was added (3 equimolar equivalents). After stirring for 2 hours, the resultant solid was filtered, washed, dried and recrystallised from ethanol to give **S8** as a yellow powder (80% yield); m.p. 125-130 °C, FTIR (ATR) ( $\text{cm}^{-1}$ ): 1687 (C=O, hydrazide), 3256 (NH), 3635 (-OH Phenolic);  $^1\text{H-NMR}$  (400 MHz,  $\text{CDCl}_3$ )  $\delta$  (ppm) = 8.53 (s, 3H, HN), 7.85 (s, 3H, HC-N), 7.19 (d,  $J = 1.8$  Hz, 3H, Ar, vanillin), 7.07 (s, 3H, Ar, vanillin), 7.03 (d,  $J = 2.7$  Hz, 3H, Ar, vanillin), 6.98 (s, 6H, Ar), 5.08 (s, 3H, phenolic), 3.68 (s, 9H, methoxy), 2.86 (t,  $J = 8.0$  Hz, 6H, ethylene), 2.60 (t,  $J = 8.2$  Hz, 6H, ethylene), 1.40 (s, 54H, tert-butyl);  $^{13}\text{C NMR}$  (100 MHz,  $\text{CDCl}_3$ ):  $\delta$  (ppm) = 173.8 (3C, triazine), 171.2 (3C, C=O), 152.2 (3C, Ar), 152.3 (3C, Ar vanillin), 142.2 (3C, C=N), 136.2 (3C, Ar vanillin), 135.7 (6C, Ar), 131.9 (3C, Ar), 130.9 (3C, Ar vanillin), 125.0 (6C, Ar), 124.9 (3C, Ar vanillin), 122.2 (3C, Ar vanillin), 114.0 (3C, Ar vanillin), 51.7 (3C, methoxy), 36.4 (3C, ethylene), 34.3 (3C, tert), 31.0 (3C, ethylene), 30.9 (18C, methyl); ESI-MS: m/z ( $[\text{M}+\text{H}]^+$ , +ESI Scan(0.129-0.596 min, 29 Scans) Frag=80.0V, 1354.7472

### 2.2.3 Synthesis of L-Series AO/MDs

#### **N',N''-bis[3-(3,5-di-tert-butyl-4-hydroxyphenyl)propanehydrazide] [L1]**

Salicylaldehyde (5.40 ml, 51.78 mmol) was combined with  $K_2CO_3$  (2.5 equiv, 17.86 g) in DMF (50mL) followed by the slow addition of 1,2-dibromoethane (2 ml, 23.20 mmol) and heated (80-100°C) with stirring for two hours. Dialdehydes are only obtained on heating, otherwise the mono product is obtained. Distilled water was added, and the precipitate filtered, washed with water and dried at room temperature to give **2,2'-[ethane-1,2-diylbis(oxy)]dibenzaldehyde** as a white solid (38% yield); FTIR (ATR) ( $cm^{-1}$ ): 1670 (Carbonyl);  $^1H$ -NMR (400 MHz,  $CDCl_3$ )  $\delta$  10.43 (s, 2H, Carbonyl), 7.84 (d, J = 6.0 Hz, 2H, Ar), 7.57 (t, J = 8.0 Hz, 2H, Ar), 7.06-7.09 (m, 2H, Ar), 7.04 (d, J = 4.1 Hz, 2H, Ar), 4.52 (s, 4H, ethylene);  $^{13}C$ -NMR (101 MHz,  $CDCl_3$ )  $\delta$  189.4 (2C, C=O), 161.0 (2C, Ar), 136.0 (2C, Ar), 128.9 (2C, Ar), 125.3 (2C, Ar), 121.8 (2C, Ar), 112.7 (2C, Ar), 66.8 (2C, ethyl-bridge)

**2,2'-[ethane-1,2-diylbis(oxy)]dibenzaldehyde** (0.5 g, 1.85 mmol) was stirred at room temperature for 2 hours with **SO** (2 equiv, 1.08 g) in methanol (30 ml). The precipitate was filtered and washed with methanol and distilled water, dried at room temperature to give **L1** as a white solid (90% yield); m.p. 245 °C ; FTIR (ATR) ( $cm^{-1}$ ): 1678 (C=O), 3539 (OH), 3330 (NH);  $^1H$ -NMR (400 MHz, DMSO- $D_6$ )  $\delta$  11.24 (d, J = 76.0 Hz, 2H, NH), 8.36 (d, J = 60.4 Hz, 2H, C=N), 7.75-7.79 (m, 2H, Ar), 7.36 (q, J = 7.8 Hz, 2H, Ar), 7.12 (d, J = 8.2 Hz, 2H, Ar), 6.90 (d, J = 22.9 Hz, 2H, Ar), 6.67 (s, 4H, Ar), 4.38 (s, 4H, bridged -CH<sub>2</sub>-), 2.86 (t, J = 8.0 Hz, 4H, -CH<sub>2</sub>-), 2.41 (t, J = 8.0 Hz, 4H, -CH<sub>2</sub>-) 1.29 (s, 36H butyl);  $^{13}C$ -NMR (101 MHz, DMSO- $D_6$ )  $\delta$  168.7(2C, -C=O), 157.3 (2C, ArC-O), 152.3 (2C, ArC-OH), 140.5 (2C, -C=N), 136.8 (4C, Ar), 132.0 (2C, Ar), 130.0 (2C, Ar), 130.0 (2C, Ar), 125.3 (4C, Ar), 124.6 (2C, Ar), 121.4 (2C, Ar), 110.0 (2C, Ar), 67.5 (2C bridged-CH<sub>2</sub>-), 36.8 (2C, -CH<sub>2</sub>-), 34.9 (4C, *tert*-C), 31.3 (2C, -CH<sub>2</sub>-), 30.7 (12C, butyl).

#### **N',N''-{butane-1,4-diylbis[oxy-2,1-phenylene(E)methanylylidene]}bis[3-(3,5-di-tert-butyl-4-hydroxyphenyl) propanehydrazide] [L2]**

Salicylaldehyde (8.73 ml, 83.72 mmol) was combined with  $K_2CO_3$  (2.5 equiv, 28.88 g) in DMF (50mL) followed by the slow addition of 1,4-dibromobutane (5 ml, 41.86 mmol) and heated (80-100°C) with

stirring for two hours. Distilled water was added, and the precipitate filtered, washed with water and dried at room temperature to give **2,2'-[butane-1,4-diylbis(oxy)]dibenzaldehyde** as a white solid (40% yield); FTIR (ATR) ( $\text{cm}^{-1}$ ): 1672 (Carbonyl);  $^1\text{H-NMR}$  (400 MHz,  $\text{CDCl}_3$ )  $\delta$  (ppm) = 10.48 (s, 2H, Carbonyl), 7.81 (d,  $J = 7.8$  Hz, 2H, Ar), 7.53 (t,  $J = 7.1$  Hz, 2H, Ar), 7.01 (t,  $J = 7.6$  Hz, 2H, Ar), 6.97 (d,  $J = 8.2$  Hz, 2H, Ar), 4.17 (s, 4H, ethylene), 2.09 (s, 4H, ethylene);  $^{13}\text{C-NMR}$  (101 MHz,  $\text{CDCl}_3$ )  $\delta$  (ppm) = 189.7 (2C, C=O), 161.5 (2C, Ar), 135.8 (2C, Ar), 128.6 (2C, Ar), 125.1 (2C, Ar), 120.8 (2C, Ar), 112.4 (2C, Ar), 67.9 (2C, ethylene), 25.8 (2C, ethylene).

**2,2'-[butane-1,4-diylbis(oxy)]dibenzaldehyde** (0.5 g, 1.67 mmol) was stirred at room temperature for 2 hours with **SO** (2 equiv, 0.98 g) in methanol (30 ml). The precipitate was filtered and washed with methanol and distilled water, dried at room temperature to give **L2** as a white solid (88% yield); m.p. 208 °C; FTIR (ATR) ( $\text{cm}^{-1}$ ): 1678 (C=O), 3540 (OH), 3331 (NH);  $^1\text{H-NMR}$  (400 MHz,  $\text{DMSO-D}_6$ )  $\delta$  (ppm) = 11.30 (d,  $J = 38.0$  Hz, 2H, NH), 8.41 (d,  $J = 49.5$  Hz, 2H, C=N), 7.74 (t,  $J = 7.8$  Hz, 2H, Ar), 7.31 (q,  $J = 8.1$  Hz, 2H, Ar), 6.93 (s, 4H, Ar), 6.90 (s, 2H, Ar), 6.68 (d,  $J = 2.3$  Hz, 2H, Ar), 4.08 (s, 4H, bridged  $-\text{CH}_2-$ ), 2.73 (t,  $J = 8.0$  Hz, 4H,  $-\text{CH}_2-$ ), 2.39 (t,  $J = 7.8$  Hz, 4H,  $-\text{CH}_2-$ ), 1.92 (s, 4H, bridged  $-\text{CH}_2-$ ), 1.31 (s, 36H, *tert*);  $^{13}\text{C-NMR}$  (101 MHz,  $\text{DMSO-D}_6$ )  $\delta$  (ppm) = 171.1 (2C, C=O), 157.3 (2C, ArC-O), 152.5 (2C, ArC-OH), 145.5 (2C, C=N), 139.6 (4C, Ar), 134.5 (2C, Ar), 132.2 (2C, Ar), 130.2 (2C, Ar), 124.7 (4C, Ar), 121.0 (2C, Ar), 119.0 (2C, Ar), 110.0 (2C, Ar), 68.1 (2C, bridged  $-\text{CH}_2-$ ), 36.7 (2C,  $-\text{CH}_2-$ ), 34.8 (4C, *tert*), 31.3 (2C,  $-\text{CH}_2-$ ), 30.7 (12C, butyl), 26.0 (2C, bridged  $-\text{CH}_2-$ ).

**$\text{N}',\text{N}''$ -{hexane-1,6-diylbis[oxy-2,1-phenylene(E)methanylylidene]}bis[3-(3,5-di-*tert*-butyl-4-hydroxyphenyl) propanehydrazide] [L3]**

Salicylaldehyde (2.72 ml, 26.09 mmol) was combined with  $\text{K}_2\text{CO}_3$  (2.5 equiv, 9 g) in DMF (50mL) followed by the slow addition of 1,6-dibromohexane (2 ml, 13 mmol) and heated (80-100°C) with stirring for two hours. Distilled water was added, and the precipitate filtered, washed with water and dried at room temperature to give **2,2'-[hexane-1,6-diylbis(oxy)]dibenzaldehyde** as a white solid (43% yield); FTIR (ATR) ( $\text{cm}^{-1}$ ):1677 (C=O);  $^1\text{H-NMR}$  (400 MHz,  $\text{CDCl}_3$ )  $\delta$  (ppm) = 10.4 (s, 2H, Carbonyl), 7.8 (d,  $J = 7.3$  Hz, 2H, Ar), 7.5 (t,  $J = 7.1$  Hz, 2H, Ar), 6.9 (d,  $J = 7.8$  Hz, 2H, Ar), 6.9 (d,  $J = 8.7$  Hz, 2H, Ar), 4.0 (t,  $J = 6.4$  Hz, 4H, ethylene), 1.8 (t,  $J = 6.2$  Hz, 4H, ethylene), 1.5 (t,  $J = 7.3$  Hz, 4H,

ethylene);  $^{13}\text{C}$ -NMR (101 MHz,  $\text{CDCl}_3$ )  $\delta$  (ppm) = 190.1 (2C, C=O), 161.6 (2C, Ar), 136.0 (2C, Ar), 128.5 (2C, Ar), 125.1 (2C, Ar), 120.6 (2C, Ar), 112.5 (2C, Ar), 68.3 (2C,  $-\text{CH}_2-$ ), 29.1 (2C,  $-\text{CH}_2-$ ), 25.7 (2C,  $-\text{CH}_2-$ ).

**2,2'-[hexane-1,6-diylbis(oxy)]dibenzaldehyde** (0.5 g, 1.53 mmol) was stirred at room temperature for 2 hours with **SO** (2 equiv, 0.90 g) in methanol (30 mL). The precipitate was filtered and washed with methanol and distilled water, dried at room temperature to give **L3** as a white solid (89% yield); m.p. 248 °C ; FTIR (ATR) ( $\text{cm}^{-1}$ ): 1678 (C=O), 3542 (OH), 3332 (NH);  $^1\text{H}$ -NMR (400 MHz, DMSO- $\text{D}_6$ )  $\delta$  (ppm) = 11.29 (d,  $J$  = 38.0 Hz, 2H, NH), 8.38 (d,  $J$  = 58.2 Hz, 2H, C=N), 7.73 (t,  $J$  = 8.7 Hz, 2H, Ar), 7.29 (d,  $J$  = 7.3 Hz, 2H, Ar), 6.93 (s, 4H, Ar), 6.90 (s, 2H, Ar), 6.68 (d,  $J$  = 4.1 Hz, 2H, Ar), 4.00 (s, 4H, bridged  $-\text{CH}_2-$ ), 2.73 (t,  $J$  = 8.0 Hz, 4H,  $-\text{CH}_2-$ ), 2.39 (t,  $J$  = 7.8 Hz, 4H,  $-\text{CH}_2-$ ), 1.72 (s, 4H, bridged  $-\text{CH}_2-$ ), 1.43 (s, 4H, bridged  $-\text{CH}_2-$ ), 1.31 (s, 36H, tert);  $^{13}\text{C}$ -NMR (101 MHz, DMSO- $\text{D}_6$ )  $\delta$  (ppm) = 174.2 (2C, C=O), 157.4 (2C, ArC-O), 152.4 (2C, ArC-OH), 141.7 (2C, C=N), 139.5 (4C, Ar), 132.7 (2C, Ar), 132.3 (2C, Ar), 131.5 (2C, Ar), 124.7 (4C, Ar), 123.1 (2C, Ar), 120.8 (2C, Ar), 113.2 (2C, Ar), 68.3 (2C, bridged  $-\text{CH}_2-$ ), 36.9 (2C,  $-\text{CH}_2-$ ), 34.9 (4C, tert), 31.5 (2C,  $-\text{CH}_2-$ ), 30.9 (12C, butyl), 29.1 (2C, bridged  $-\text{CH}_2-$ ), 25.7 (2C, bridged  $-\text{CH}_2-$ ).

#### **$\text{N}',\text{N}''$ -bis[3-(3,5-di-tert-butyl-4-hydroxyphenyl)propanehydrazide] [**L1A**]**

Vanillin (7.05 g, 46.38 mmol) was combined with  $\text{K}_2\text{CO}_3$  (2.5 equiv, 16.0 g) in DMF (50 mL) followed by the slow addition of 1,2-dibromoethane (2 ml, 23.19 mmol) and heated (80-100 °C) with stirring for two hours. Distilled water was added, and the precipitate filtered, washed with water and dried at room temperature to give **4,4'-[ethane-1,2-diylbis(oxy)]bis(3-methoxybenzaldehyde)** as a white solid (41% yield); FTIR (ATR) ( $\text{cm}^{-1}$ ): 1677 (C=O). NMR data is unavailable due to solubility issues.

**4,4'-[ethane-1,2-diylbis(oxy)]bis(3-methoxybenzaldehyde)** (0.5 g, 1.51 mmol) was stirred at room temperature for 2 hours with **SO** (2 equiv, 0.88 g) in methanol (30 mL). The precipitate was filtered and washed with methanol and distilled water, dried at room temperature to give **L1A** as a white solid (89% yield); m.p. 149 °C , FTIR (ATR) ( $\text{cm}^{-1}$ ): 1678 (C=O), 3539 (OH), 3330 (NH);  $^1\text{H}$ -NMR (400 MHz,  $\text{CDCl}_3$ )  $\delta$  (ppm) = 9.85 (s, 2H, NH), 8.11 (2H, C=N), 7.45 (dd,  $J$  = 8.0, 1.6 Hz, 4H, Ar), 7.09 (d,  $J$  = 8.2 Hz, 2H, Ar), 6.97 (s, 4H, Ar), 5.09 (s, 2H, -OH), 4.54 (s, 4H, bridged  $-\text{CH}_2-$ ), 3.90 (s, 6H,  $-\text{CH}_3$ ), 2.86

(t,  $J = 8.0$  Hz, 4H,  $-\text{CH}_2-$ ), 2.41 (t,  $J = 8.0$  Hz, 4H,  $-\text{CH}_2-$ ), 1.41 (s, 36H, butyl);  $^{13}\text{C}$ -NMR (101 MHz,  $\text{CDCl}_3$ )  $\delta$  (ppm) = 190.1 (2C, C=O), 172.3 (2C, vanillin ArC-O- $\text{CH}_2-$ ), 152.5 (2C, ArC-OH), 151.4 (2C, vanillin ArC-O- $\text{CH}_3$ ), 148.9 (2C, C=N), 135.1 (4C, Ar), 130.1 (2C, Ar), 129.5 (2C, vanillin ring C-C=N), 125.7 (4C, Ar), 123.8 (2C, vanillin ring), 111.4 (2C, vanillin ring), 108.4 (2C, vanillin ring), 66.4 (2C, bridged  $-\text{CH}_2-$ ), 55.1 (2C, methyl), 35.9 (4C, *tert*-C), 33.5 (2C,  $-\text{CH}_2-$ ), 30.5 (2C,  $-\text{CH}_2-$ ), 29.1 (12C, butyl).

**$\text{N}',\text{N}''$ -{butane-1,4-diylbis[oxy(3-methoxy-4,1-phenylene)(E)methanylylidene]}bis[3-(3,5-di-*tert*-butyl-4-hydroxyphenyl)propanehydrazide] [L2A]**

Vanillin (12.72 g, 84.83 mmol) was combined with  $\text{K}_2\text{CO}_3$  (2.5 equiv, 29.26 g) in DMF (50 mL) followed by the slow addition of 1,4-dibromobutane (5 ml, 41.86 mmol) and heated (80-100°C) with stirring for two hours. Distilled water was added, and the precipitate filtered, washed with water and dried at room temperature to give **4,4'-[butane-1,4-diylbis(oxy)]bis(3-methoxybenzaldehyde)** as a white solid (47% yield); FTIR (ATR) ( $\text{cm}^{-1}$ ): 1680 (C=O);  $^1\text{H}$ -NMR (400 MHz,  $\text{CDCl}_3$ )  $\delta$  (ppm) = 9.81 (s, 2H, Carbonyl), 7.41 (d,  $J = 8.2$  Hz, 2H, Ar), 7.36 (s, 2H, Ar), 6.96 (d,  $J = 8.2$  Hz, 2H, Ar), 4.18 (s, 4H,  $-\text{CH}_2-$ ), 3.86 (s, 6H, methoxy group), 2.08 (s, 4H,  $-\text{CH}_2-$ );  $^{13}\text{C}$ -NMR (101 MHz,  $\text{CDCl}_3$ )  $\delta$  (ppm) = 191.0 (2C, C=O), 153.9 (2C, Ar), 149.9 (2C, Ar), 129.9 (2C, Ar), 126.8 (2C, Ar), 111.4 (2C, Ar), 108.7 (2C, Ar), 68.8 (2C,  $-\text{CH}_2-$ ), 55.7 (2C,  $-\text{CH}_3$ ), 27.4 (2C,  $-\text{CH}_2-$ ), 25.6 (2C,  $-\text{CH}_2-$ ).

**4,4'-[butane-1,4-diylbis(oxy)]bis(3-methoxybenzaldehyde)** (0.5 g, 1.40 mmol) was stirred at room temperature for 2 hours with **SO** (2 equiv, 0.82g) in methanol (30 ml). The precipitate was filtered and washed with methanol and distilled water, dried at room temperature to give **L2A** as a white solid (92% yield); m.p. 132 °C, FTIR (ATR) ( $\text{cm}^{-1}$ ): 1678 (C=O), 3539 (OH), 3330 (NH);  $^1\text{H}$ -NMR (400 MHz,  $\text{CDCl}_3$ )  $\delta$  (ppm) = 9.84 (s, 2H, NH), 8.10 (2H, C=N), 7.43 (dd,  $J = 8.0, 1.6$  Hz, 4H, Ar), 7.10 (d,  $J = 8.2$  Hz, 2H, Ar), 6.97 (s, 4H, Ar), 5.10 (s, 2H, -OH), 4.07 (t,  $J = 1.6$  Hz, 4H, bridged  $-\text{CH}_2-$ ), 3.89 (s, 6H,  $-\text{CH}_3$ ), 2.87 (t,  $J = 8.0$  Hz, 4H,  $-\text{CH}_2-$ ), 2.43 (t,  $J = 8.0$  Hz, 4H,  $-\text{CH}_2-$ ), 1.98 (m, 4H, bridged  $-\text{CH}_2-$ ), 1.41 (s, 36H, butyl);  $^{13}\text{C}$ -NMR (101 MHz,  $\text{CDCl}_3$ )  $\delta$  (ppm) = 175.5 (2C, C=O), 152.1 (2C, ArC-OH), 150.3 (2C, ArC-OH), 149.7 (2C, C=N), 143.8 (2C, vanillin ArC-O- $\text{CH}_3$ ), 135.9 (4C, Ar), 131.8 (2C, Ar), 127.7 (2C, vanillin ring C-C=N), 125.0 (4C, Ar), 121.6 (2C, vanillin ring), 112.4 (2C, vanillin ring), 109.0 (2C, vanillin

ring), 67.9 (2C, bridged -CH<sub>2</sub>-), 56.0 (2C, methyl), 35.1 (4C, tert-C), 34.4 (2C, -CH<sub>2</sub>-), 33.5 (2C, -CH<sub>2</sub>-), 30.4 (12C, butyl), 27.8 (2C, bridged -CH<sub>2</sub>-).

**N',N''-{hexane-1,6-diylbis[oxy(3-methoxy-4,1-phenylene)(E)methanylylidene]}bis[3-(3,5-di-tert-butyl-4-hydroxyphenyl)propanehydrazide] [L3A]**

Vanillin (5.85 g, 38.5 mmol) was combined with K<sub>2</sub>CO<sub>3</sub> (2.5 equiv, 13.28 g) in DMF (50mL) followed by the slow addition of 1,6-dibromohexane (3.0 ml, 19.26 mmol) and heated (80-100 °C) with stirring for two hours. Distilled water was added, and the precipitate filtered, washed with water and dried at room temperature to give **4,4'-[hexane-1,6-diylbis(oxy)]bis(3-methoxybenzaldehyde)** as a white solid (52% yield); FTIR (ATR) (cm<sup>-1</sup>): 1681 (C=O); <sup>1</sup>H-NMR (400 MHz, CDCl<sub>3</sub>) δ (ppm) = 9.82 (s, 2H, Carbonyl), 7.40 (d, *J* = 7.8 Hz, 2H, Ar), 7.38 (s, 2H, Ar), 6.94 (d, *J* = 7.8 Hz, 2H, Ar), 4.09 (t, *J* = 6.6 Hz, 4H, -CH<sub>2</sub>-), 3.89 (s, 6H, methoxy), 1.90 (t, *J* = 6.6 Hz, 4H, -CH<sub>2</sub>-), 1.55 (t, *J* = 3.4 Hz, 4H, -CH<sub>2</sub>-); <sup>13</sup>C-NMR (101 MHz, CDCl<sub>3</sub>) δ (ppm) = 191.0 (2C, C=O), 154.1 (2C, Ar), 149.8 (2C, Ar), 129.8 (2C, Ar), 126.9 (2C, Ar), 111.3 (2C, Ar), 109.2 (2C, Ar), 68.9 (2C, -CH<sub>2</sub>-), 55.8 (2C, -CH<sub>3</sub>), 28.9 (2C, -CH<sub>2</sub>-), 25.8 (2C, -CH<sub>2</sub>-).

**4,4'-[hexane-1,6-diylbis(oxy)]bis(3-methoxybenzaldehyde)** (0.5 g, 1.29 mmol) was stirred at room temperature for 2 hours with **SO** (2 equiv, 0.76 g) in methanol (30 mL). The precipitate was filtered and washed with methanol and distilled water, dried at room temperature to give **L3A** as a white solid (93% yield); m.p. 143 °C; FTIR (ATR) (cm<sup>-1</sup>): 1678 (C=O), 3539 (OH), 3330 (NH); <sup>1</sup>H-NMR (400 MHz, CDCl<sub>3</sub>) δ (ppm) = 9.83 (s, 2H, NH), 7.67 (2H, C=N), 7.42 (dd, *J* = 8.2, 1.8 Hz, 4H, Ar), 6.97 (s, 4H, Ar), 6.82 (s, 2H, Ar), 5.09 (2H, -OH), 4.10 (t, *J* = 6.6 Hz, 4H, bridged -CH<sub>2</sub>-), 3.93 (s, 6H, -CH<sub>3</sub>), 2.86 (t, *J* = 8.0 Hz, 4H, -CH<sub>2</sub>-), 2.41 (t, *J* = 7.8 Hz, 4H, -CH<sub>2</sub>-), 1.92 (t, *J* = 6.6 Hz, 4H, bridged -CH<sub>2</sub>-), 1.56 (t, *J* = 6.6 Hz, 4H, bridged -CH<sub>2</sub>-), 1.41 (s, 36H, butyl); <sup>13</sup>C-NMR (101 MHz, CDCl<sub>3</sub>) δ (ppm) = 176.6 (2C, C=O), 153.0 (2C, ArC-OH), 150.8 (2C, ArC-OH), 148.9 (2C, -C=N), 144.6 (2C, vanillin ArC-O-CH<sub>3</sub>), 136.0 (4C, Ar), 131.3 (2C, Ar), 126.5 (2C, vanillin ring C=C=N), 125.1 (4C, Ar), 120.6 (2C, vanillin ring), 111.5 (2C, vanillin ring), 110.3 (2C, vanillin ring), 66.7 (2C, bridged -CH<sub>2</sub>-), 56.4 (2C, methyl), 35.3 (4C, tert-C), 34.7 (2C, -CH<sub>2</sub>-), 32.5 (2C, -CH<sub>2</sub>-), 30.4 (12C, butyl), 29.5 (2C, bridged -CH<sub>2</sub>-), 26.5 (2C, bridged -CH<sub>2</sub>-).

## 2.2.4 Synthesis of T-Series AO/MDs

### 3,3'-thiodi(propanehydrazide) [T0]

Dilauryl thiodipropionate (DLTDP) (5 g, 9.7 mmol) was refluxed with an excess of hydrazine monohydrate (20 ml, 40 mmol) in 2-propanol and diethyl ether (50:50 mixture, 100 mL). The reaction mixture was refluxed (2-4 hours) and left to cool down to room temperature. Filtration and washing with water then ethanol gave **S0** as a white, shiny solid (40% yield); m.p. 48-155°C, FTIR (ATR) ( $\text{cm}^{-1}$ ): 1626 (C=O, Amide);  $^1\text{H-NMR}$  (400 MHz, DMSO- $d_6$ )  $\delta$  (ppm) = 9.02 (s, 2H, NH), 4.19 (s, 4H,  $\text{NH}_2$ ), 2.64 (t,  $J = 7.3$  Hz 4H,  $\text{H}_2\text{C-C=O}$ ), 2.27 (t,  $J = 7.3$  Hz, 4H,  $\text{H}_2\text{C-CH}_2\text{C=O}$ );  $^1\text{H-NMR}$  (400 MHz,  $\text{D}_2\text{O}$ )  $\delta$  (ppm) = 3.16 (t,  $J = 6.9$  Hz, 4H,  $\text{H}_2\text{C-C=O}$ ), 2.93 (t,  $J = 6.9$  Hz, 4H,  $\text{H}_2\text{C-CH}_2\text{C=O}$ );  $^{13}\text{C NMR}$  (100 MHz, DMSO- $d_6$ ):  $\delta$  (ppm) = 27.4 (2C, CSC) 34.3 (2C, C-CO) 170.4 (2C, CO); ESI-MS: m/z ( $[\text{M}+\text{H}]^+$ , +ESI Scan (0.291 min) Frag=80.0V  $\text{MNa}^{+1}$  229.073 and 207.0906.

### 3(2Hydrazinocarbonylethylsulfanyl)propionic acid dodecyl ester or dodecyl 3-((3-hydrazinyl-3-oxopropyl)thio)propanoate [TOA]

Dilauryl thiodipropionate (5g, 9.708 mmol) dissolved in 2-propanol (100 mL). An excess of hydrazine monohydrate (10ml) was added dropwise with care, whilst stirring the solution. The reaction mixture was stirred for 2 days at room temperature. After filtration, washing with water then ethanol **TOA** was obtained as a white solid (80% yield); m.p. 60-62 °C, FTIR (ATR) ( $\text{cm}^{-1}$ ): 1626 (C=O, hydrazide), 1732 (C=O, ester);  $^1\text{H-NMR}$  (400 MHz,  $\text{CDCl}_3$ )  $\delta$  (ppm) = 8.36 (s, 1H, NH), 4.07 (t,  $J = 6.6$  Hz, 2H, O- $\text{CH}_2$ ), 3.62 (t,  $J = 6.6$  Hz, 2H,  $\text{CH}_2\text{CH}_2\text{CH}_2\text{CH}_2\text{O}$ ), 2.79 (t,  $J = 7.3$  Hz, 4H,  $\text{SCH}_2$ ), 2.59 (t,  $J = 7.3$  Hz, 4H,  $\text{CH}_2\text{CH}_2\text{S}$ ), 2.44 (t,  $J = 7.1$  Hz, 2H,  $\text{NH}_2$ ), 1.61 (t,  $J = 7.1$  Hz, 2H,  $\text{CH}_2\text{CH}_2\text{O}$ ), 1.55 (t,  $J = 7.3$  Hz, 2H,  $\text{CH}_2\text{CH}_2\text{CH}_2\text{O}$ ), 1.24 (s, 14H,  $(\text{CH}_2)_7\text{CH}_3$ ), 0.85 (t,  $J = 6.9$  Hz, 3H, Terminal methyl);  $^{13}\text{C NMR}$  (100 MHz,  $\text{CDCl}_3$ ):  $\delta$  (ppm) = 173.5 (1C Azide Carbon C=O), 172.0 (1C, OC=O), 65.0 (1C, OC ester), 63.0 (1C,  $\text{CH}_2\text{CH}_2\text{CH}_2\text{CH}_2\text{O}$ ), 34.8 (1C CC=O), 32.8 (1C,  $\text{CH}_2\text{CH}_2\text{CH}_2\text{O}$ ) 31.9 (1C CC=O carboxylic), 29.7 (4C, Chain), 28.6 (1C,  $\text{CH}_2\text{CH}_2\text{O}$ ), 27 (2C, CS), 25.9-25.8(2C,  $\text{CH}_2\text{CH}_2\text{CH}_2\text{CH}_2\text{CH}_2\text{CH}_2\text{O}$ ), 22.7 (1C, C- $\text{CH}_3$ ), 14.2 (1C Terminal methyl); ESI-MS: m/z ( $[\text{M}+\text{H}]^+$ , +ESI Scan (0.291 min) Frag=80.0V  $\text{MNa}^{+1}$  383.2339 and 361.2523

### **3,3'-sulfanediybis{N'-[(E)-(3,5-di-tert-butyl-4-hydroxyphenyl)methylidene]propanehydrazide}[T1]**

3,3'-thiodi(propane hydrazide) **T0** (0.5 g, 4.85 mmol) and 3,5-di-tert-butyl-4-hydroxybenzaldehyde hemihydrate (2 equiv, 2.35 g) were dissolved in methanol (50 mL) by heating at 60 °C. Stirring for 30 minutes, followed by filtration gave **T1** as a white solid (75% yield); m.p. 250-255 °C, FTIR (ATR) (cm<sup>-1</sup>): 1667 (C=O, Azide), 3207 (NH), 3631 (-OH); <sup>1</sup>H-NMR (400 MHz, CD<sub>3</sub>OD) δ (ppm) = 7.72 (d, *J* = 11.9 Hz, 2H, C=N), 7.37 (s, 4H, Ar), 7.28 (d, *J* = 8.7 Hz, 2H, NH), 2.68-2.62 (m, 4H, CS), 2.36-2.31 (m, 4H, CCS), 1.13 (s, 36H); <sup>1</sup>H-NMR (400 MHz, DMSO-D<sub>6</sub>) δ (ppm) = 11.19 (t, *J* = 8.9 Hz, 2H, OH), 8.07 (d, *J* = 3.7 Hz, 1H, C=N), 7.88 (d, *J* = 7.3 Hz, 1H, C=N), 7.41 (s, 4H, Ar), 7.38 (s, 2H, NH), 2.90 (t, *J* = 3.0 Hz, 4H, CS), 2.81 (t, *J* = 5.7 Hz, 4H, CCS), 1.41 (36H); <sup>13</sup>C NMR (100 MHz, CD<sub>3</sub>OD): δ (ppm) = 170.0 (2C, C=O), 150.0 (2C, C-OH), 139.0 (2C, C=N), 126.0 (4C, ArC-C-tert-butyl), 125.0 (2C, ArC-C=N), 124.0 (4C, Ar), 35.0 (2C, C-C=O), 34.0 (4C, C-tert), 31.0 (12C), 28.0 (2C, C-S)

### **3-[2-(Furan-2-ylmethylene-hydrazinocarbonyl)-ethylsulfanyl]-propionic acid furan-2-ylmethylene-hydrazide [T2]**

3,3'-thiodi(propane hydrazide) **T0** (0.5 g, 4.85 mmol) and 2-furaldehyde (2 equiv, 0.80 mL) were dissolved in methanol (30 mL) by heating at 60 °C. Stirring for 30 minutes, followed by filtration gave **T2** as a white solid (72% yield); m.p. 189-194 °C; FTIR (ATR) (cm<sup>-1</sup>): 1664 (C=O, hydrazide), 1626 (C=N); <sup>1</sup>H-NMR (400 MHz, DMSO-D<sub>6</sub>): δ (ppm) = 11.34 (d, *J* = 27.0 Hz, 2H, NH), 8.04 (s, 2H, C=N), 7.90-7.72 (m, 2H, Furyl), 6.95-6.73 (m, 2H, Furyl), 6.67-6.38 (m, 2H, Furyl), 2.75 (t, *J* = 6.6 Hz, 4H CSC), 2.63 (t, *J* = 6.6 Hz, 4H, CC=O); <sup>13</sup>C NMR (100 MHz, DMSO-D<sub>6</sub>, D<sub>2</sub>O): δ (ppm) = 168.0 (2C, C=O), 150.2 (2C, furyl), 145.0 (2C, furyl), 137.0 (2C, C=N), 114.3 (2C, furyl), 113.110 (2C, furyl), 35.62 (2C, CC=O), 30 (2C, CSC=O); ESI-MS: m/z ([M+H]<sup>+</sup>, +ESI Scan (0.302 min) Frag=80.0V 363.1122

### **3-[2-(2-Hydroxy-benzylidene-hydrazinocarbonyl)-ethylsulfanyl]-propionic acid (2-hydroxy-benzylidene)-hydrazide [T3]**

3,3'-thiodi(propane hydrazide) **T0** (0.5 g, 4.85 mmol) and 2-hydroxybenzaldehyde (2 equiv, 1.0 mL) were dissolved in methanol by heating at 60 °C. Stirring for 30 minutes, followed by filtration gave **T3** as a white solid (76% yield); m.p. 245-250 °C, FTIR (ATR) (cm<sup>-1</sup>): 1665 (C=O, hydrazide), 1622 (C=N); <sup>1</sup>H-NMR (400 MHz, DMSO-D<sub>6</sub>, D<sub>2</sub>O) δ (ppm) = 8.39-8.21 (m, 2H C=N), 7.66-7.50 (m, 2H ring),

7.48-7.46 (m, 2H, ring), 7.32-7.18 (m, 2H ring), 6.95-6.83 (m, 2H ring), 2.83 (t,  $J = 6.4$  Hz, 4H, ethylene), 2.71 (t,  $J = 6.4$  Hz, 4H, ethylene);  $^1\text{H-NMR}$  (400 MHz, DMSO- $\text{D}_6$ )  $\delta$  (ppm) = 11.72-9.98 (m, 2H, OH), 10.08 (2H, NH), 8.40-8.15 (m, 2H C=N), 7.65-6.70 (m, 6H Aromatic), 2.97 (t,  $J = 6.6$  Hz, 4H, ethylene), 2.43 (t,  $J = 6.6$  Hz, 4H, ethylene);  $^{13}\text{C NMR}$  (100 MHz, DMSO- $\text{D}_6$ ,  $\text{D}_2\text{O}$ ):  $\delta$  (ppm) = 168.2 (2C, C=O), 157.913 (2C, Phenolic), 148.0 (2C, C=N), 132.3 (2C, CC=COH ring), 130.4 (2C, C=CCOH ring), 120.6 (2C, Para carbons), 119.3 (2C, CCOH ring), 117.2 (2C, C=COH), 35.1 (2C, CC=O), 27.5 (2C, SC); ESI-MS:  $m/z$  ([M+H] $^+$ , +ESI Scan (0.220 min) Frag=80.0V 415.1435

**N'-[(Z)-(4-hydroxy-3-methoxyphenyl)methylidene]-3-[(3-[(2E)-2-[(4-hydroxy-3-)methylidene]hydrazinyl)-3-oxopropyl)sulfanyl]propanehydrazide [T4]**

3,3'-thiodi(propane hydrazide) **T0** (0.5 g, 4.85 mmol) and vanillin (2 equiv, 1.47 g) were dissolved in methanol (50 mL) by heating at 60 °C. Stirring for 30 minutes, followed by filtration gave **T4** as a white solid (82% yield); FTIR (ATR) ( $\text{cm}^{-1}$ ): 1663 (C=O, hydrazide), 1632 (C=N);  $^1\text{H-NMR}$  (400 MHz, DMSO- $\text{D}_6$ )  $\delta$  (ppm) = 11.19 (d,  $J = 20.1$  Hz, 2H, -OH), 9.45 (s, 2H, NH), 7.89 (d,  $J = 66.4$  Hz, 2H C=N), 7.21 (s, 2H, Ar C-C=N), 6.92 (d,  $J = 8.2$  Hz, 2H, Ar), 6.77 (d,  $J = 9.2$  Hz, 2H, Ar), 3.76 (s, 6H, - $\text{CH}_3$ ), 2.88 (t,  $J = 6.9$  Hz, 2H, - $\text{CH}_2$ -), 2.77 (t,  $J = 7.6$  Hz, 2H, - $\text{CH}_2$ -);  $^{13}\text{C-NMR}$  (101 MHz, DMSO- $\text{D}_6$ )  $\delta$  (ppm) = 167.2 (2C, C=O), 149.3 (2C, C-OH), 148.4 (2C, C-O $\text{CH}_3$ ), 143.8 (2C, C-N), 126.1 (2C, Ar), 122.4 (2C, Ar), 116.04 (2C, Ar), 109.8 (2C, Ar), 56.0 (2C, O $\text{CH}_3$ ), 33.0 (2C, CC=O), 27.4 (2C, CS).

## 2.2.5 Synthesis of MD-Series AO/MDs

### 2-hydroxybenzohydrazide [MD1]

2-hydroxybenzohydrazide **MD1** was prepared<sup>132</sup> by reaction of hydrazine monohydrate (excess) with methyl salicylate (2 mL) in methanol (30 mL) by refluxing for one hour. After reducing the volume of the solvent, the solution was left to stand for 12 hours. **MD1** was obtained as a green solid which turned white after washing with water (92% yield); m.p. 150 °C; FTIR (ATR) (cm<sup>-1</sup>): 1642 (C=O, hydrazide); <sup>1</sup>H-NMR (400 MHz, DMSO-D<sub>6</sub>) δ (ppm) = 11.61 (s, 1H, -OH), 9.18 (s, 1H, -NH), 6.91 (d, *J* = 6.7 Hz, 1H, Ar), 6.48 (t, *J* = 7.0 Hz, 1H, Ar), 6.01 (d, *J* = 8.3 Hz, 1H, Ar), 5.97 (t, *J* = 7.5 Hz, 1H, Ar), 3.77 (s, 2H, -NH<sub>2</sub>); <sup>13</sup>C NMR (100 MHz, CD<sub>3</sub>OD): δ (ppm) = 1668.4 (1C, C=O), 160 (1C C-OH), 133 (1C, Ar), 127.8 (1C, Ar), 119 (1C, Ar), 117.8 (1C, Ar), 114.89 (1C, Ar).

### (N',N'''E,N',N'''E)-N',N'''-(pentane-1,5-diylidene)bis(2-hydroxybenzohydrazide) [MD1B]

**MD1** was stirred for one hour with glutaraldehyde in methanol and **MD1B** obtained as a white powder (85% yield); m.p. 200 °C, IR (cm<sup>-1</sup>): 1636 (C=N, Imine); <sup>1</sup>H-NMR (400 MHz, CDCl<sub>3</sub>) δ (ppm) = 11.98 (2H, NH), 11.61 (s, 2H, OH), 7.94 (d, *J* = 8.2 Hz, 2H, Ar), 7.60 (t, *J* = 5.5 Hz, 2H, C=N), 7.39 (t, *J* = 7.8 Hz, 2H, Ar), 6.97 (d, *J* = 8.2 Hz, 2H, Ar), 6.84 (t, *J* = 7.6 Hz, 2H, Ar), 2.04 (d, *J* = 6.0 Hz, 4H, -CH<sub>2</sub>-), 1.45 (t, *J* = 6.9 Hz, 2H, -CH<sub>2</sub>-); <sup>13</sup>C-NMR (101 MHz, DMSO-D<sub>6</sub>) δ (ppm) = 165.92 (2C, C=O), 158.83 (2C, ArC-OH), 152.14 (2C, C=N), 135.03 (2C, Ar), 129.65 (2C, Ar), 120.17 (2C, Ar), 117.49 (4C, Ar), 30.61 (2C, -CH<sub>2</sub>-), 19.50 (1C, -CH<sub>2</sub>-).

### (E)-2-hydroxy-N'-(4-hydroxy-3-methoxybenzylidene)benzohydrazide [MD1C]

**MD1** was stirred for one hour with vanillin in methanol and **MD1C** obtained as a white powder (90% yield); m.p. 212 °C, FTIR (ATR) (cm<sup>-1</sup>): 1639 (C=N, Imine); <sup>1</sup>H-NMR (400 MHz, DMSO-D<sub>6</sub>) δ (ppm) = 12.04 (s, 1H, Phenolic), 11.60 (s, 1H, Vanillin phenolic), 9.26 (s, 1H, NH), 8.22 (s, 1H, C=N), 7.83 (d, *J* = 7.8 Hz, 1H, Ar), 7.36 (s, 1H, Vanillin Ar), 7.28 (t, *J* = 7.8 Hz, 1H, Ar), 6.97 (d, *J* = 8.2 Hz, 1H, Vanillin Ar), 6.84 (d, *J* = 8.2 Hz, 1H, Ar), 6.80 (t, *J* = 7.8 Hz, 1H, Ar), 6.75 (d, *J* = 8.2 Hz, 1H, Vanillin Ar), 3.79 (s, 3H, methyl); <sup>1</sup>H-NMR (400 MHz, DMSO-D<sub>6</sub> + D<sub>2</sub>O) δ (ppm) = 8.22 (s, 1H, C=N), 7.83 (d, *J* = 7.8 Hz, 1H,

Ar), 7.36 (s, 1H, Vanillin Ar), 7.28 (t,  $J = 7.8$  Hz, 1H, Ar), 6.97 (d,  $J = 8.2$  Hz, 1H, Vanillin Ar), 6.84 (d,  $J = 8.2$  Hz, 1H, Ar), 6.80 (t,  $J = 7.8$  Hz, 1H, Ar), 6.75 (d,  $J = 8.2$  Hz, 1H, Vanillin Ar), 3.79 (s, 3H, methyl);  $^{13}\text{C}$ -NMR (101 MHz, DMSO- $\text{D}_6$ )  $\delta$  (ppm) = 165.82 (1C, C=O), 160.65 (1C, ArC-OH), 150.20 (1C, Vanillin ArC-O- $\text{CH}_3$ ), 149.70 (1C, vanillin ArC-OH), 148.34 (1C, C=N), 134.12 (1C, Ar), 128.22 (1C, Ar), 125.76 (1C, vanillin Ar), 123.21 (1C, vanillin Ar), 118.90 (1C, Ar), 117.87 (1C, Ar), 115.58 (1C, vanillin Ar), 114.96 (1C, Ar), 109.13 (1C, vanillin Ar), 56.03 (1C, methyl).

### **2,2'-(hydrazine-1,2-diylidenebis(methanylylidene))diphenol [MD0]**

**MD0** was synthesised according to the procedure described in literature<sup>133</sup>. Salicylaldehyde and hydrazine hydrate (2:1) in ethanol with stirring gave **MD0** as a yellow solid (60% yield); m.p. 215 °C, FTIR (ATR) ( $\text{cm}^{-1}$ ): 1615 (C=N);  $^1\text{H}$ -NMR (400 MHz,  $\text{CDCl}_3$ )  $\delta$  11.39 (s, 2H, OH), 8.70 (s, 2H, C=N), 7.39 (d,  $J = 7.3$  Hz, 2H, Ar), 7.35 (t,  $J = 5.7$  Hz, 2H, Ar), 7.03 (d,  $J = 8.2$  Hz, 2H, Ar), 6.96 (t,  $J = 7.6$  Hz, 2H, Ar);  $^{13}\text{C}$  NMR (100 MHz,  $\text{CDCl}_3$ ):  $\delta = 164.72$  (2C, C=N), 159.82 (2C, ArC-OH), 133.35 (2C, Ar), 132.32 (2C, Ar), 119.82 (2C, Ar), 117.78 (2C, Ar), 117.01 (2C, Ar).

### **2,2'-((1E,1'E)-((2E,2'E)-ethane-1,2-diylidenebis(hydrazine-2,1-diylidene))bis(methanylylidene))diphenol [MD2A]**

Glyoxal bishydrazone (synthesis described in the literature<sup>134</sup>) (2 g, mol, 23.25 mmol) in 30 mL of methanol was refluxed for 2 hours with 2-hydroxybenzaldehyde (2 equiv. 4.85 mL) to give **MD2A** white crystals (77% yield); m.p. 220-225 °C, FTIR (ATR) ( $\text{cm}^{-1}$ ): 1632 (C=N);  $^1\text{H}$ -NMR (400 MHz, DMSO- $\text{D}_6$ )  $\delta$  (ppm) = 8.96 (s, 2H, -C=N), 8.53 (s, 2H, N=C-C=N), 7.75 (dd,  $J = 7.8, 1.8$  Hz, 2H), 7.46-7.39 (m, 2H), 6.99 (d,  $J = 1.4$  Hz, 2H), 6.98-6.95 (m, 2H), 5.08 (d,  $J = 49.5$  Hz, 2H, OH);  $^{13}\text{C}$  NMR (100 MHz, DMSO- $\text{D}_6$ ,  $\text{D}_2\text{O}$ ):  $\delta$  (ppm) = 164.7 (2C, C=N), 160.3 (2C, C-OH), 159.5 (2C, C=N), 134.5 (2C, Ring C-C=C-OH), 131.3 (2C, Ring C=C-C-OH), 120.1 (2C, Para carbon), 118.6 (2C, Ring C-C-OH), 117.2 (2C, Ring C=C-OH); ESI-MS: m/z ([M+H]<sup>+</sup>, +ESI Scan (0.220 min) Frag=80.0V 295.11

### **(1E,2E)-1,2-bis((E)-(furan-2-ylmethylene)hydrazono)ethane [MD2B]**

Glyoxal bishydrazone (synthesis described in the literature<sup>134</sup>) (2 g, mol, 23.25 mmol) in 30 mL of methanol was refluxed for 2 hours with 2-furaldehyde (2 equiv. 3.84 mL) to give **MD2B** (67% yield); m.p. 155-160 °C, FTIR (ATR) (cm<sup>-1</sup>): 1616 (C=N); <sup>1</sup>H-NMR (400 MHz, DMSO-D<sub>6</sub>) δ (ppm) = 8.55 (s, 2H, -N=HC-CH=N-), 8.37 (s, 2H, -C=N-), 8.02 (d, *J* = 1.4 Hz, 2H, -C-O), 7.25 (d, *J* = 3.2 Hz, 2H, furyl -C=C-C=N-), 6.75 (q, *J* = 1.7 Hz, 2H, furyl -C=C-O-); <sup>13</sup>C NMR (100 MHz, DMSO-D<sub>6</sub>, D<sub>2</sub>O):δ (ppm) = 159.725 (2C, -C=N-), 152.688 (2C, -N=C-C=N-), 149.198 (2C, C-O furyl), 148.188 (2C, Furyl -O-C), 120.070 (2C, furyl -O-C=C-), 113.549 (2C, furyl C=C-O-); ESI-MS: m/z ([M+H]<sup>+</sup>, +ESI Scan (0.220 min) Frag=80.0V 242.1023

### **Synthesis of metal deactivator 4,4'-(ethane-1,2-diylidenebis(azanylylidene)) bis(1,5-dimethyl-2-phenyl-1H-pyrazol-3(2H)-one) [MD4]**

Synthesis of MD4 was undertaken by a modified procedure to that reported in the literature<sup>135</sup>. 4-aminoantipyrine(4-amino-1,5-dimethyl-2-phenyl-1H-pyrazol-3(2H)-one) (1.55 g, 7.6 mmol) was dissolved in absolute ethanol (25 mL). A clear, light brown solution was obtained to which glyoxal (0.222 mL, 3.82 mmol) was added and this solution was stirred for 30 minutes. A yellow precipitate was formed, which was washed with ethanol and water and dried at room temperature to give **MD4** (62% yield); FTIR (ATR) (cm<sup>-1</sup>): 1650 (C=O), 1575 (C=N, Imine); <sup>1</sup>H-NMR (400 MHz, CDCl<sub>3</sub>) δ (ppm) = 9.34 (s, 2H N=CH), 7.47 (dd, *J* = 8.2, 7.3 Hz, 4H), 7.40-7.35 (m, 4H), 7.31 (t, *J* = 7.6 Hz, 2H), 3.17 (s, 6H N-CH<sub>3</sub>), 2.42 (s, 6H CH<sub>3</sub>); <sup>13</sup>C NMR (100 MHz, CDCl<sub>3</sub>): δ (ppm) = 160.1 (2C, C=O), 159.0 (2C, C-CH<sub>3</sub> Pyrazole), 152.7 (2C, C=N), 134.7 (2C, PyrazoleN-CH benzene ring), 129.2 (4C, Ar), 127.1 (2C, Ar), 124.7 (4C, Ar), 119.0 (2C, Pyrazole C-N=C), 35.6 (2C, N-CH<sub>3</sub> Pyrazole), 10.15 (2C, C-CH<sub>3</sub> Pyrazole)

### **Synthesis of metal deactivators 2,3-dihydroxybutanedihydrazide [MD7] and 2,3-dihydroxy butanedioyl bis(salicylidenehydrazone) [MD7A]**

**MD7**<sup>136</sup> and **MD7A** were synthesised by following procedures described in the literature<sup>137</sup>. IR and NMR assignments were identical to those given in this method, confirming the structures, and so are not given here.

## Chapter 3: Results and Discussion

### Section A: Novel Antioxidant-Metal Deactivator Performance

A wide range of novel antioxidant-metal deactivator structures have been synthesised in this study. For the sake of clarity, not all of these are described in the results and discussion section. Where samples have been omitted performance data (MFI and YI) is tabulated in the Appendix, namely data for a combination of base stabilisers (CaSt, ALKANOX<sup>®</sup>240, ANOX<sup>®</sup>20) and novel antioxidant-metal deactivators, evaluated by conventional multi-pass extrusion (this data will be discussed briefly in the section on Future Work).

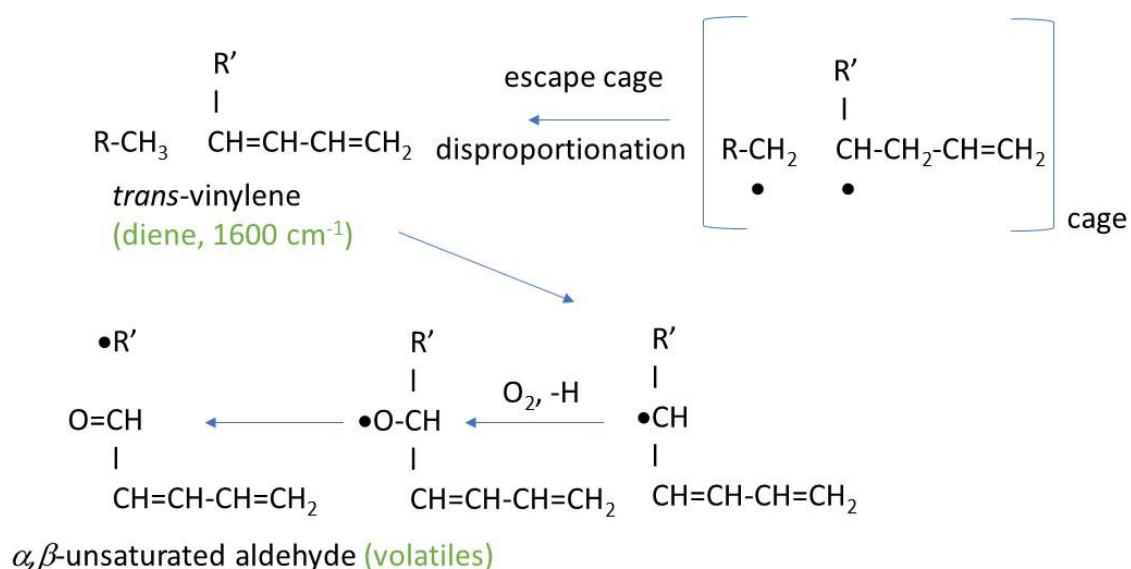
In the first part of this study Commercial-Series antioxidant-metal deactivators have been examined to give confidence that the methodology is broadly in line with the existing literature and, to provide a baseline to compare the novel metal deactivators synthesised in this study. Here the ability of the Commercial structures to coordinate copper has been assessed by FTIR and NMR, their performance evaluated by MFI and YI and, interactions with the polymer by FTIR in LDPE. The ability of the novel metal deactivators to complex with copper was assessed by mixing an excess of the copper salts with the ligand and precipitating out the complex from methanol followed by filtration and drying. Although these experiments were not performed on base commercial stabilisers, there is evidence in the literature to corroborate the formation of their complexes with copper.

Throughout the results and discussion section the data is examined in the context of key degradation mechanisms for LDPE, as explained in detail in the introduction and summarised as follows.

During extrusion, the viscosity of the polymer is high, even in the melt, especially during the initial stages of degradation. Once radical chain degradation is underway termination reactions can take place by radical combination or disproportionation. The probability of radical recombination is 2-5 times higher than disproportionation. However, both types have zero activation energy and cage effects predominate, due to the lower rate of diffusion of reactions outside the cage.

In the absence of oxygen, combination reactions leading to long chain branching (LCB) and molecular enlargement are likely. Where disproportionation takes place unsaturated groups (*trans*-vinylene)

are formed. If *trans*-vinylene groups form adjacent to end-chain vinyl groups these reactions will lead to the formation of volatiles that will diffuse out of the polymer matrix (**Scheme 3.1**).

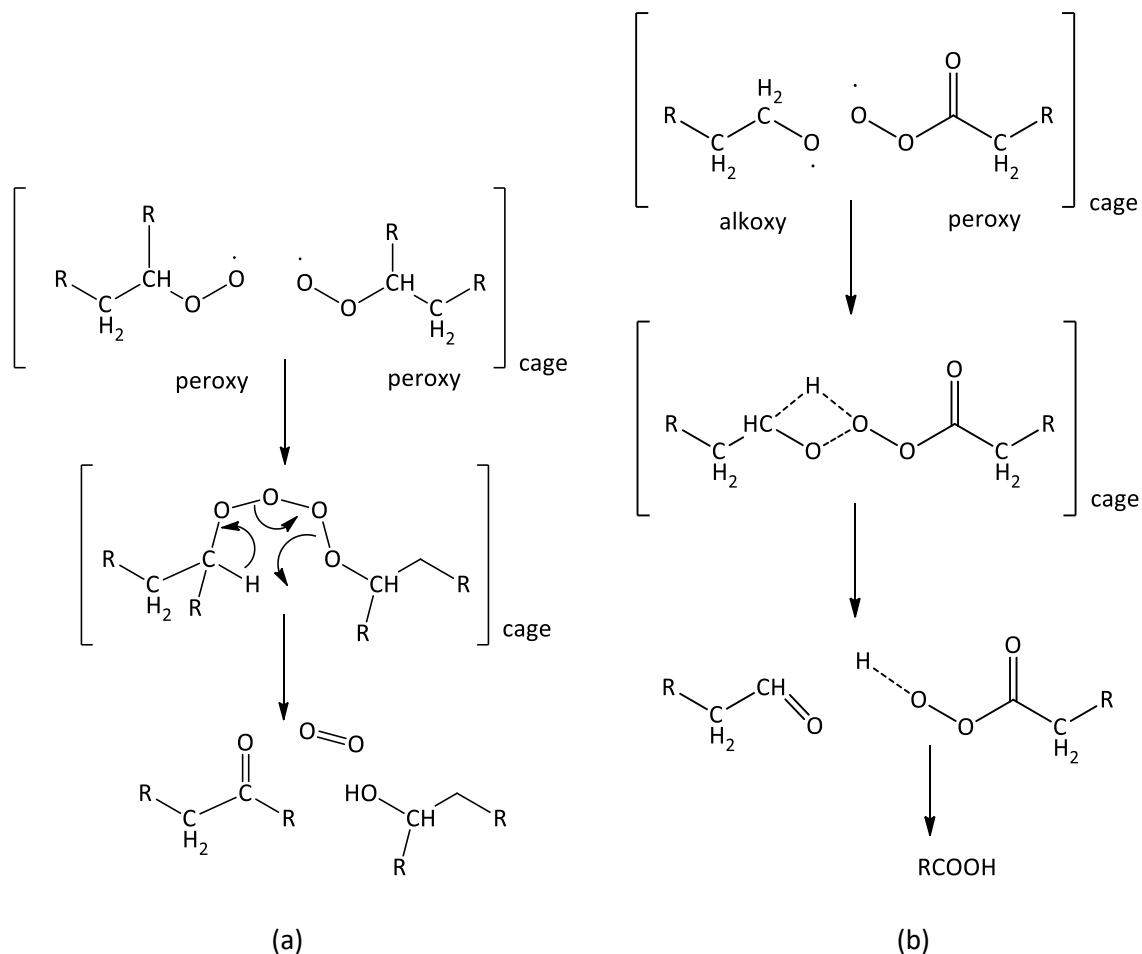


**Scheme 3-1** Formation of volatiles from chain-ends during LDPE oxidation

If the radicals react with oxygen to form peroxy radicals, cage recombination leads to the formation of aldehyde and alcohol groups, for primary and secondary peroxy radicals. This reaction results in the generation of chemiluminescence and oxygen. The aldehydes readily form acyl radicals oxidising to the corresponding carboxylic acid via peracids. Within the cage the acids and alcohols may combine to form saturated esters. At low concentrations of peroxide, alkoxy and hydroxyl radicals are formed.

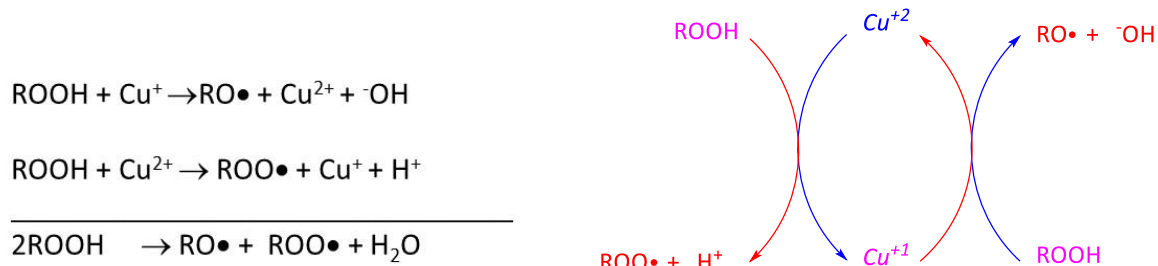
Tertiary radicals escape the cage since they are unable to undergo these reactions because they have no available  $\alpha$ -hydrogen, leading to the formation alcohols and ketones.

The alkoxy and peroxy radicals in the cage can react to yield similar products to the peroxy cage reaction, via a hydride shift (**Scheme 3-2**).



**Scheme 3-2** Cage reactions of peroxy and alkoxy radicals in LDPE

In the presence of metal ions, such as copper, redox reactions will take place according to the equations and redox couple given in **Scheme 3-3**.



**Scheme 3-3** Equations and Redox Couple for the copper catalysed decomposition of peroxide

### 3.1 Commercial Stabilizer Performance

Different synthetic metal deactivators (LOWINOX<sup>®</sup>MD24 and NAUGARD<sup>®</sup>XL-1) and commercial additives (CaSt, ALKANOX<sup>®</sup>240, ANOX<sup>®</sup>20), were formulated in LDPE without and with copper (I) chloride and analysed by FTIR, yellowness index (YI) and melt flow index (MFI).

#### 3.1.1 MFI and Yellowness Index (Commercial Series)

**Figure 3-1** shows the changes in MFI of the Commercial-Series formulations, relative to LDPE. The ranking of the MD-Series with respect to MFI follows the order:

Without copper:      **LOWINOX<sup>®</sup>MD24  $\cong$  NAUGARD<sup>®</sup>XL-1  $\cong$  ANOX<sup>®</sup>20** < CaSt < ALKANOX<sup>®</sup>240

With Copper:        **NAUGARD<sup>®</sup>XL-1  $\cong$  ANOX<sup>®</sup>20** < **LOWINOX<sup>®</sup>MD24** < ALKANOX<sup>®</sup>240 < CaSt

In the absence of copper, the MFI of all the Commercial-Series increases with residence time in the extruder. The rate of increase of MFI is highest for ALKANOX<sup>®</sup>240, which shows a higher MFI throughout processing. In the case of ANOX<sup>®</sup>20 and the metal deactivators the MFI remains lower than LDPE, showing that they can reduce chain-scission during the process time.

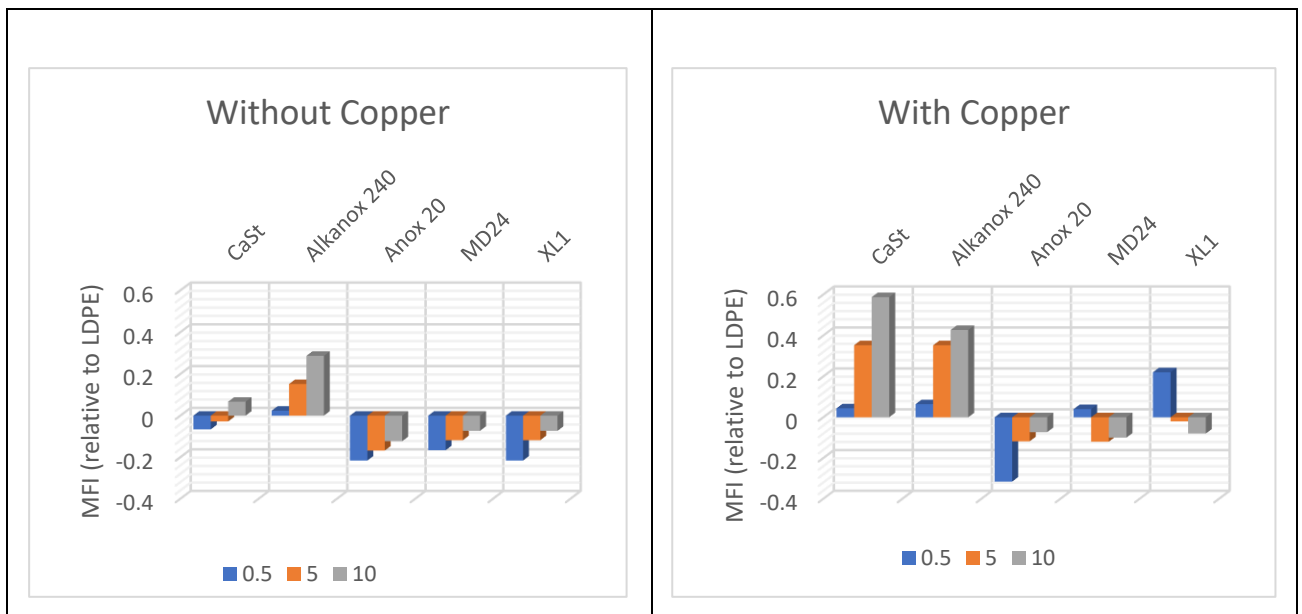
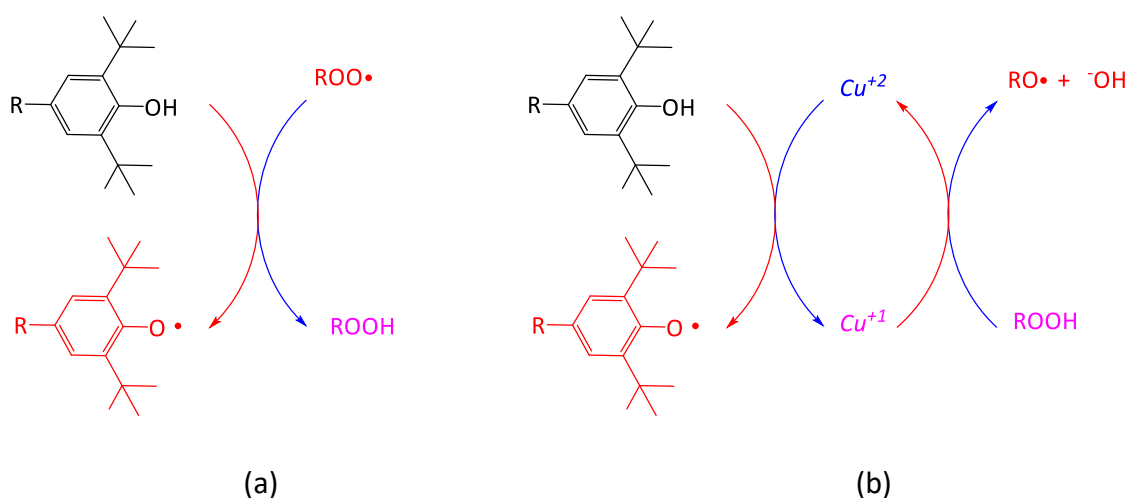


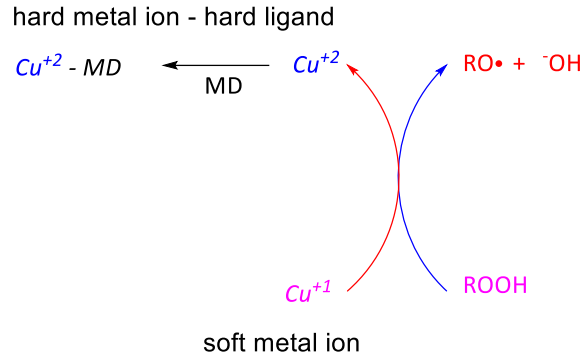
**Figure 3.1** MFI values relative to LDPE, for Commercial-Series formulations in LDPE extruded without and with CuCl (*s.d* = 0.01 g/10 min)

In the presence of copper, the MFI of all the Commercial-Series formulations increases with residence time in the extruder, except for *LOWINOX*<sup>®</sup>*MD24* and *NAUGARD*<sup>®</sup>*XL-1*. For *ANOX*<sup>®</sup>*20* the MFI in the initial stage of degradation is the lowest of all values demonstrating its effective antioxidant performance. In contrast in the presence of copper, *LOWINOX*<sup>®</sup>*MD24* and *NAUGARD*<sup>®</sup>*XL-1* show MFI values, though initially higher than LDPE, that decreased to values similar to *ANOX*<sup>®</sup>*20* after 10 minutes. This suggests that *ANOX*<sup>®</sup>*20* is an effective antioxidant (**Scheme 3-4 (a)**) but poor metal deactivator (**Scheme 3-4 (b)**) and, that its reduction in performance in the presence copper is a consequence of the two competing reactions.



**Scheme 3-4** Phenolic antioxidant redox couple in the absence (a) and presence (b) of copper

In the absence of copper, *LOWINOX*<sup>®</sup>*MD24* and *NAUGARD*<sup>®</sup>*XL-1* are less-effective antioxidants than *ANOX*<sup>®</sup>*20*, which can be explained by their lower molar ratio of active phenol groups (2x -OH c.f. 4x -OH). In the presence of copper, some chain scission to form peroxy radicals during propagation will have taken place *before* coordination of copper (II) by the metal deactivators can prevent chain-branching by peroxide decomposition (**Scheme 3-5**). This is the reason why *LOWINOX*<sup>®</sup>*MD24* and *NAUGARD*<sup>®</sup>*XL-1* show an initial MFI that is higher than that of LDPE.



*Scheme 3-5 Oxidation of Cu<sup>+</sup> by peroxide and complexation of Cu<sup>2+</sup> by a metal deactivator*

**Figures 3-2** shows the  $\Delta b^*$  values of the Commercial-Series formulations, relative to LDPE. The ranking of the MD-Series with respect to  $\Delta b^*$  follows the order:

Without copper: CaSt < ALKANOX<sup>®</sup>240 < LOWINOX<sup>®</sup>MD24 < NAUGARD<sup>®</sup>XL-1 < ANOX<sup>®</sup>20

With Copper: NAUGARD<sup>®</sup>XL-1 < CaSt < LOWINOX<sup>®</sup>MD24 < ALKANOX<sup>®</sup>240 < ANOX<sup>®</sup>20

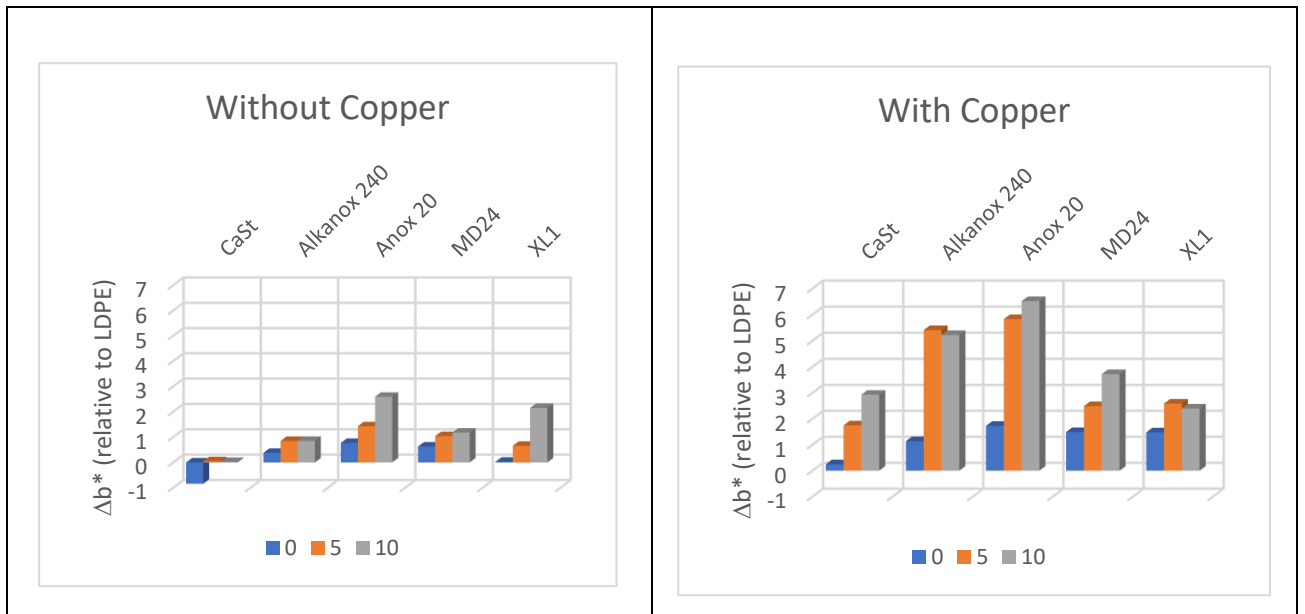
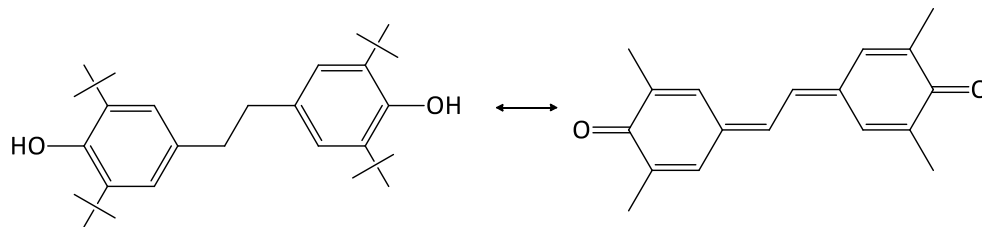


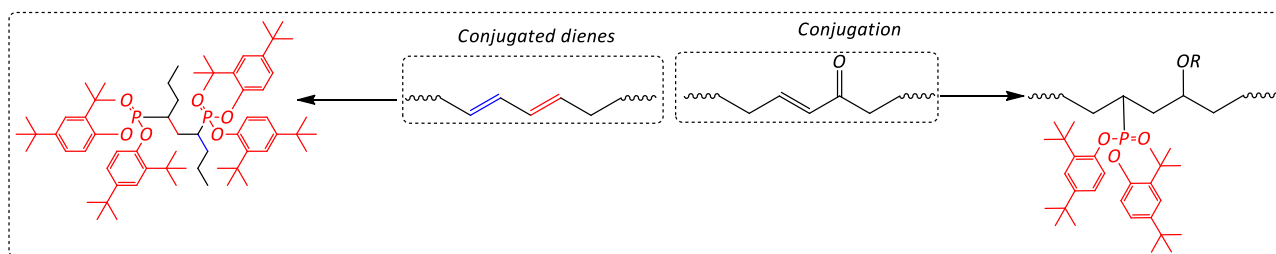
**Figure 3-2** Yellowness ( $\Delta b^*$ ) values relative to LDPE, for Commercial-Series formulations in LDPE extruded without and with CuCl (s.d = 0.04)

In both the absence and presence of copper the  $\Delta b^*$  value for ANOX<sup>®</sup>20 has the highest value after 10 minutes residence time in the extruder. Yellowness may arise from oxidation of the LDPE polymer or the transformation products of the antioxidant, the latter being the major contributor. The phenoxy radical can transform to give quinonoid structures, which have high extinction coefficients. Generally, the more conjugated the quinone the more intense the yellowness (**Scheme 3-6**). This can also be seen in LOWINOX<sup>®</sup>MD24 and NAUGARD<sup>®</sup>XL-1, which also have relatively high  $\Delta b^*$  values.



**Scheme 3-6** Quinonoid transformation product of a hindered phenol

The ALKANOX<sup>®</sup>240 is added as a colour inhibitor and shows low  $\Delta b^*$  in the absence of copper (**Scheme 3-7**): In the presence of copper its coordination leads to enhanced  $\Delta b^*$ . The calcium stearate can block colour in the polymer initially, in the absence of copper, but in the presence of copper, metal exchange results in the formation of copper stearate which can act as a prooxidant.



**Scheme 3-7** Proposed mechanism of action of phosphite in the destruction of conjugation in LDPE

The above observations raise two main possibilities about the chemical processes taking place during the extrusion residence time, namely that:

- I. *Discoloration is caused mainly by the stabiliser.*
- II. *The reactions are similar during the extrusion residence time, but their specific rates differ.*

### 3.1.2 FTIR Analysis of Commercial-Series Antioxidants and Metal Deactivators in LDPE

**Figures 3-3 and 3-5** give the FTIR spectra in the range 1800-1500  $\text{cm}^{-1}$  for the Commercial Series AO/MDs. Absorptions in the range 3000-3300  $\text{cm}^{-1}$  are referred to in the text and not depicted. Because some spectra display baseline shift (which has not been corrected due to software issues) and for ease of comparison **Figures 3-4 and 3-6** shows the relative rate of change of key functional group absorptions, where intensity is corrected for baseline drift.

The assignment of bands is detailed in **Table 3-1**. The absorbances in the range 1600-1660  $\text{cm}^{-1}$  correspond to *trans*-1,2-disubstituted alkenes (*trans*-vinylene) at 1660  $\text{cm}^{-1}$ , dienes (1645  $\text{cm}^{-1}$ ), conjugated dienes associated with carbonyl groups (1633  $\text{cm}^{-1}$ ) and conjugated dienes (1600  $\text{cm}^{-1}$ ). In the range 1700-1750  $\text{cm}^{-1}$  carbonyl absorptions are associated with esters (1745  $\text{cm}^{-1}$ ), aldehyde/ketone groups (1720  $\text{cm}^{-1}$ , influenced by unsaturation) carboxylic acids (1710  $\text{cm}^{-1}$ ).

*Table 3-1 Assignment of FTIR absorptions of oxidised species in LDPE*

Wavenumber ( $\text{cm}^{-1}$ )	Assignment
1600	conjugated dienes
1633	conjugated dienes associated with carbonyl groups
1645	dienes
1660	<i>trans</i> -1,2-disubstituted alkenes
1710	Carboxylic acids
1720	Carbonyl groups of ketones and aldehydes*
1745	Carbonyl of esters

\*position influenced by unsaturation

The FTIR spectrum of LDPE powder before processing showed negligible absorptions indicating thermal or oxidative degradation and so is not shown here. In the absence of copper (**Figure 3-3**), a broad band is shown for LDPE, that increases in intensity between 1560-1700  $\text{cm}^{-1}$ . This broad band shows evidence for absorptions peaking at 1600  $\text{cm}^{-1}$  and 1660  $\text{cm}^{-1}$ . A distinct absorption at 1645  $\text{cm}^{-1}$  is also seen to develop with time, attributed to the formation of ester groups. **Figure 3-4** also shows the rate of development of these groups. During the first five minutes of processing all absorptions develop at a relatively low rate. From five to ten minutes there is a rapid increase in the

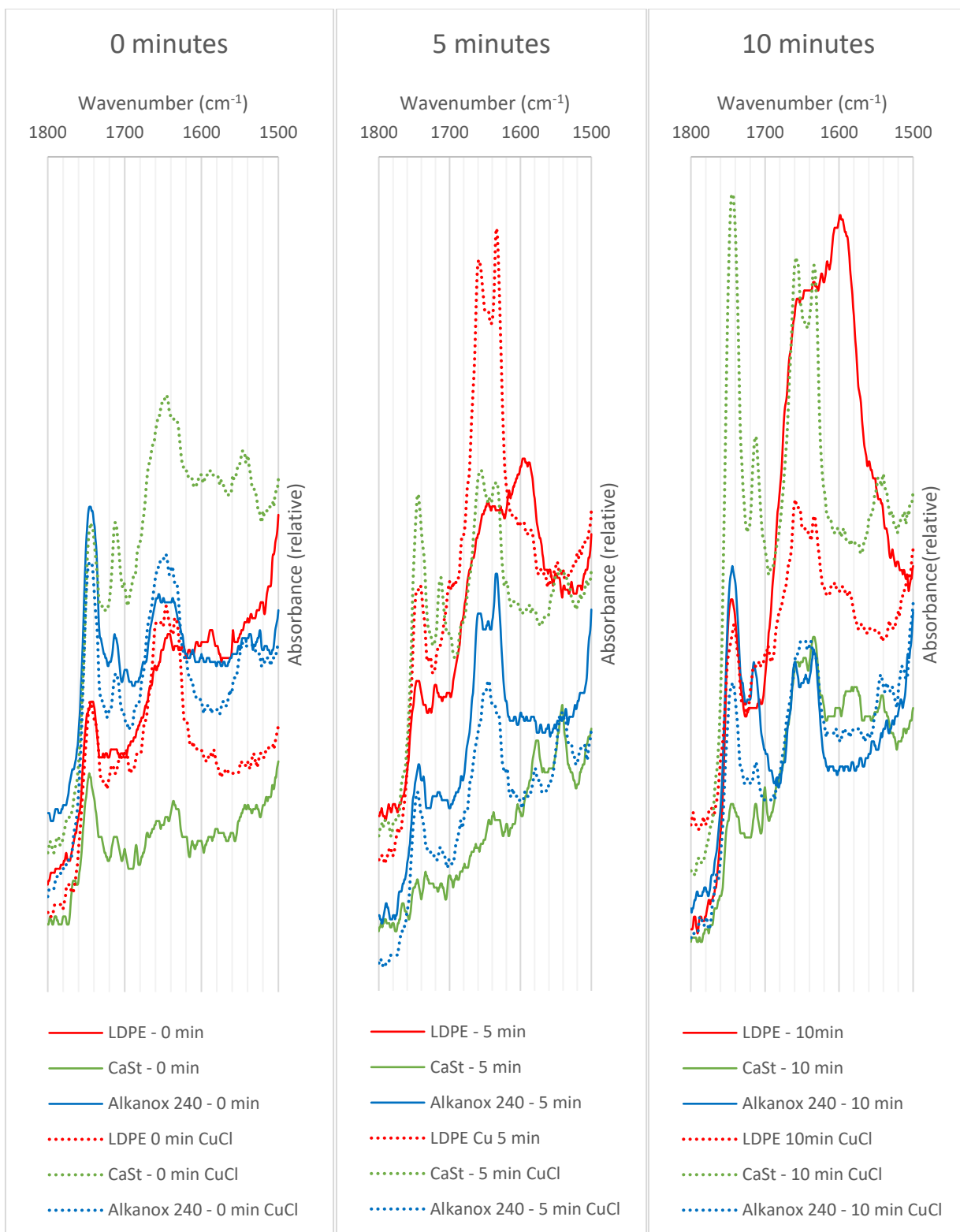


**Figure 3-3:** FTIR spectra (1800-1500 cm<sup>-1</sup>) of LDPE and, CaSt and Alkanox 240 in LDPE; extruded for 0, 5 and 10 minutes without and with CuCl

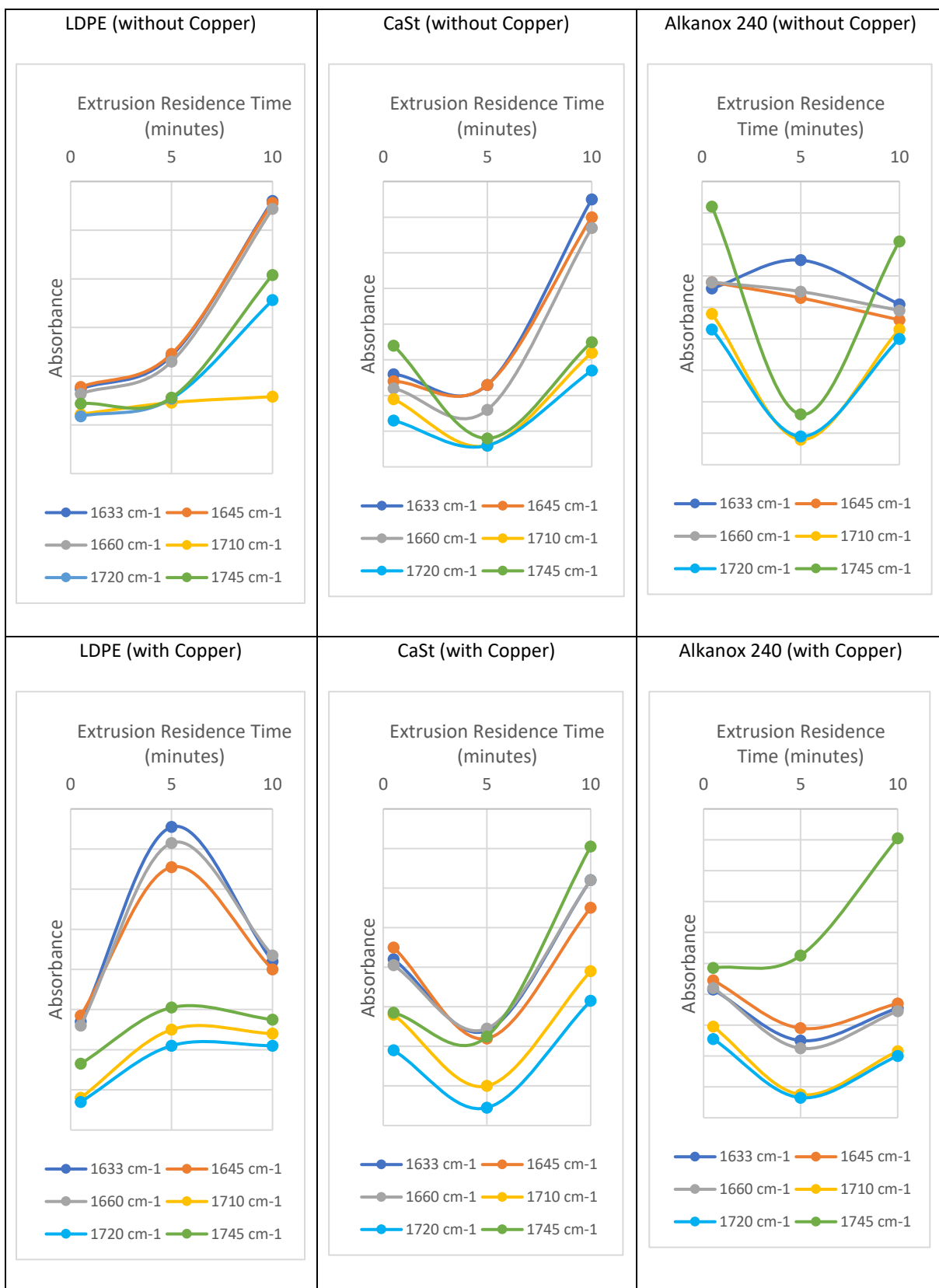


Figure 3-4: FTIR absorption intensities of carbonyl and unsaturated species in LDPE and, CaSt and Alkanox 240 in LDPE; extruded for 0, 5 and 10 minutes without and with CuCl

intensities of the peaks in the range 1600-1660  $\text{cm}^{-1}$ . This supports the proposition that as oxidation proceeds and peroxy radical and peroxide concentrations increase, cage recombination and cage disproportionation of radicals in the presence of oxygen is leading to the formation of unsaturation, unsaturated carbonyls, and saturated esters.

For LDPE in the presence of copper (**Figure 3-3**), the band at 1600  $\text{cm}^{-1}$  is diminished, and a doublet at 1633 and 1660  $\text{cm}^{-1}$  is intensified during the first 5 minutes of processing that decreases rapidly from 5-10 minutes. The C=O absorptions at 1710, 1720 and 1745  $\text{cm}^{-1}$  increase at a slower rate in the first 5 minutes and decrease slightly from 5-10 minutes. This suggests that copper is catalysing the decomposition of peroxides or cage recombination of peroxy radicals to rapidly form unsaturated carbonyls. After 5 minutes these groups are then rapidly converted to ketones, carboxylic acids and esters. Further evidence comes from the hydroxyl region (not shown here) between 3700 -3300  $\text{cm}^{-1}$ . The non-hydrogen-bonded hydroxyl group (free OH) and hydrogen-bonded hydroxyl group were absent in samples without CuCl. In addition, a small absorption attributed to the hydrogen-bonded hydroxyl group is growing gradually at 3367  $\text{cm}^{-1}$  in presence of CuCl which is due to the formation of carboxylic acids, while carboxylic C-O stretch is appearing at 1584  $\text{cm}^{-1}$ .

For calcium stearate, in the first 5 minutes of processing, there is a decrease in all the absorptions that characterise degradation. Following this there is a rapid increase in the intensity of the absorptions and a very marked increase in the ester band. The doublet at 1540 and 1575  $\text{cm}^{-1}$  arises from carboxylate groups associated with calcium ions in unidentate and bidentate modes. In the presence of copper in the first 5 minutes of degradation the bands decrease and from 5-10 minutes increase rapidly, especially the ester band. For, LDPE with *Calcium Stearate* in the presence of CuCl showed the growth of several groups (ester, carbonyl C=O, and alkene C=C) at frequencies of 1745  $\text{cm}^{-1}$ , 1720  $\text{cm}^{-1}$  and 1659  $\text{cm}^{-1}$  and 1633  $\text{cm}^{-1}$ . This indicates that the calcium stearate, having a long alkyl chain, is susceptible to oxidation catalysed by the presence of the CuCl.

In the presence of the phosphite, ALKANOX<sup>®</sup>240, the band at 1633  $\text{cm}^{-1}$  increases slightly then decreases after 5 minutes, whilst the bands at 1660 and 1645  $\text{cm}^{-1}$  decrease throughout the

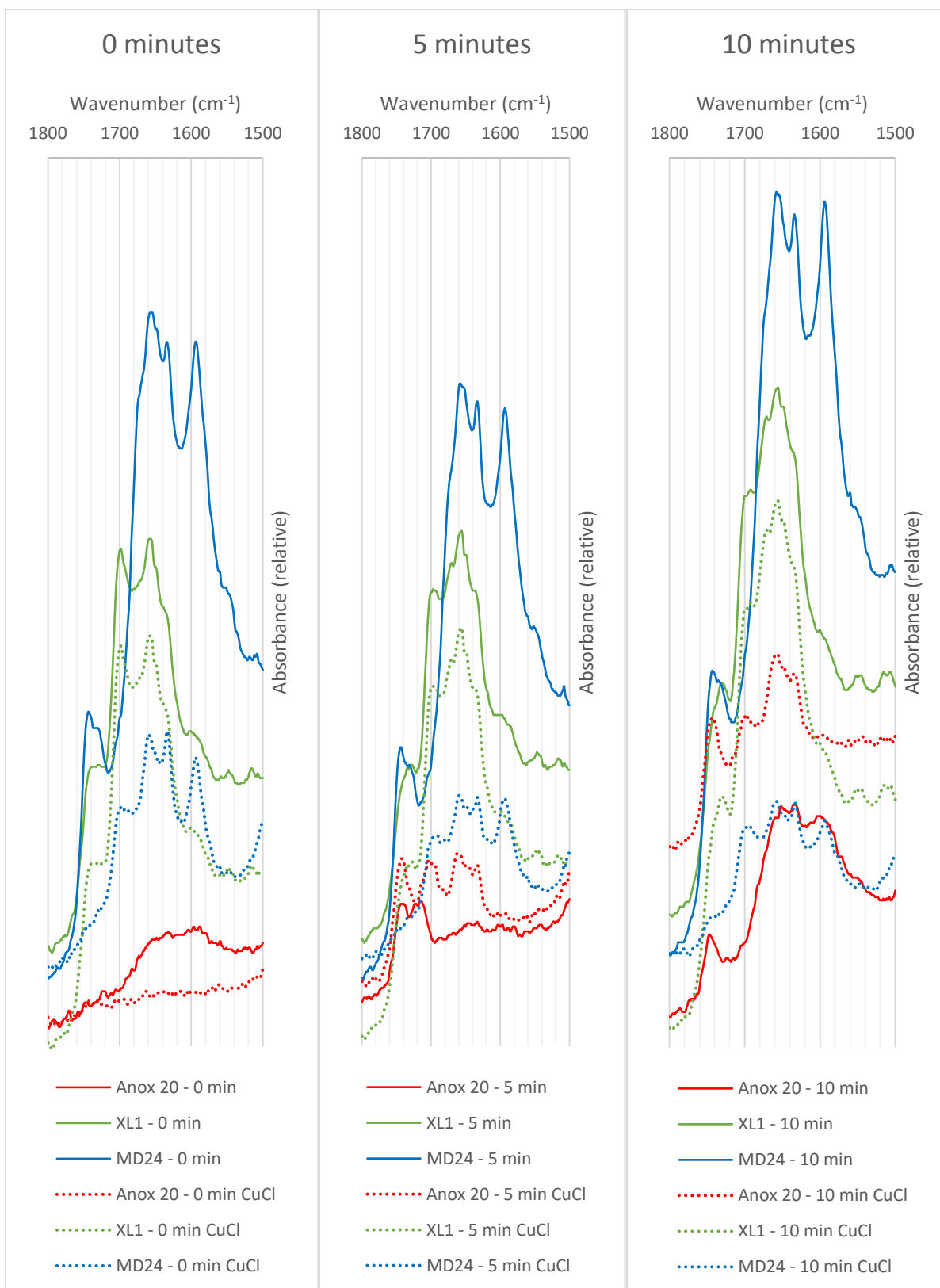


**Figure 3-5:** FTIR spectra (1800-1500 cm<sup>-1</sup>) of Anox 20, Naugard XL-1 and Lowinox MD24 in LDPE extruded for 0, 5 and 10 minutes without and with CuCl

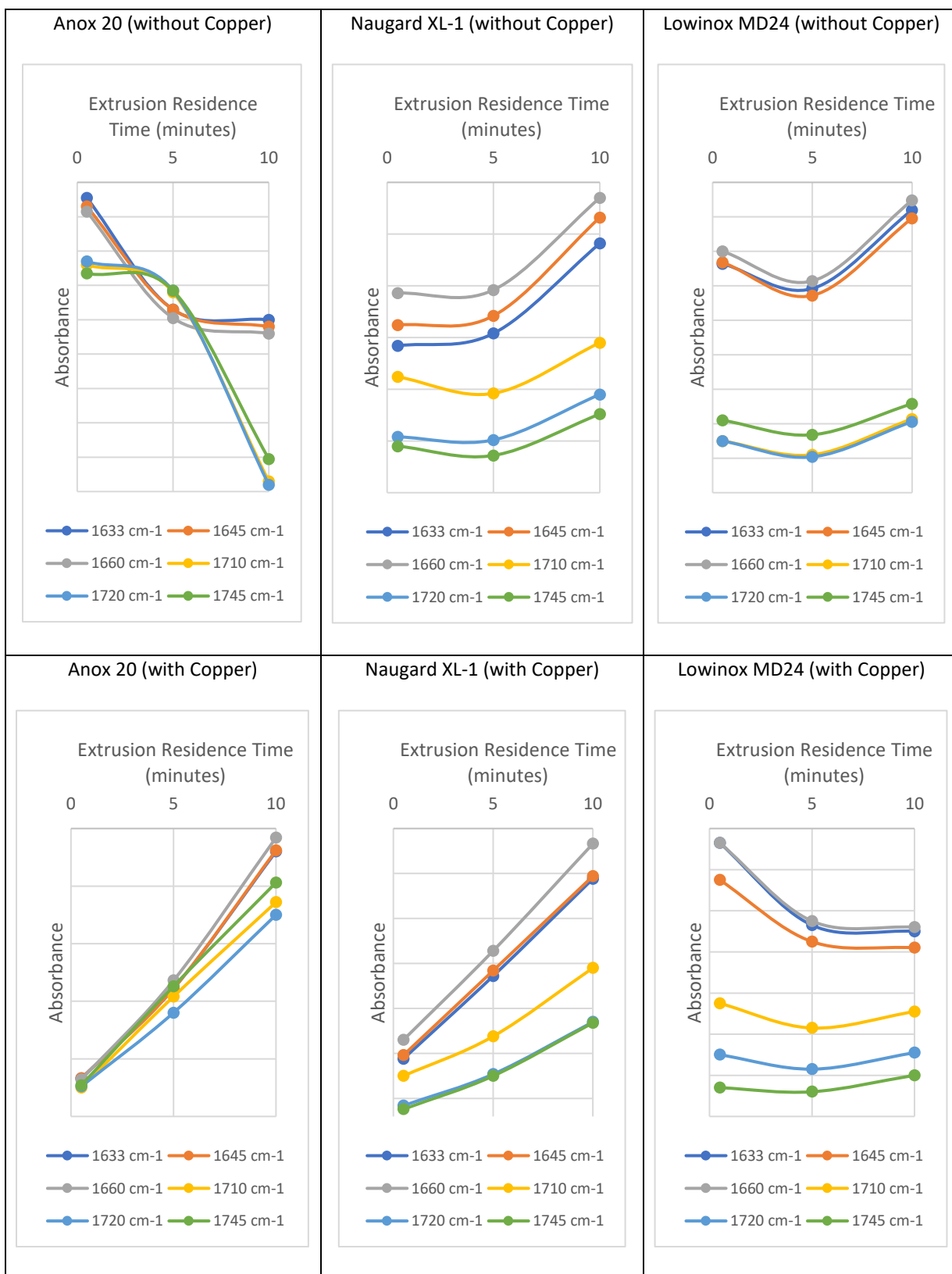
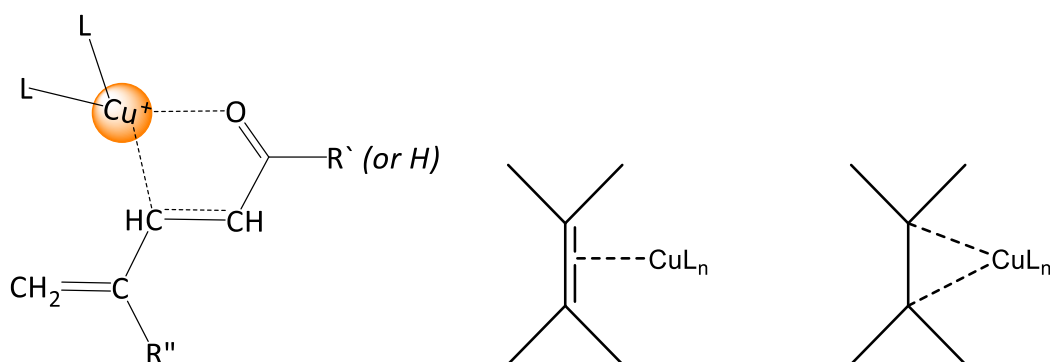


**Figure 3-6:** FTIR absorption intensities of carbonyl and unsaturated species for Anox 20, XL1 and MD24 in LDPE extruded for 0, 5 and 10 minutes without and with CuCl

processing time. In contrast the C=O bands decrease dramatically in the first 5 minutes then increase dramatically from 5-10 minutes. In the presence of copper, the ester band is more pronounced after 10 minutes extrusion. The decrease in the absorptions in the absence and presence of copper, although the latter is less pronounced, confirm the ability of ALKANOX®240 to decompose peroxides. However, without the combination of a primary antioxidant it is relatively ineffective after the initial stages of oxidation.

In the absence of copper ANOX®20 shows the opposite (mirror image) behaviour to that of ALKANOX®240 with respect to oxidation. Here the concentration of unsaturation/unsaturated carbonyls decreases, since at low oxidation levels phenol is an effective scavenger of peroxy radicals. Because the levels of peroxide are not able to build-up during this initial period, the level of carbonyls in the 1700-1750  $\text{cm}^{-1}$  band remain relatively constant. After 5 minutes, there is a rapid decrease in the absorptions of carbonyls (ketones, esters, carboxylic acids), demonstrating that ANOX®20 is a superior antioxidant to ALKANOX®240.

The rapid build-up of unsaturation/unsaturated carbonyls after 10 minutes extrusion for LDPE, followed by a rapid decrease in these bands may be due to their association with copper and its ligands. It is known that the polymerisation copper can inhibit the polymerisation of MVK (methyl vinyl ketone) by coordination with copper (**Scheme 3-8**). This would be of interest because copper may be bound by both the novel metal deactivators in this study in competition with binding to unsaturated carbonyls.



**Scheme 3-8** Coordination of copper with unsaturated carbonyls

The LDPE+LOWINOX<sup>®</sup>MD24 formulation showed an ester stretch at 1745 cm<sup>-1</sup> in all samples extruded for 0, 5 and 10 minutes which disappeared in the presence of copper. However, a peak can be seen at 1698 cm<sup>-1</sup> as a result of the presence of carbonyl C=O. In addition to this, alkene C=C (1659 cm<sup>-1</sup>, 1633 cm<sup>-1</sup>) and conjugated diene absorptions (1594 cm<sup>-1</sup>, not present in LDPE alone) appeared after 10 minutes.

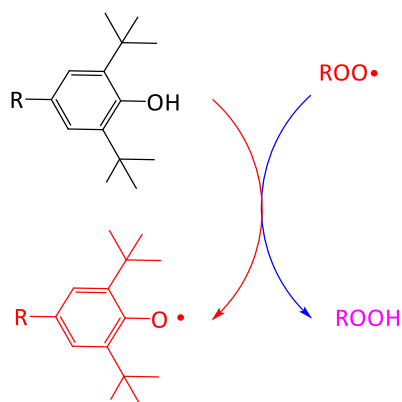
In contrast for LDPE + NAUGARD<sup>®</sup>XL-1 formulations, ester; carbonyl C=O and alkene C=C stretches were evident in the presence and absence of CuCl and, a small absorption attributed to conjugated dienes was seen in formulations containing CuCl. In addition, an absorption band at 1696 cm<sup>-1</sup> was present in both treated and untreated LLDPE+ NAUGARD<sup>®</sup>XL-1 formulations due to the presence of a weak ester link in this additive, where chain scission could lead to the formation of aldehyde.

### 3.1.3 FTIR spectra of Commercial-Series antioxidants and metal deactivators and their copper complexes

To better understand the performance of the Commercial-Series structures in LDPE, their ability to complex with copper was assessed by mixing an excess of the copper salts with the ligand and precipitating out the complex from methanol followed by filtration and drying. FTIR spectra (and in some cases <sup>1</sup>H NMR spectra) were then obtained for these samples.

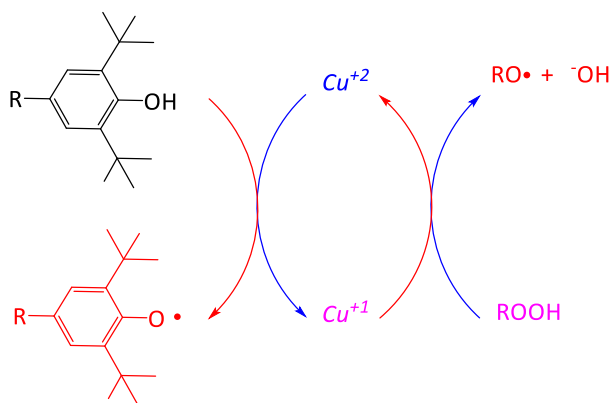
As stated earlier, although these experiments were not performed on base commercial stabilisers, there is evidence in the literature to corroborate the formation of their complexes with copper

The normal antioxidant role of hindered phenols is to scavenge peroxy radicals, but hindered phenols can participate in other redox mechanisms (**Scheme 3-9**). Phenols interact strongly with Cu<sup>2+</sup> (hard Lewis acid) via Fenton type reactions. Cu<sup>+</sup> has little affinity for phenols being a soft Lewis acid.



**Scheme 3-9** Removal of peroxy radicals by hydrogen atom transfer (HAT) from a hindered phenol

The one of interest here being the redox decomposition of peroxide in the presence of copper (**Scheme 3-10**). Here  $\text{Cu}^+$  is regenerated through redox conversion of the phenol to a resonance stabilised phenoxyl radical. In effect this process decreases the concentration of the phenol available for the removal of active peroxy radicals.



**Scheme 3-10** Regeneration of  $\text{Cu}^+$  by redox reaction with hindered phenol

EXAFS spectroscopy has shown that phosphite copper(I) complexes are tetrahedral with Cu–P bond distances in the range 2.24–2.28 Å in both solution and solid state. A regular tetrahedral configuration has been proposed based on the fact that  $[\text{Cu}(\text{P}(\text{OC}_6\text{H}_5)_3)_4]^+$  is  $^{63}\text{Cu}$  and  $^{65}\text{Cu}$  NMR silent.

In the case of CaSt, metal exchange reactions have been cited. Whilst the CaSt is an acid scavenger in the presence of metal ions, like copper it can exchange to form the metal stearates, which act as pro-oxidants. There is the possibility that both copper (I) stearate  $[\text{Cu}(\text{C}_{18}\text{H}_{35}\text{O}_2)]$  or copper (II) stearate  $[\text{Cu}(\text{C}_{18}\text{H}_{35}\text{O}_2)_2]$  may be formed.

The binding mode of *LOWINOX*<sup>®</sup>*MD24* and *NAUGARD*<sup>®</sup>*XL-1* to copper (II) ions is given in **Figure 3-7**. Coordination was confirmed by the shift in the stretching vibration of C=O ( $1661\text{ cm}^{-1}$ ) towards a lower frequency range ( $1601\text{ cm}^{-1}$ ). The ester C=O stretch appeared in the same absorption range ( $1731\text{ cm}^{-1}$ ) in *NAUGARD*<sup>®</sup>*XL-1* and its complex. A shift of the N-H band in the *Cu-LOWINOX*<sup>®</sup>*MD24* complex from  $3240\text{ cm}^{-1}$  to lower absorption frequency  $3217\text{ cm}^{-1}$  suggested that this site was coordinated to the central metal ( $\text{Cu}^{2+}$ ) by transferring its proton to the oxygen atom of the carbonyl group. Similarly, the band due to N-H stretch in the *Cu-NAUGARD*<sup>®</sup>*XL-1* complex was shifted from lower frequency ( $3242\text{ cm}^{-1}$ ) to higher frequency ( $3356\text{ cm}^{-1}$ ) on coordination showing the involvement of the nitrogen atom by transferring its proton to the oxygen atom of carbonyl group as shown in **Figure 3-8**.

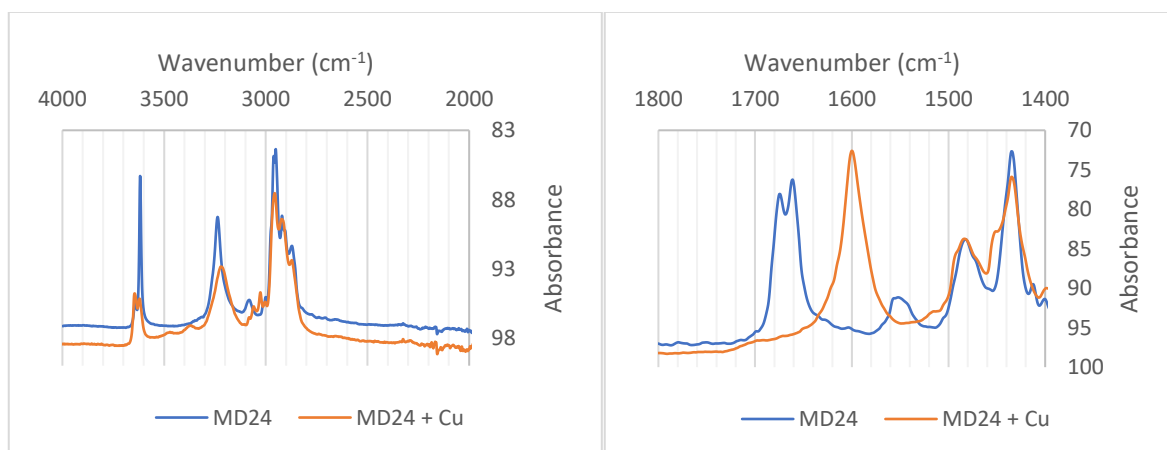


**Figure 3-7** FTIR spectra of *Cu-LOWINOX*<sup>®</sup>*MD24* and its copper complex

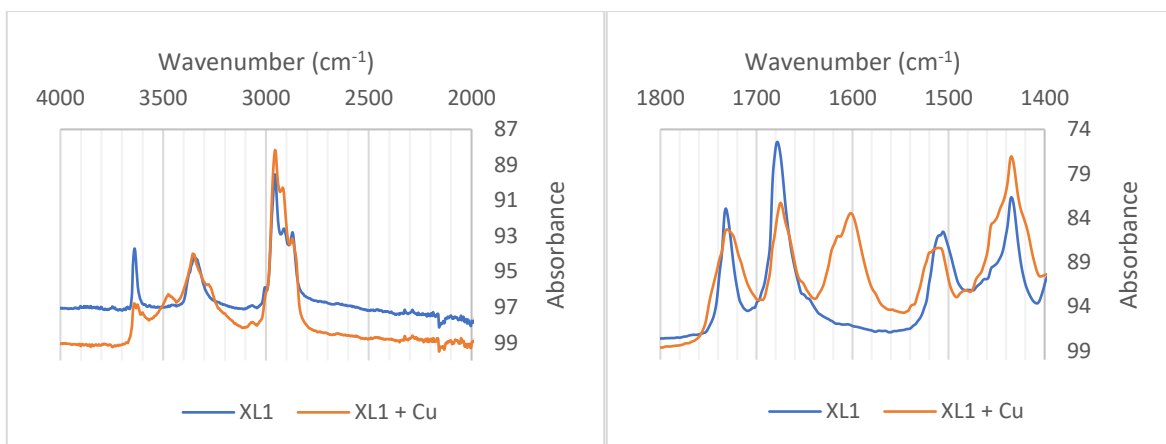
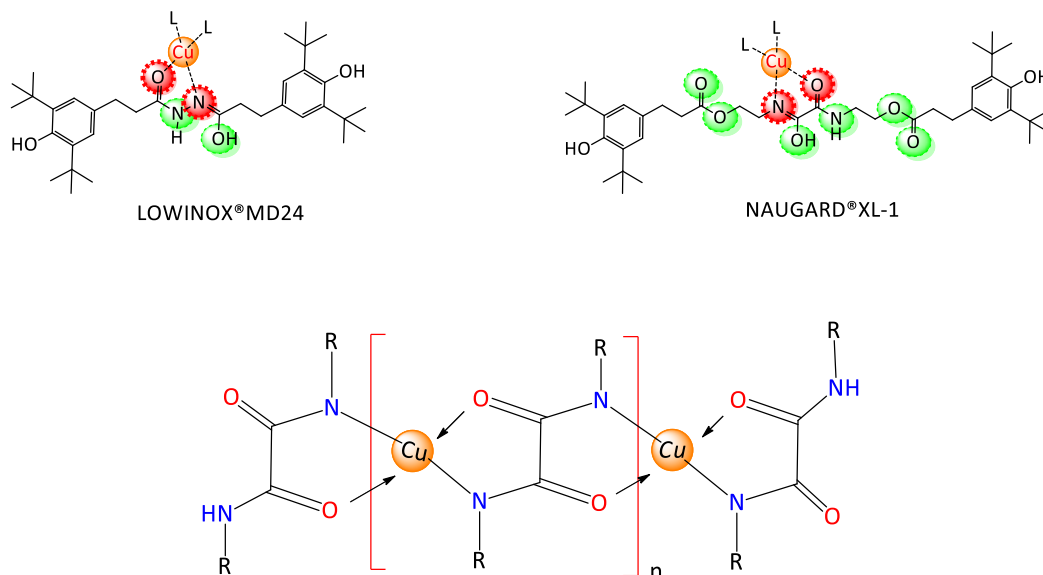


**Figure 3-8** FTIR spectra of Cu-NAUGARD<sup>®</sup>XL-1 and its copper complex

Metal-complex formation of LOWINOX<sup>®</sup>MD24 has already been described in the literature<sup>138</sup> using differential scanning calorimetry and thermogravimetric analysis. The likely modes of binding to copper in LOWINOX<sup>®</sup>MD24 and NAUGARD<sup>®</sup>XL-1 are given in **Scheme 3-11**:

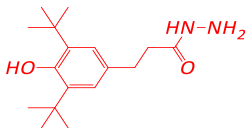
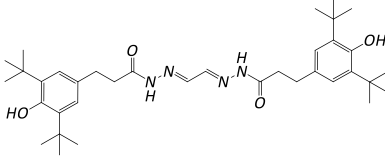
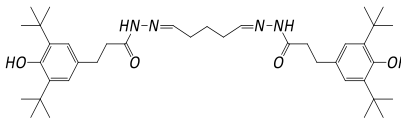
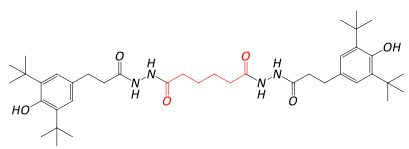
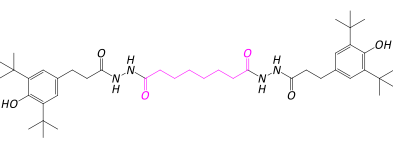
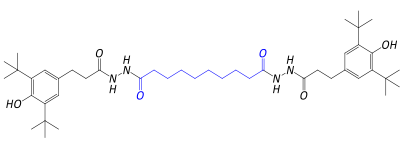
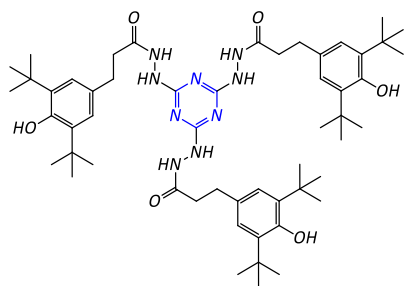
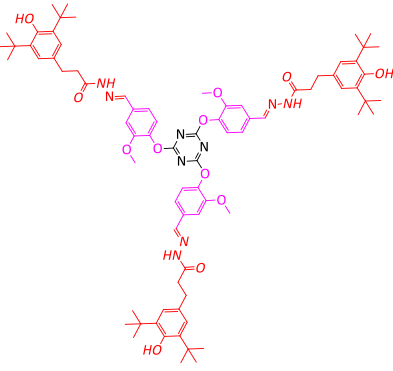
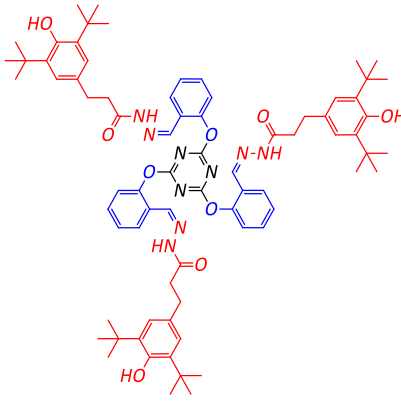


**Scheme 3-11** Structures of copper complexes of LOWINOX<sup>®</sup>MD24 and NAUGARD<sup>®</sup>XL-1

Overall, the performance data is consistent with that given for these commercial additives throughout the literature and so lends confidence to the extrusion methodology used here.

### 3.2 Novel Stabilizer Performance (S-Series)

The S-Series AO/MDs are analogues of *3,5-di-tert-butyl-4-hydroxyhydrocinnamic acid hydrazide*. This presents the possibility of intra-molecular hydrogen bonding or, coordination with copper thereby modifying the antioxidant activity of the molecule. Again, the hindered phenol possessing potential antioxidant activity is linked by hydrazide groups with different spacers e.g. alkyl chains of varying length or a triazine ring.

 <p style="text-align: center;"><b>S0</b> (292 g mol<sup>-1</sup>, m.p.156-160°C)</p>	 <p style="text-align: center;"><b>S1</b> (607 g mol<sup>-1</sup>, m.p.275-277°C)</p>	 <p style="text-align: center;"><b>S2</b> (649 g mol<sup>-1</sup>, m.p.98-102°C)</p>
 <p style="text-align: center;"><b>S3</b> (695 g mol<sup>-1</sup>, m.p.224°C)</p>	 <p style="text-align: center;"><b>S4</b> (723 g mol<sup>-1</sup>, m.p.178°C)</p>	 <p style="text-align: center;"><b>S5</b> (751 g mol<sup>-1</sup>, m.p.168°C)</p>
 <p style="text-align: center;"><b>S6</b> (952 g mol<sup>-1</sup>, m.p.179-183°C)</p>	 <p style="text-align: center;"><b>S7</b> (1355 g mol<sup>-1</sup>, m.p.155-160°C)</p>	 <p style="text-align: center;"><b>S8</b> (1265 g mol<sup>-1</sup>, m.p.125-130°C)</p>

### 3.2.1 MFI and Yellowness Index (S-Series)

**Figures 3-9 and 3-10** show the changes in MFI of the MD-Series structures, relative to LDPE. The ranking of the MD-Series with respect to MFI follows the order:

Without copper: **S5** << S7 < S1 < S0 < S2  $\cong$  S8 < S6 < S4 < S3

With Copper: **S5** < S0  $\cong$  S6 < S8  $\cong$  S2 < S1  $\cong$  S4 < S3 < S7

All the MFI values for S-Series molecules increase with extrusion time, except S5 which decreases, to a value lower than that for the commercial metal deactivators (*LOWINOX<sup>®</sup>MD24* and *NAUGARD<sup>®</sup>XL-1*). S5 therefore exhibits improved antioxidant behaviour in comparison to the commercial metal deactivators.

In the presence of copper, the antioxidant performance is reduced for S5, but it remains comparable with the commercial antioxidants and the best performance of the S-Series antioxidant-metal deactivators. The MFI of all the molecules decreases with extrusion time, except S7.

The performance of S3 is the poorest of the S-Series both in the absence and presence of copper.

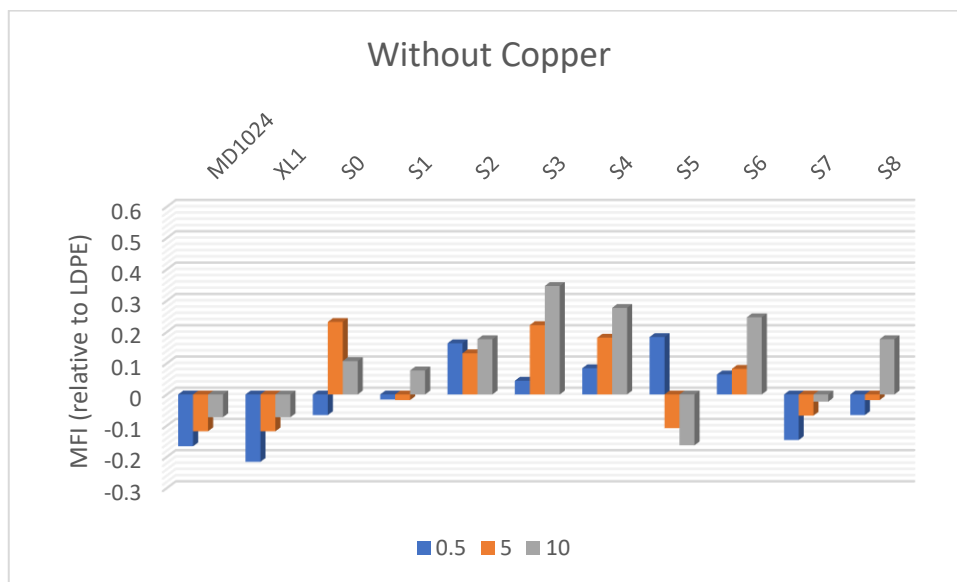


**Figure 3-9** MFI of S-Series formulations in LDPE extruded for 0, 5 and 10 minutes without CuCl (*s.d* = 0.01 g/10 min)

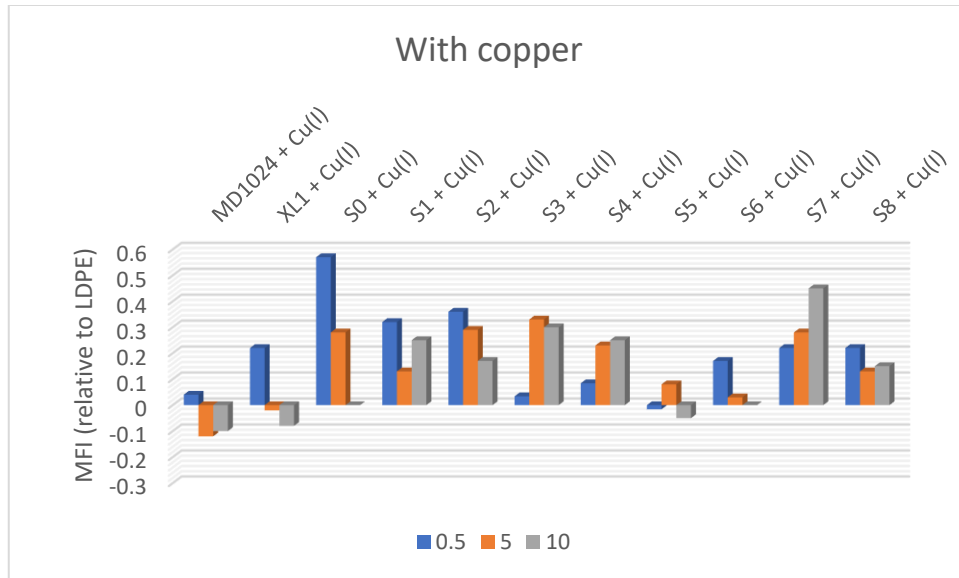


Figure 3-10 MFI of S-Series formulations in LDPE extruded for 0, 5 and 10 minutes with CuCl (s.d = 0.01 g/10 min)

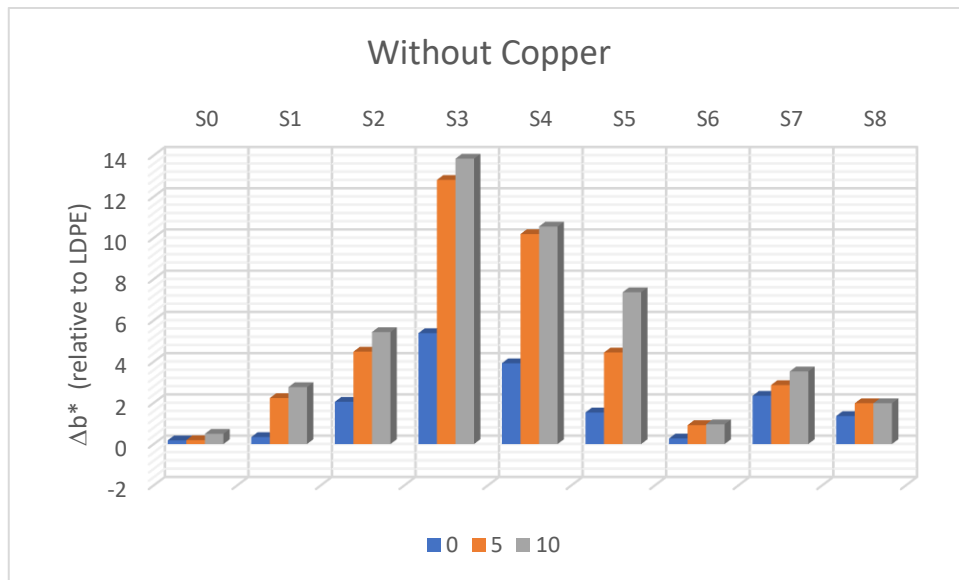
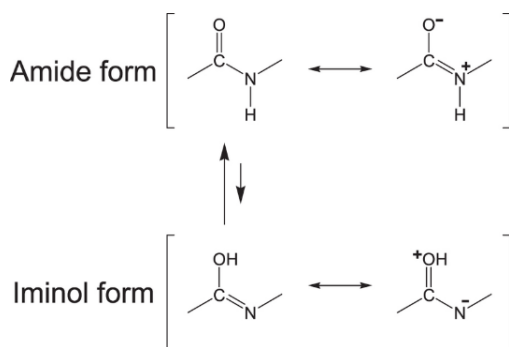
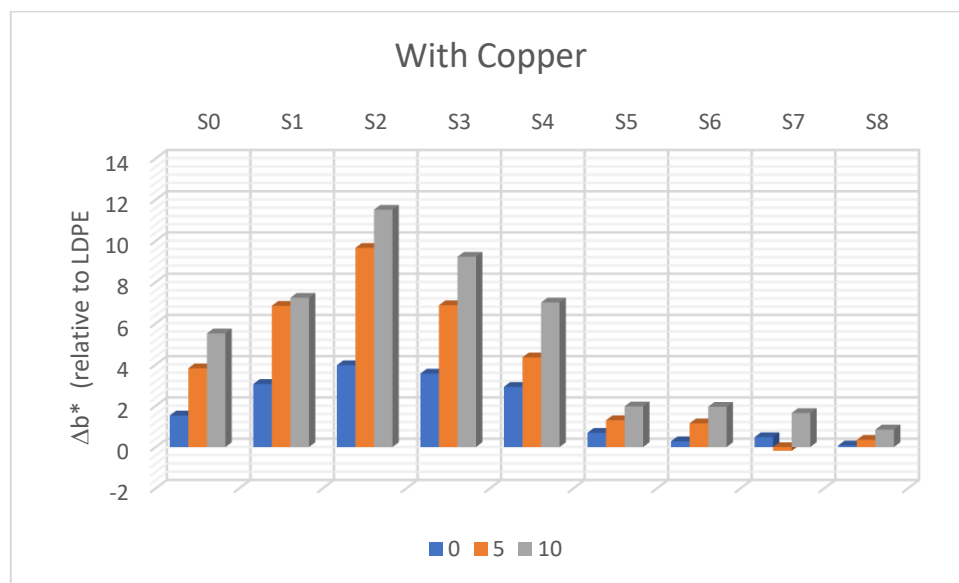


Figure 3-11 Yellowing ( $\Delta b^*$ ) of S-Series formulations in LDPE extruded for 0, 5 and 10 minutes without CuCl (s.d = 0.04)

In the absence of copper, the  $\Delta b^*$  value is very high for S3 and S4. Since colour usually arises from transformations of the antioxidant, this suggests that the phenol has been oxidised to quinone. Also, if there is tautomerism of the amide to iminol, this would give extended conjugation in these structures (**Scheme 3-12**). For S5 the  $\Delta b^*$  value is significantly lower, suggesting that this does not take place, or to the same extent.

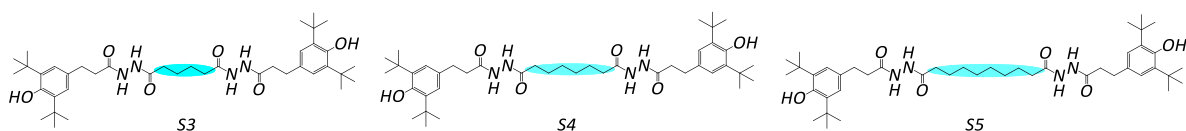


**Scheme 3-12** Amide-Iminol tautomerism



**Figure 3-12** Yellowness ( $\Delta b^*$ ) of S-Series formulations in LDPE extruded for 0, 5 and 10 minutes with CuCl ( $s.d = 0.04$ )

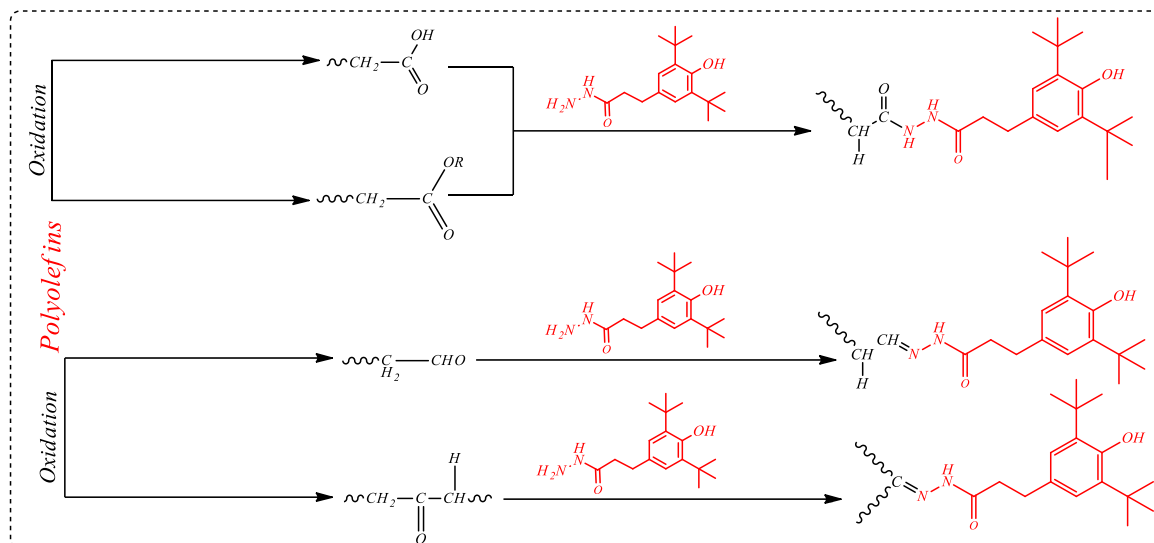
In the presence of copper, the  $\Delta b^*$  value is reduced, providing evidence that the extended conjugation is not present to the same degree. Here the disparity in performance of S3 and S5 is very clear, with the S5 showing a much greater reduction in yellowness. In general, there is an inverse relationship between yellowness ( $\Delta b^*$ ), MFI and the number of carbon atoms joining two azide groups as shown in the chemical structures below



### 3.2.2 FTIR Analysis of S-Series Antioxidants and Metal Deactivators in LDPE

**Figure 3-13 and 3-14** show the FTIR spectra of **S0** in the range  $1800\text{-}1500\text{ cm}^{-1}$  and the rates of change of functional groups respectively. A broad band at  $1545\text{ cm}^{-1}$  (NH stretch out of plane) and a sharp band at  $1633\text{ cm}^{-1}$  (amide) arise from the additive. In the latter case this band is superimposed on the band due to conjugated dienes associated with carbonyl groups. In the absence of copper, a band at  $1720\text{ cm}^{-1}$  due to the carbonyl group of aldehydes/ketones/carboxylic acids decreases throughout the extrusion time. The intensities of alkene C=C ( $1659\text{ cm}^{-1}$ ,  $1633\text{ cm}^{-1}$ ) bands remain very low, confirming the excellent performance of additive (**S0**) in the formulation (**Figure 3-13**).

The additive **S0** with its active -OH and amino groups can act as an antioxidant and metal and a metal deactivator. The phenolic part contributes towards trapping free radicals while the terminal amino group can bind copper ion and carbonyl compounds such as ester, aldehyde, ketones and carboxylic acids (**Scheme 3-13**)



**Scheme 3-13** Reaction of ester, aldehydes, ketones and carboxylic acids by the additive **S0**

For **S0** in the presence of copper the reduction of the band at  $1720\text{ cm}^{-1}$  (**Figure 3-13**) and the rapid decrease in the band at  $1633\text{ cm}^{-1}$  (**Figure 3-14**) suggests that the reactions with aldehydes and ketones may be taking place, or that the **S0** is effectively binding copper to prevent the cage reactions that lead to these species. The reduction in the band at  $1540\text{ cm}^{-1}$  is further evidence for this.

The performance of additive **S1** in LDPE in the absence of CuCl was good (low absorbance  $1600\text{-}1750\text{ cm}^{-1}$ ), but it could not slow down the degradation in the presence of CuCl as shown in **Figure 3-13** and **Figure 3-14**. The intensity of ester-stretch ( $1745\text{ cm}^{-1}$ ) present in samples extruded for 0, 5 and 10 minutes remained high in the samples extruded for 0, 5 and 10 minutes in the presence of CuCl. This could be due to the presence of a double bond between carbon and donor nitrogen ( $\text{-C=N}$ ), the distance between them ( $\text{-N=C-C=N-}$ ) and the fact that Schiff bases can revert to their original components during processing.

In contrast, for **S2** the most notable change in the absence of copper is the increase in intensity of the broad band at  $1600\text{ cm}^{-1}$ . In the presence of copper, the band at  $1600\text{ cm}^{-1}$  is less pronounced. This is accompanied by an increase in the ester band from 5-10 minutes. This suggests that **S2** is

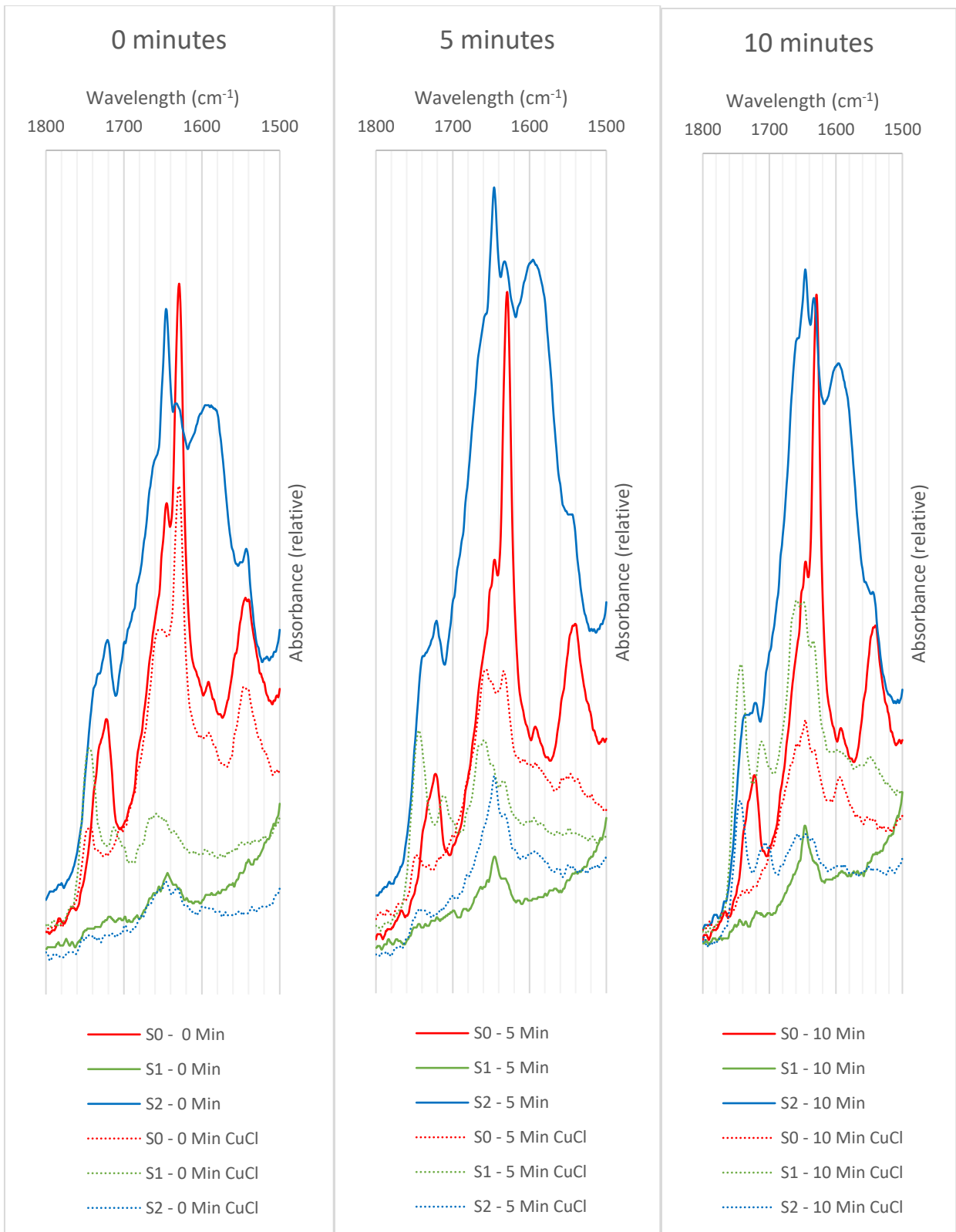


**Figure 3-13:** FTIR spectra (1800-1500 cm<sup>-1</sup>) of S0, S1 and S2 in LDPE extruded for 0, 5 and 10 minutes without and with CuCl

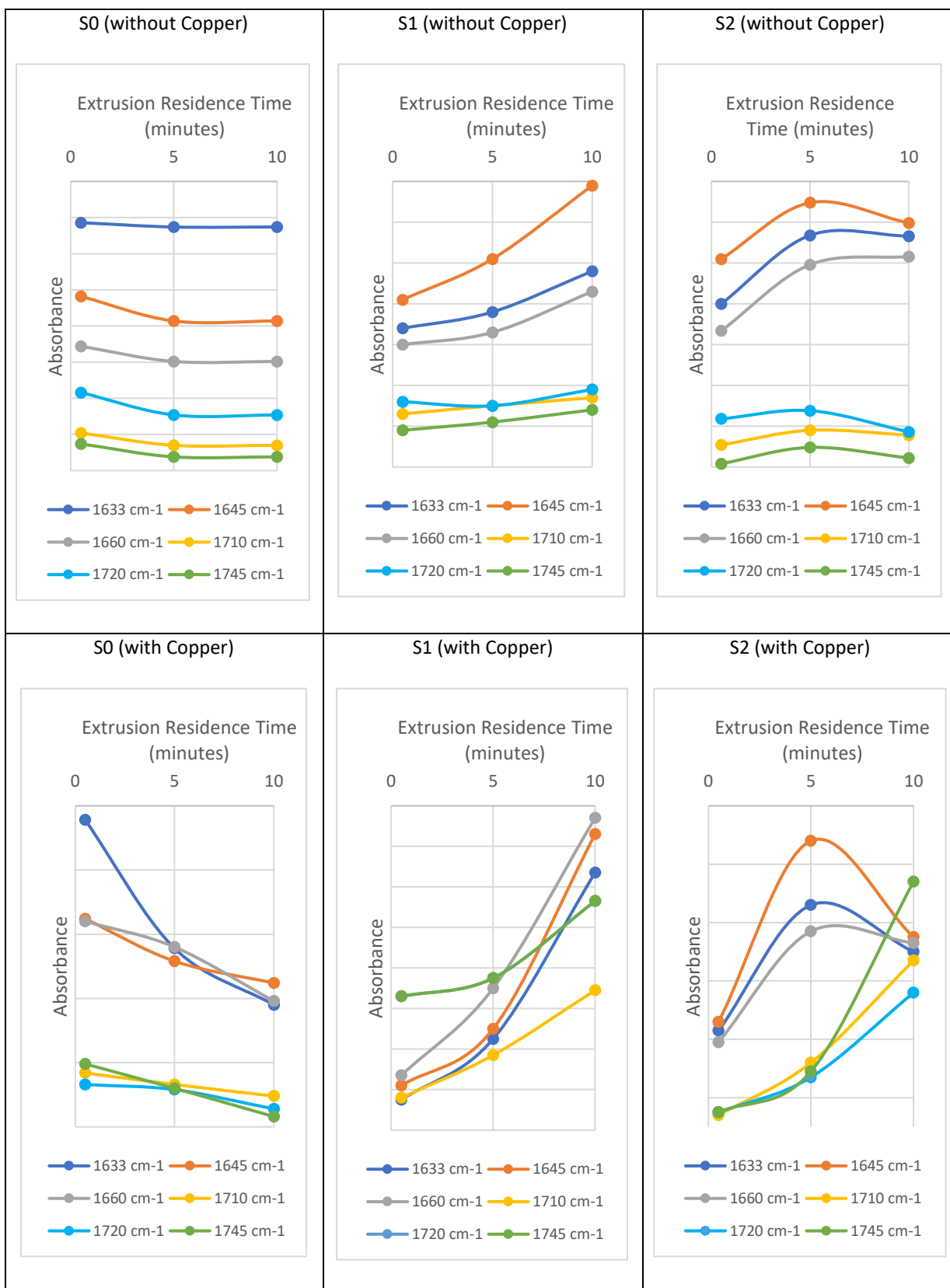


**Figure 3-14:** FTIR absorption intensities of carbonyl and unsaturated species for S0, S1 and S2 in LDPE extruded for 0, 5 and 10 minutes without and with CuCl

unable to prevent the cage recombination of peroxy radicals. This is consistent with the MFI values showing that **S1** and **S2** are less effective metal deactivators than **S0**.

Comparison of changes between the three structures **S3** to **S5** and the effect of chain length is further confirmed by the FTIR spectra (**Figures 3-15 and 3-16**). Spectra for **S3** in the presence of copper show the  $1633\text{cm}^{-1}$  (unsaturated carbonyls) is the mirror of the ester band at  $1745\text{ cm}^{-1}$ , whereas for **S4** the ester band decreases with time. The poor antioxidant performance of **S3** and **S4** is seen not just in the broad bands in the FTIR spectra, signifying the presence of a range of oxidised species (**Figures 3-15**), but in the high MFI values relative to LDPE demonstrating significant chain-scission has taken place (**Figure 3-9**). For **S3** the high intensity of the band at  $1600\text{ cm}^{-1}$  in the presence of copper suggests a high level of unsaturation

In contrast for **S5** the bands increase to 5 minutes then decrease. What is notable from the rates of change of key functional groups is that this effective metal deactivator for copper shows a rapid increase in absorptions in the range  $1600\text{-}1750\text{ cm}^{-1}$  and hence growth of oxidised species in the initial stages of degradation, but this is followed by a rapid reduction in these bands. This suggests there is a time lag to the effective operation of **S5** and this is also seen in the changes in MFI (**Figure 3-8**). Although, in the absence of copper, **S5** can inhibit growth of oxidised species in the first 5 minutes of extrusion (**Figure 3-16**), it is not a particularly effective antioxidant after this. Furthermore, the initial level of unsaturated groups ( $1633\text{ cm}^{-1}$  and  $1660\text{ cm}^{-1}$ ) is relatively high which is consistent with the initial MFI value being higher than LDPE in the absence of copper (**Figure 3-9**).

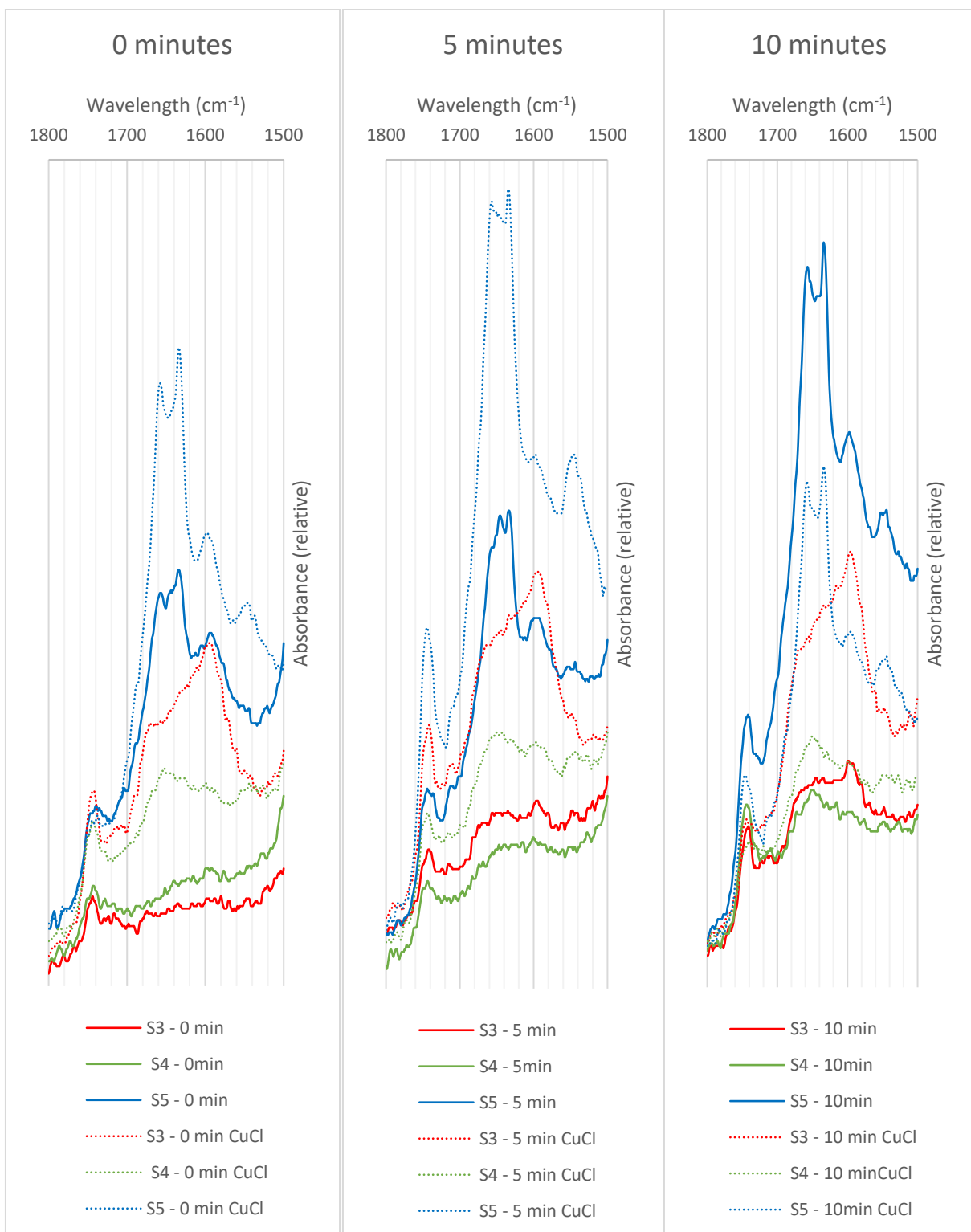


**Figure 3-15:** FTIR spectra ( $1800\text{-}1500\text{ cm}^{-1}$ ) of S3, S4 and S5 in LDPE extruded for 0, 5 and 10 minutes without and with CuCl

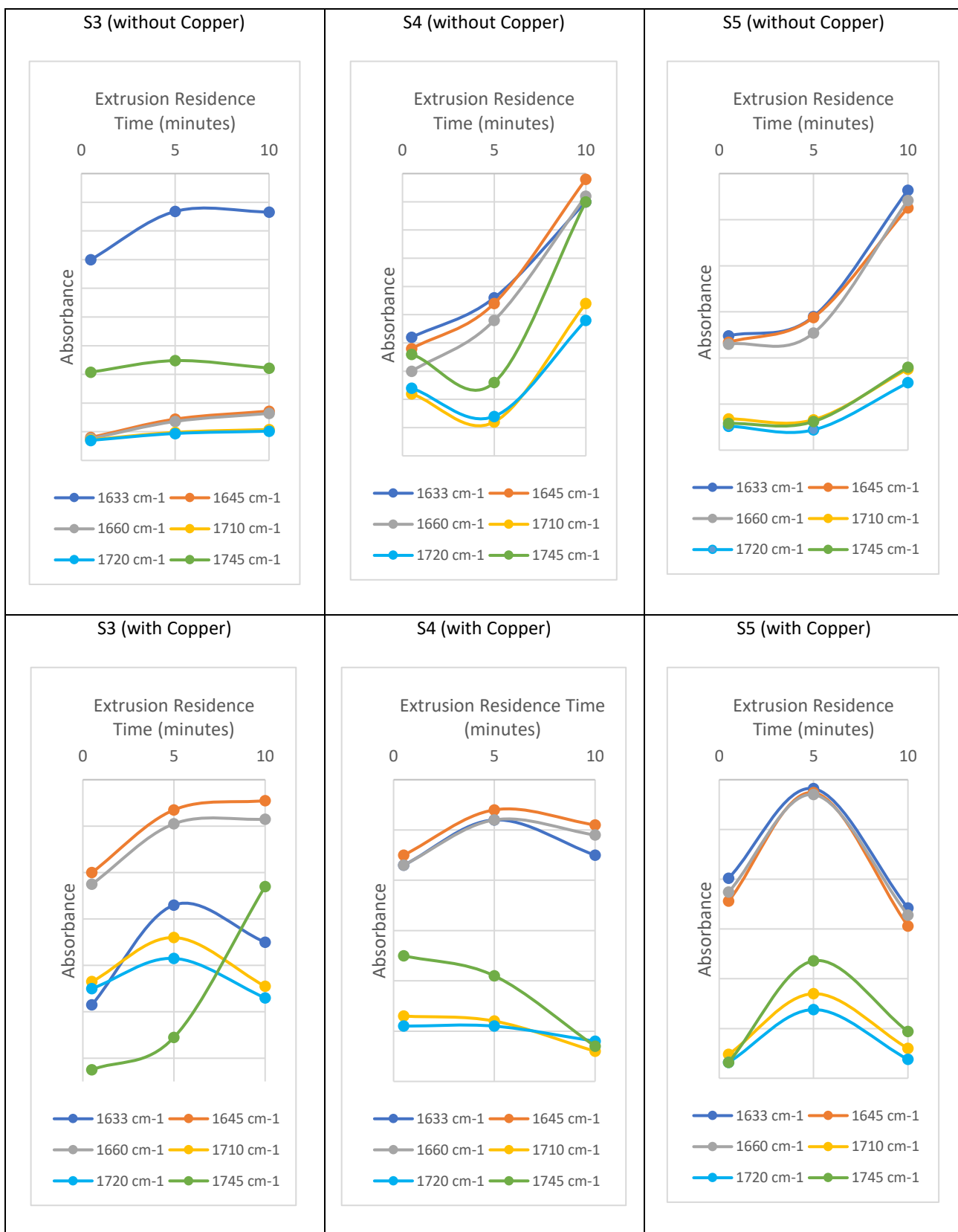


**Figure 3-16:** FTIR absorption intensities of carbonyl and unsaturated species for S3, S4 and S5 in LDPE extruded for 0, 5 and 10 minutes without and with CuCl

For **S6**, **S7** and **S8**, (*Figures S-17 and S-18*) the hydrazide groups are linked by a triazine ring. Usually this structure offers greater thermal stability. We might expect the higher molar ratio of phenol groups to give better antioxidant performance and this is indeed the case in the absence of copper for **S7**, but less so for **S6** and **S8**. This can be explained by the presence of the methoxy group, which is an effective radical scavenger, enhancing the antioxidant performance of **S7**.

In the presence of copper **S8** shows a strong absorption due to the carboxylic C=O vibrational stretch at  $1720\text{ cm}^{-1}$ , which decreases significantly during the extrusion degradation time. In the presence of copper, the ability of **S6** to chelate copper adjacent to the triazine ring is effective in metal deactivation. This also explains the intermediate behaviour of **S8**, which does not possess the methoxy group like its **S7** analogue, suggesting that performance is a careful balance between the ability of the structure to act as an antioxidant and/or metal deactivator.

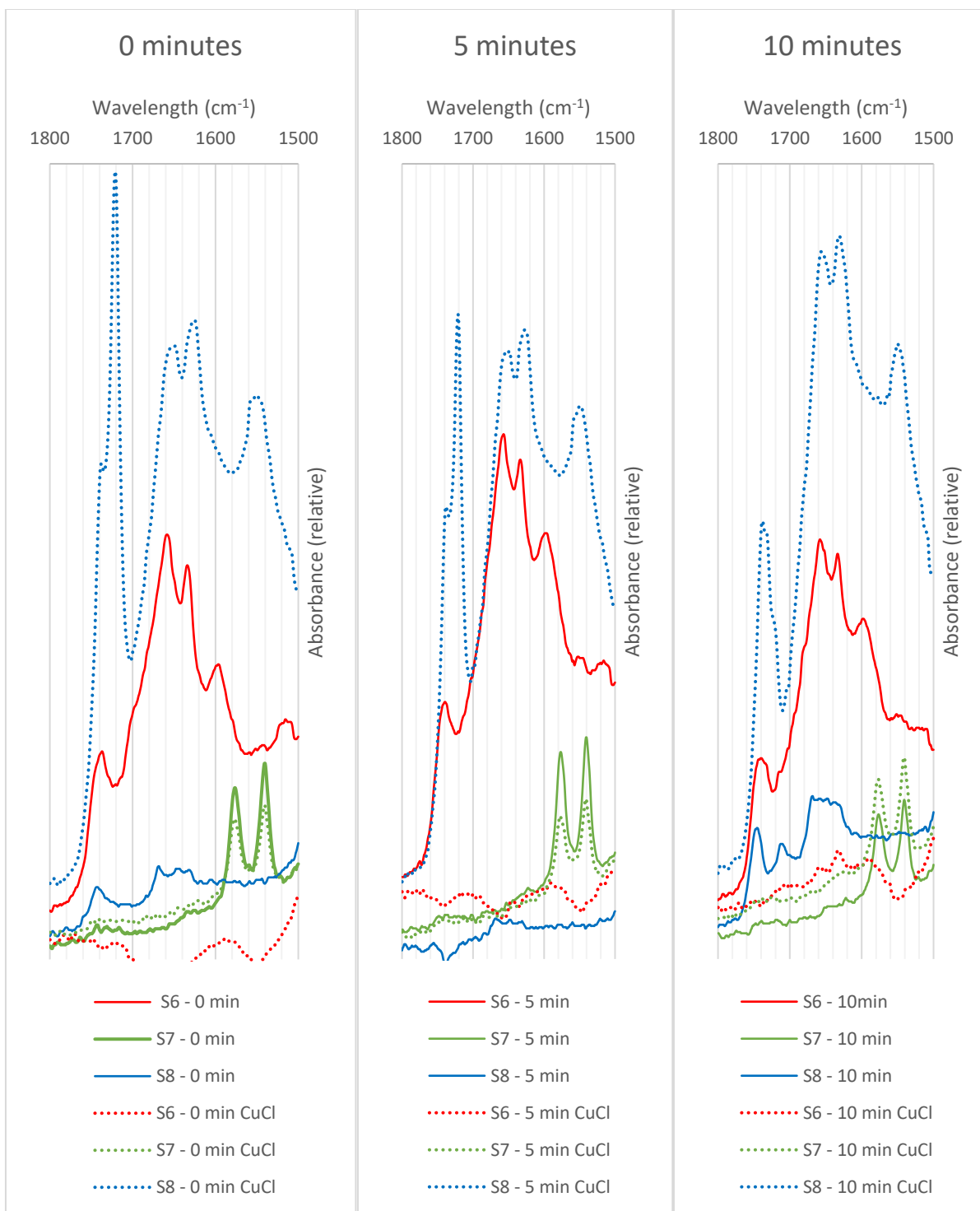


**Figure 3-17:** FTIR spectra (1800-1500  $\text{cm}^{-1}$ ) of S6, S7 and S8 in LDPE extruded for 0, 5 and 10 minutes without and with CuCl

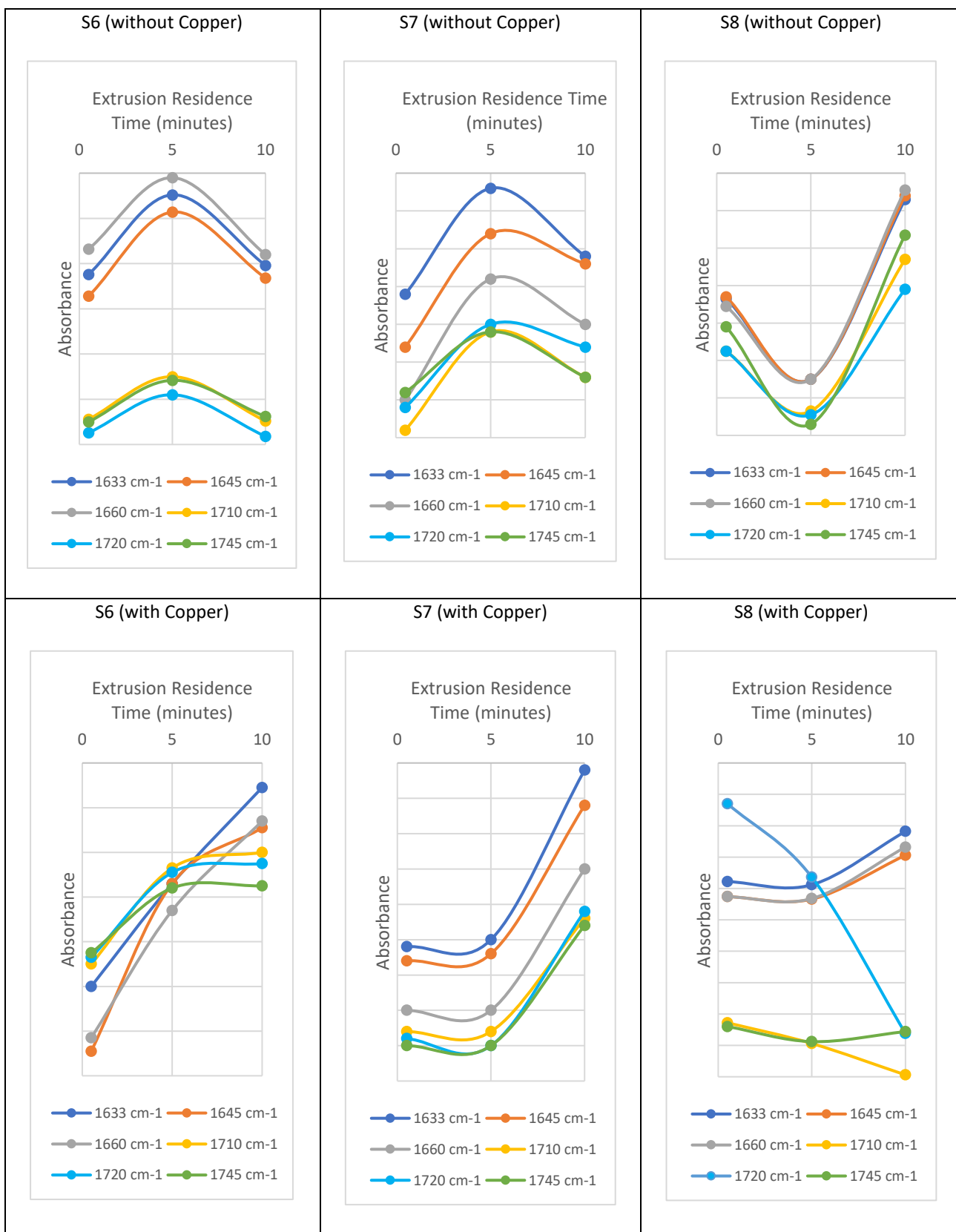


**Figure 3-18:** FTIR absorption intensities of carbonyl and unsaturated species for S6, S7 and S8 in LDPE extruded for 0, 5 and 10 minutes without and with CuCl

### 3.2.3 FTIR spectra of S-Series antioxidants and metal deactivators and their copper complexes

The performance of **SO** was also supported by the  $^1\text{H}$ NMR,  $^{13}\text{C}$ NMR and FTIR (**Figure 3-19**). FTIR spectra shows that azide C=O stretch shifted from  $1626\text{ cm}^{-1}$  to  $1704\text{ cm}^{-1}$ , NH out of plane shifted from lower frequency ( $1540\text{ cm}^{-1}$ ) to a higher frequency ( $1599\text{ cm}^{-1}$ ). In the FTIR spectrum of the free ligand, the  $\text{NH}_2$  stretch is seen at  $3329\text{ cm}^{-1}$ , whereas in the complex it appeared at  $3363\text{ cm}^{-1}$ . The phenolic (-OH) proton remained unaltered upon coordination.

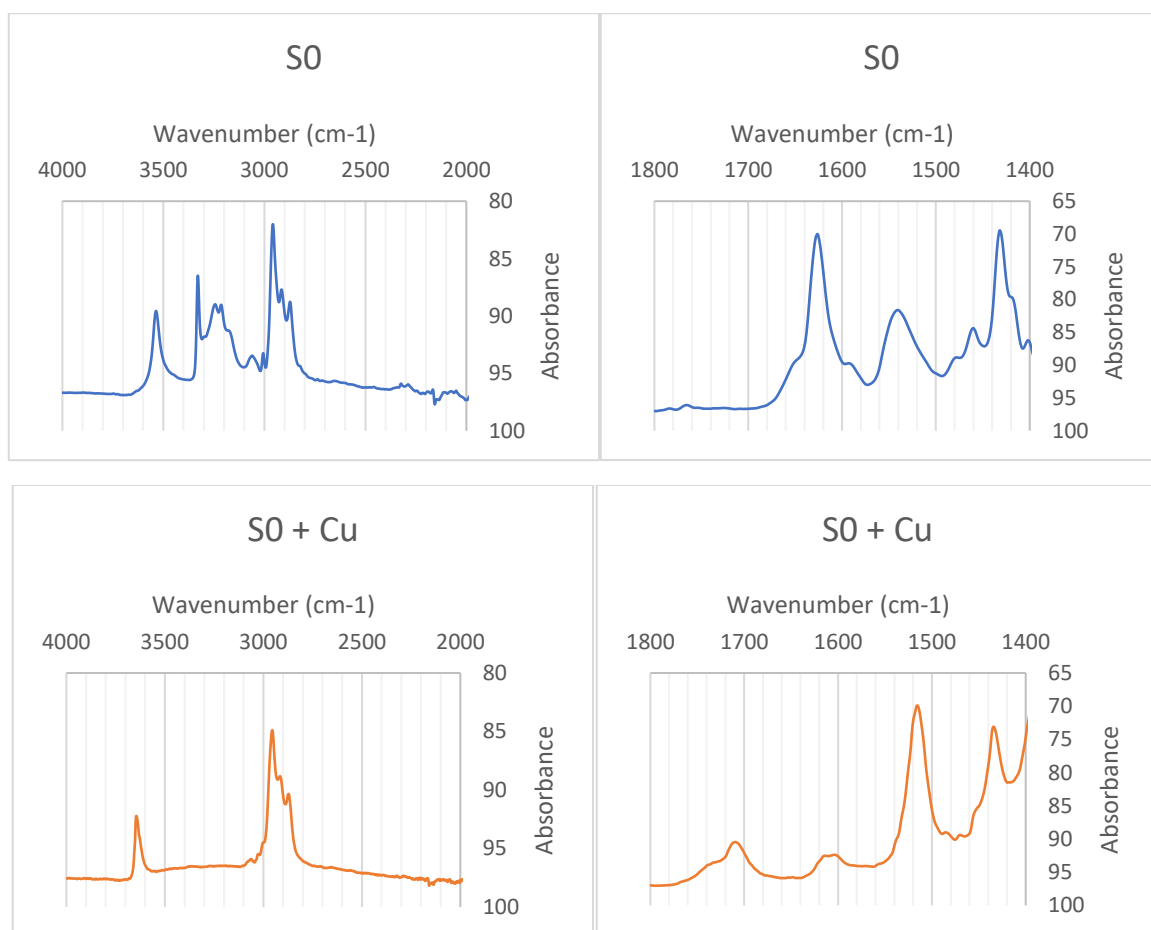


**Figure 3-19** FTIR spectra of free ligand **SO** and its copper complex

$^1\text{H}$ NMR and  $^{13}\text{C}$ NMR spectral observations of the copper chloride/copper acetate complexes of **SO** demonstrate that only two sites are taking part in chelation. In the complex, selective proton and carbon line broadening were observed. This might be due to the large enhancement of transverse relaxation rates, resulting from scalar coupling between the copper unpaired electron and the **SO**

proton and carbon nuclear magnetic moments. The hydrogens most affected included NH and terminal amino group, although the four protons (-CH<sub>2</sub>-) were also somehow affected. The participation of carbonyl C=O was judged by the chemical shift of carbon atom from ( $\delta$ 172.27) to ( $\delta$ 138.20), although two carbon (-CH<sub>2</sub>-) were also somehow affected. Proton shifts (black) and carbon shifts (red) can be seen in the chemical structure of ligand and complex below.

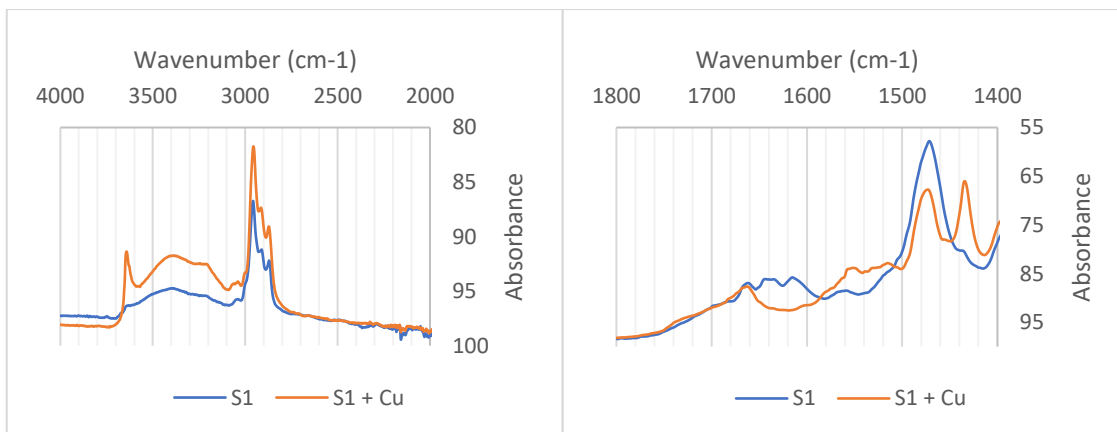


**Figure 3-20** FTIR spectra of free ligand *S1* and its copper complex

For *S1* normal C=N and NH absorptions are noted but their intensity was very weak as given in **Figure 3-20**. <sup>1</sup>HNMR data of *S1* and *S1-Cu* complex showed that NH hydrogen resonated at the same frequency (6.54ppm) in both molecules. The azomethine proton (HC=N-) was affected and disappeared due to the nitrogen atom involvement in the chelation. The phenolic (-OH) and ethylene protons are found in the same resonating frequency range. This reveals that the NH, and carbonyl C=O are not taking part in coordination in agreement with the FTIR results.

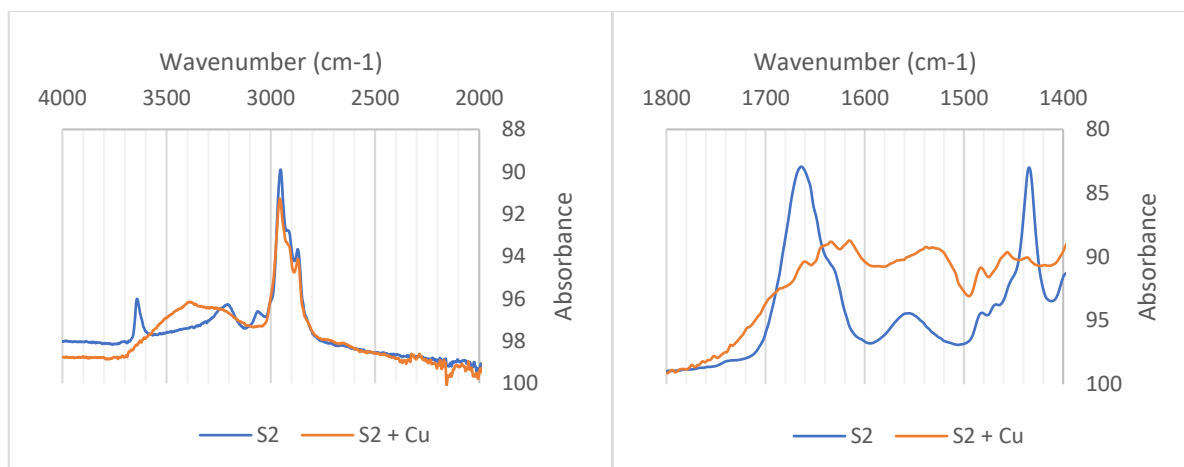


**Figure 3-21** FTIR spectra of free ligand **S2** and its copper complex

For **S2**, a normal N-H stretching vibration is observed at  $3225\text{ cm}^{-1}$  as a broad band. This band shifted towards lower frequency ( $3210\text{ cm}^{-1}$ ) upon metal complex formation for the related ligand. The N-H out of plane stretching vibration was observed at  $1555\text{ cm}^{-1}$  in the ligand and shifts towards lower frequency ( $1517\text{ cm}^{-1}$ ) in the complex. The azide (C=O) absorption is also affected and the shifting of bands from  $1666\text{ cm}^{-1}$  to a lower absorption frequency ( $1608\text{ cm}^{-1}$ ) suggested that C=O group was also coordinated to a metal atom as shown in **Figure 3-21**.

The data obtained from  $^1\text{H}$  NMR spectroscopic studies provides support to the binding mode of the ligand's coordinating sites.  $^1\text{H}$ NMR data of **S2** and **S2-Cu** complexes showed that the position of proton attached to a nitrogen atom (NH) in the ligand (9.44ppm) shows a downfield shift (6.54ppm) in complexation with the binding of a copper ion by the neighbouring chelation sites (N and C=O).

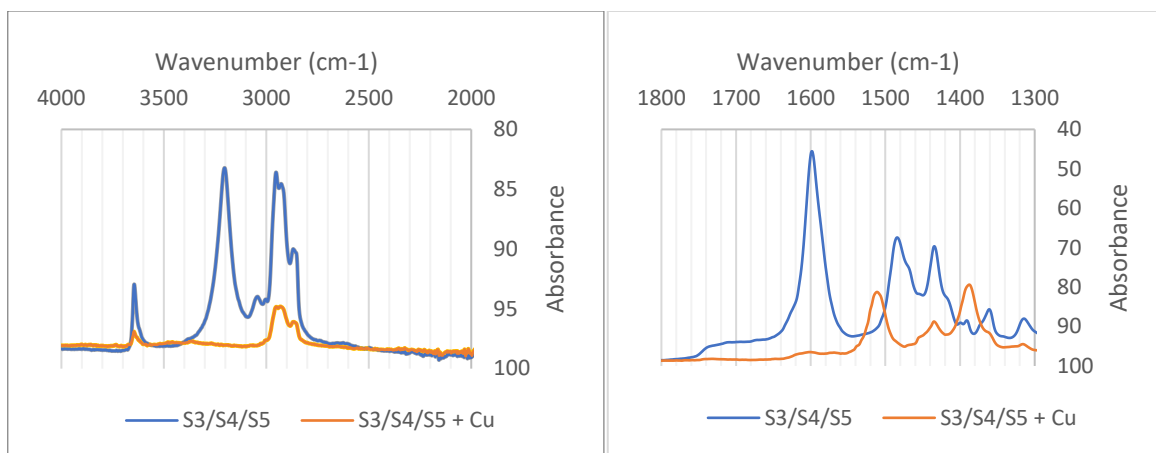
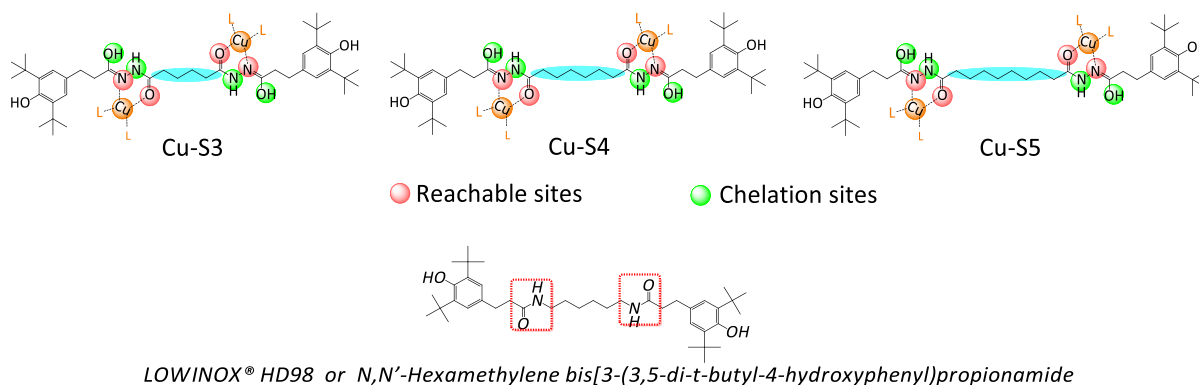


**Figure 3-22** FTIR spectra of free ligands S3/S4/S5 and their copper complex

When complexed with copper, free ligands (**S3**, **S4** and **S5**) displayed intense bands of two symmetrical azide C=O groups at  $1601\text{ cm}^{-1}$  and shifted towards lower frequency range ( $1512\text{ cm}^{-1}$ ) by accepting a proton (-C-OH) from the -NH- site. The NH absorption stretch at  $3205\text{ cm}^{-1}$  showed changes in absorption intensity and shifted to a higher frequency range ( $3252\text{ cm}^{-1}$ ) as shown in **Figure 3-22**.

To better understand the coordination geometry and stability of the S3/S4/S5-copper complexes, a commercial additive (*LOWINOX<sup>®</sup> HD98*) was studied since it has some common structural characteristics with the S3, S4 and S5 molecules. *LOWINOX<sup>®</sup> HD98* is *N,N'*-Hexamethylene bis[3-(3,5-di-*t*-butyl-4-hydroxyphenyl)propionamide] which acts as an antioxidant but not as a metal deactivator. Analytical information showed that the Cu-*LOWINOX<sup>®</sup> HD98* complex was not formed because of its chemical structure (see structure below).



$^1\text{H}$  NMR spectroscopic studies showed the chemical shift of -NH protons from 9.71ppm to 8.2ppm, in addition to this, the signals of bridged-ethylene protons shifted from  $\delta$ 1.55 to  $\delta$  3.1 and  $\delta$  2.12 to  $\delta$  4.0 in the complexes indicating that the NH attached to bridged-ethylene is associated with the central metal atom.

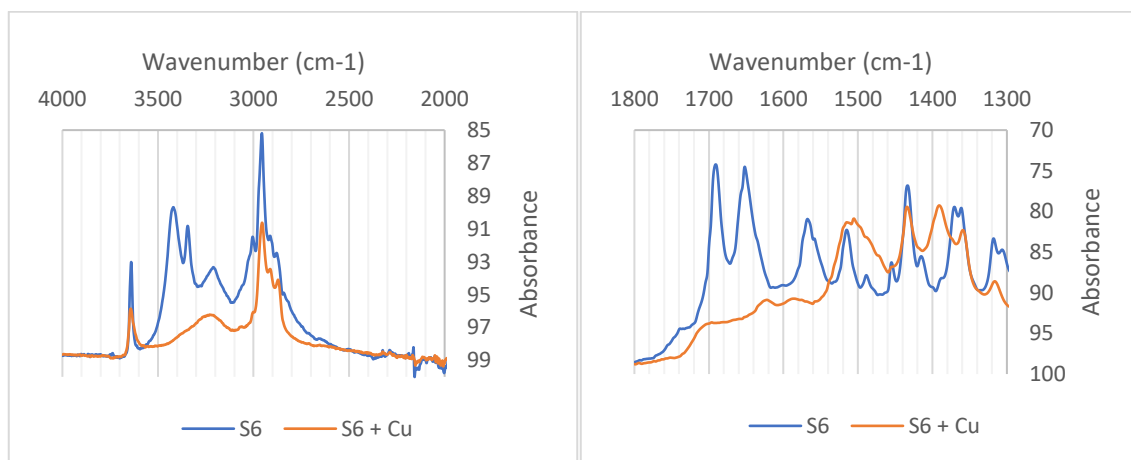
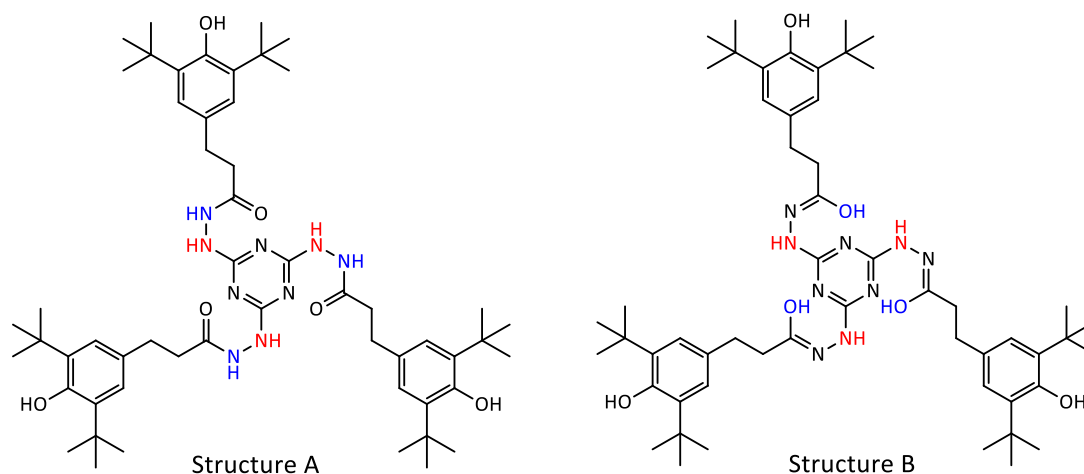


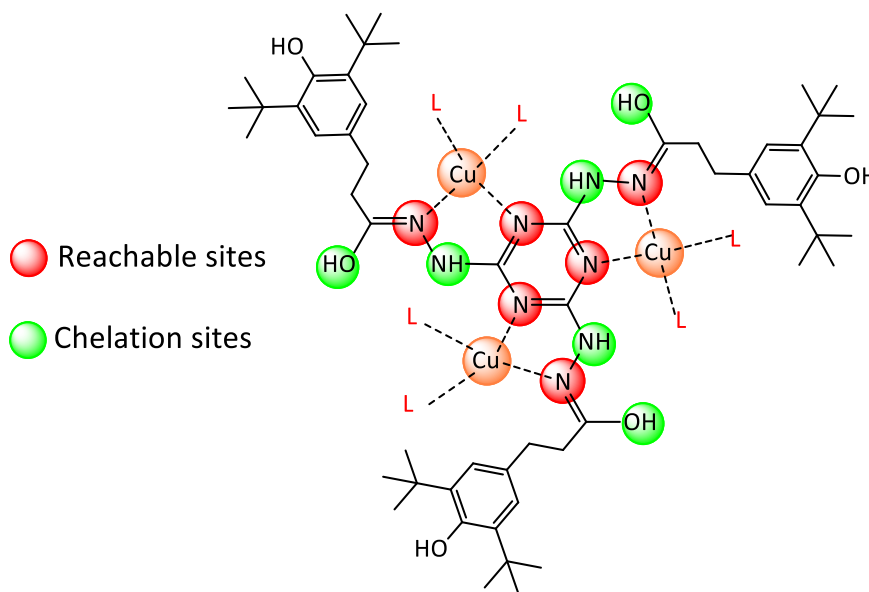
**Figure 3-23** FTIR spectra of free ligand **S6** and its copper complex

The performance of **S6**, **S7** and **S8** was further explored with the help of their ability to bind copper atoms. Free ligand **S6** had displayed intense bands of azide C=O at  $1691\text{ cm}^{-1}$  which disappear in the **Cu-S6** complex and appeared towards lower frequency range ( $1507\text{ cm}^{-1}$ ) by accepting a proton (C-OH) from -NH- site. The peak at  $1568\text{ cm}^{-1}$  and  $1370\text{ cm}^{-1}$  in the free ligand is assigned to the vibration of a triazine C=N and C-N respectively. The triazine C=N vibrational stretch disappears in the complex while C-N stretch showed a small band at  $1358\text{ cm}^{-1}$  (**Figure 3-23**).

In the free ligand **S6**, two different vibrational bands (-NH-) in the range between  $3312\text{ cm}^{-1}$  -  $3345\text{ cm}^{-1}$  were present but one band ( $3345\text{ cm}^{-1}$ ) disappeared due to the transfer of an N-H proton to the azide C=O group as shown in the chemical structure below.



A comparative  $^1\text{H}$ NMR spectral study of the free ligand **56** and its complex revealed that the N–H signal appears at 8.6 and 9.02 ppm in the  $^1\text{H}$  NMR spectrum of the free ligand and shifted to 9.0 and 9.28 ppm in the complex. The integration value confirms the allocation of amine protons to the azide  $-\text{C}=\text{O}$  in agreement with the IR results. A new signal appears at 5.2ppm which was assigned to a  $-\text{C}-\text{OH}$  group (structure B) and this indicates that the triazine ring is taking part in the coordination as shown below.



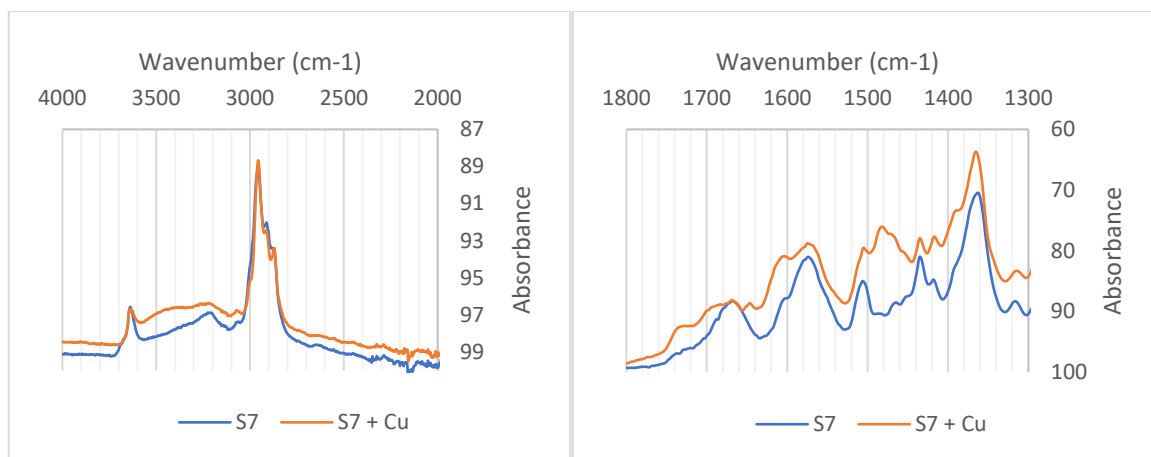
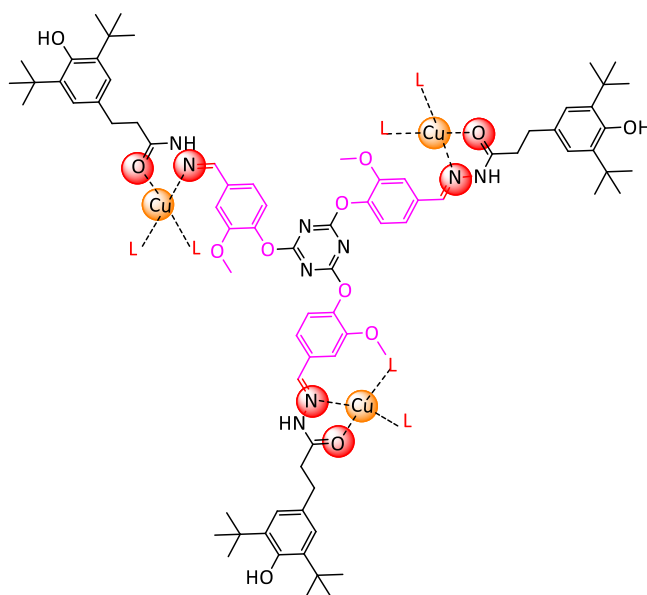


**Figure 3-24** FTIR spectra of free ligand **S7** and its copper complex

The free ligand **S7** had displayed strong bands of azide C=O at  $1667\text{ cm}^{-1}$  which disappeared upon coordination with the copper atom and appeared at a lower absorption range ( $1601\text{ cm}^{-1}$ ). The triazine vibrational stretch of C=N at  $1574\text{ cm}^{-1}$  and C-N at  $1366\text{ cm}^{-1}$  was observed in the normal range. This indicates that the triazine ring is not taking part in coordination as shown in **Figure 3-24**.

The FTIR spectra of the **Cu-S7** complex compared to the ligand also accounted for the involvement of the azide C=O and azomethine (-C=N) in coordination as shown in the chemical structure below.



A comparative  $^1\text{H}$ NMR spectral study of the free ligand **S7** and its complex revealed shift of the N–H signal from 8.53 to 5.41 ppm upon coordination of the C=O and C=N sites with copper.

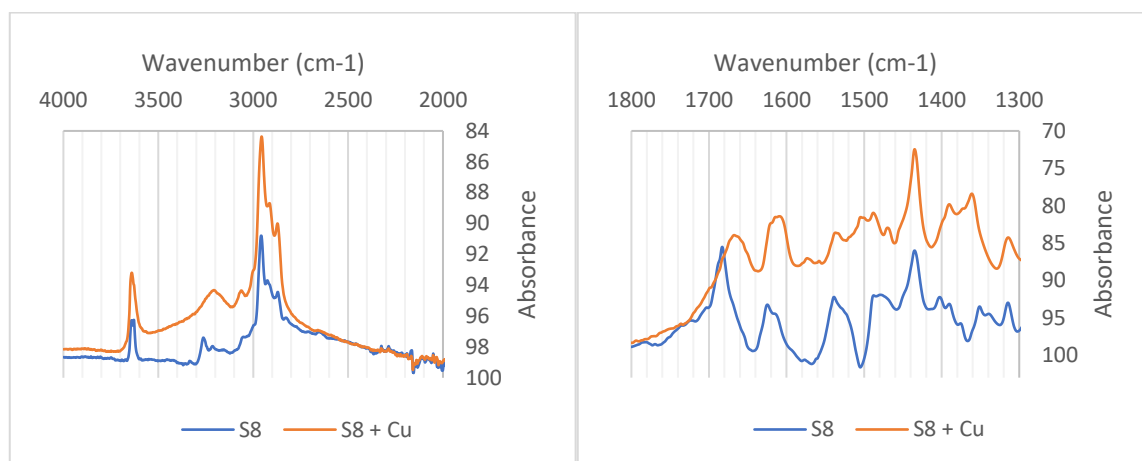
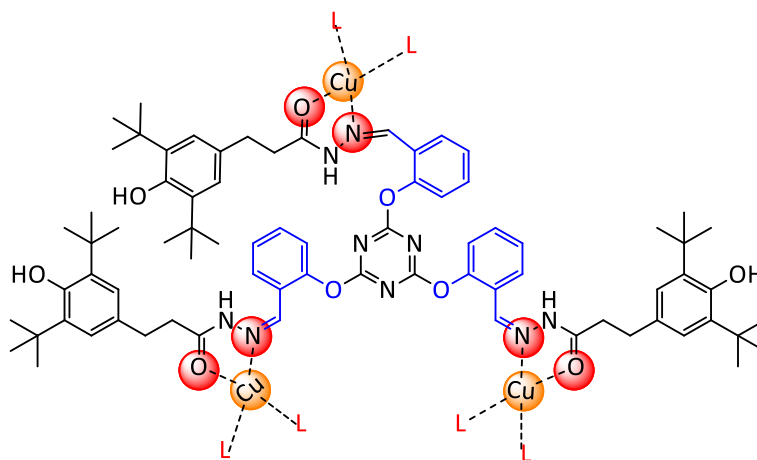


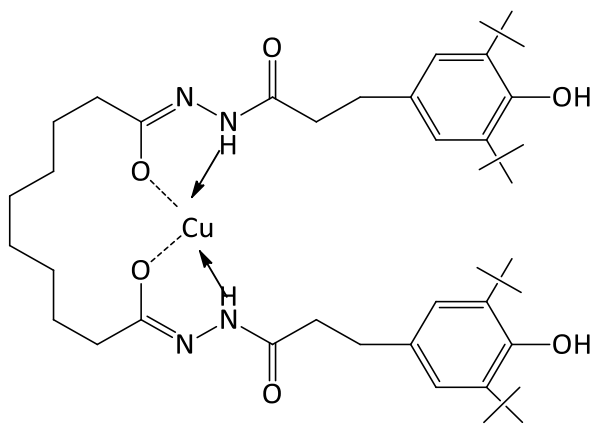
**Figure 3-25** FTIR spectra of free ligand **S8** and its copper complex

The free ligand **S8** displayed strong bands of azide C=O at  $1684\text{ cm}^{-1}$  which disappeared upon coordination with the copper atom and appeared at a lower absorption range ( $1601\text{ cm}^{-1}$ ). The azomethine stretch (C=N) at  $1624\text{ cm}^{-1}$  slightly shifted to lower stretching frequency ( $1615\text{ cm}^{-1}$ ). These changes in absorption stretches in the coordinated compound as compared to free ligand also accounted for the involvement of the azide C=O and azomethine (-C=N) in coordination as shown in the chemical structure below.



The stretching vibration of N-H proton shifted from  $3264\text{ cm}^{-1}$  to  $3192\text{ cm}^{-1}$  on the coordination of the C=O and C=N groups to the copper atom as shown in **Figure 3-25**. The  $^1\text{H}$ NMR spectrum of the free ligand **S8** and its complex revealed slight shifts for the N-H signal from 10.19 to 10.22 ppm upon coordination of the C=O and -C=N sites with copper.

For the S-Series several factors are involved in performance. For the group **S0**, **S1** and **S2** the relatively short links between the active functional groups restricts activity and the best stabiliser performance is seen for **S0**, which may coordinate in a 1:1 or 2:1 arrangement with copper. For the series **S3** to **S5** the superior performance of **S5** is attributed to the increased length of the alkyl chain coordinating the functional groups. Here 'back-biting' allows effective coordination of copper, but also leaves the phenol groups free to act as primary antioxidant:

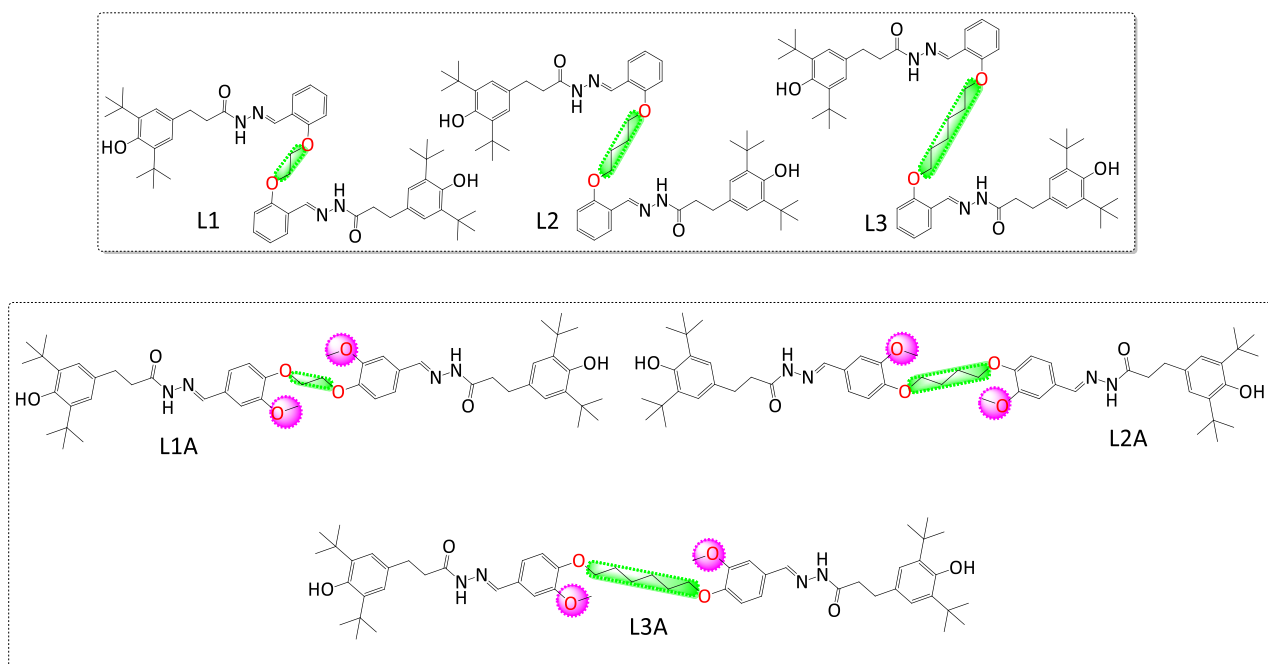


**S5**

For **S6**, **S7** and **S8** the spacer group coordinated to the triazine ring has a marked effect. For **S7** the superior antioxidant activity is attributed to a methoxy phenyl adjacent to the triazine ring. These groups are efficient hydroxyl radical scavengers. However, on coordination with copper at adjacent sites the activity of this group is rendered ineffective. For **S6** coordination with copper allows for the activity of phenol groups to scavenge peroxy and alkoxy radicals in conjunction with prevention of decomposition of peroxide to peroxy radicals afforded by complexation of **S6** with the oxidised copper.

### 3.3 Novel Stabilizer Performance (L-Series)

The L-Series AO/MDs are all hydrazides based on bis[3-(3,5-di-tert-butyl-4-hydroxyphenyl)propanehydrazide. Essentially, they are analogues of the commercial antioxidant MD24, they differ according to the length of a spacer (ethyl-bridge, butyl-bridge and hexyl-bridge) connecting the two functionalities. Here the influence of chain length on antioxidant versus metal deactivator capacity is assessed.



#### 3.3.1 MFI and Yellowness Index (L-Series)

**Figure 3-26** show the changes in MFI of the L-Series structures, relative to LDPE. The ranking of the L-Series with respect to MFI follows the order:

Without Copper:  $L3A < L1A < L2 \cong L3 \cong L2A < L1$

With Copper:  $L3 < L3A < L1A < L2A < L1 \cong L2$

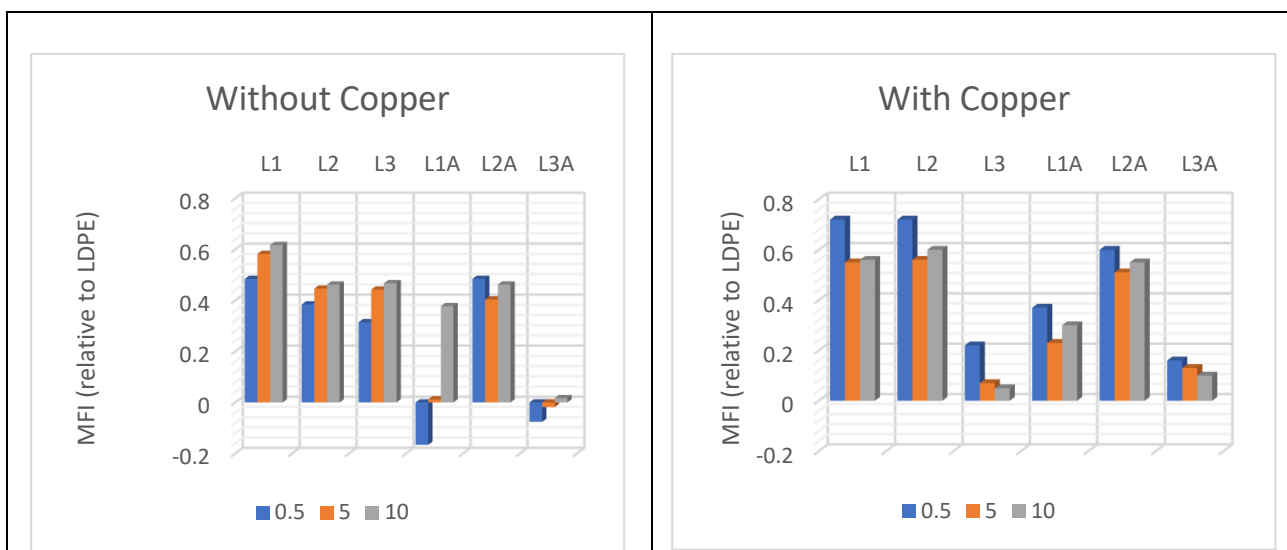
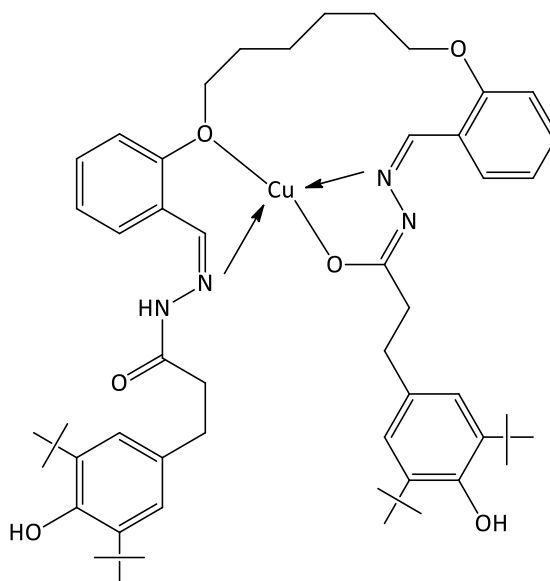
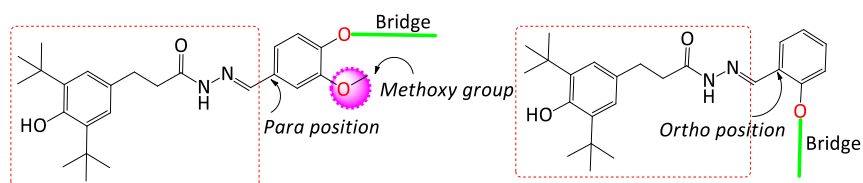


**Figure 3-26** Effect of methoxy group on Melt Flow Index of LDPE+ L1, LDPE+L2, LDPE+L3 and LDPE+ L1A, LDPE+L2A, LDPE+L3A formulations in the presence and absence of CuCl (*s.d* = 0.01 g/10 min)

Of all the molecules tested in this study the L-Series show the poorest melt stability, only **L3**, **L3A** and **L1A** show good melt stability. Both **L3** and **L3A** have a longer alkyl chain spacer joining their AO/MD functionalities. Here the chain will allow an ‘back-biting’ conformation allowing the formation of a more stable copper complex (analogous to that of **S5**):



From the results shown in **Figure 3-26**, it can be seen that in the presence of a methoxy group the MFI is decreasing. The reason is primarily due to the position of the methoxy (ortho) and azide groups (para) in L1A, L2A and L3A additives as shown in the chemical structure below, which operates as an effective hydroxyl radical scavenger in conjunction with the peroxy radical scavenging activity of the phenol.



However, this effect is minor in comparison to the influence of increasing the alkyl chain length between the functional groups.

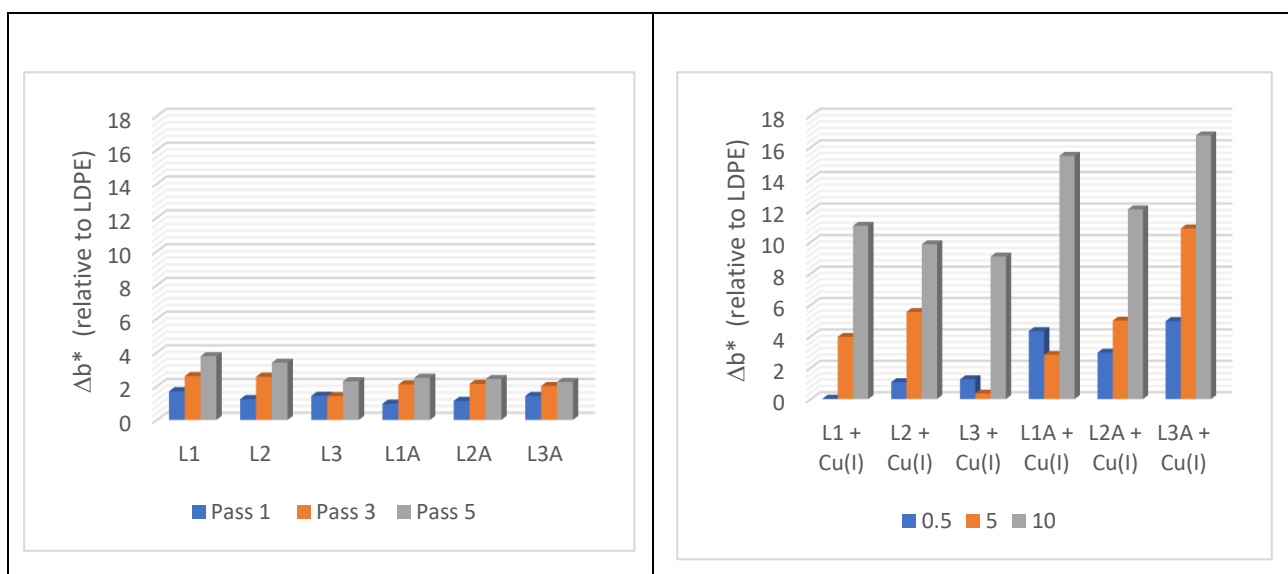


**Figure 3-27** Yellowness ( $\Delta b^*$ ) for LDPE+ L1, LDPE+L2, LDPE+L3 and LDPE+ L1A, LDPE+L2A, LDPE+L3A formulations in the presence and absence of CuCl (*s.d* = 0.04)

From **Figure 3-27** a direct link is found between colour development and the chain length (ethyl-bridge, butyl-bridge and hexyl-bridge). The colour development in LDPE+L1A, LDPE+L2A and LDPE+L3A formulations in the presence and absence of CuCl depend very strongly on the presence

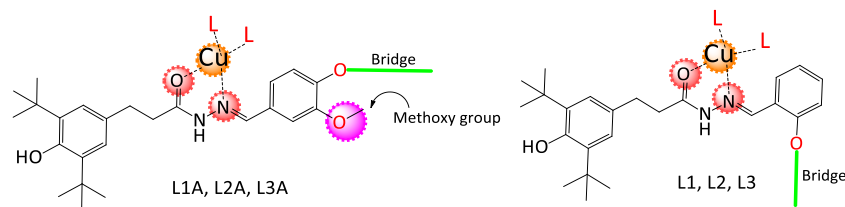
of the methoxy functional group in the stabiliser. In addition to this, *LDPE+L1*, *LDPE+L2* and *LDPE+L3* formulations in the absence and presence of CuCl showed less intense yellowness (lower  $\Delta b^*$ ).

### 3.3.2 FTIR Analysis of L-Series Antioxidants and Metal Deactivators in LDPE

On comparison of the FTIR spectra, along with the rates of change of functional group, of **L1**, **L2** and **L3** several features are notable (**Figures 3-28 and 3-29**). In **L1** the absorption bands of ester stretch ( $1745\text{ cm}^{-1}$ ) increase significantly with extrusion time. In comparison, the ester band is less pronounced for **L2**, while for **L3** the broad absorptions of unsaturated groups is dominant. This suggests **L3**, in the presence of copper can effectively inhibit the concentration of peroxy and alkoxy radicals that lead to the cage reactions producing ester groups.

For **L1A**, **L3A** and **L3A** (**Figures 3-30 to 3-31**) absorptions are partly masked by the antioxidant itself. However, rates of change of functional groups (**Figure 3-31**) support the MFI data. For **L1A** in the absence of copper, the ability of the methoxy group adjacent to the phenol for a short chain length to scavenge radicals, as seen by a decrease in the intensity of functional groups over the extrusion time, supports the observations from the MFI data. For **L3A** the ability to reduce oxidation for 5 minutes in the presence of copper and reduce oxidation after 5 minutes in the absence of copper indicates that the point at which the structure is able to scavenge radicals, according to their relative concentrations is important. These subtle differences mean that **L3A** is the best antioxidant-metal deactivator in the L-Series.

Here not only chain length but the position of the methoxy group and the presence of the azide group at the para position are likely to be important.



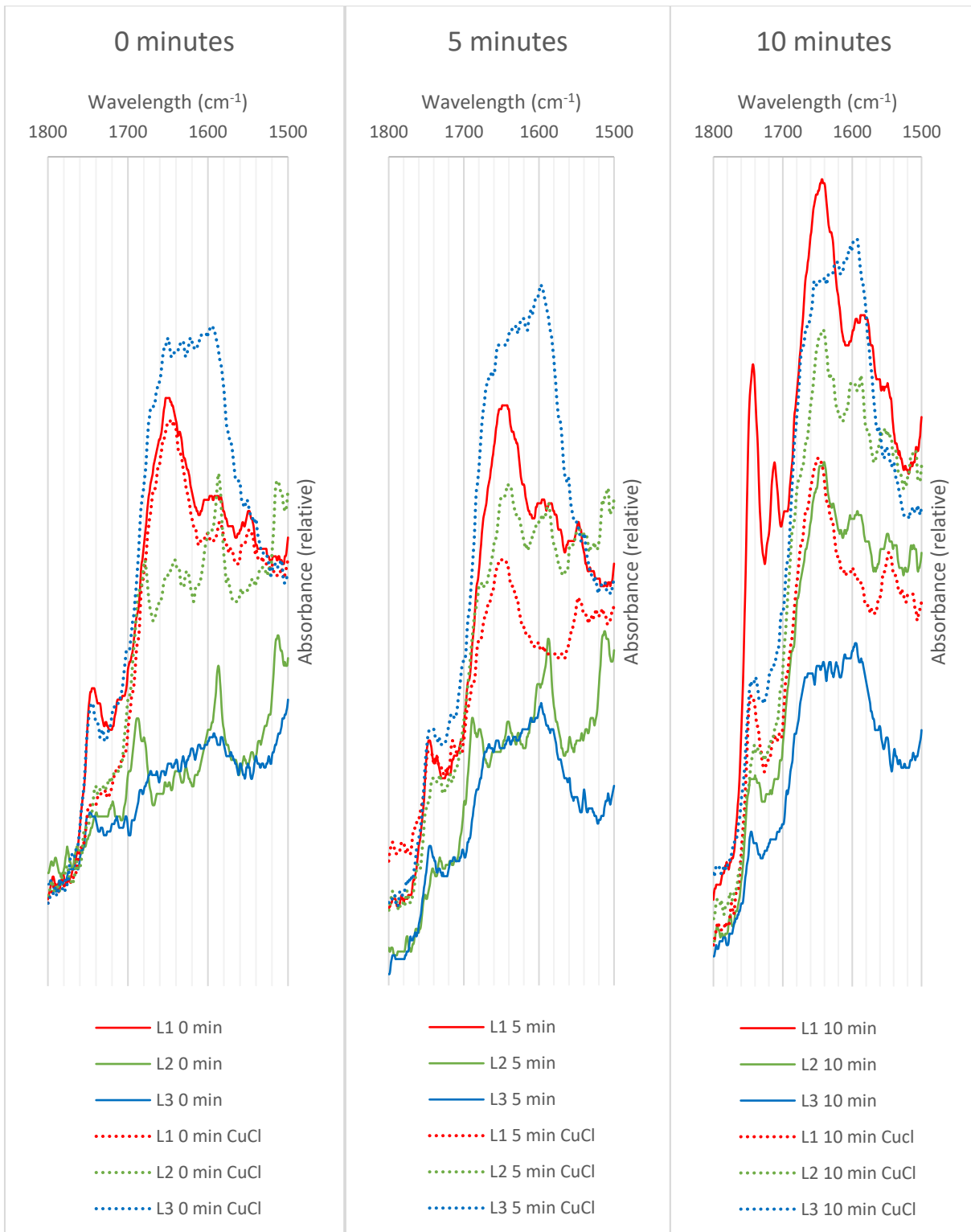


**Figure 3-28:** FTIR spectra ( $1800\text{-}1500\text{ cm}^{-1}$ ) of L1, L2 and L3 in LDPE extruded for 0, 5 and 10 minutes without and with CuCl

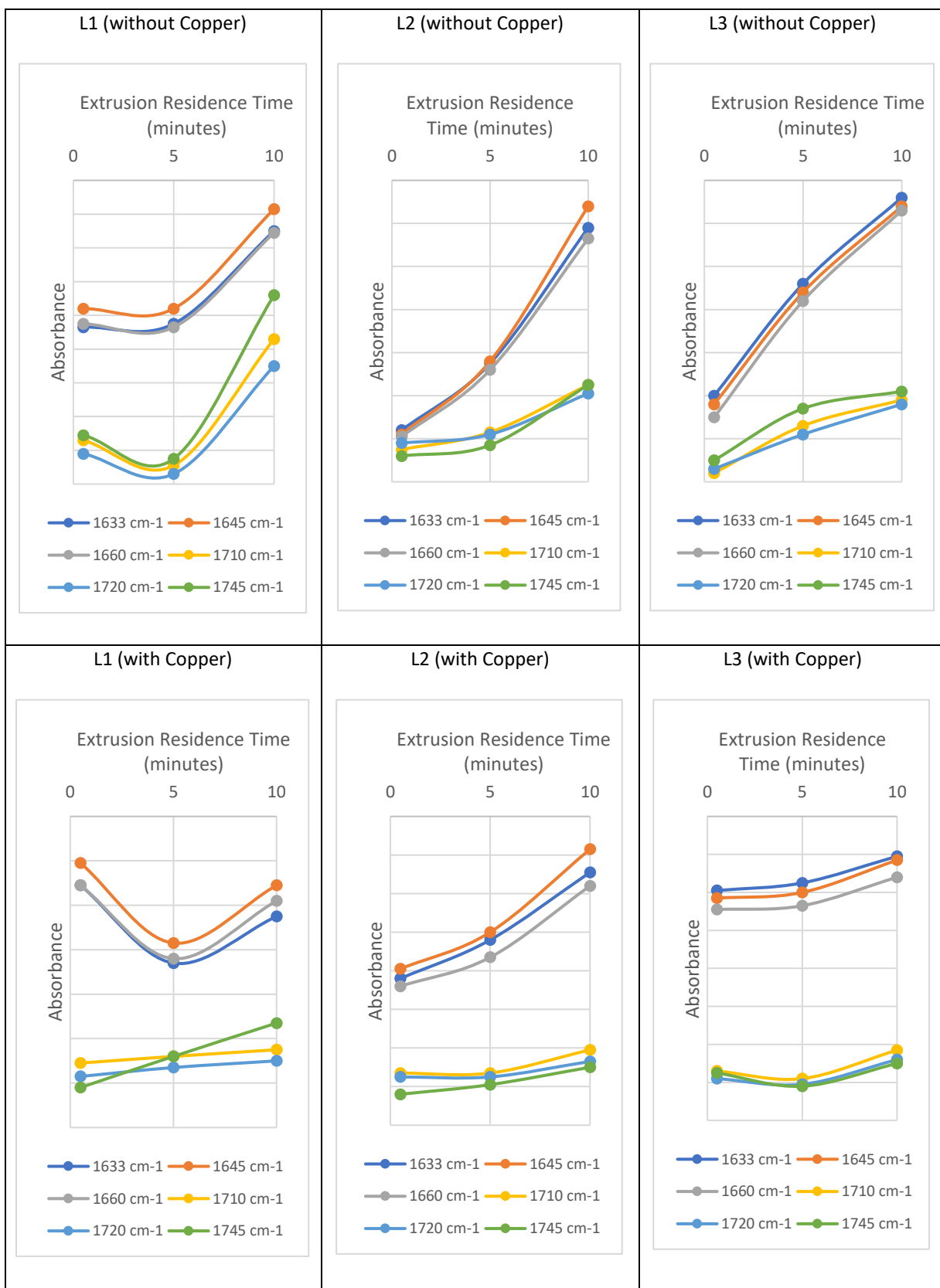


**Figure 3-29:** FTIR absorption intensities of carbonyl and unsaturated species for L1, L2 and L3 in LDPE extruded for 0, 5 and 10 minutes without and with CuCl

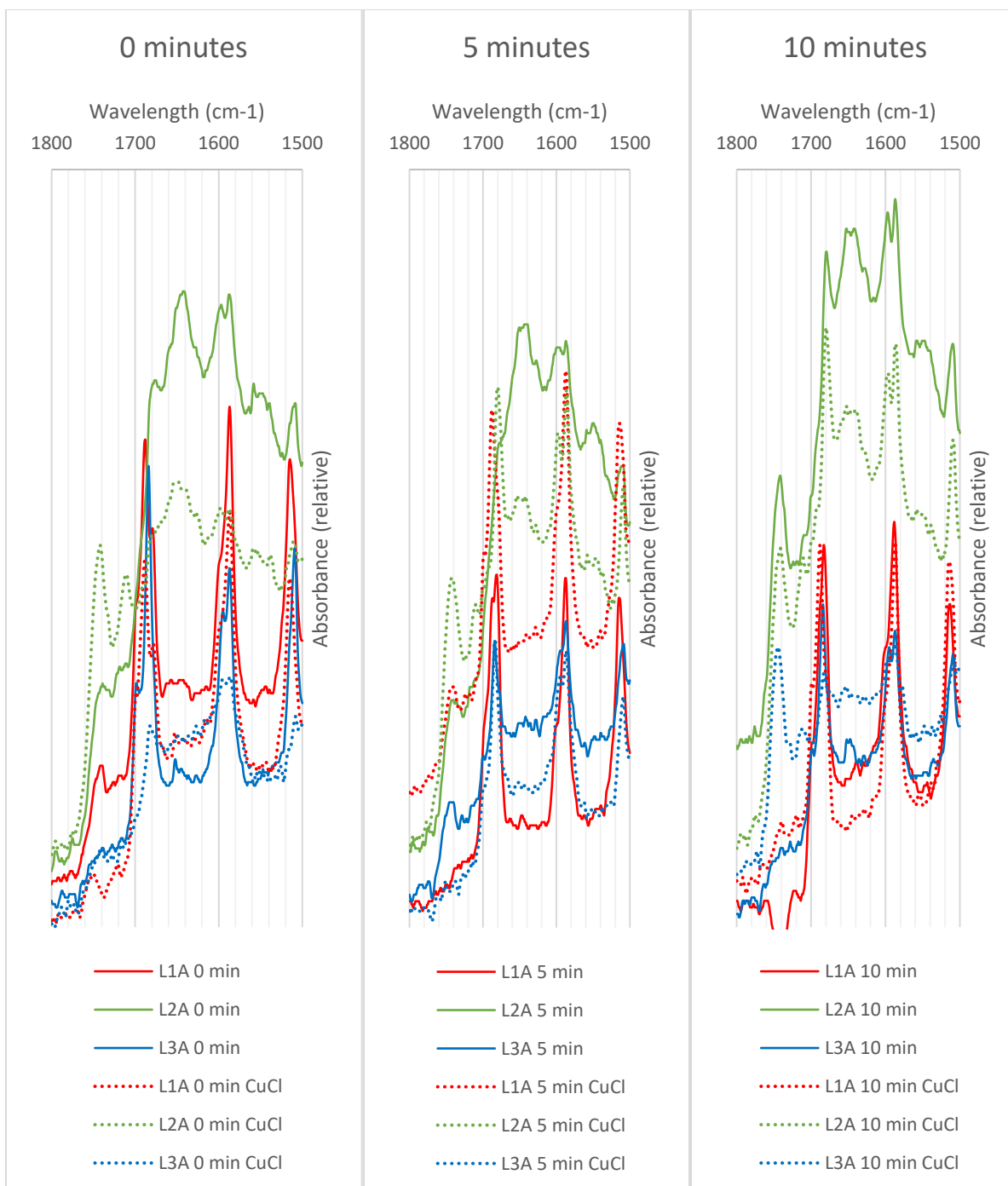


**Figure 3-30:** FTIR spectra (1800-1500  $\text{cm}^{-1}$ ) of L1A, L2A and L3A in LDPE extruded for 0, 5 and 10 minutes without and with CuCl

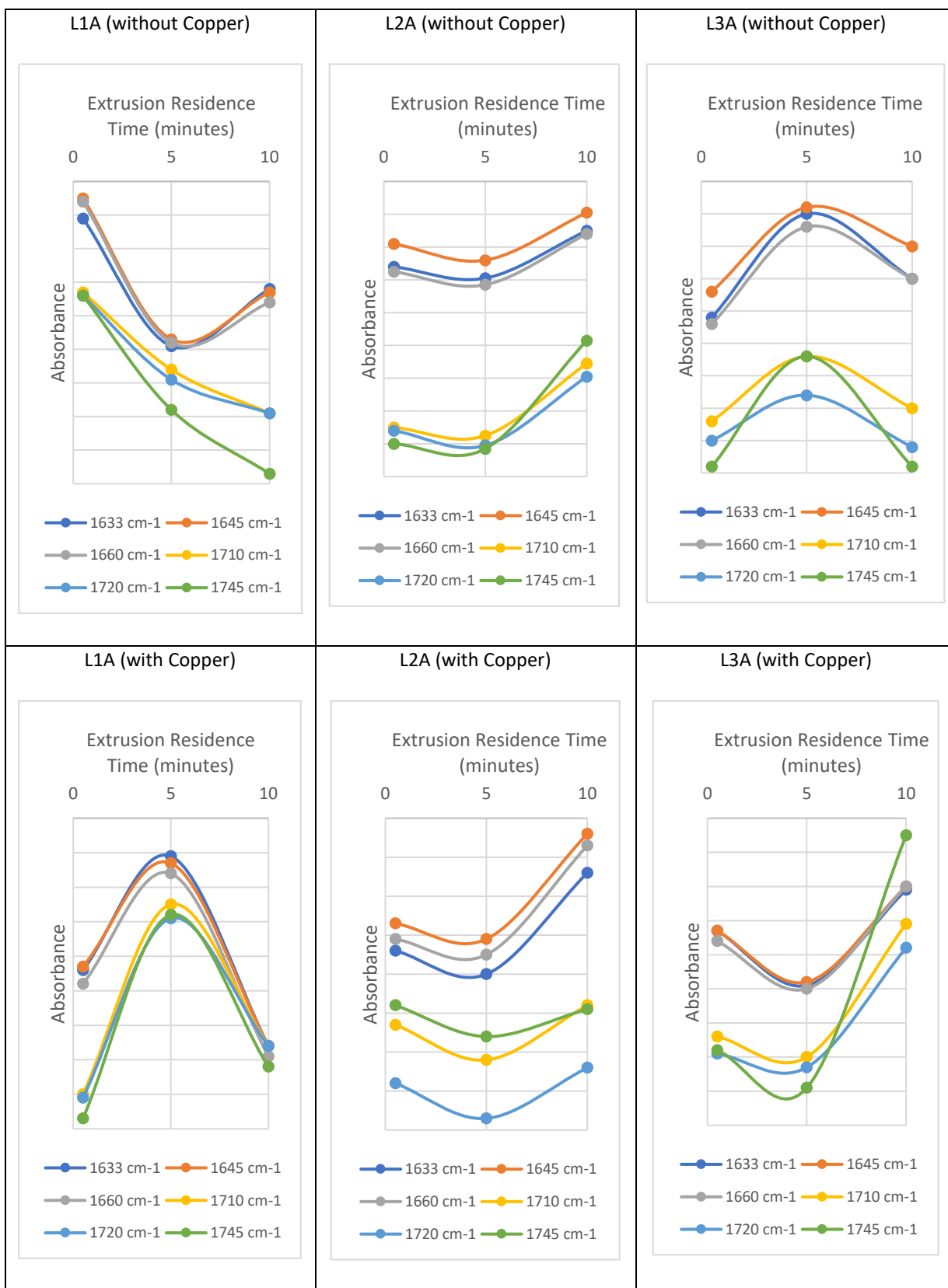


**Figure 3-31:** FTIR absorption intensities of carbonyl and unsaturated species for L1A, L2A and L3A in LDPE extruded for 0, 5 and 10 minutes without and with CuCl

### 3.3.3 FTIR spectra of L-Series antioxidants and metal deactivators and their copper complexes

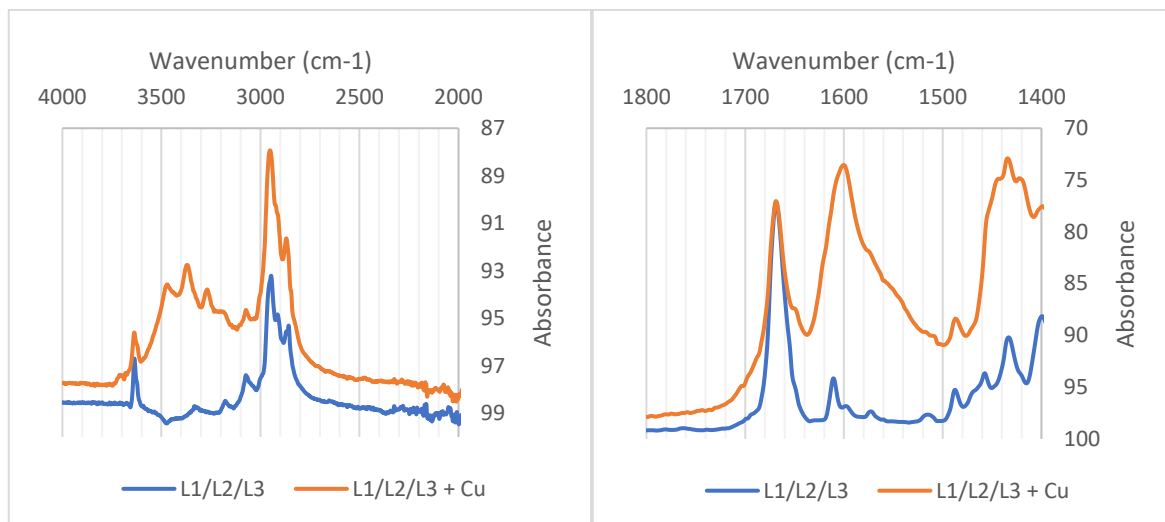


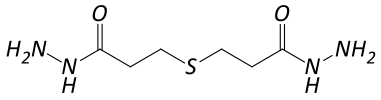
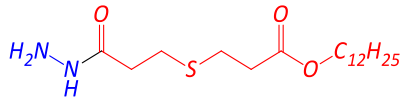
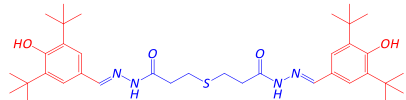
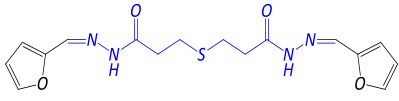
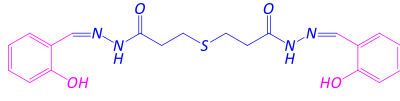
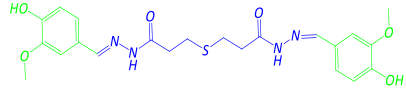
**Figure 3-32** FTIR spectra of free ligands L1, L2, L3, L1A, L2A, L3A and their copper complex

For the L-Series, the formation of a Cu-ligand complex was confirmed by the disappearance of the azomethine C=N stretch ( $1626\text{ cm}^{-1}$ ) and absence of stretching vibrations due to the azide C=O ( $1687\text{ cm}^{-1}$ ) and instead, a strong new band appeared at ( $1602\text{ cm}^{-1}$ ) corresponding to the Cu-O-C as shown in **Figure 3-32**.

Collectively the data underlines the fact that increasing chain length as means to improve the activity of antioxidant-metal deactivators is not the best method to optimise performance

### 3.4 Novel Stabilizer Performance (T-Series)

Like the S-Series, the T-Series antioxidant-metal deactivators are analogues of hydrazides, here linked by an alkyl chain containing sulphur. Given that sulphur can reduce peroxides in a catalytic mechanism generating oxidised sulphur species, this opens-up the possibility for improved antioxidant behaviour.

 <p style="text-align: center;"><b>T0</b> (206 g mol<sup>-1</sup>, m.p.148-155°C)</p>	 <p style="text-align: center;"><b>T0A</b> (361 g mol<sup>-1</sup>, m.p.60-62°C)</p>	 <p style="text-align: center;"><b>T1</b> (639 g mol<sup>-1</sup>, m.p.250-255°C)</p>
 <p style="text-align: center;"><b>T2</b> (362 g mol<sup>-1</sup>, m.p.189-194°C)</p>	 <p style="text-align: center;"><b>T3</b> (414 g mol<sup>-1</sup>, m.p.245-250°C)</p>	 <p style="text-align: center;"><b>T4</b> (475 g mol<sup>-1</sup>, m.p. not available)</p>

#### 3.4.1 MFI and Yellowness Index (T-Series)

**Figures 3-33** shows the changes in MFI of the T-Series structures, relative to LDPE. The ranking of the T-Series with respect to MFI follows the order:

Without copper: **T0 < T3 < T1** < T0A < T4 < T2

With Copper: **T0 < T3 < T1** < T2 < T0A < T4

**Figure 3-33** also show the changes in YI of the T-Series structures, relative to LDPE. The ranking of the MD-Series with respect to YI follows the order:

Without copper: **T0A < T1 < T0**  $\cong$  T3 < T4 < T2

With Copper: **T0A << T1 < T0** < T3 < T4 < T2

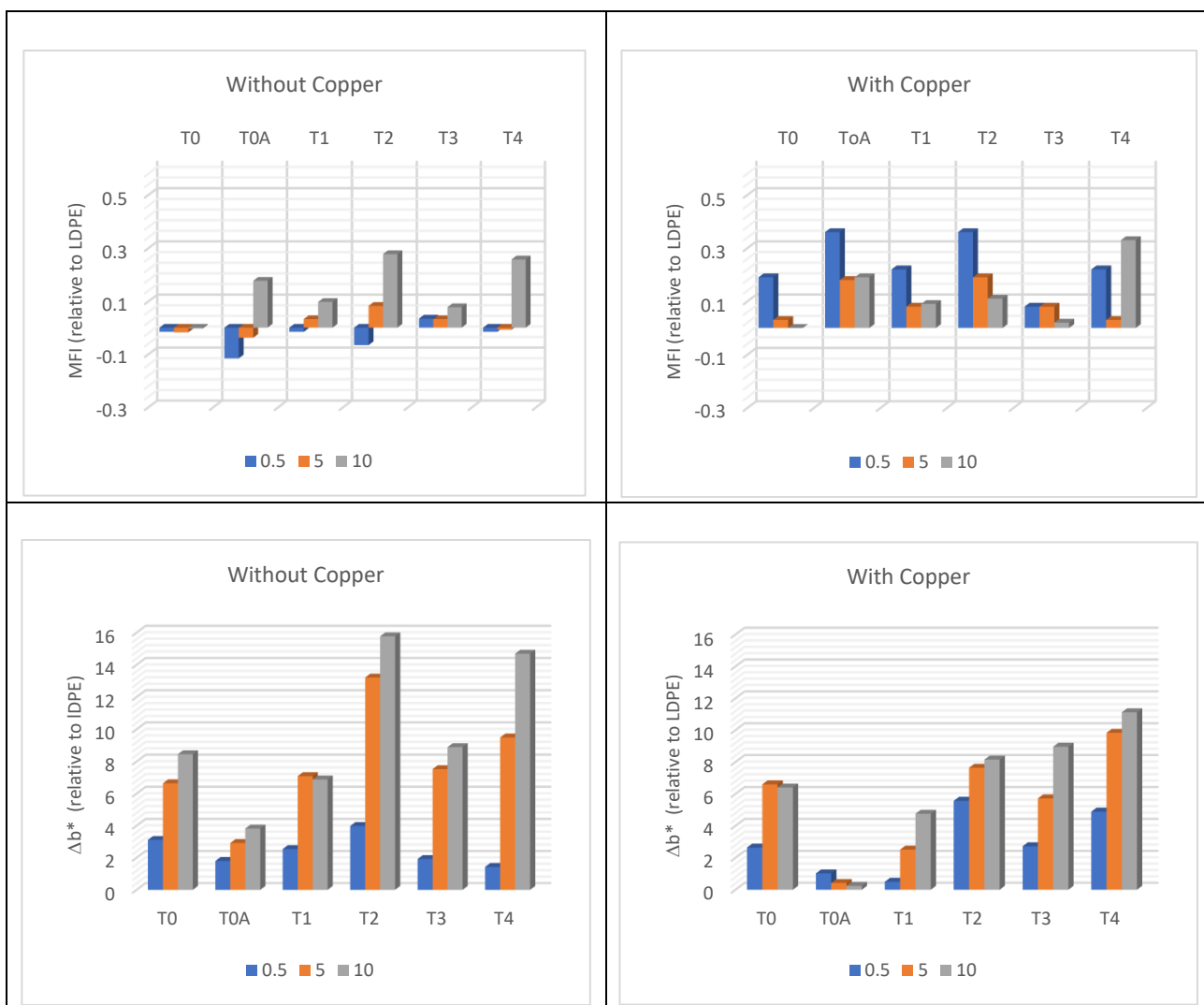


**Figure 3-33** MFI ( $s.d = 0.01$  g/10 min) and Yellowness ( $\Delta b^*$ ) ( $s.d = 0.04$ ) for T-Series antioxidant-metal deactivators in LDPE in the absence and presence of CuCl extruded for 0, 5 and 10 minutes.

When copper is not present, the antioxidant activity of all T-Series structures shows an improvement in the initial stages of extrusion oxidation. However, within 10 minutes there is a significant increase in MFI, apart from **T3** which shows anomalous behaviour. In the presence of copper, only samples **T1** and **T3** show a comparable MFI to that of LDPE. All samples show a reduction in MFI in the presence of copper suggesting they act as metal deactivators.

The YI values gradually increased in the samples extruded for 0, 5 and 10 minutes without copper and with copper. The difference being that overall magnitude of the YI value was less with copper.

### 3.4.2 FTIR Analysis of T-Series Antioxidants and Metal Deactivators in LDPE

The FTIR spectra and corresponding data for **LDPE+T0** and **LDPE + T1** are given in **Figures 3-34 and 3-35** respectively. In the absence of copper **T0** shows strong growth in the ester band in the first 5 minutes of extrusion. When copper is present a similar profile is seen. This indicates that the two azide group attached to a sulphur atom in **T0** are slowing down oxidation catalysed by the CuCl.

The data for **T2**, **T3** and **T4** (**Figures 3-36 and 3-37**) indicates variable performance. **T2** shows increased levels of unsaturated group ( $1630-1660\text{ cm}^{-1}$ ) and an ester band ( $1745\text{ cm}^{-1}$ ) that grows in during the degradation over 10 minutes. This suggests that although **T2** can reduce oxidation in the presence of copper it is not effective over this timescale. For the LDPE sample containing **T3** the best performance is seen. Although this stabiliser is not particularly good in the absence of copper (strong growth of ester and unsaturated carbonyl absorptions over 10 minutes), in the presence of copper it is able to reduce the concentration of oxidised species at a reasonable rate. In particular there is a sharp decrease in the ester band ( $1745\text{ cm}^{-1}$ ) after 10 minutes in the extruder. For **T4** oxidised species increase rapidly in the presence and absence of copper in the first 5 minutes of extrusion and only slowly decrease in the absence of copper. Where copper is present the carbonyl bands continue to increase throughout the extrusion time.

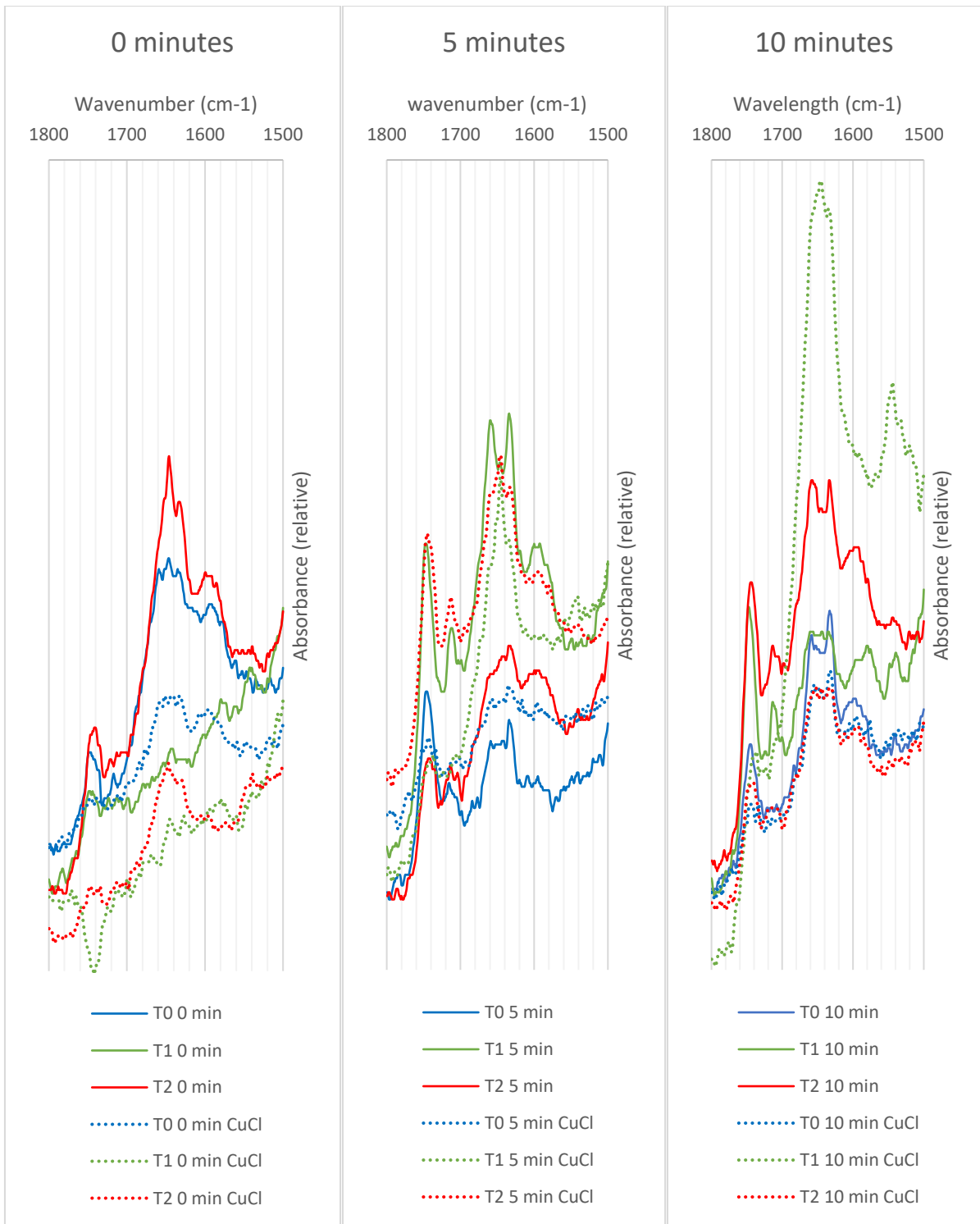


**Figure 3-34:** FTIR spectra (1800-1500 cm<sup>-1</sup>) of T0, T1 and T2 in LDPE extruded for 0, 5 and 10 minutes without and with CuCl

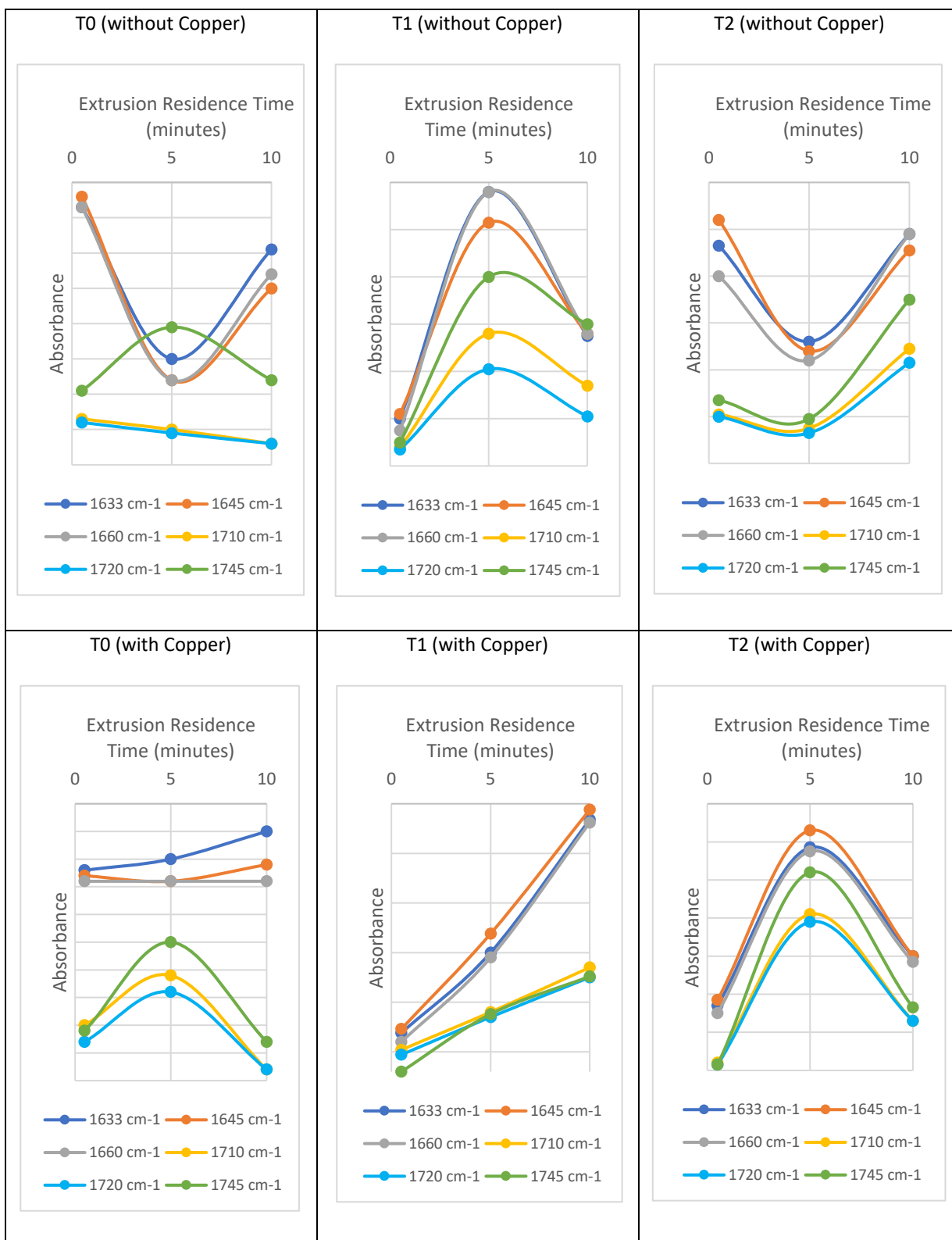


**Figure 3-35:** FTIR absorption intensities of carbonyl and unsaturated species for T0, T1 and T2 in LDPE extruded for 0, 5 and 10 minutes without and with CuCl

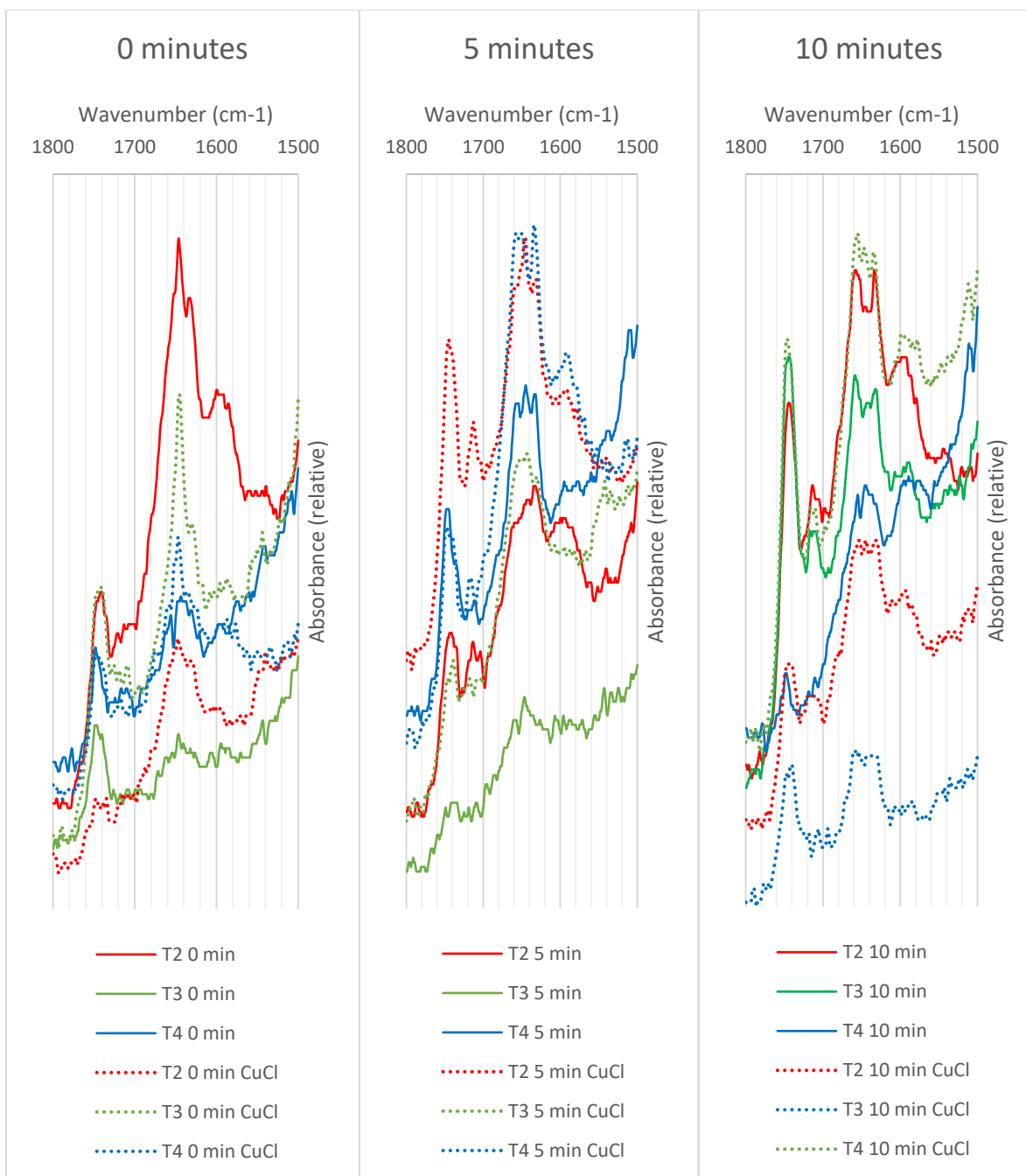


**Figure 3-36:** FTIR spectra ( $1800\text{-}1500\text{ cm}^{-1}$ ) of T2, T3 and T4 in LDPE extruded for 0, 5 and 10 minutes without and with CuCl

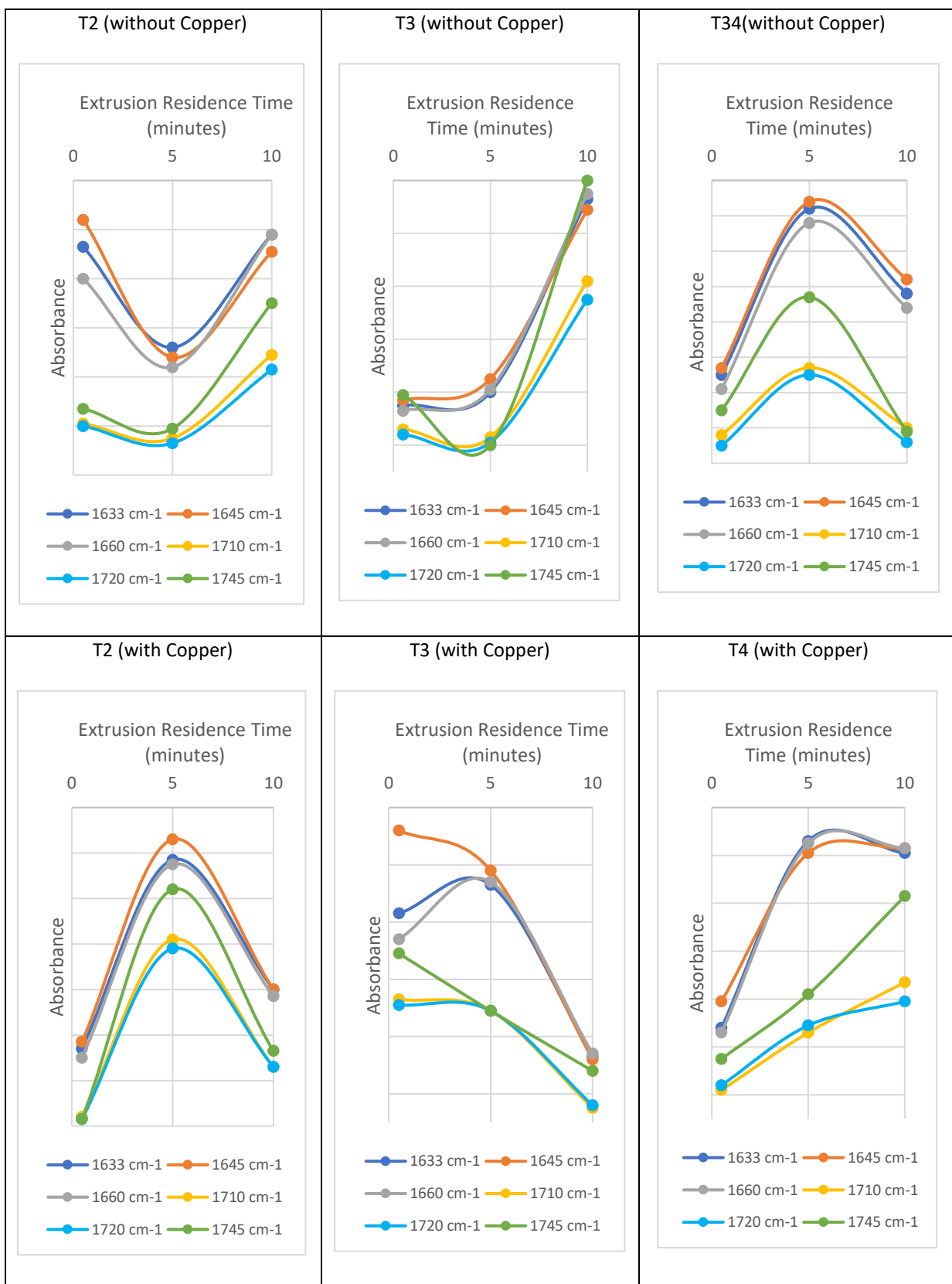


**Figure 3-37:** FTIR absorption intensities of carbonyl and unsaturated species for T2, T3 and T4 in LDPE extruded for 0, 5 and 10 minutes without and with CuCl

### 3.4.3 FTIR spectra of T-Series antioxidants and metal deactivators and their copper complexes

The  $^1\text{H}$ NMR and  $^{13}\text{C}$ NMR spectra of the free ligand **T0** and its complex with copper revealed significant changes in chemical shifts. FTIR analysis showed that the vibrational stretch of the terminal amino group ( $-\text{NH}_2$ ) at  $3288\text{ cm}^{-1}$  shifted towards a higher frequency range ( $3308\text{ cm}^{-1}$ ), while the NH out of plane ( $1532\text{ cm}^{-1}$ ) shifted slightly towards a lower frequency ( $1520\text{ cm}^{-1}$ ). The formation of a Cu-ligand complex was confirmed by the absence of the stretching vibration due to azide C=O ( $1626\text{ cm}^{-1}$ ) and instead, a strong new band appeared at ( $1640\text{ cm}^{-1}$ ) corresponding to Cu-O-C as shown in **Figure 3-38**.

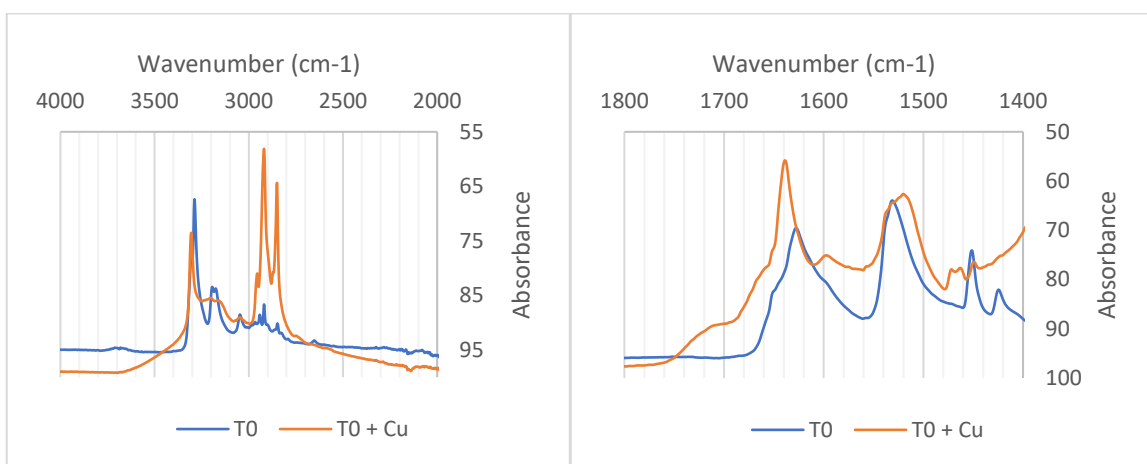
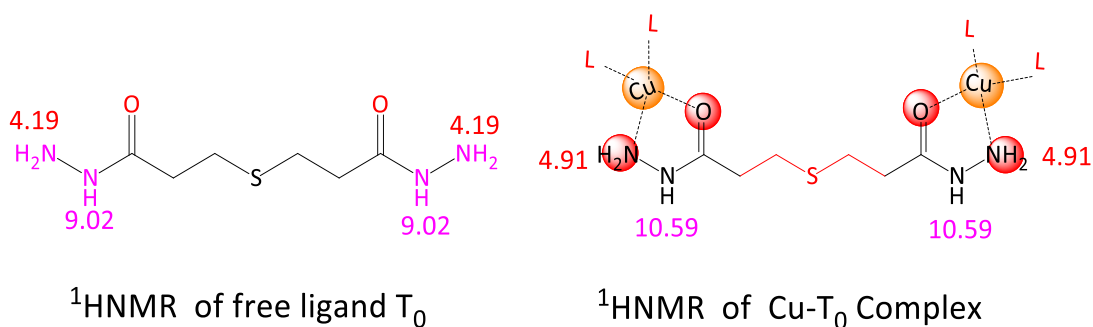


**Figure 3-38** FTIR spectra of free ligand **T0** and its complex with copper

This indicates that the terminal amine ( $\text{NH}_2$ ) and azide C=O in the thio-based metal deactivator **T0** are taking part in coordination as shown in the structure below.



The complex itself is likely to coordinate through amide-iminol tautomerism.

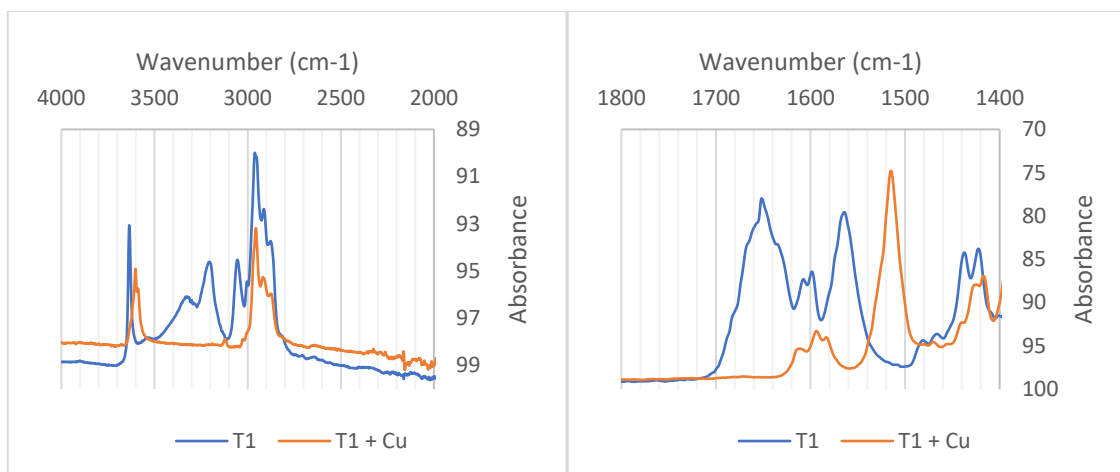
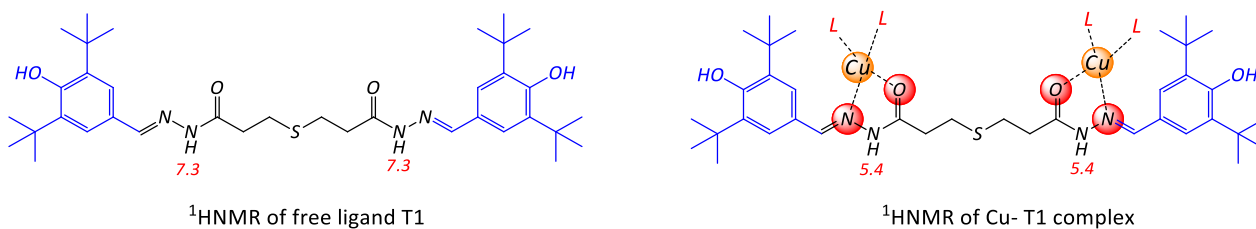
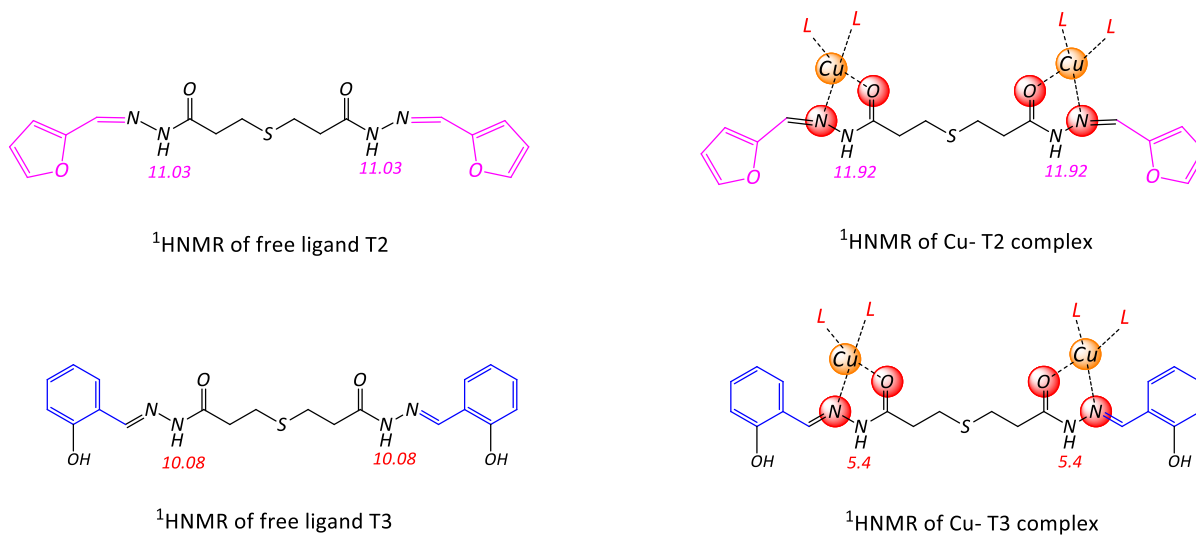


**Figure 3-39** FTIR spectra of free ligand **T1** and its complex with copper

The  $^1\text{H}$ NMR and IR spectra of the free ligand **T1** and its complex with copper reveal significant changes in chemical shifts. This indicates that the azomethine (C=N) and azide C=O are taking part in coordination. The formation of Cu-ligand complex was confirmed by the absence of the stretching vibration due to the azide C=O instead, a strong new band appeared at  $1515\text{ cm}^{-1}$  corresponding to the C-O-Cu group as shown in **Figure 3-39**.



A comparative  $^1\text{H}$ NMR and IR spectral study of the free ligand **T2** and **T3** and their complexes with copper reveal that both additives are binding copper in a similar way (see structures below).



The formation of Cu-ligand complex was confirmed by the absence of stretching vibrations due to the azide C=O but instead, a strong new band appeared at  $1601\text{ cm}^{-1}$  corresponding to the C-O-Cu group as shown in **Figure 3-40**. The  $^1\text{H}$ NMR and FTIR study of the Cu-T3 complex confirms that phenolic OH is not taking part in coordination while the furyl ring is a weak chelating site.

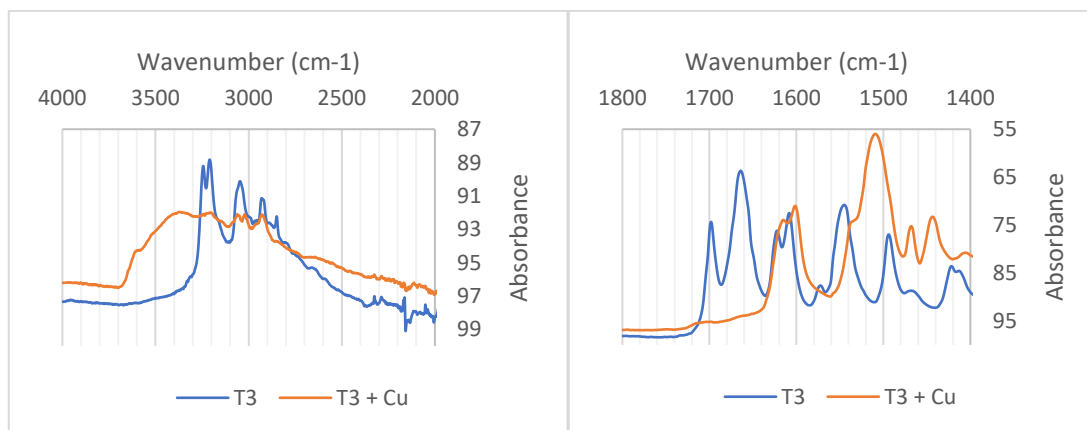
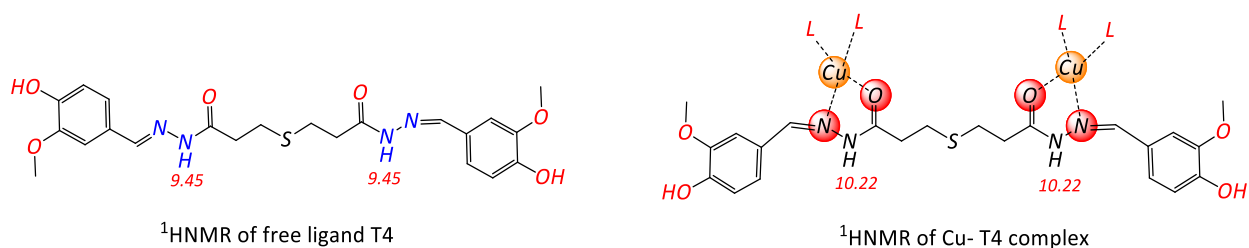
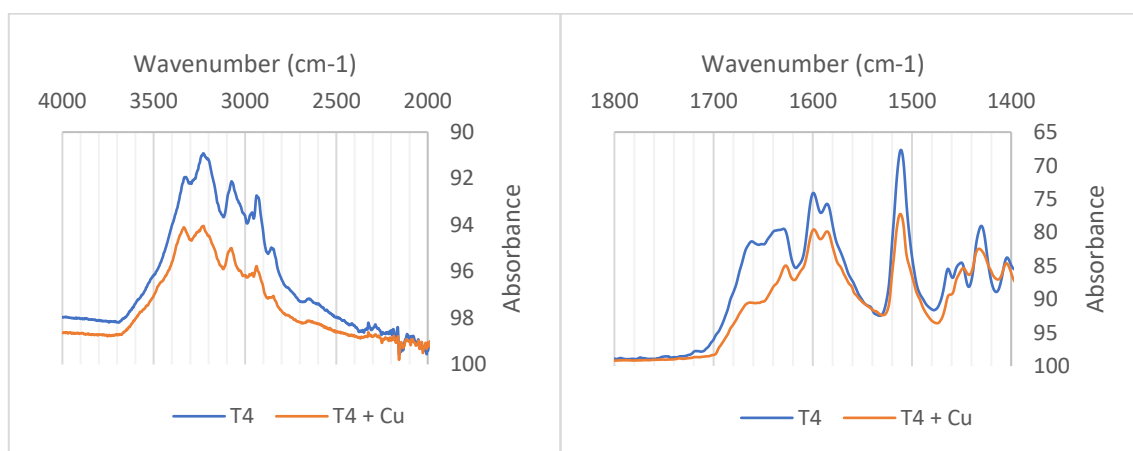


**Figure 3-40** FTIR spectra of free ligand T3 and its complex with copper

A comparative  $^1\text{H}$ NMR and FTIR spectral study of the free ligand T4 and its complex with copper reveals that the additive T4 is binding copper by using azomethine C=N and carbonyl C=O groups.  $^1\text{H}$ NMR and IR spectral information of the Cu-T3 complex confirms that phenolic OH is not taking part in coordination (see structures below).



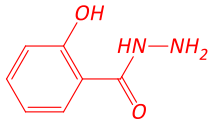
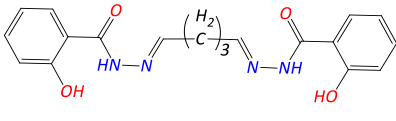
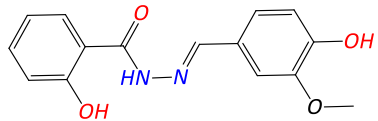
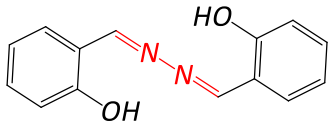
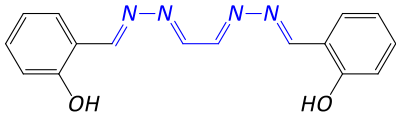
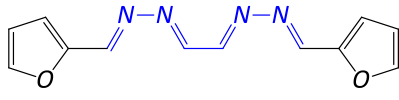
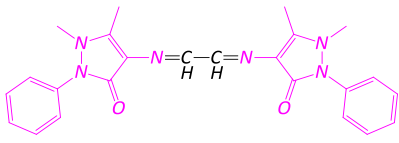
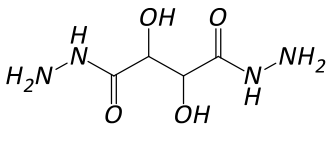
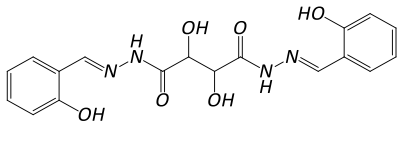
FTIR spectra showed the absence of important stretching vibrations due to azide C=O but instead, a strong new band appeared at  $1601\text{ cm}^{-1}$  corresponding to the C-O-Cu group as shown in **Figure 3-41**.



**Figure 3-41** FTIR spectra of free ligand T3 and its complex with copper

### 3.5 Novel Stabilizer Performance (MD-Series)

The MD-Series AO/MDs are analogues of hydrazides and hydrazines. Most of the structures in this series have a hydroxy phenyl group in proximity to nitrogen. This presents the possibility of intra-molecular hydrogen bonding or, coordination with copper.

 <p>MD1 (152 g mol<sup>-1</sup>, m.p.150°C)</p>	 <p>MD1B (368 g mol<sup>-1</sup>, m.p. not available)</p>	 <p>MD1C (286 g mol<sup>-1</sup>, m.p.212°C)</p>
 <p>MD0 (240 g mol<sup>-1</sup>, m.p.215°C)</p>	 <p>MD2A (294 g mol<sup>-1</sup>, m.p.220-225°C)</p>	 <p>MD2B (242 g mol<sup>-1</sup>, m.p.155-160°C)</p>
 <p>MD4 (428 g mol<sup>-1</sup>, m.p.not available)</p>	 <p>MD7 (178 g mol<sup>-1</sup>, m.p.208-209°C)</p>	 <p>MD7A (386 g mol<sup>-1</sup>, m.p. not available)</p>

### 3.5.1 MFI and Yellowness Index (MD-Series)

**Figure 3-42** shows the changes in MFI of the MD-Series structures, relative to LDPE. The ranking of the MD-Series with respect to MFI follows the order:

Without copper: **MD7A >> MD0  $\cong$  MD2A  $\cong$  MD4 > MD7 > MD1B > MD1C > MD2B > MD1**

With Copper: **MD7A >> MD0  $\cong$  MD2A  $\cong$  MD2B > MD1C  $\cong$  MD4 > MD7 > MD1  $\cong$  MD1B**

Unlike the other compounds examined in this study, all the MD-Series molecules (except MD1) show an initial improvement in MFI compared with LDPE in the absence of copper. This suggests that these structures are effective antioxidants in the initial stages of circulation mode extrusion.

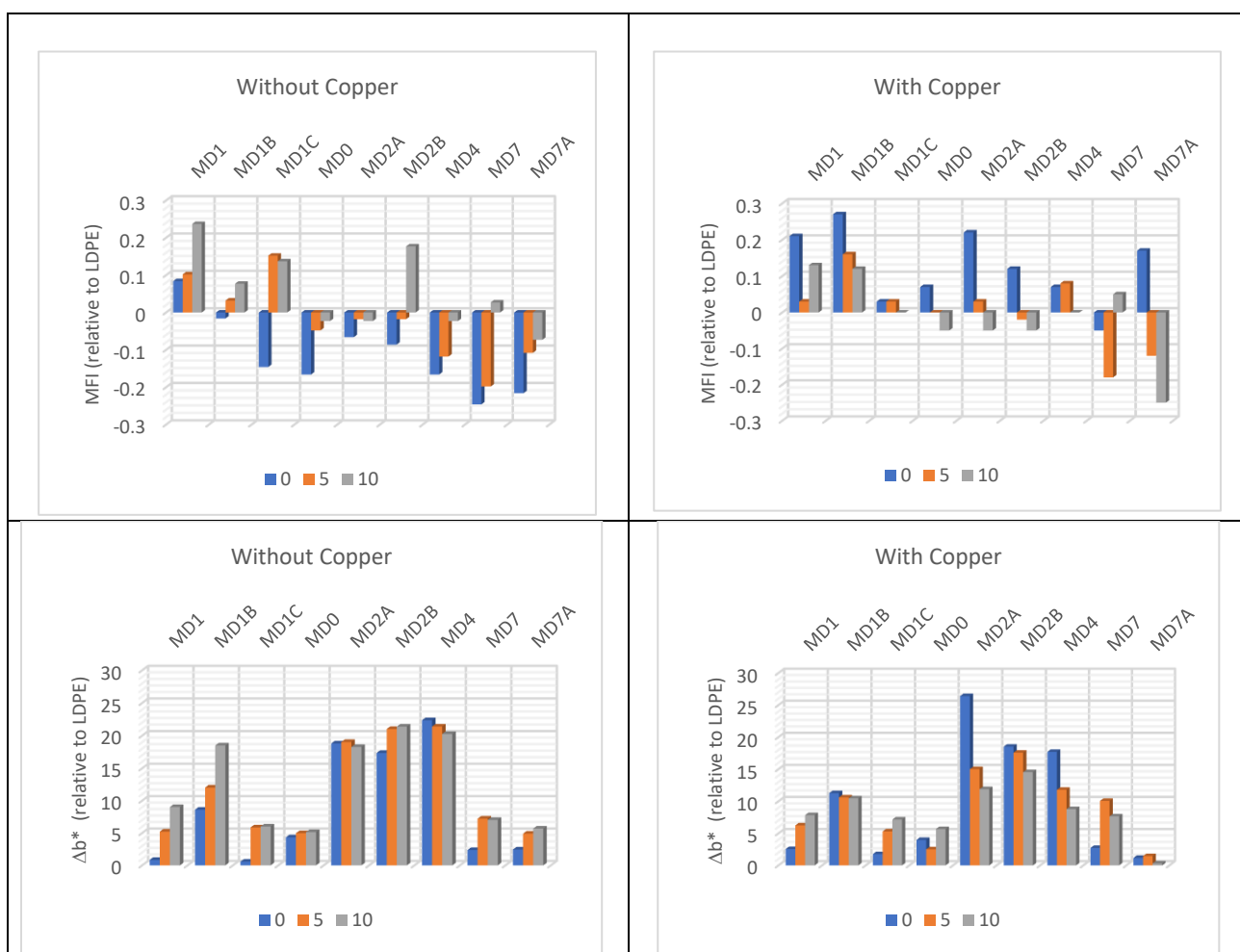


**Figure 3-42** Melt flow index (MFI) ( $s.d = 0.01$  g/10 min) and Yellowness ( $\Delta b^*$ ) ( $s.d = 0.04$ ) for LDPE+MD1A, LDPE +MD1B and LDPE+MD1C formulations in the absence and presence of CuCl during circulation mode extrusion for 0, 5 and 10 minutes.

**Figure 3-42** also shows the changes in Yellowness ( $\Delta b^*$ ) of the MD-Series structures, relative to LDPE. The ranking of the MD-Series with respect to YI follows the order:

Without copper: **MD7A  $\cong$  MD0  $\cong$  MD1C  $\cong$  MD4** > MD7 > MD1B > MD1C > MD2B > MD1

With Copper: **MD7A  $\ll$  MD0 < MD1C  $\cong$  MD7** > MD1C  $\cong$  MD4 > MD7 > MD1  $\cong$  MD1B

One key observation is that in contrast to other AO/MDs in this study, the Yellowness ( $\Delta b^*$ ) for the MD-Series reveals that some of the molecules that show good melt stability also show good YI or rapid reduction in Yellowness ( $\Delta b^*$ ) during the extrusion process (namely MD7A, MD0).

### 3.5.2 FTIR Analysis of MD-Series Antioxidants and Metal Deactivators in LDPE

The FTIR spectra, and the rates of change of key functional groups, for **MD0**, **MD1B** and **MD1C** are given in **Figures 3-43 and 3-44**. For **MD1**, the ester bands ( $1745\text{ cm}^{-1}$ ) increase dramatically in the absence of copper. Although the relative absorption of ester groups is diminished in the presence of copper, overall, it suggests that substantial oxidation has occurred. For **MD1B** although absorptions are suppressed in the absence of copper marked absorptions are evident in **MD1C** formulation extruded for 0, 5 and 10 minutes without CuCl showed increased oxidative stability in the presence of CuCl, this is due to the methoxy phenol which is an effective radical scavenger. The MFI values are also the best of this group, though they are only equivalent to LDPE.

Better performance is seen for LDPE containing **MD0**, **MD2A** and **MD2B** (**Figures 3-45 and 3-46**). Here peaks for oxidation are obscured by additive peaks, but from **Figure 3-46** it can be seen that the intensities of key functional groups are reduced over the extrusion time, suggesting this group of structures are particularly effective antioxidants on a par with the commercial metal deactivators.

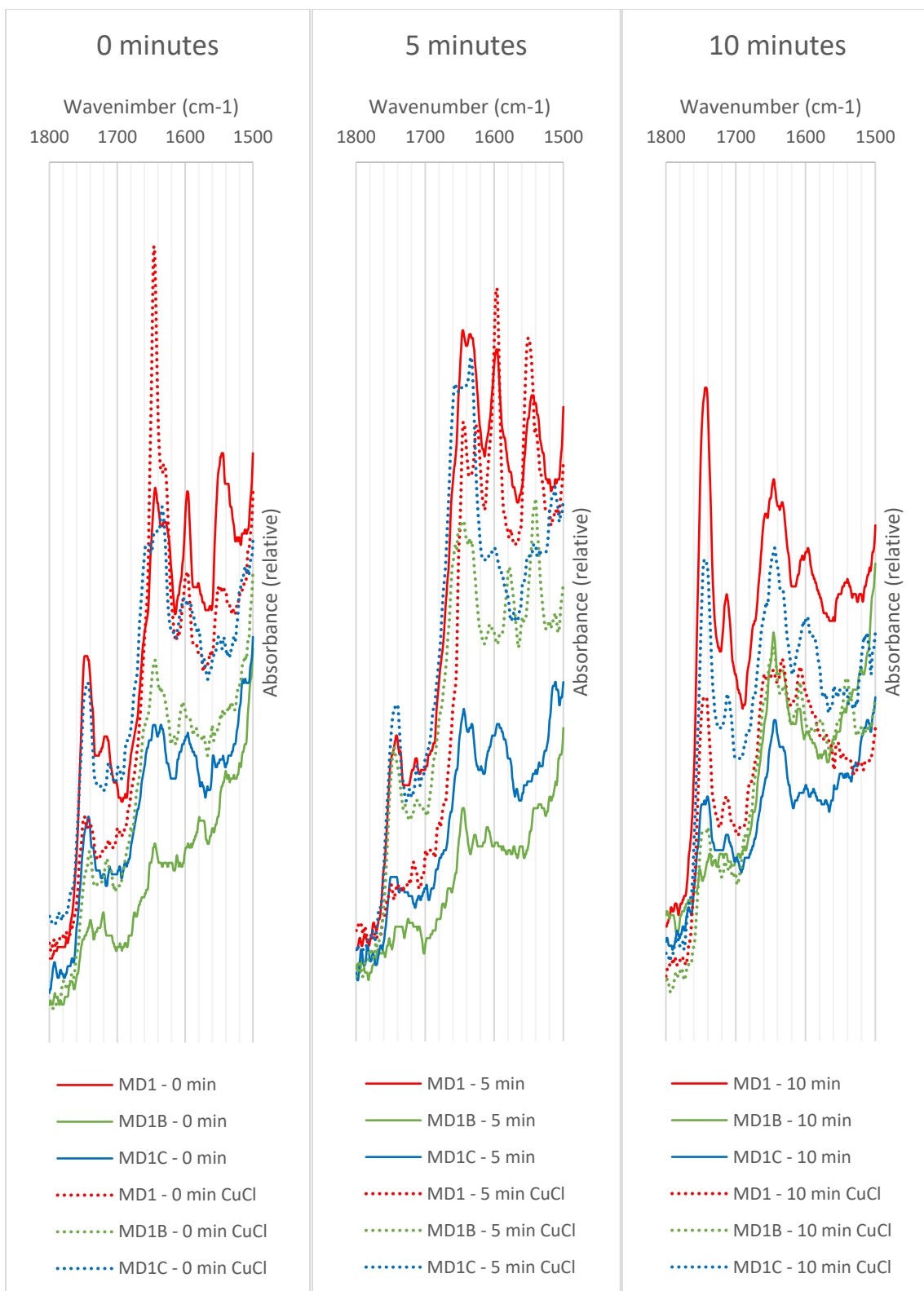


**Figure 3-43:** FTIR spectra (1800-1500 cm<sup>-1</sup>) of MD1, MD1B and MD1C in LDPE extruded for 0, 5 and 10 minutes without and with CuCl

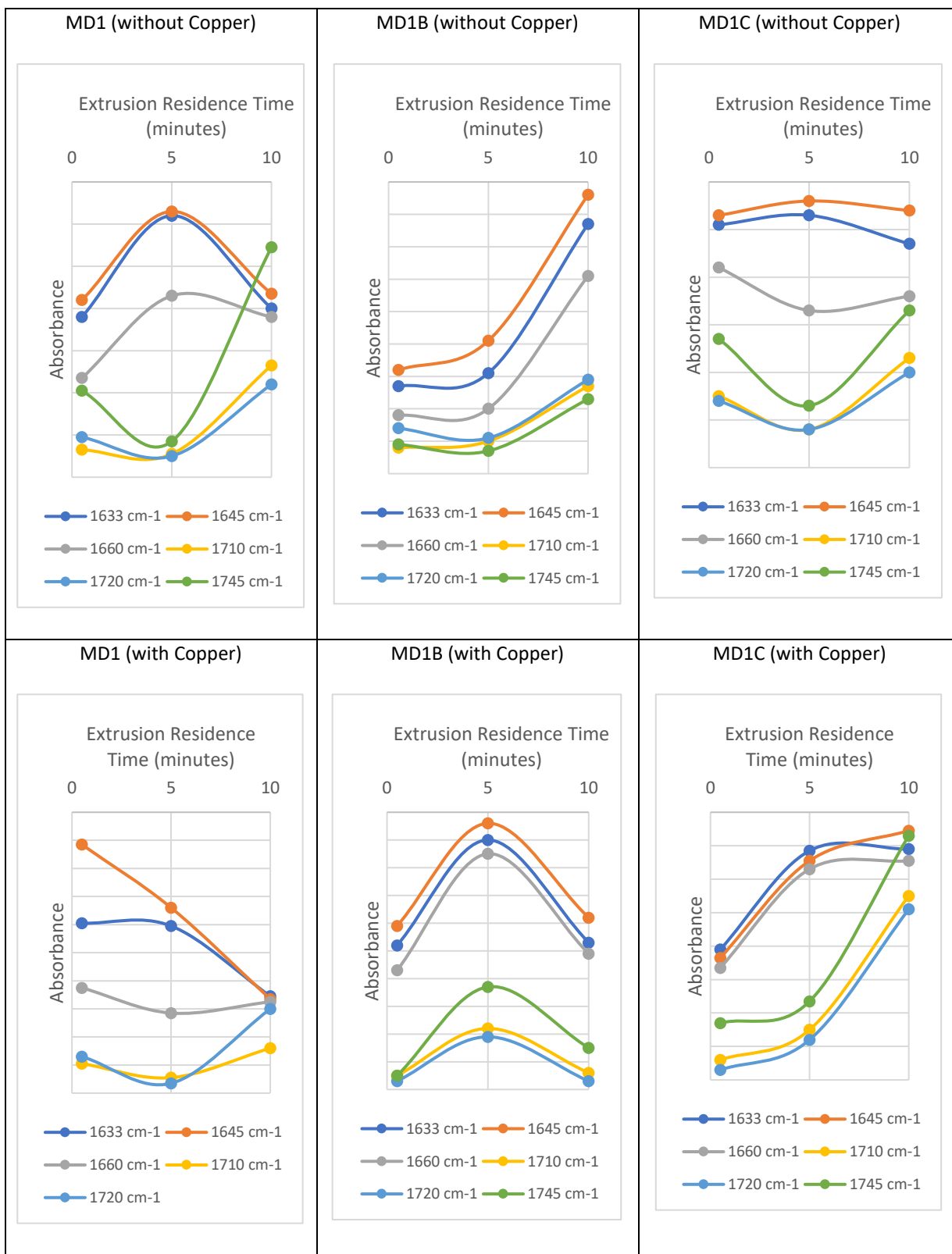


**Figure 3-44:** FTIR absorption intensities of carbonyl and unsaturated species for MD1, MD1B and MD1C in LDPE extruded for 0, 5 and 10 minutes without and with CuCl

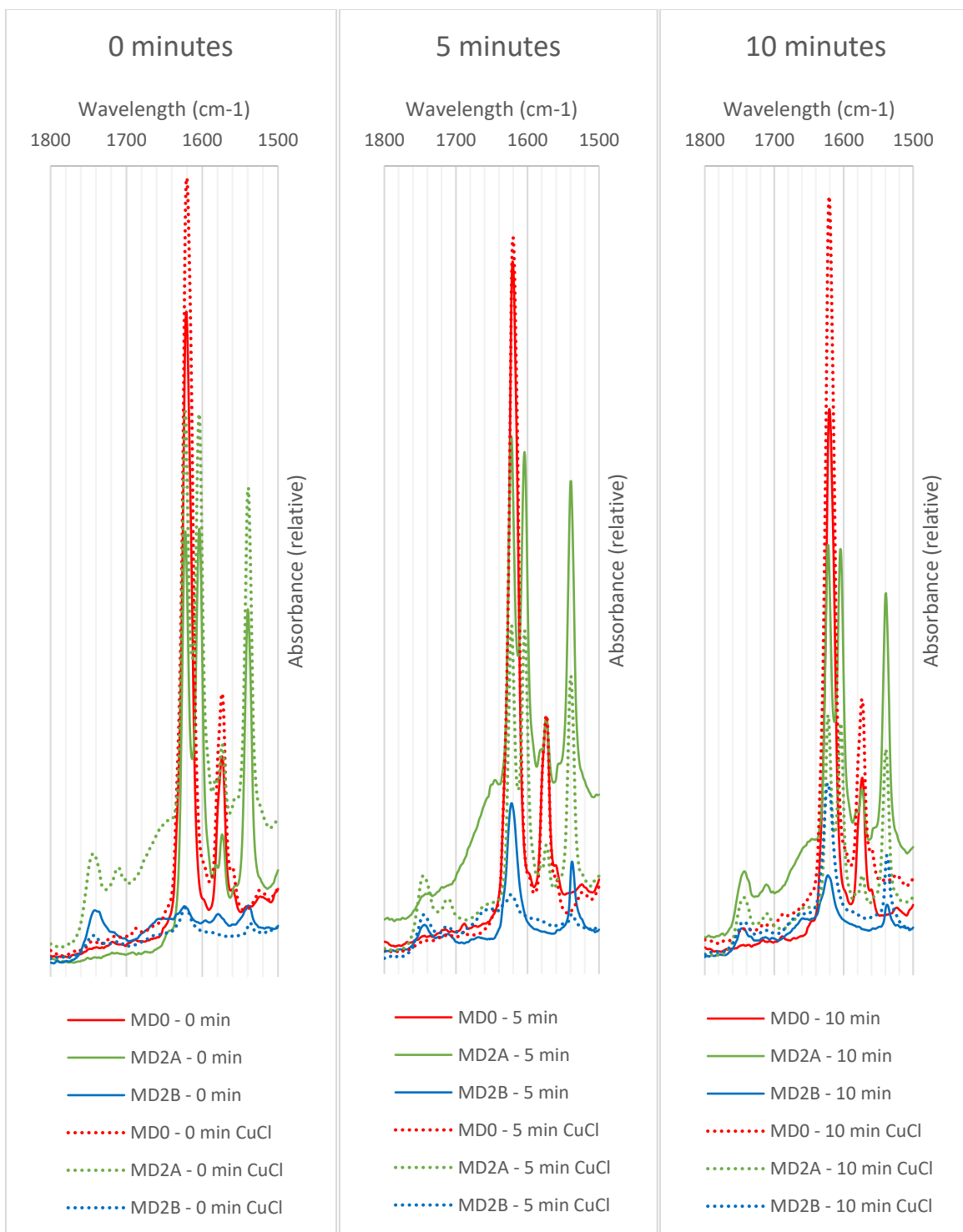


**Figure 3-45:** FTIR spectra ( $1800\text{-}1500\text{ cm}^{-1}$ ) of MD0, MD2A and MD2B in LDPE extruded for 0, 5 and 10 minutes without and with CuCl

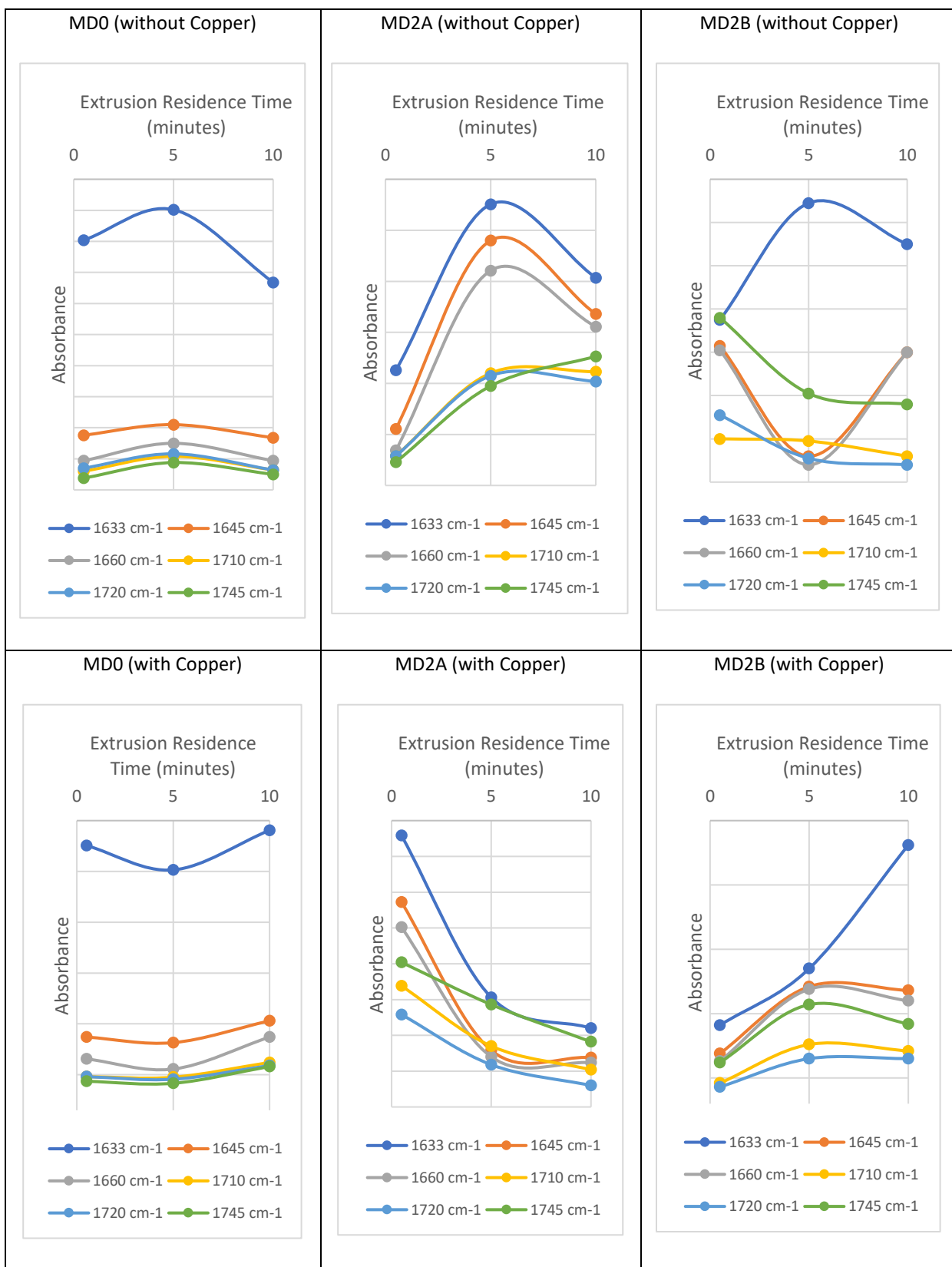


**Figure 3-46:** FTIR absorption intensities of carbonyl and unsaturated species for MD0, MD2A and MD2B in LDPE extruded for 0, 5 and 10 minutes without and with CuCl

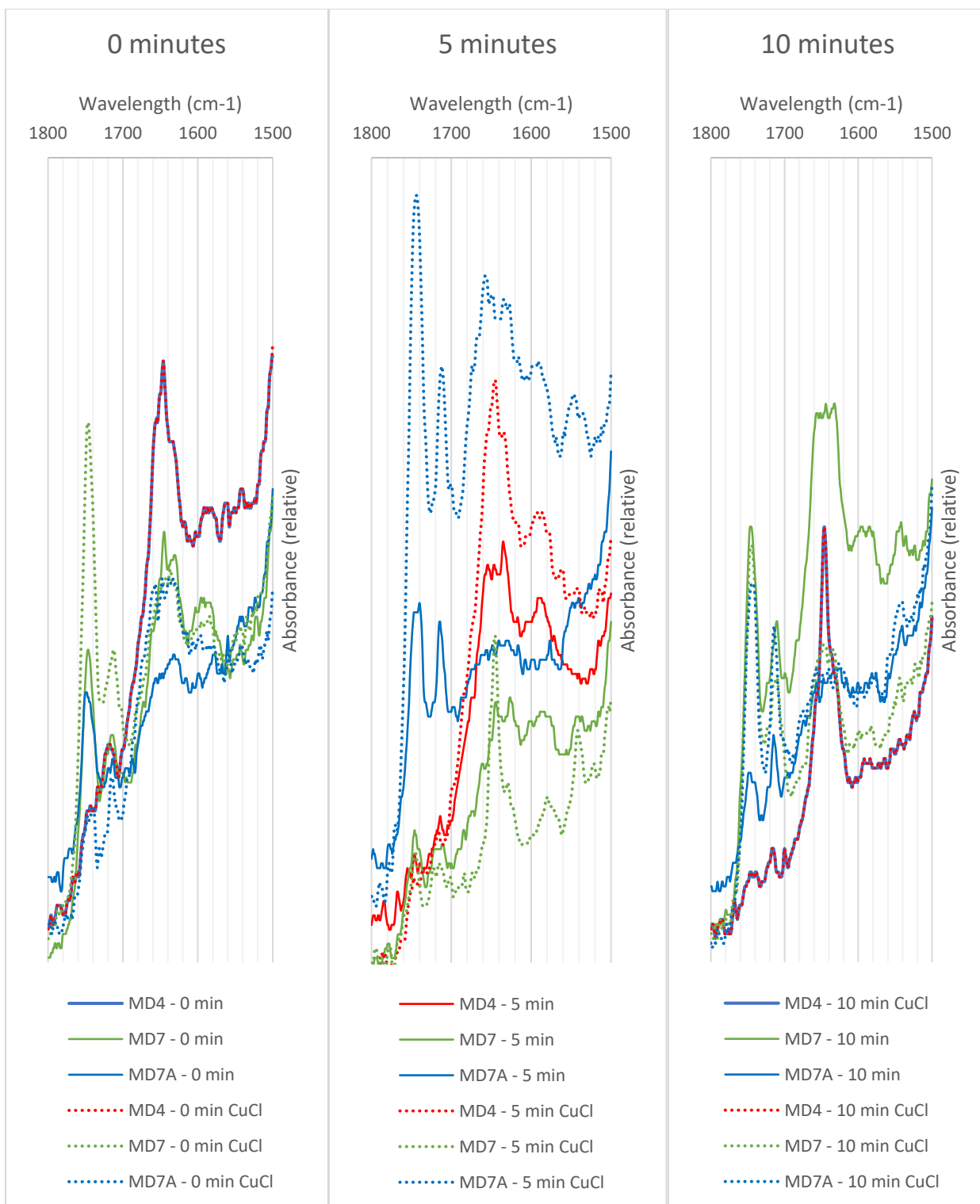


**Figure 3-47:** FTIR spectra MD4, MD7 and MD7A extruded for 0, 5 and 10 minutes without and with CuCl in carbonyl region

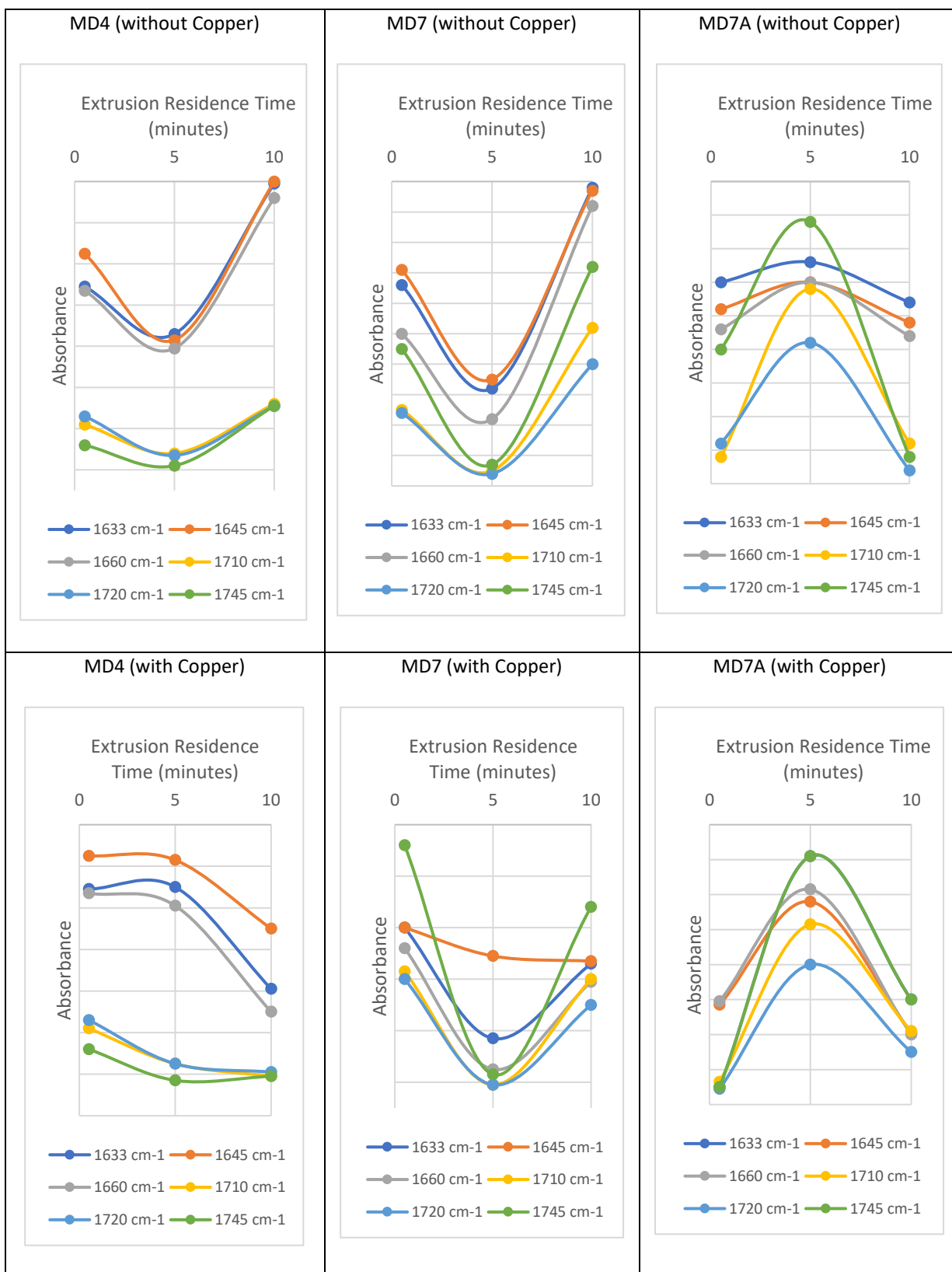


**Figure 3-48:** FTIR absorption intensities of carbonyl and unsaturated species for MD4, MD7 and MD7A in LDPE extruded for 0, 5 and 10 minutes without and with CuCl

The FTIR spectra and rates of change of key functional groups for formulations containing **MD4**, **MD7** and **MD7A** are given in **Figures 3-47 and 3-48** respectively. The FTIR spectra of LDPE+MD4 without CuCl show strong absorptions due to unsaturation that are reduced in the presence of copper, but this occurs at a relatively low rate. For **MD7** a significant ester band ( $1745\text{ cm}^{-1}$ ) is evident throughout the degradation time in the presence of copper but this is significantly lower in the absence of copper suggesting that this molecule is a much better antioxidant than it is a metal deactivator.

For **MD7A** the rates of change of carbonyl groups and spectral profiles are similar in both the absence and presence of copper. Although cage reactions of peroxy and alkoxy radicals coupled with the activity of phenol groups leads to a rapid increase in the rate of functional group formation and, this might suggest that a poorer performance of this additive, after five minutes the decrease in these groups in the most rapid of all the novel antioxidant-metal deactivators in this study. This means that MD7A is effectively complexing a higher stoichiometric ratio of  $\text{Cu}^{2+}$  as soon as it is formed by the peroxide redox couple. The results are consistent with both the YI and MFI data where **MD7A** shows the best melt stability over the extrusion time in both the absence and presence of copper.

### **3.5.3 FTIR spectra of MD-Series antioxidants and metal deactivators and their copper complexes**

The function of the metal deactivator MD1 in the formulation can be understood by its coordination geometry. The FTIR spectrum of 2-hydroxybenzohydrazide (MD1) showed absorptions at 1644 and  $1583\text{ cm}^{-1}$  corresponding to C=O and C-N stretching vibrations of the amide group. Two bands at 3269 and  $3320\text{ cm}^{-1}$  appeared due to the presence of OH and  $\text{NH}_2$  groups respectively. The absence of a band due to the  $\text{NH}_2$  group confirms its coordination with copper. Azide C=O and C-N stretching vibrations appeared at lower frequency range 1601 and  $1559\text{ cm}^{-1}$  respectively (**Figure 3-49**).

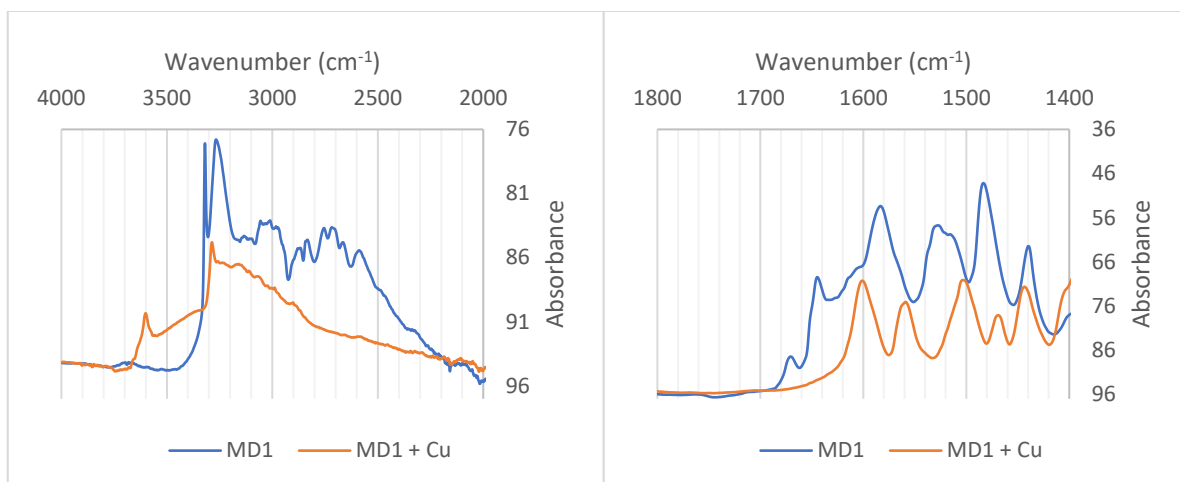
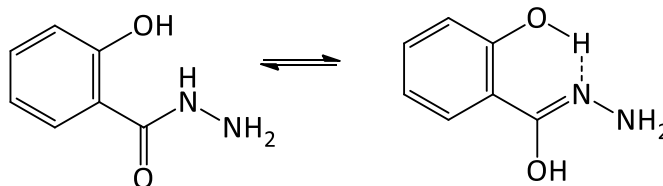


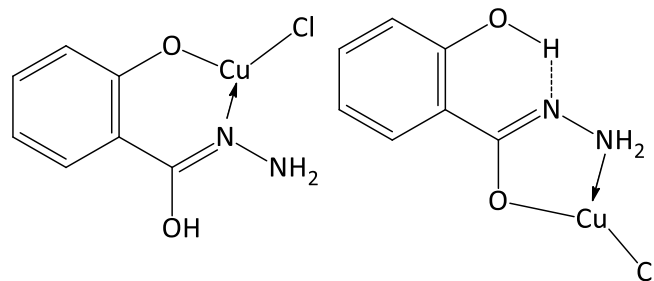
**Figure 3-49** FTIR spectra of free ligand MD1 and its complex with copper

The free OH group shifted towards higher frequency and appeared at  $3601\text{ cm}^{-1}$  and is not taking part in coordination.  $^1\text{H}$ NMR assignments of the free ligand MD1 and its complex with copper revealed that the terminal amino proton (3.77) disappeared in complexation due to coordination with copper while the NH proton slightly shifted from 9.17 ppm to 8.9 ppm.  $^{13}\text{C}$ NMR showed the shift of azide C=O carbon from 168 ppm to 165 ppm, the result of binding the copper.

Scheme \* below shows that **MD1** may possess an intra-molecular hydrogen bond.



This, and its innate structure, will prevent its antioxidant activity through formation of nitroxyl from the NH and restrict the antioxidant activity of the phenol to phenoxy radical by scavenging of peroxy. This accounts for the poor antioxidant performance of this molecule. Performance is improved in the presence of copper by its coordination capacity as shown in the structure below:



However, copper (I) is a soft Lewis acid and unlikely to coordinate to MD1, which is a hard ligand. Coordination of the metal ions is likely only after metal catalysed oxidation of peroxide (ROOH) to alkoxy (RO•) and conversion of Cu<sup>+</sup> to Cu<sup>2+</sup>. This is seen in both poor initial MFI and in the FTIR spectra of LDPE oxidation.

<sup>1</sup>HNMR for MD1B showed a shift of the NH proton from  $\delta$  11.98 to  $\delta$  12.3 ppm, and singlet of the hydroxyl proton  $\delta$  11.61 to  $\delta$  11.16. Nothing was observed in the <sup>13</sup>CNMR due to solubility issues. From the FTIR spectra, the azide C=O and C-N stretching vibrations appeared at lower frequency range 1601 and 1559 cm<sup>-1</sup> respectively, as shown in **Figure 3-50**.

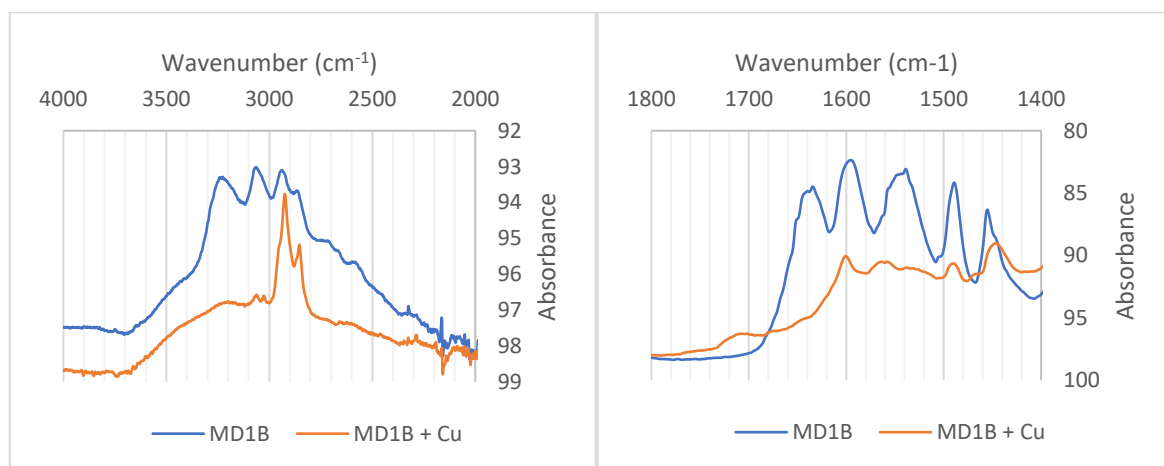
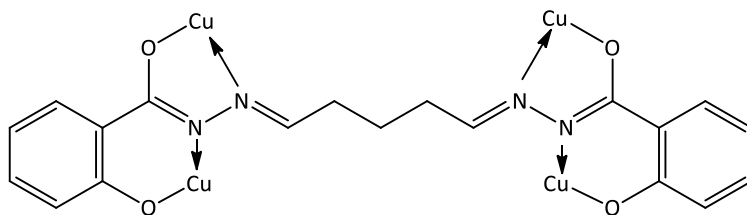


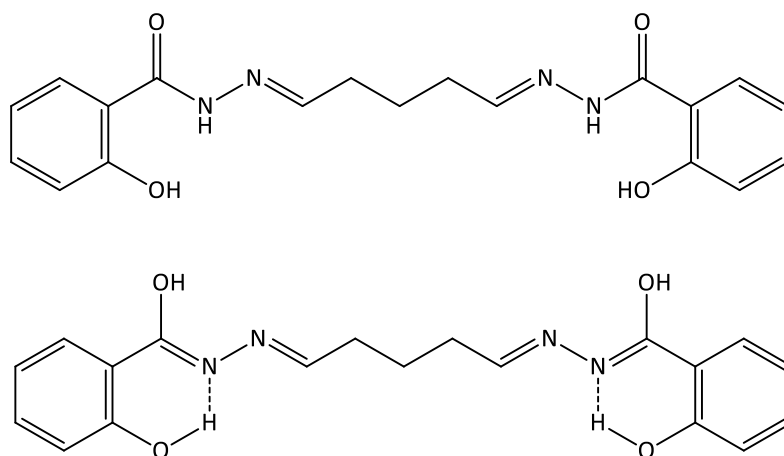
**Figure 3-50** FTIR spectra of free ligand MD1B and its complex with copper

Collectively, these observations suggest that **MD1B** can coordinate copper via its imidol tautomer. Although this will lead to effective coordination of the metal ion it will also remove antioxidant capacity from the molecule. Given the previous arguments for **MD1**, the likelihood is that **MD1B** will

only be able to coordinate and thereby reduce the activity of  $\text{Cu}^{2+}$  ions in metal catalysed decomposition of peroxide, by a redox couple.



The better antioxidant of **MD1B** performance compared with **MD1** is due to a higher molar ratio of active phenol groups.



$^1\text{H}$  NMR showed that the phenolic OH and vanillin OH proton shifted from  $\delta$  12.04 to  $\delta$  10.60 and  $\delta$  11.60 to  $\delta$  10.30 respectively while the NH proton slightly shifted from  $\delta$  9.26 to  $\delta$  9.20. Nothing was observed in the  $^{13}\text{C}$ NMR due to solubility problems. The FTIR showed, the azide C=O and C-N stretching vibrations appeared at lower frequency range 1601 and 1559  $\text{cm}^{-1}$  in the complex, as was the case for **MD1B** (Figure 3-51).

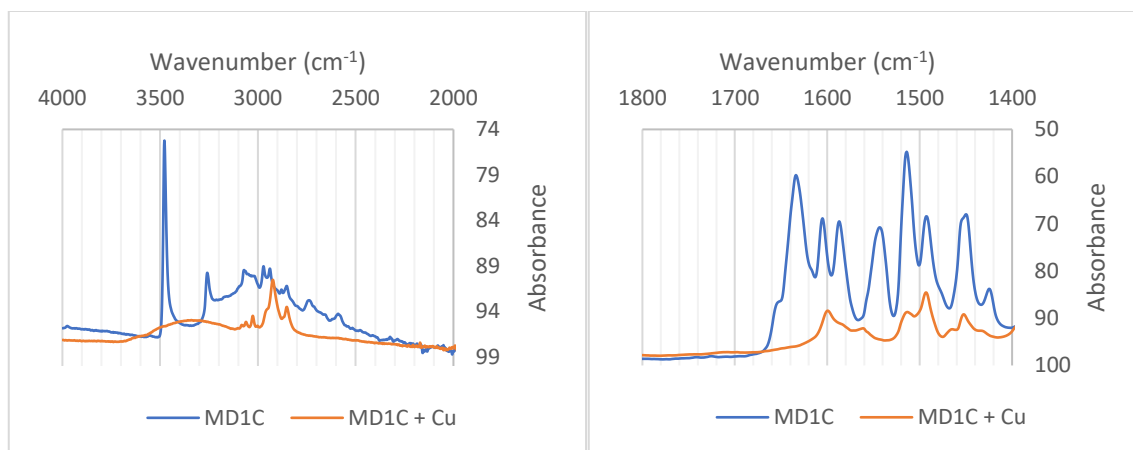
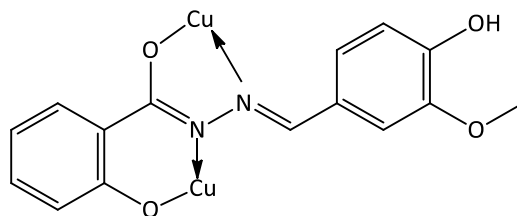


**Figure 3-51** FTIR spectra of free ligand MD1C and its complex with copper

The improved performance of **MD1C** in comparison with **MD1** and **MD1B** is a consequence of the *ortho*-methoxy phenyl group. This group has superior antioxidant activity compared with phenol alone, due to its ability to scavenge hydroxyl radicals. Therefore, it shows better initial antioxidant activity in the absence of copper and improved performance in the presence of copper. In the latter case this is due to its ability to scavenge alkoxy ( $\text{RO}\bullet$ ) and hydroxyl ( $\bullet\text{OH}$ ) radicals from peroxide decomposition formed by the  $\text{Cu}^+$  to  $\text{Cu}^{2+}$  redox couple.



The good performance of **MDO** was further supported by complexation data. FTIR spectra showed that the azomethine  $\text{C}=\text{N}$  vibration ( $1615\text{ cm}^{-1}$ ) shifted towards lower frequency ( $1601\text{ cm}^{-1}$ ). The formation of Cu-ligand complex was confirmed by the absence of important stretching vibrations due to two symmetric  $\text{-OH}$  ( $3499\text{ cm}^{-1}$ ) functional groups as shown in **Figure 3-52**.

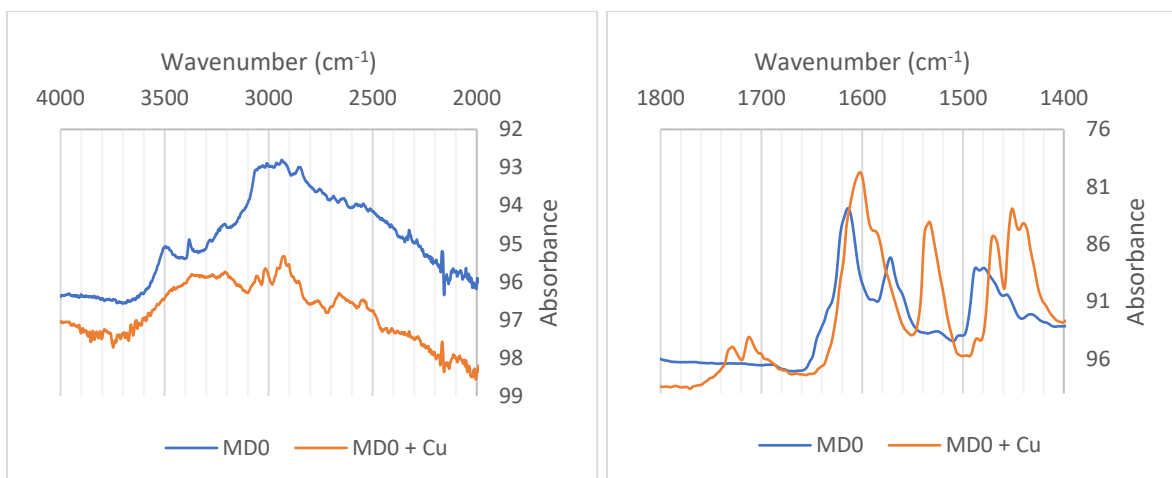
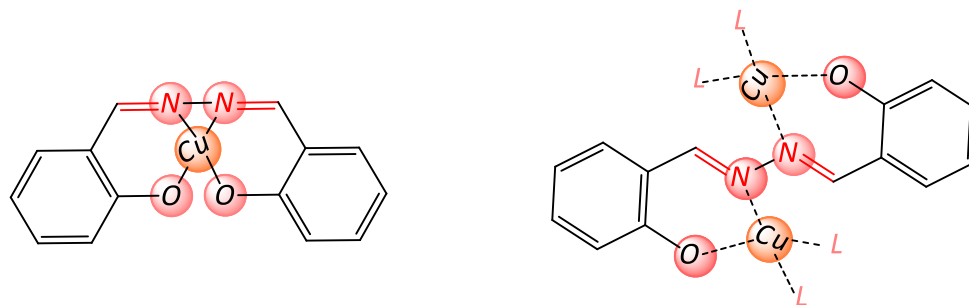
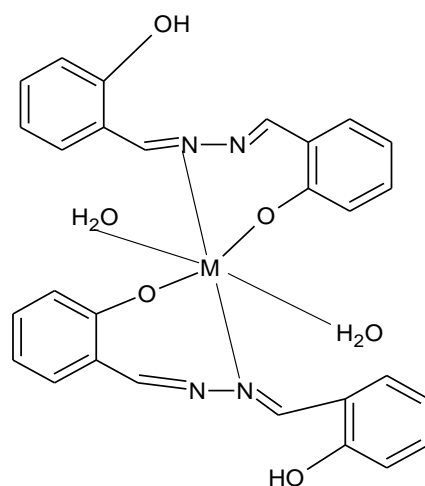


**Figure 3-52** FTIR spectra of free ligand MD0 and its copper complex

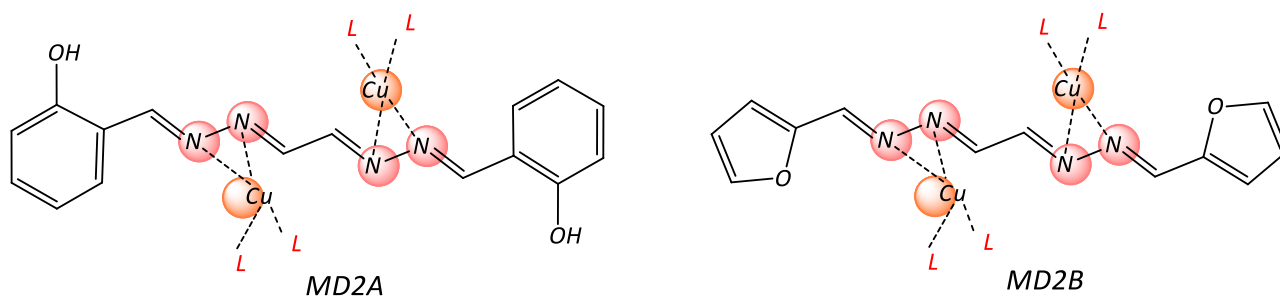
On the addition of 1.0 equiv.  $\text{Cu}(\text{OAc})_2$  to MD0, the  $-\text{OH}$  peak at 11.39 ppm does not disappear fully, probably due to the presence of two symmetric  $-\text{OH}$  units that can equally interact with two molecules of  $\text{Cu}(\text{OAc})_2$  (see structures below) but upon addition of two equiv. of  $\text{Cu}(\text{OAc})_2$ , the  $-\text{OH}$  peak almost disappears.



The literature characterises copper (II) salicylaldazine<sup>139</sup> by the following absorptions: C=N peak at  $1617\text{ cm}^{-1}$ , C-O peak at  $1196\text{ cm}^{-1}$ , N – N peak at  $983\text{ cm}^{-1}$ , C-C peak at  $1147\text{ cm}^{-1}$ , M-O peak at  $571$  and M-N peak at  $601.7\text{ cm}^{-1}$ . This is consistent with the data obtained in this study. On this basis a complex with octahedral geometry is proposed.



The FTIR spectra of **MD2A** and **MD2B** complexes are given in **Figure 3-53**. The absorption at  $1632\text{ cm}^{-1}$  and  $1616\text{ cm}^{-1}$  can be attributed to the azomethine C=N for the free ligand MD2A and MD2B respectively and these strong absorption bands are shifted towards lower frequency at  $1612\text{ cm}^{-1}$  and  $1601\text{ cm}^{-1}$  in the complex, confirming the coordination of the imino nitrogen to the Cu(II) ion.



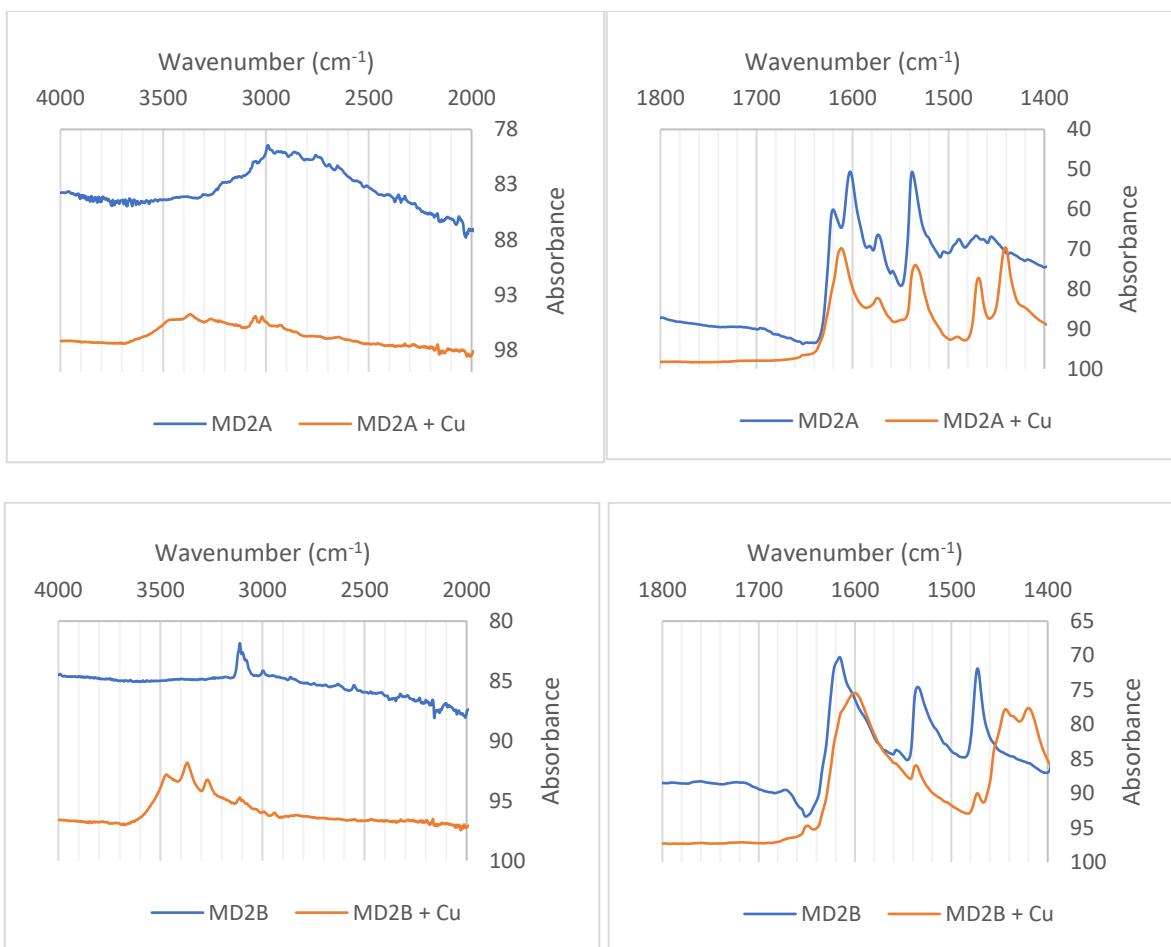
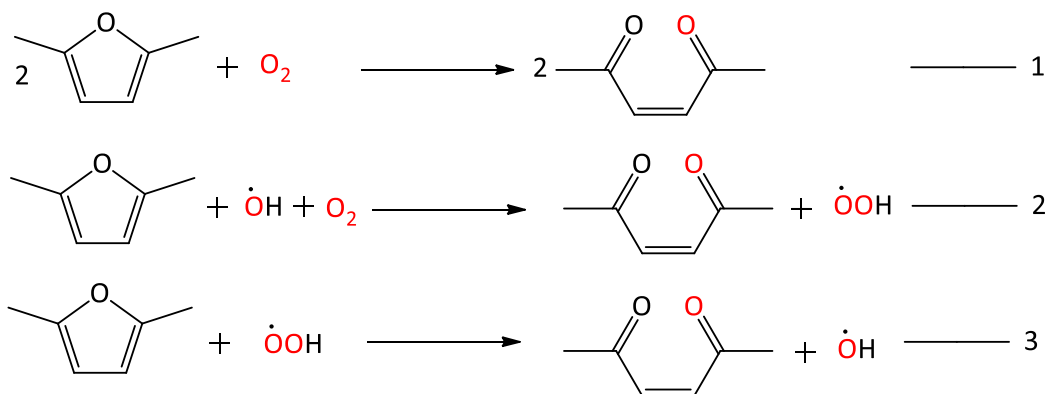
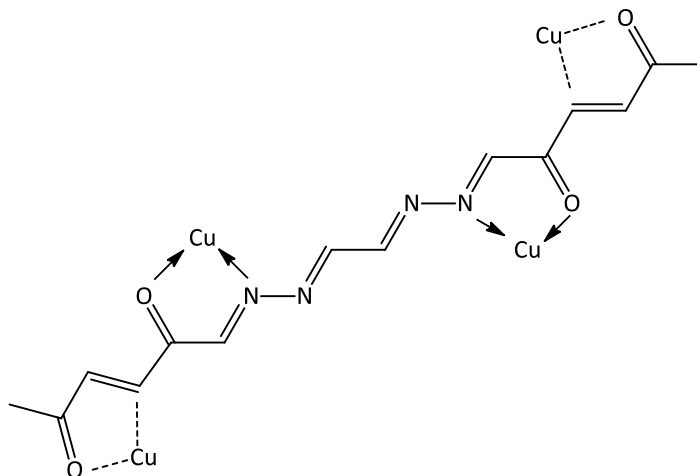


Figure 3-53 FTIR spectra of Cu-MD2A and Cu-MD2B complex

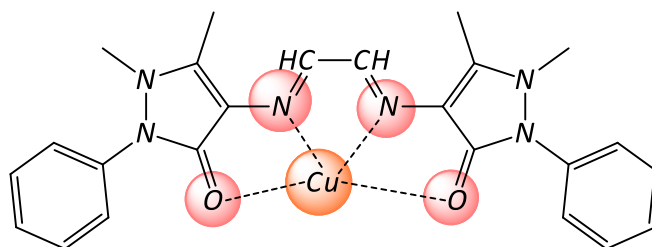
For **MD2B** it is known that the furan ring could act as a radical scavenger leading to ring opening by the steps given below:



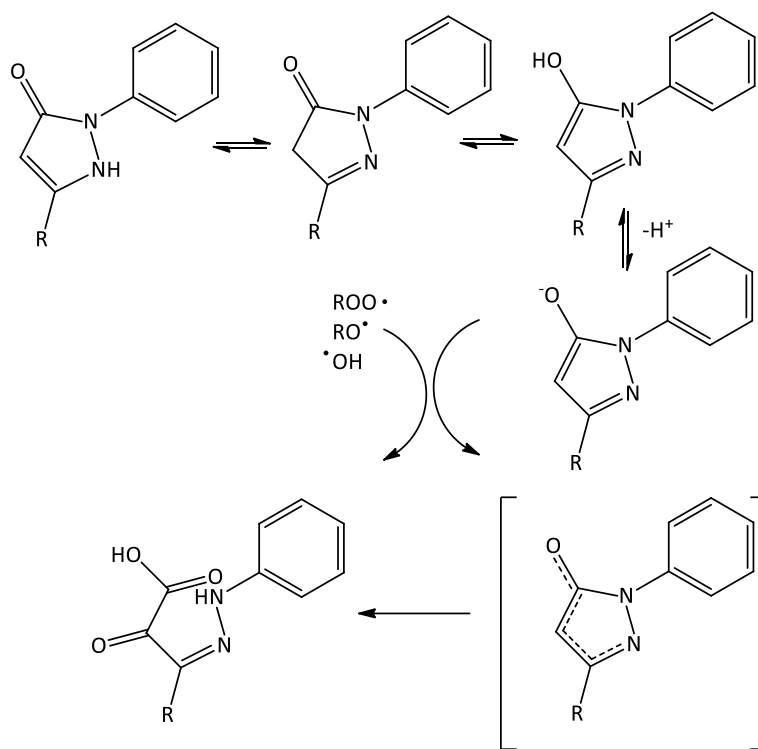
This would enable a higher stoichiometric ratio of Copper (II) to be complexed with the oxidised structure according to:



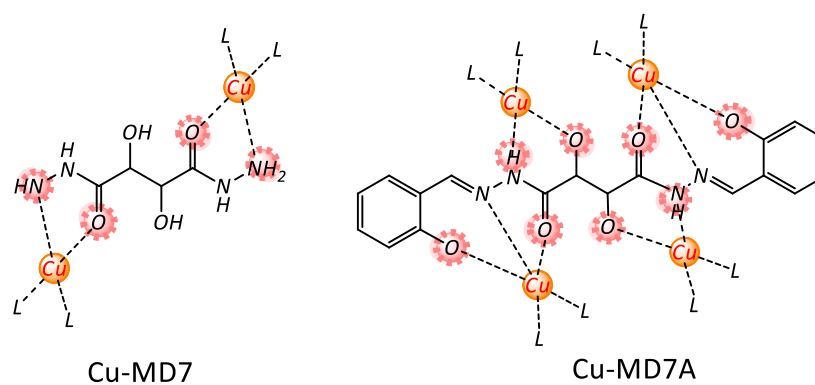
The complexation data of **MD4** is available in the literature<sup>135</sup>. The absorption at  $1650\text{ cm}^{-1}$  in free ligand MD4 is attributed to the azomethine C=N shifted towards lower frequency at  $1630\text{ cm}^{-1}$  in the complex confirming the coordination of the imino nitrogen to the Cu(II) ion as shown in the structure below.



Pyrazolone rings are also good radical scavengers. They undergo a redox coupled reaction leading to ring opening. The most effective of these structures are those where the anionic form is stabilised by an intra molecular base: as the case with **MD4**. This makes **MD4** a good antioxidant in the absence of copper. However, in the presence of copper coordination effectively removes this function.



Complexation information of **MD7A** is also reported in the literature<sup>137</sup>. The FTIR spectra of **MD7** and its complex were acquired to gain some information about the mechanism of complexation and consequently formation by probing the interaction of Cu ion with  $>C=O$  groups (see structure below).



The band at  $1673\text{ cm}^{-1}$  corresponding to  $>C=O$  stretching in the vibrational spectra of free ligand shifted to  $1646\text{ cm}^{-1}$  in the complex, confirming weakening of the  $>C=O$  bond due to  $>C=O\cdots Cu^{++}$  interaction as shown in **Figure 3-54**.

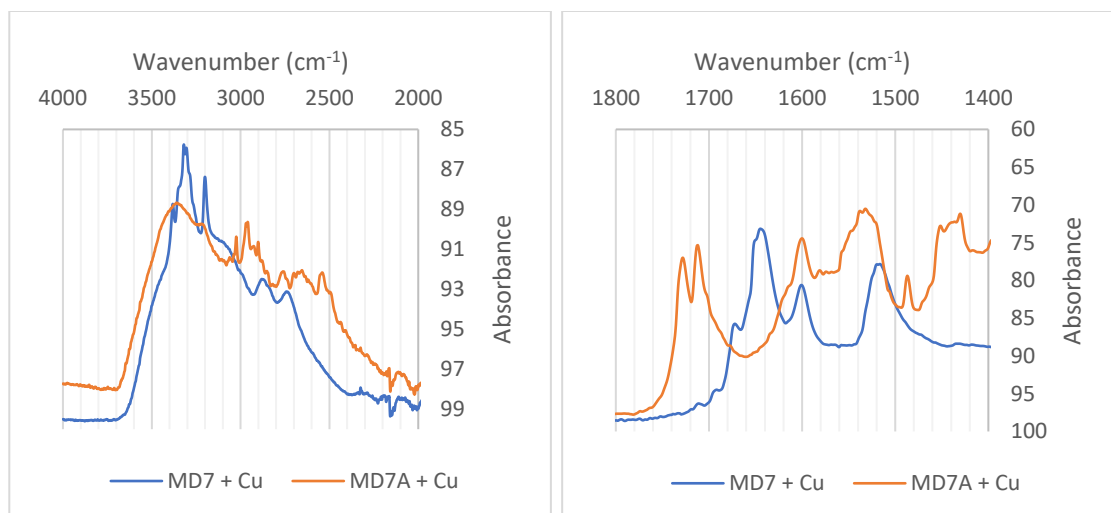
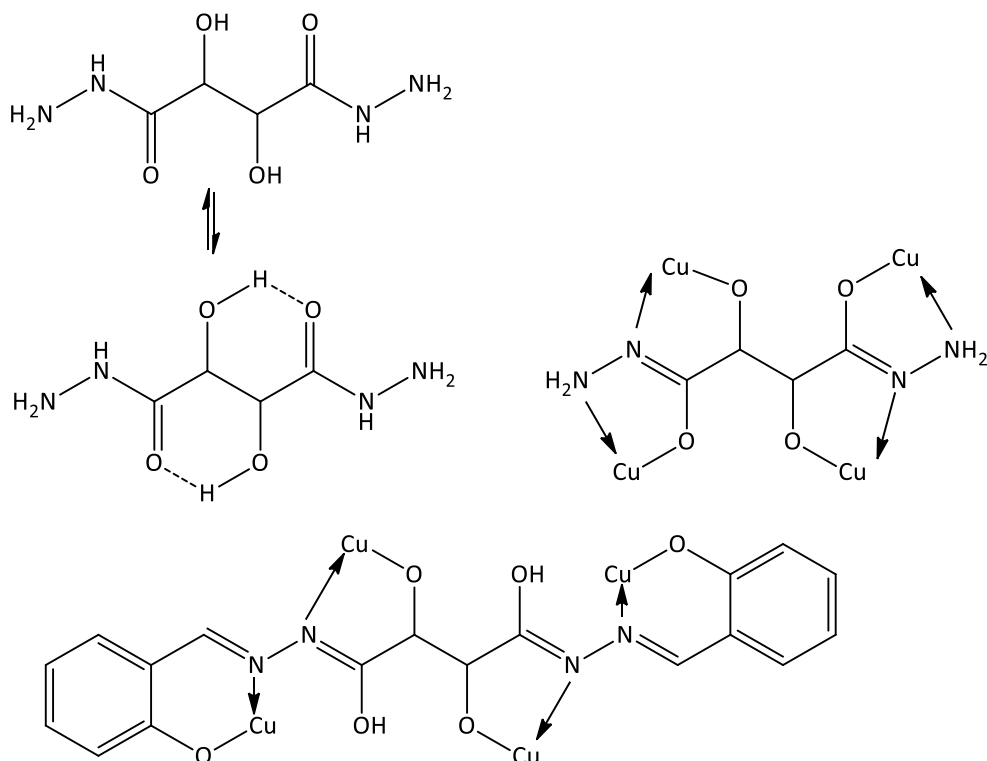


Figure 3-54 FTIR spectra of Cu-MD7 and Cu-MD7A complex

Allowing for hydrogen bonding and tautomerism the following structures are proposed for **MD7** and **MD7A** :



## Section B: Novel Antioxidant-Metal Deactivator Performance Summary

**Figures 3-55 to 3-58** show the combined MFI and YI data for all the additives processed by circulation mode extrusion in this study. At least 5 of the structures have equal or superior performance to the commercial metal deactivators *LOWINOX<sup>®</sup>MD24* and *NAUGARD<sup>®</sup>XL-1*. The L-Series structures show the poorest performance in terms of melt stability both in the absence and presence of copper. The best performing structures are the MD series. The T-series show good initial antioxidant performance, as do many of the MD-Series. L1A, L3A, T0A, S7 and S8 also show an initial MFI that is lower than that of LDPE alone. In all cases, in the absence of copper, the MFI increases with extrusion (oxidation) time, with the notable exception of S5.

Most of the structures show a decrease in MFI (improved melt stability) in the presence of copper, over the extrusion time, except several of the S-Series ligands. Here only S0, S5, S6 and S8 show a reduction in MFI. The relative rates of reduction in MFI vary considerably across the different Series and more data points would have enabled a better evaluation of kinetic rates.

The yellowness index (YI) data displays high colour for the L-Series and many of the MD-Series structures in both the absence and presence of copper. The best retention of colour relative to LDPE is seen for samples and MD7A T0A, S5, S6, S7, as well as for the commercial metal deactivators *LOWINOX<sup>®</sup>MD24* and *NAUGARD<sup>®</sup>XL-1*. However, in many commercial plastics applications colour is not a problem (e.g. cable) and in other cases formulations can be colour balanced.

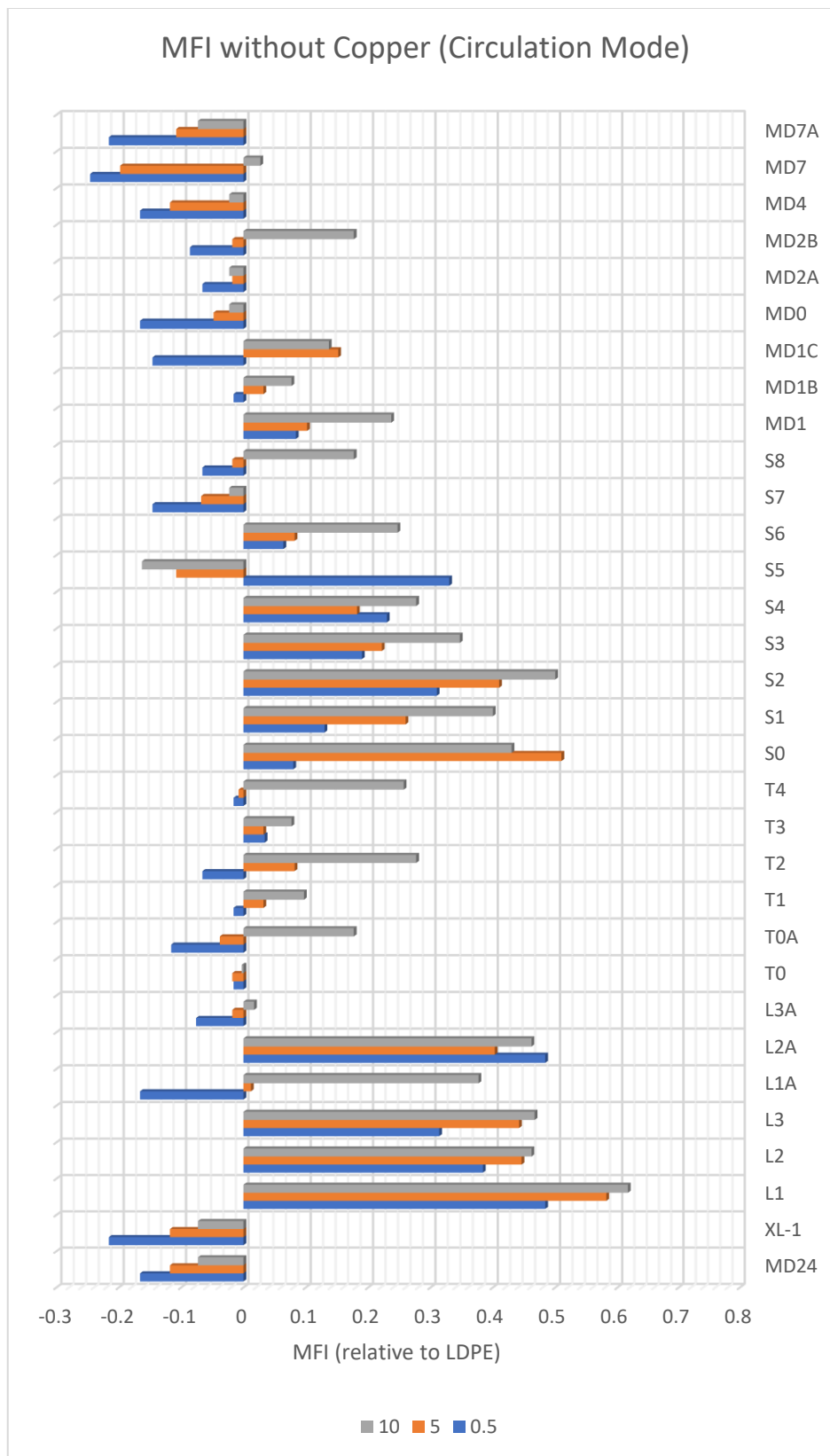


Figure 3-55 MFI of novel antioxidant-metal deactivators in LDPE in the absence of copper (I) chloride

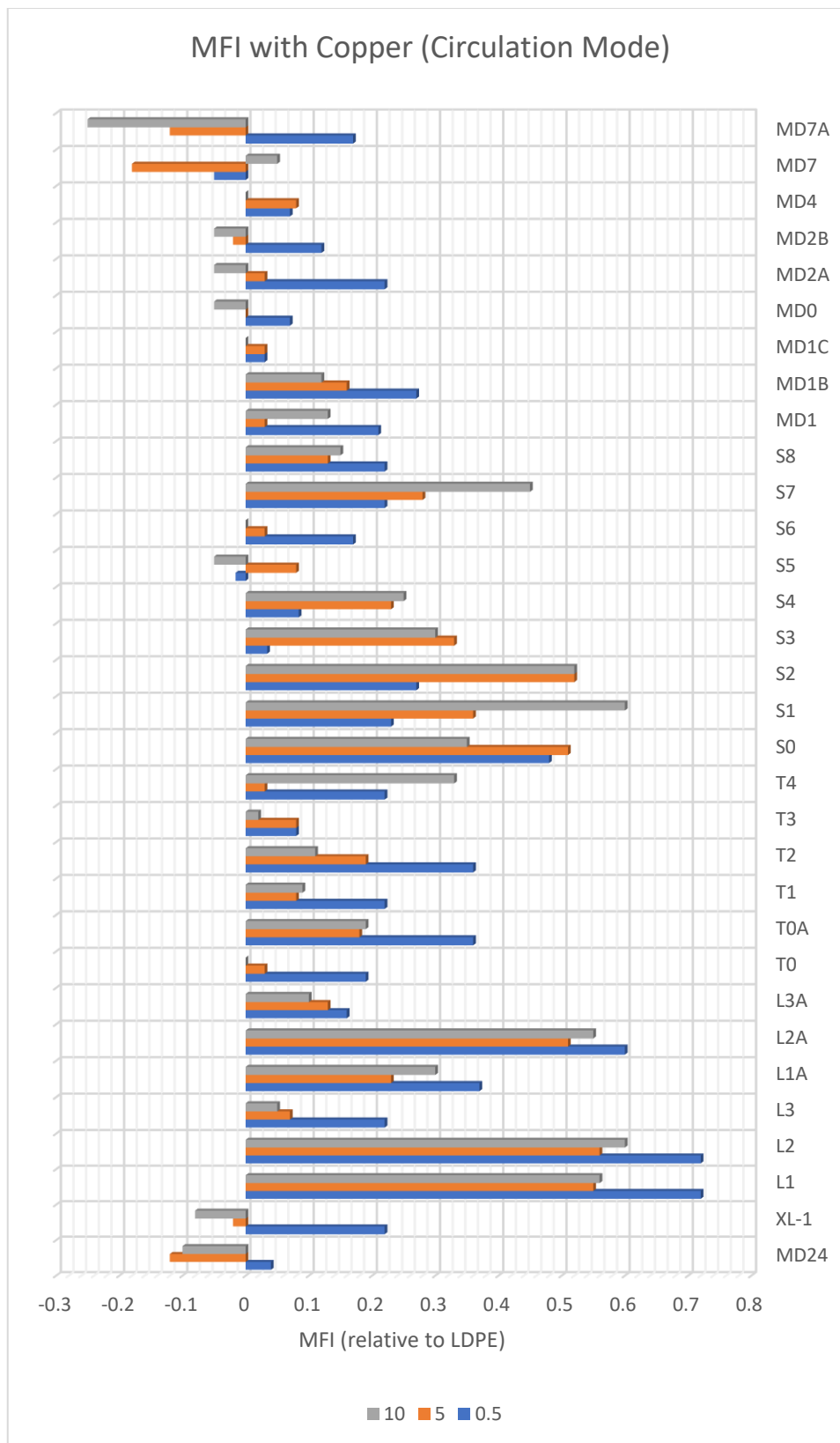


Figure 3-56 MFI of novel antioxidant-metal deactivators in LDPE in the presence of copper (I) chloride

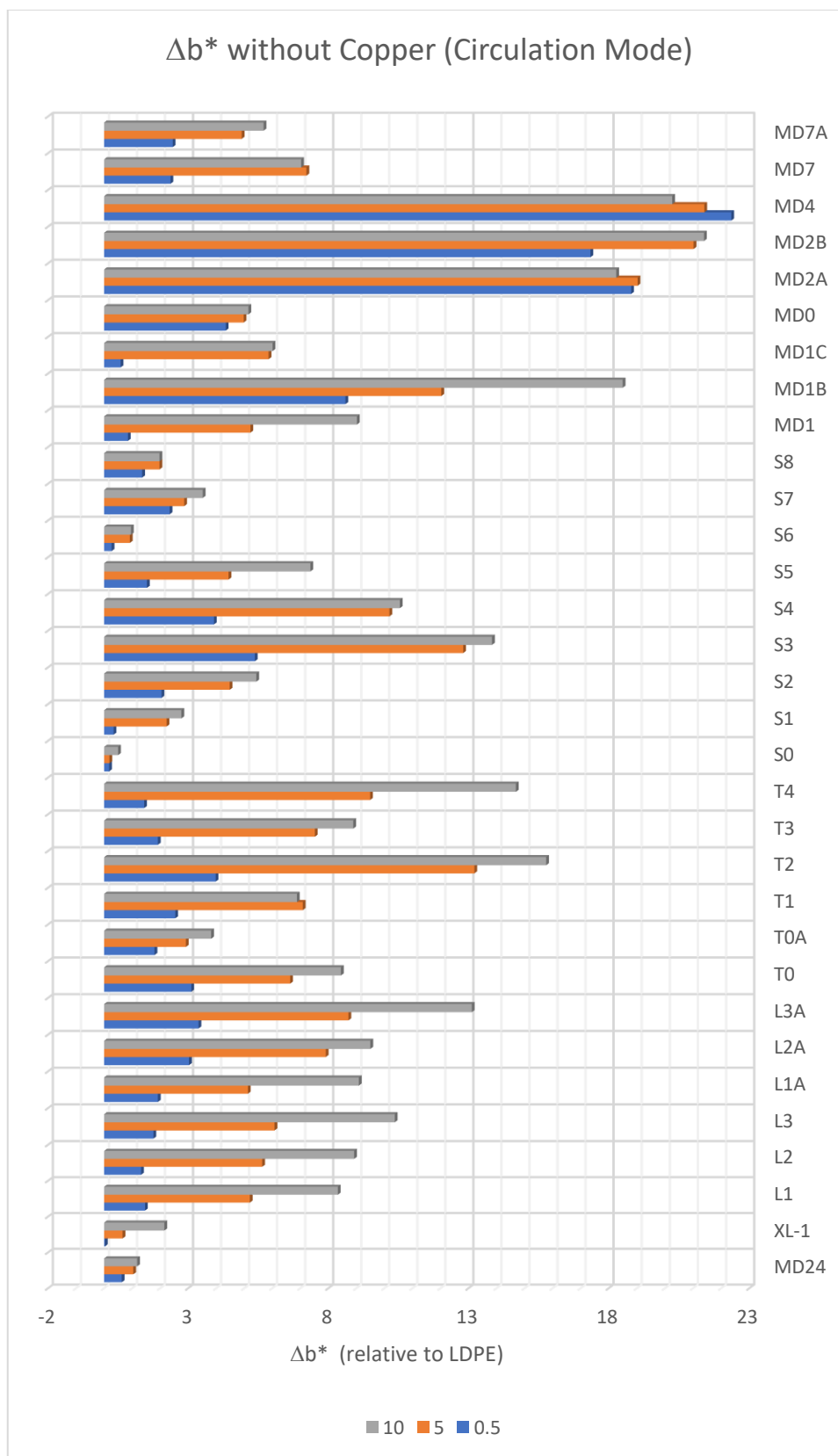


Figure 3-57 Δb\* of novel antioxidant-metal deactivators in LDPE in the absence of copper (I) chloride

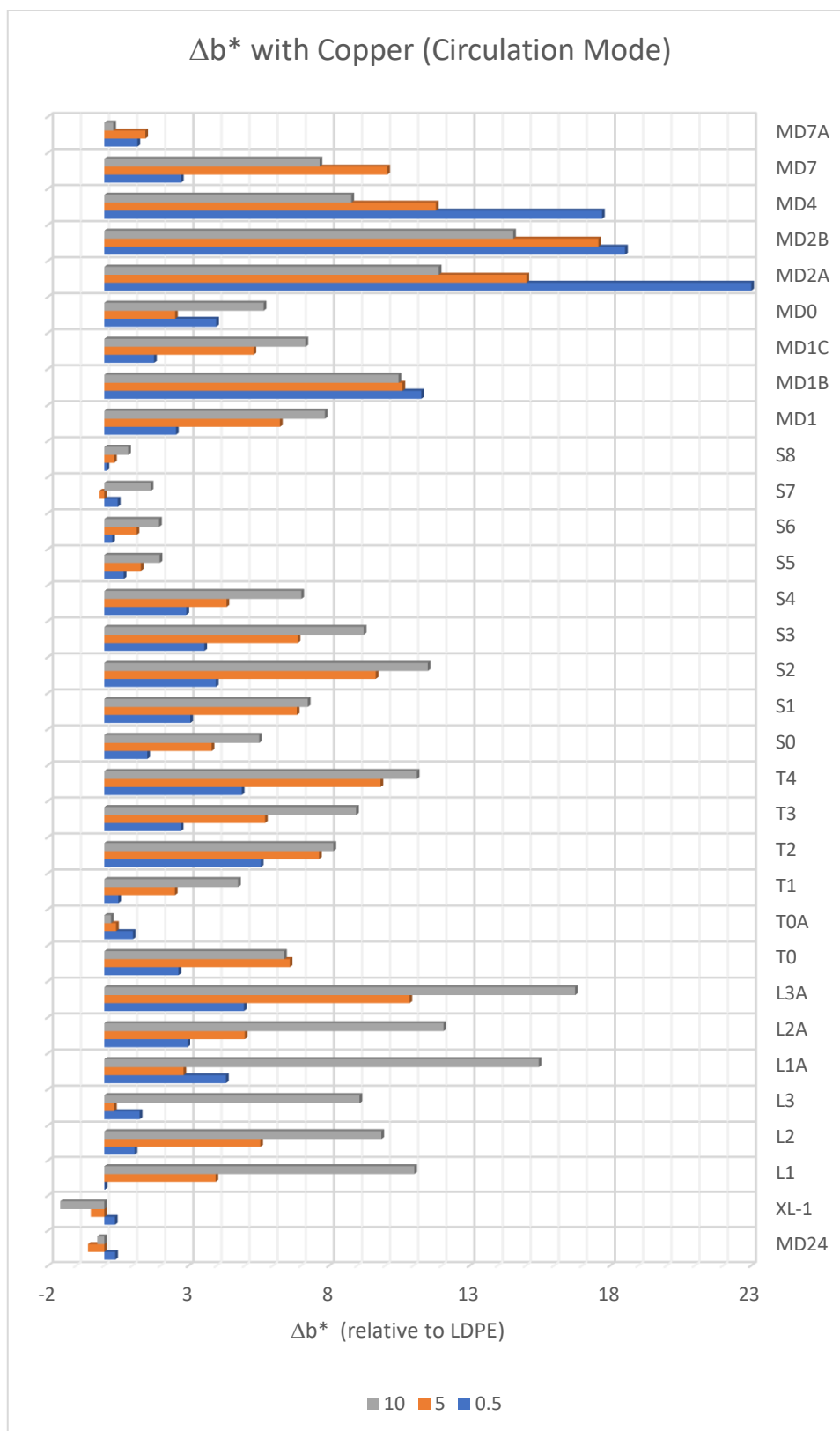


Figure 3-58  $\Delta b^*$  of novel antioxidant-metal deactivators in LDPE in the presence of copper (I) chloride

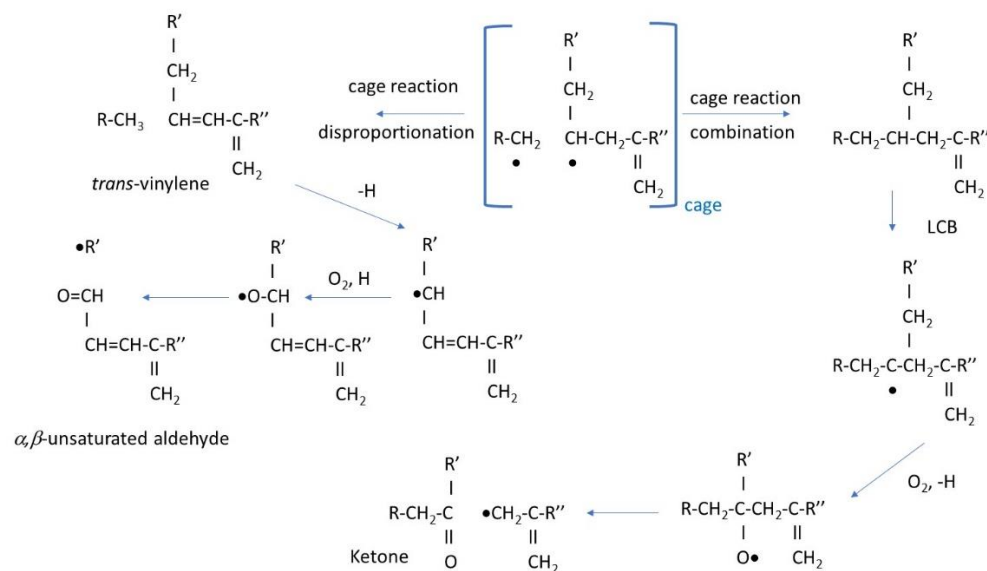
## Chapter 4: Conclusion and Further work

### 4.1 Conclusions

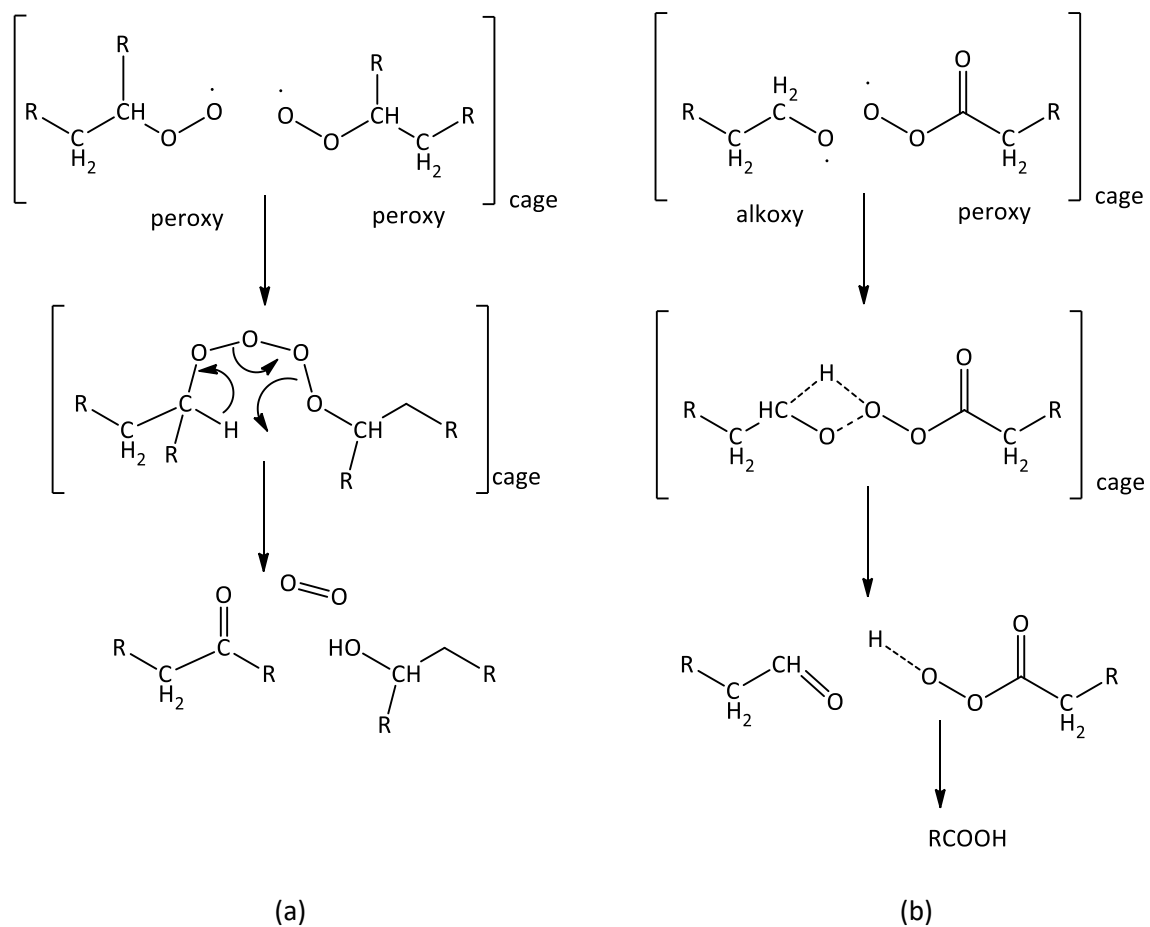
A wide range of structures have been synthesised that combine antioxidant and metal deactivator functions in a single molecule. The performance of these novel structures has been evaluated in LDPE oxidised during circulation mode extrusion, using MFI, YI and FTIR spectroscopy. Nearly all the structures have an ability to complex  $\text{Cu}^{2+}$  and demonstrate wide ranging performance. Inhibition of oxidative degradation by these antioxidant-metal deactivators is complex and arises from a subtle balance of antioxidant and metal deactivator functions.

The work highlights the complex interplay between different routes to degradation and their inhibition, particularly the concentration profile of peroxy radicals and peroxides that leads to the carbonyls (aldehyde, ketone, ester) that predominate the degradation profile of polymers such as LDPE.

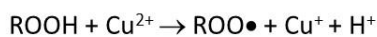
At low levels of oxidation, cage recombination for radicals competes effectively with disproportionation, and cage escape is limited by diffusion, leading to low concentrations of peroxy radical and peroxide.



At higher levels of oxidation, the opportunity for cage reactions involving alkoxy, peroxy and peroxide radicals increases.

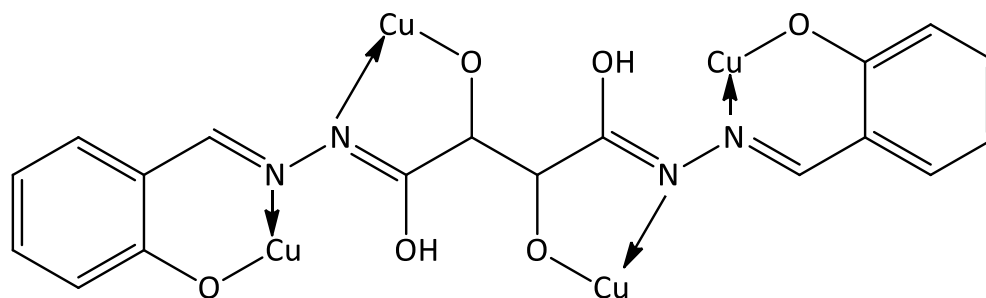


In the presence of metal ions both routes to generation of oxidised species will be promoted according to the accepted mechanisms for the redox decomposition of peroxides and generation of peroxy and alkoxy radicals.

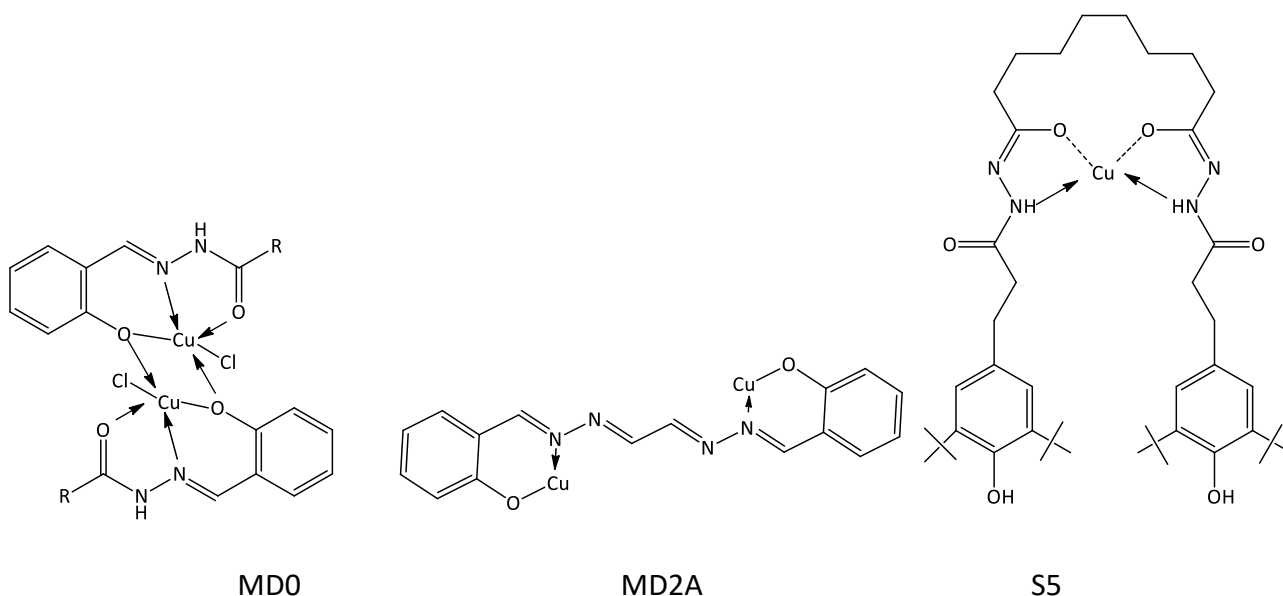


The best performance of antioxidant-metal deactivator structures is presented therefore by molecules that optimise metal coordination at multiple sites with proximity to an effective peroxy

and alkoxy radical scavenger (i.e. primary antioxidants of the phenolic type). This is demonstrated by the excellent performance of MD7A which shows a comparable antioxidant performance (in the absence of copper) to the commercial metal deactivators (LOWINOX<sup>®</sup>MD24 and NAUGARD<sup>®</sup>XL-1) but 2.5x the improvement in melt stability in the presence of copper, meaning it is a significantly better metal deactivator. Although not as effective MD0, MD2A and S5 also show good performance (comparable to the commercial metal deactivators).



MD7A



MD0

MD2A

S5

Here the role of  $\text{Cu}^+$  as a soft Lewis acid prevents initial coordination with the metal deactivator until it has been oxidised to  $\text{Cu}^{2+}$ , when it can then bind with the hard ligands of these novel structures. This allows the phenol in the initial stages of oxidation to scavenge peroxy and alkoxy radicals. MD7A and S5 also shows a low value of YI, since the potential for extended conjugation of quinone arising from the phenoxy radical is prevented.

These principles may be used to tailor antioxidant-metal deactivator ligands to metal redox systems (e.g.  $\text{Fe}^{2+}/\text{Fe}^{3+}$ ) and so improve the performance of metal deactivators in commercial polymers.

## 4.2 Further Work

Though a-number-of important trends have been highlighted in this study there is considerable scope for further work. Indeed, it is surprising that more extensive work on metal deactivators is not evident in the published literature, given that these important additives have a central role in many plastics applications and have wider implications in other areas of commercial concern (petrochemical, biological).

The work undertaken here has used circulation mode extrusion to highlight any difference in the performance of the antioxidant-metal deactivators, but the work should be repeated using multi-pass extrusion which is the traditional method used by industry to assess the performance of additives. A comparison is given here to give an initial comparison of the differences in these different extrusion methods: **Figure 3-59** shows the MFI values.

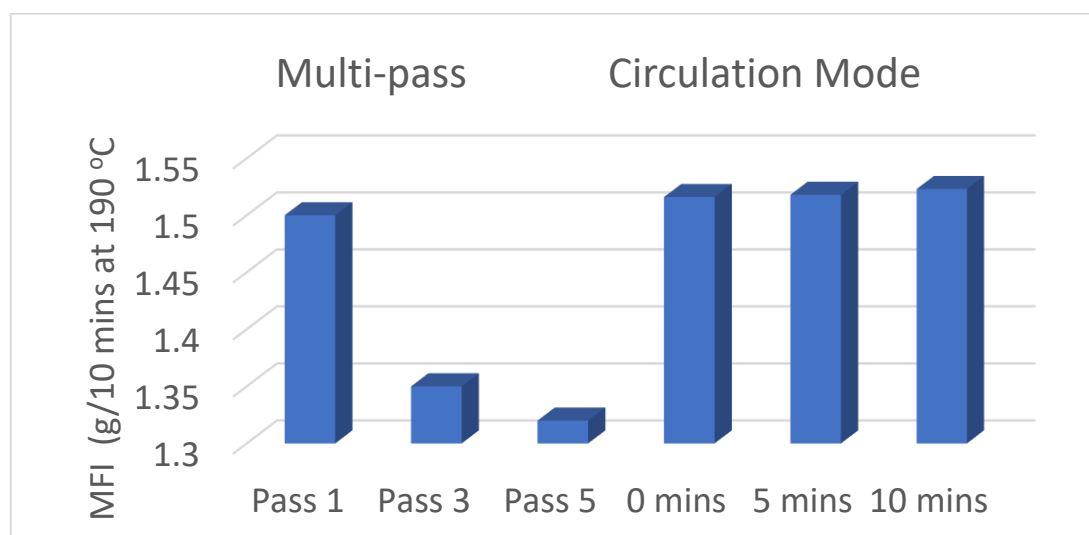


**Figure 3-59** MFI values for LDPE subjected to multi-pass and circulation mode extrusion (*s.d* = 0.01 g/10 min)

The time evolution of changes in MFI is as an indirect measure of molecular weight changes for LDPE during oxidation, by measuring melt viscosity under a constant load and low shear rates. During circulation mode the MFI is increasing very slightly during the oxidation time (0 to 10 minutes), which

demonstrates competition between chain-scission and chain-branching/cross-linking. Note that throughout this study, 0 minutes corresponds to about 30 seconds residence time to achieve throughput of the material. For multi-pass extrusion the MFI shows a noticeable decrease, indicating that chain-branching/cross-linking are the dominant modes of degradation. Note that the MFI values for Pass 1 and 0 minutes are similar, consistent with a standard deviation of  $\pm 1\%$  (pass time is about 30 seconds). The data for MFI and YI by multi pass extrusion is given in the **Appendix (Tables A-7 to A-10)**. This data will be published separately in a peer-reviewed polymer journal. Again, the type of species generated on degradation is similar, but their distribution and concentrations differ over the extrusion time, leading to subtle differences in the performance of the antioxidant-metal deactivators.

This thesis has been focused mainly on the synthesis of novel metal deactivators and understanding their performance within a polymer matrix, but a more critical evaluation requires widening the scope of the investigations including but not limited to:

- more in-depth analysis of the specific chelation process and binding strengths of the antioxidant-metal deactivators. This would be particularly useful if complex formation constants were assimilated as a function of temperature.
- quantification of the synthetic antioxidant-metal deactivator after each extruder pass via HPLC analysis following solvent extraction. Loss of the metal deactivators or their transformation products is important in relation to their activity.
- polymer oxidation studies in situ on copper metal surfaces would provide real-life activity and efficacy.
- combination of the structures with commercial additives to assess any synergism or antagonism (a start to this work is provided in the multi-pass extrusion data in the Appendix)
- concentration profiles of antioxidants also influence performance, and combinations of additives may improve solubility arising from eutectic mixtures.
- many of the molecules synthesised are similar in structure to antimicrobial structures and as such their microbiological activity should be assessed. In conjunction an assessment of the

toxicity profile of the best performing structures should be undertaken. This would then extend the applicability of the antioxidant-metal-deactivators into biological and other areas.

- Many metal deactivators are also utilised for the protection of polymers in contact with other metals not just Cu with iron ranking second in importance and here their utilisation and efficacy with various types of doped iron would be valuable, such as Chromium vs C-doped steels. Activity with Ferrite species play an important role here.
- In terms of further changes to the structures developed here, the following modifications are suggested:
  - The addition of a phosphorus atom in the backbone chain of the chelation agents would be of value in terms of anti-corrosion activity.
  - Enhancement of the additives by the introduction of a greater number of azomethine units at its core, in-line with the trends observed in this study.

## References

1. Z. Osawa, *Polymer Degradation and Stability*, 1988, **20**, 203-236.
2. E. Blatt, H. J. Griesser, J. H. Hodgkin and A. W.-H. Mau, *Polymer degradation and stability*, 1989, **25**, 19-29.
3. *Fundamentals of Polymer Degradation and Stabilization* | N.S. Allen | Springer, 2016.
4. M.G.Chan, *Journal of Colloid and Interface*, 1974, **47**, 589-805.
5. J. Cogen and A. Hilmer, *Polymer Degradation and Stability*, 2008, **93**, 2193-2198.
6. J. Pospíšil, Z. Horák, Z. Kruliš, S. Nešpůrek and S.-i. Kuroda, *Polymer Degradation and Stability*, 1999, **65**, 405-414.
7. L. M. Gorghiu, S. Jipa, T. Zaharescu, R. Setnescu and I. Mihalcea, *Polymer Degradation and Stability*, 2004, **84**, 7-11.
8. F. Gugumus, Paper presented at the 4e Conférence Européenne des plastiques et des caoutchoucs, and J. Paris, *Kunstst. Plast.* (1975) 22, p. 11–19, *Caout. Plast.* (1976) 558, p. 67–71.
9. H.Staudinger, *Die Hochmolecularen*, Springer-Verlag, Berlin, 1932.
10. Raymond B. Seymour and Charles.E.Carraher.Jr, *Structure-Property Relationships in Polymers*, Plenum Press, New York, a division of Plenum Publishing Corporation, 233 Spring Street, New York, N.Y.10013, New York, 1984.
11. M. Kutz, *Applied Plastics Engineering Handbook - Processing, Materials, and Applications (2nd Edition)*, Elsevier.
12. D. Abraham, K. E. George and D. J. Francis, *Polymer*, 1998, **39**, 117-121.
13. A.J Peacock, ed. *Handbook of Polyethylene*, Marcel Dekker, New York. , 2000.
14. V. R. Sastri, in *Plastics in Medical Devices - Properties, Requirements, and Applications*, Elsevier, p. 89.
15. A.J Peacock, *Catalytic activity and control of the nascent morphology of polyethylenes obtained with first and second generation of Ziegler-Natta catalysts. ed. Handbook of Polyethylene*, Marcel Dekker, New York. , 2000.
16. C. Brown, J. Krzystek, R. Achey, A. Lita, R. Fu, R. W. Meulenberg, M. Polinski, N. Peek, Y. Wang, L. J. van de Burgt, S. Profeta, A. E. Stiegman and S. L. Scott, *ACS Catalysis*, 2015, **5**, 5574-5583.
17. M. P. McDaniel, *Advances in Catalysis*, 1985, **33**, 47-98.
18. K. H. Theopold, R. A. Heintz, S. K. Noh and B. J. Thomas, in *Homogeneous Transition Metal Catalyzed Reactions*, American Chemical Society, 1992, vol. 230, ch. 41, pp. 591-602.
19. K.W.Swogger, *An Outlook for Metallocene and Single Site Catalyst Technology into 21st Century*, Polyethylene and Insite Technology.
20. D.Yan, W.J. Wang and S. Zhu, *Polymer*, 1999, **40**, 1737-1744.

21. W.A.Fraser and C.C.Williamm, *Manufacturing efficiencies from metallocene cattalyst in gas-pashe polyethylene production*, 1971.
22. M.Bochmann, G.J. Pindado and S.J. Lancaster, *Journal of Molecular Catalysis A: Chemical*, 1999, **146**, 179-190.
23. G.M. Benedikt and B.L. Goodall, eds. *Metallocene Catalyzed Polymers*, Plastic Desing Library: New York., 1998.
24. W. Kaminsky and A. Laban, *Applied Catalysis A: General*, 2001, **222**, 47-61.
25. W. Kaminsky, *Journal of the Chemical Society, Dalton Transactions*, 1998, 1413-1418.
26. Devesh Tripathi, *Practical Guide to Polypropylene*, Smithers Rapra Technology, Shawbury, Shrewsbury, Shropshire, SY4 4NR, UK, 2002.
27. S. Arjmand, *IOSR Journal of Polymer and Textile Engineering (IOSR-JPTE)*, 2014, **1**, 37-45.
28. C. Maier and T. Calafut, *Polypropylene - The Definitive User's Guide and Databook*, William Andrew Publishing/Plastics Design Library, United States of America, Norwich, NY, 1998.
29. Thomas Carl Ward, *Journal of Chemical Education*, 1981, **58**, 867.
30. D. M. Mowery, R. L. Clough and R. A. Assink, *Macromolecules*, 2007, **40**, 3615-3623.
31. D. J. Carlsson and D. M. Wiles, *J.Macromol. Sci., ReV. Macromol. Chem* 1976, **C14**, 65-106
32. G. A. George and M. Celina, *Homogeneous and Heterogeneous Oxidation of Polypropylene. In Handbook of Polymer Degradation, 2nd ed.; Hamid, S. H., Ed., Marcel Dekker: New York New York 2000.*
33. F. M. Mirabella, *Polymer*, 1993, **34**, 1729-1735.
34. H. Frostling, A. Hoff, S. Jacobsson, P. Pfäffli, S. and Vainiotalo and A. Zitting, *Scandinavian Journal of Work, Environment & Health,,* 1984, 163-169.
35. J. Bolland and G. Gee, *Transactions of the Faraday Society*, 1946, **42**, 236-252.
36. J. Bolland, *Proceedings of the Royal Society of London. Series A. Mathematical and Physical Sciences*, 1946, **186**, 218-236. .
37. A.V.Tobolsky, *Discussions of the Faraday Society*, 1947, **2**, 384-388.
38. J. L. Bolland, *Quarterly Reviews, Chemical Society*, 1949, **3**, 1-21.
39. *J. Bolland, Faraday Trans Soc., 1948, 44, 669-677.*
40. J. F. Cavalli, X.Fernandez, L.Lizzani-Cuvelier and A. M. Loiseau, *Journal of agricultural and food chemistry*, 2003, **51**, 7709-7716.
41. J. Dewulf, H.Van.Langenhove and G. Wittmann, *TrAC Trends in Analytical Chemistry*, 2002, **21**, 637-646
42. C. Henneuse and T. Pacary, *Emissions from plastics, iSmithers Rapra Publishing*, 2003.
43. B. Singh and N. Sharma, *Polymer Degradation and Stability*, 2008, **93**, 561-584
44. G. Mitchell, C. Higgitt and L. T. Gibson, *Polymer Degradation and Stability*, 2014, **107**, 328-340.
45. A.Hoff and S.Jacobsson, *Journal of applied polymer science*, 1984, **29**, 465-480.
46. F. Severini, R. Gallo and S. Ipsale, *Polymer degradation and stability*, 1988, **22**, 185-194

47. D. Bertin, M. Leblanc, S. R. Marque and a. D. Siri, *Polymer Degradation and Stability*, 2010, **95**, 782-791
48. R. Bernstein, S. M. Thornberg, R. A. Assink, A. N. Irwin, J. M., Hochrein, J. R. Brown, D. K. Derzon, S. B. Klamo and R.L.Clough, *Polymer Degradation and Stability* 2007, **92**, 2076-2094.
49. J.L. Philippart, F. Posada and J. L. Gardette, *Polymer degradation and stability*, 1995, **49**, 285-290. .
50. A.François-Heude, E. Richaud, J. Leprovost, M. Heninger, H., Mestdagh, E. Desnoux and X. Colin, *Polymer Testing*, 2013, **32**, 907-917.
51. L. Bateman, *Quarterly Reviews, Chemical Society*, 1954, **8**, 147-167.
52. T. Hatanaka, H. Mori and M. Terano, *Polymer Degradation and Stability*, 1999, **64**, 313-319.
53. H. Frostling, A. Hoff, S. Jacobsson, P. Pfaffli, S. Vainiotalo and A. Zitting, *Scand J Work Environ Health*, 1984, **10**, 163-169.
54. X. Xue, K. Hanna, C. Despas, F. Wu and N. Deng, *Journal of Molecular Catalysis A: Chemical*, 2009, **311**, 29-35.
55. J.Bolland., *Trans. Faraday Soc*, , 1950, **46**, 358-368.
56. F. Gugumus, *Polymer Degradation and Stability*, 2001, **74**, 327-339
57. J.K.Kochi, ed. *Free Radicals*, New York: Wiley, 1973, 665-710.
58. Evgeny T. Denisov and Igor B. Afanas'ev, *Oxidation and Antioxidants in Organic Chemistry and Biology*, CRC Press Taylor & Francis Group, 6000 Broken Sound Parkway NW ,Boca Raton, FL 33487-2742, 2005.
59. K.J.Laidler, LF.Loucks, In: CH Bamford and C. F. H. Tipper, eds. *Comprehensive Chemical Kinetics*, Amsterdam: Elsevier, 1972,1-148.
60. G.C.Eastmond, In:C.H.Bamford and C.F.H.Tipper, eds. *Comprehensive Chemical Kinetics*, Amsterdam: Elsevier, , 1976,105–152
61. F. F. Rust, *Journal of the American Chemical Society*, 1957, **79**, 4000-4003.
62. F.Gugumus, *Re-examination of the thermal oxidation reactions of polymers 2.Thermal oxidation of polyethylene. Polymer Degradation and Stability*, 2002, **76(2)**, 329-340.
63. F.Gugumus, 2002, **77**, 147-155.
64. G. A. Russell, *J Am Chem Soc* 1957, **79**, 3871
65. E. G. E. Hawkins, *Organic Peroxides* . London: Spon, 1961.
66. S. Patai, *The Chemistry Peroxides* . New York: Wiley, 1983.
67. NM Emanuel, ET Denisov and Z. Maizus, *Liquid-Phase Oxidation of Hydrocarbons* .New York: Plenum Press, 1967.
68. V. L. Antonovskii, *Organic Peroxide Initiators* . Moscow: Khimiya, [in Russian]. 1972.
69. L Bateman, H Hughes and A. Moris., *Disc Faraday Soc*, 1953, **14**, 190.
70. A. Hoff and S. Jacobsson, *Journal of Applied Polymer Science*, 1982, **27**, 2539-2551.
71. A. Hoff and S. Jacobsson, *Journal of applied polymer science*, 1984, **29**, 465-480.

72. A. François-Heude, E. Richaud, J. Leprovost, M. Heninger, H. Mestdagh, E. Desnoux and X. Colin, *Polymer Testing*, 2013.
73. E.T.Denisov and I.B.Afanas.ev, *Oxidation and antioxidants in organic chemistry and biology*, CRC press, 2010. E.T. CRC press, 2010.
74. Crompton.T.R, *Thermal Stability of Polymers*, Smithers Rapra Technology, 2012.
75. J.Andrew.Waynick, *American Chemical Society*, 2001, **15**, 1326.
76. George.P and Robertson.A, *Trans. Faraday Soc*, 1946, **43**, 217.
77. George.P and Robertson.A, *J. Inst. Pet*, 1946, **32**, 382.
78. Bernhard.R.A and Marr.A.G, *Food Res*, 1960, **25**, 517.
79. Klaus.E.E. and Wang.J.C.Tribol, *Trans*, 1992, **35**, 316.
80. Hazlett.R.N, *Thermal Oxidation Stability of Aviation Turbine Fuels; ASTM: Philadelphia,1991; Chapters 2,6,8,9.*
81. Reich.L and Stivala.S.S, *Autoxidation of Hydrocarbon and Polyolefins,Kinetics, and Mechanisms;* , Marcel Dekker, New York 1969.
82. Scott.G, *Atmospheric Oxidation and Antioxidants*, Elsevier, New York, 1965.
83. J.D. Holdsworth, G.Scot and D.Williams, *J.Chem.Soc*, 1964, 4692.
84. G.Scott, *Atmospheric Oxidation and Antioxidants. Elsevier, Amsterdam*, 1965, 188.
85. F.Rasti and G.Scott, *Eur.Polym.j*, 1980, **16**, 1153.
86. L.L.Yasina, V.B.Miller and Y.A.Shalyapnikov, *Vysokomol,Soedin, Ser.B*, 1969, **11**, 467-470.
87. R. L. Spore, Oxidative degradation of Polyethylene, Master of Science in Chemical Engineering, Texas Tech University, 1971.
88. L. M. Gorghiu, S. Jipa, T. Zaharescu, R. Setnescu and I. Mihalcea, *Elsevier*, 2004, **84**, 7-11.
89. ET.Denisov and TG.Denisova, *Handbook of Antioxidants*, Boca Raton, FL:CRC Press, 2000.
90. Jasso-Gastinel, Carlos.F and Kenny.José.M, *Modification of Polymer Properties*, Elsevier, 2016.
91. J.Tocháček, *Polymer degradation and stability*, 2004.
92. Geoffrey.Pritchard, *Plastics Additives*, Chapman and Hall, 2-6 Boundary Row,London, SE1 8HN,UK, London, 1998
93. Hans Zweifel, Ralph D. Maier and Michael Schiller, *Plastics Additives Handbook*, Hanser Publishers, Munich, 6 edn., 2009.
94. Gerald.Scott, *Polymers and The Environment*, The Royal Society of Chemistry, Thomas Graham House, Science Park, Milton Road, Cambridge CB4 0WF, UK, 1999.
95. AP.Griva and ET.Denisov, *Int J Chem Kinet* 1973, **5**, 869–877
96. K.D.Breese, J.-F.Lamethe and C.DeArmitt, *Polymer Degradation and Stability*, 2000, **70**, 89-94.
97. Burton.GW and Ingold.KU, *Journal of American Chemical Society*, 1981, **103**, 6472.
98. Zweifel.H, *Stabilization of polymeric materials*, Springer-Verlag, Berlin, Heidelberg, 1998.

99. Erik.Klein, Vladimír.Lukeš and Zuzana.Cibulková, *Petroleum & Coal* 2005, **47**, 33-39.
100. Kwek.S.Q, Leong.L.P. and Bettens.R, *Effects of Different Functional Group on Antioxidant Activity. Department of Chemistry, Faculty of Science, National University of Singapore 10,Kent Ridge Road, Singapore 117546*
101. C.J.Pedersen, *Ind. Eng. Chem*, 1949, **41**, 924-928.
102. Jonathan.W.Steed and Jerry.L.Atwood, *Supramolecular Chemistry, 2nd Edition*, 2009.
103. Jones.Chris and Thornback.John, *Medicinal Applications of Coordination Chemistry*, Royal Society of Chemistry, 2007 88-89.
104. Michael.T.Ashby, John.H.Enemark and Dennis.L.Lichtenberger, *Inorganic Chemistry*, 1988, **27**, 191-197.
105. Masato.Kamata, Ken.Hirotsu, Taiichi.Higuchi, Kazuyuki.Tatsumi, Roald.Hoffann, Toshikatsu.Yoshida and S. Otsuka, *Journal of American Chemical Society*, 1981, **103**, 5772-5778.
106. Michael.T.Ashby and John.H.Enemark, *Journal of Americal Society*, 1986, **108**, 730-733.
107. Craig.A.Grappnerhaus and Marcetta.Y.Darensbourg, *Accounts of Chemical Research*, 1998, **31**, 451-459.
108. Chaurin.Valerie, Constable.Edwin.C and Housecroft.Catherine.E, *New Journal of Chemistry*, 2006, **30**, 1740-1744.
109. Jipa.S, Setnescu.R, Setnescu.T and Zaharescu.T, *Polym Degrad Sta*, 2000, **68**, 159.
110. Howard.J, *Polym Eng Sci*, 1973, **13**, 429.
111. Marcetta.Darensbourg, *Coordination Chemistry Transition Metal Complexes*, <http://www.chem.tamu.edu/rgroup/marcetta/chem104/lectures/104-l-w04.pdf>).
112. Dave.Berg, *Stability of Transition Metal Complexes*, <http://web.uvic.ca/~djberg/Chem324/Chem324-14.pdf>).
113. J. A. Waynick, *Energy & Fuels*, 2001, **15**, 1325-1340.
114. J. Pospisil and P. P. Klemchuk, CRC Press: Boca Rotan, 1990, vol. 1, ch. 3,7.
115. U.S, *Patent 2,181,121*.
116. U.S, *Patent 2,181,122*.
117. U.S, *Patent 2,282,513*.
118. U.S, *Patent 2.284.267*.
119. U.S, *Patent 2,285,259*.
120. U.S, *Patent 2,285,260*.
121. U.S, *Patent 3,110,696*.
122. U.S, *Patent 3,772,245*.
123. U.S, *Patent 4,043,976*.
124. U.S, **Patent 3,993,622**.
125. U.K, *Patent 974,274*.
126. U.S, *Patent 4,154,723*.

127. U.S, *Patent 3,367,907*.
128. M. Tramontini and L. Angiolini, *Tetrahedron*, 1990, **46**, 1791 - 1837
129. U.S, *Patent 4,749,468*.
130. M. Arifuzzaman, M. R. Karim, T. A. Siddiquee, A. H. Mirza and M. A. Ali, *International Journal of Organic Chemistry*, 2013, **03**, 81.
131. J. B. Kramer, D. H. Boschelli and D. T. Connor, *Journal of Heterocyclic Chemistry*, 1994, **31**, 1439-1443.
132. M. Taha, N. H. Ismail, S. Imran, M. Selvaraj, A. Rahim, M. Ali, S. Siddiqui, F. Rahim and K. M. Khan, *Bioorganic & Medicinal Chemistry*, 2015, **23**, 7394-7404.
133. Somnath.Khanra, Sabyasachi.Ta, Milan.Ghosh, Sudeshna.Chatterjee and Debasis.Das, *RSC Adv.* , 2019, **9** , 21302, 2019.
134. Zhao.Xiao-Hui and Ye.Zhi-Wen, *Chinese Chemical Letters*, 2014, **25**, 209-211.
135. N. T. Madhu and P. K. Radhakrishnan, *SYNTH. REACT. INORG. MET.-ORG. CHEM.*,, 2001, **31**, 315-330.
136. Hany.F.Nour, Nadim.Hourani and Nikolai.Kuhnert, *Org. Biomol. Chem*, 2012, **10**, 4382.
137. S. Z. Zilu Chen, Yanling Shen, Huahong, Dongcheng and Fupei Liang, *Eur. J. Inorg. Chem*, 2014, 5783-5792.
138. Lays.B. Fitaroni, Juliana.A.d e.Lima, Sandra.A. Cruz and Walter.R.Waldman, *Polymer Testing*, 2016, **53**, 165-173.
139. Jamila Wazir, *International Journal of Medical Works* 2016, 11(2), 13-18.

## Appendix

**Table A-1** MFI and Colour Index ( $L^*$ ,  $a^*$ ,  $b^*$ ) values of Commercial-Series AO/MDs in LDPE (unstabilised) in the absence and presence of CuCl with extruder (circulation mode) residence time of 0, 5 and 10 minutes

Sample Code/time 0,5,10 min	Sample values			Difference				MFI g/10min@190 °C
	$L^*$	$a^*$	$b^*$	$\Delta L^*$	$\Delta a^*$	$\Delta b^*$	$\Delta E^*_{Lab}$	
Paper	87.67	2.61	-9.16					
LDPE	79.83	-0.25	-2.14	-7.85	-2.85	7.02	10.91	1.50
ANOX®20	30.06	-0.32	-1.64	-57.61	-2.93	7.52	58.17	1.30
ANOX®20	32.03	-0.60	-0.85	-55.64	-3.21	8.31	56.35	1.35
ANOX®20	30.32	-0.48	0.50	-57.35	-3.09	9.67	58.24	1.40
LOWINOX®MD24	38.02	-0.40	-1.78	-49.66	-3.01	7.38	50.29	1.35
LOWINOX®MD24	33.32	-0.33	-1.24	-54.36	-2.94	7.92	55.01	1.40
LOWINOX®MD24	35.31	-0.34	-0.97	-52.36	-2.94	8.26	53.08	1.45
NAUGARD®XL-1	43.47	-0.29	-2.39	-44.20	-2.90	6.78	44.81	1.30
NAUGARD®XL-1	33.66	-0.40	-1.62	-54.07	-3.00	7.54	54.67	1.40
NAUGARD®XL-1	30.50	-0.37	0.06	-57.17	-2.98	9.23	57.99	1.45
ALKANOX®240	43.56	-0.33	-2.04	-44.11	-2.93	7.13	44.78	1.54
ALKANOX®240	42.43	-0.39	-1.43	-45.25	-3.00	7.73	46.00	1.67
ALKANOX®240	35.69	-0.31	-1.23	-51.98	-2.91	7.93	52.66	1.81
CaSt	42.58	-0.25	-3.25	-45.10	-2.86	5.91	45.57	1.45
CaSt	44.17	0.28	-2.24	-43.50	-2.33	6.93	44.11	1.49
CaSt	42.74	-0.07	-2.06	-44.94	-2.67	7.10	45.57	1.59
Cu- ANOX®20	32.51	-0.61	-0.68	-55.16	-3.21	8.48	55.91	1.20
Cu- ANOX®20	40.47	-0.85	3.55	-47.20	-3.46	12.71	47.20	1.40
Cu- ANOX®20	32.97	-0.81	4.43	-54.70	-3.41	13.60	56.47	1.45
Cu- LOWINOX®MD24	41.56	-0.31	-0.92	-46.11	-2.92	8.24	46.93	1.32
Cu- LOWINOX®MD24	34.65	-0.48	0.20	-53.02	-3.09	9.37	53.93	1.35
Cu- LOWINOX®MD24	31.96	-0.35	1.63	-55.72	-2.96	10.80	56.83	1.45
Cu- ALKANOX®240	30.91	-0.38	-0.94	-56.77	-2.99	8.23	57.44	1.50
Cu- ALKANOX®240	21.86	-0.19	0.30	-65.81	-2.80	9.47	66.65	1.45
Cu- ALKANOX®240	30.91	-0.29	0.32	-59.87	-2.89	9.48	60.68	1.47
Cu- ALKANOX®240	41.92	-1.14	-1.27	-45.76	-3.74	7.89	46.58	1.58
Cu- ALKANOX®240	41.95	-1.17	3.13	-45.72	-3.78	12.29	47.49	1.87
Cu- ALKANOX®240	41.39	-0.86	3.13	-46.28	-3.46	12.30	48.01	1.95
Cu- CaSt	45.91	-0.56	-2.17	-41.76	-3.17	7.00	42.46	1.56
Cu- CaSt	44.46	-0.56	-0.54	-43.22	-3.17	8.63	44.18	1.87
Cu- CaSt	49.38	-0.57	0.85	-38.29	-3.17	10.01	39.70	2.11

**Table A-2** MFI and Colour Index ( $L^*, a^*, b^*$ ) values of S-Series AO/MDs in LDPE (unstabilised) in the absence of CuCl with extruder (circulation mode) residence time of 0, 5 and 10 minutes

Sample Code/time 0,5,10 min	Sample values			Difference				MFI g/10min@190°C
	$L^*$	$a^*$	$b^*$	$\Delta L^*$	$\Delta a^*$	$\Delta b^*$	$\Delta E^*_{Lab}$	
LDPE	38.14	-0.31	-2.41	-49.53	-2.91	6.75	50.08	1.516
LDPE	45.25	-0.37	-2.28	-42.42	-2.97	6.88	43.08	1.518
LDPE	38.61	-0.28	-2.09	-49.06	-2.88	7.08	49.66	1.523
S0	41.95	-0.28	-2.23	-45.72	-2.88	6.93	46.33	1.45
S0	41.53	-0.37	-2.10	-46.15	-2.98	7.07	46.78	1.75
S0	40.46	-0.59	-1.58	-47.21	-3.20	7.58	47.92	1.63
S1	45.93	-0.48	-2.08	-41.75	-3.09	7.09	42.46	1.5
S1	48.61	-0.63	-0.06	-39.07	-3.23	9.11	40.24	1.5
S1	47.59	-0.74	0.67	-40.08	-3.35	9.84	41.41	1.6
S2	40.42	-0.97	-0.37	-47.25	-3.58	8.80	48.19	1.68
S2	38.67	-0.67	2.20	-49.00	-3.28	11.36	50.41	1.65
S2	38.46	-0.47	3.35	-49.21	-3.08	12.51	50.87	1.70
S3	50.51	-1.40	2.96	-37.16	-4.00	12.13	39.29	1.56
S3	40.07	-0.42	10.53	-47.61	-3.02	19.69	51.61	1.74
S3	33.12	-0.45	11.75	-54.55	-3.06	20.92	58.50	1.87
S4	40.68	-0.82	1.50	-46.99	-3.42	10.67	48.31	1.60
S4	37.06	-0.70	7.89	-50.61	-3.30	17.06	53.51	1.70
S4	34.69	-0.13	8.46	-52.98	-2.73	17.63	55.90	1.80
S5	38.60	-0.20	-0.89	-49.07	-2.81	8.28	49.84	1.70
S5	36.56	0.33	2.16	-51.11	-2.28	11.32	50.40	1.41
S5	36.40	-0.28	5.28	-51.26	-2.88	14.44	53.34	1.36
S6	37.31	-0.30	-2.15	-50.36	-2.90	7.02	50.93	1.58
S6	36.95	-0.52	-1.37	-50.72	-3.13	7.80	51.41	1.60
S6	42.66	-0.65	-1.12	-45.01	-3.25	8.04	45.84	1.77
S7	33.54	-1.09	-0.07	-54.14	-3.64	9.09	55.01	1.37
S7	39.50	-1.07	0.58	-48.17	-3.68	9.74	49.29	1.45
S7	32.45	-0.83	1.41	-55.22	-3.43	10.58	56.33	1.50
S8	45.11	-0.94	-1.06	-42.56	-3.35	8.11	43.47	1.45
S8	35.81	-1.03	-0.30	-51.86	-3.64	8.86	52.74	1.50
S8	42.53	-1.09	-0.11	-45.15	-3.70	9.06	46.19	1.70

**Table A-3** MFI and Colour Index ( $L^*, a^*, b^*$ ) values of S-Series AO/MDs in LDPE (unstabilised) in the presence of CuCl with extruder (circulation mode) residence time of 0, 5 and 10 minutes

Sample Code/time 0,5,10 min	Sample values			Difference				MFI g/10min@190°C
	$L^*$	$a^*$	$b^*$	$\Delta L^*$	$\Delta a^*$	$\Delta b^*$	$\Delta E^*_{Lab}$	
Cu-LDPE	34.46	-0.36	-1.31	-53.21	-2.97	7.85	53.87	1.28
Cu-LDPE	41.70	-0.71	0.79	-45.97	-3.31	9.95	47.15	1.47
Cu-LDPE	41.97	-0.90	1.89	-45.70	-3.50	11.05	47.15	1.55
Cu-S0	37.30	-0.51	-0.88	-50.37	-3.12	8.28	51.14	1.85
Cu-S0	31.87	-0.91	1.53	-55.80	-3.52	10.70	56.93	1.75
Cu-S0	32.07	-1.15	3.43	-55.61	-3.75	12.59	57.14	1.55
Cu-S1	36.83	-0.84	0.64	-50.84	-3.45	9.81	51.89	1.6
Cu-S1	32.13	0.85	4.56	-55.54	-2.56	13.73	57.27	1.6
Cu-S1	33.14	0.67	5.15	-54.33	-1.94	14.32	56.22	1.8
Cu-S2	33.30	-0.97	1.56	-54.37	-3.58	10.72	55.53	1.64
Cu-S2	28.13	0.72	7.38	-59.55	-1.89	16.54	61.83	1.76
Cu-S2	22.21	5.81	9.43	-65.46	3.20	18.59	68.13	1.72
Cu-S3	44.70	-0.73	2.25	-42.97	-3.34	11.41	44.59	1.55
Cu-S3	34.66	-0.01	7.66	-53.01	-2.62	16.83	55.68	1.80
Cu-S3	45.22	-0.32	11.11	-42.45	-2.93	20.28	47.14	1.85
Cu-S4	41.04	-0.92	1.61	-46.63	-3.53	10.77	47.99	1.60
Cu-S4	37.13	-0.58	5.13	-50.54	-3.19	14.30	52.62	1.70
Cu-S4	32.50	-0.07	8.90	-55.17	-2.67	18.06	58.11	1.80
Cu-S5	47.87	-0.12	-0.63	-39.80	-2.73	8.54	40.80	1.50
Cu-S5	39.41	-0.64	2.09	-48.26	-3.24	11.25	49.66	1.55
Cu-S5	35.98	0.34	3.85	-51.70	-2.27	13.02	53.36	1.50
Cu-S6	40.82	-0.31	-1.03	-46.85	-2.92	8.13	47.65	1.45
Cu-S6	35.69	0.06	1.95	-51.39	-2.55	11.11	53.22	1.50
Cu-S6	34.05	-0.08	3.83	-53.63	-2.68	13.00	54.24	1.55
Cu-S7	41.63	-0.86	-0.83	-46.04	-3.46	8.33	49.92	1.50
Cu-S7	38.61	-0.95	0.60	-49.04	-3.55	9.77	50.15	1.75
Cu-S7	29.23	-0.82	3.53	-58.44	-3.43	12.70	59.90	2.00
Cu-S8	41.73	-1.15	-1.24	-45.94	-3.75	7.93	46.77	1.50
Cu-S8	40.82	-0.83	1.15	-46.85	-3.43	10.32	48.09	1.60
Cu-S8	41.76	-0.92	2.71	-45.92	-3.53	11.88	47.56	1.70

**Table A-4** MFI and Colour Index ( $L^*$ ,  $a^*$ ,  $b^*$ ) values of MD-Series AO/MDs in LDPE (unstabilised) in the absence and presence of CuCl with extruder (circulation mode) residence time of 0, 5 and 10 minutes

Sample Code/time 0,5,10 min	Sample values			Difference				MFI g/10min@190°C
	$L^*$	$a^*$	$b^*$	$\Delta L^*$	$\Delta a^*$	$\Delta b^*$	$\Delta E^*_{Lab}$	
MD0A	48.11	-3.47	3.02	-39.56	-6.08	12.19	41.84	1.53
MD0A	49.79	-3.14	4.06	-37.89	-5.75	13.22	40.54	1.76
MD0A	38.36	-2.51	4.86	-49.31	-5.12	14.02	51.52	1.85
Cu-MD0A	39.53	-4.04	5.57	-48.15	-6.64	14.73	50.78	1.53
Cu-MD0A	34.25	-3.12	7.65	-53.42	-5.72	16.81	56.30	1.75
Cu-MD0A	37.67	-2.29	10.25	-50.00	-4.89	19.42	53.86	1.75
MD0	39.97	-1.33	1.93	-47.70	-3.94	11.09	49.13	1.35
MD0	41.73	-1.51	2.69	-45.94	-4.11	11.86	47.62	1.47
MD0	36.02	-1.73	3.07	-51.65	-4.34	12.23	53.25	1.5
Cu-MD0	38.89	-1.87	2.67	-48.78	-4.47	11.83	50.40	1.35
Cu-MD0	42.45	-1.62	3.30	-45.22	-4.22	12.47	47.10	1.47
Cu-MD0	34.33	-1.65	7.55	-53.34	-4.26	16.72	56.06	1.50
MD2B	38.06	-2.77	14.93	-49.61	-5.37	24.10	55.42	1.43
MD2B	37.92	-1.59	18.74	-49.75	-4.20	27.90	57.19	1.5
MD2B	30.40	0.13	19.30	-57.27	-2.48	28.47	64.01	1.7
Cu-MD2B	33.24	-1.60	17.21	-54.43	-4.20	26.38	60.63	1.40
Cu-MD2B	21.23	0.97	18.37	-66.64	-1.64	27.53	71.94	1.45
Cu-MD2B	33.97	-1.79	16.44	-53.70	-4.40	25.60	59.65	1.50
MD2A	38.24	-6.44	16.38	-49.43	-9.05	25.55	56.37	1.45
MD2A	32.59	-1.57	16.75	-55.08	-4.17	25.91	61.02	1.50
MD2A	39.71	-4.16	16.18	-47.96	-6.77	25.35	54.67	1.50
Cu-MD2A	43.22	-8.06	25.09	-44.45	-10.66	34.26	57.12	1.5
Cu-MD2A	37.42	-3.19	15.81	-50.25	-5.80	24.97	56.41	1.5
Cu-MD2A	37.54	-0.24	13.78	-50.53	-2.84	22.95	55.21	1.5
MD4	44.34	-9.87	19.95	-43.33	-12.48	29.11	53.68	1.35
MD4	30.00	-1.56	19.12	-57.67	-4.16	28.28	64.36	1.40
MD4	46.55	-6.22	18.17	-41.12	-8.82	27.34	50.16	1.50
Cu-MD4	38.00	-6.47	16.39	-49.67	-9.07	25.56	56.59	1.35
Cu-MD4	38.41	-2.29	12.58	-49.56	-4.90	21.75	54.07	1.55
Cu-MD4	27.41	-0.25	10.68	-60.27	-2.86	19.84	63.51	1.55
MD7A	41.09	-1.49	0.03	-46.58	-4.10	9.20	47.66	1.30
MD7A	40.87	-1.53	2.62	-46.80	-4.13	11.79	48.44	1.41
MD7A	37.54	-2.17	3.61	-50.14	-4.78	12.77	51.96	1.45
Cu-MD7A	35.02	-1.31	-0.14	-52.65	-3.91	9.03	53.57	1.45
Cu-MD7A	46.48	-1.65	2.24	-41.19	-4.24	11.41	42.95	1.35
Cu-MD7A	49.41	-1.94	2.21	-38.26	-4.55	11.37	40.17	1.30
MD7	41.82	-0.97	-0.04	-45.85	-3.57	9.12	46.89	1.27
MD7	41.69	-1.22	4.93	-45.99	-3.82	14.10	48.25	1.32
MD7	40.85	-0.92	4.95	-46.82	-3.52	14.11	49.03	1.55
Cu-MD7	44.01	-1.13	1.41	-43.66	-3.74	10.58	45.08	1.23
Cu-MD7	33.47	-0.71	10.86	-54.20	-3.32	20.02	57.87	1.29
Cu-MD7	30.14	0.12	9.55	-57.53	-2.49	18.71	60.55	1.60

**Table A-5** MFI and Colour Index ( $L^*$ , $a^*$ , $b^*$ ) values of L-Series AO/MDs in LDPE (unstabilised) in the absence of CuCl with extruder (circulation mode) residence time of 0, 5 and 10 minutes

Sample Code/time 0,5,10 min	Sample values			Difference				MFI g/10min@190°C
	$L^*$	$a^*$	$b^*$	$\Delta L^*$	$\Delta a^*$	$\Delta b^*$	$\Delta E^*_{Lab}$	
Paper	87.67	2.61	-9.16					
L1	42.61	-0.84	-0.95	-45.06	-3.44	8.21	45.93	2.0
L1	36.31	0.78	2.92	-51.36	-1.82	12.08	52.79	2.1
L1	38.26	1.94	6.26	-49.42	-0.67	15.42	51.77	2.14
L1A	50.55	-0.51	-0.50	-37.12	-3.12	8.67	38.24	1.35
L1A	49.05	-1.23	2.85	-38.63	-3.83	12.01	40.63	1.53
L1A	37.15	-0.71	7.01	-50.52	-3.31	16.17	53.15	1.9
L2	40.55	-0.79	-1.09	-47.12	-3.39	8.07	47.93	1.9
L2	36.81	-1.32	3.79	-50.86	-3.82	12.96	52.63	1.964
L2	44.07	-1.34	8.29	-43.60	-3.95	17.45	47.13	1.985
L2A	39.87	-0.25	0.02	-47.80	-2.86	9.78	48.88	2.0
L2A	47.08	-0.75	6.43	-40.59	-3.36	15.60	43.62	1.921
L2A	41.13	-1.04	7.41	-46.54	-3.64	16.58	49.54	1.985
L3	44.04	-0.54	-0.65	-43.63	-3.14	8.51	44.57	1.83
L3	38.97	-0.68	3.36	-48.70	-3.29	12.52	50.39	1.96
L3	44.35	-0.03	6.90	-43.32	-2.64	16.06	46.28	1.99
L3A	34.44	-0.59	0.95	-53.23	-3.19	10.12	54.28	1.44
L3A	38.48	-1.49	5.63	-49.19	-4.10	14.79	51.53	1.50
L3A	36.08	-0.81	11.04	-51.60	-3.42	20.20	55.52	1.54
Cu-L1	40.10	-0.66	-1.29	-47.58	-3.26	7.87	48.33	2.0
Cu-L1	43.91	0.41	4.74	-43.76	-2.19	13.91	45.97	2.02
Cu-L1	38.26	1.89	12.92	-49.41	-0.71	22.08	54.12	2.11
Cu-L1A	41.03	-0.59	3.02	-46.64	-3.20	12.18	48.31	1.65
Cu-L1A	43.27	-1.03	12.60	-44.40	-3.64	21.77	49.58	1.70
Cu-L1A	38.34	2.27	17.34	-49.33	-0.33	26.51	56.00	1.85
Cu-L2	44.98	-0.82	-0.23	-42.70	-3.42	8.93	43.76	2.0
Cu-L2	43.25	-0.97	5.57	-44.42	-3.58	14.74	46.94	2.03
Cu-L2	33.15	2.32	11.75	-54.52	-0.28	20.91	58.40	2.15
Cu-L2A	41.50	-0.40	1.65	-46.17	-3.01	10.81	47.51	1.88
Cu-L2A	36.46	-0.84	5.79	-51.21	-3.45	14.95	53.46	1.98
Cu-L2A	24.67	1.12	13.95	-63.00	-1.48	23.12	67.12	2.1
Cu-L3	45.32	-0.62	-0.05	-42.36	-3.23	9.11	43.45	1.5
Cu-L3	31.15	-0.51	6.34	-56.52	-3.12	15.50	58.69	1.54
Cu-L3	41.19	-0.10	10.96	-46.48	-2.71	20.13	50.73	1.6
Cu-L3A	35.71	-1.21	3.65	-51.96	-3.81	12.82	53.66	1.44
Cu-L3A	37.09	-0.95	11.64	-50.58	-3.56	20.81	54.81	1.6
Cu-L3A	29.27	1.48	18.63	-58.40	-1.13	27.80	64.69	1.65

**Table A-6** MFI and Colour Index ( $L^*$ ,  $a^*$ ,  $b^*$ ) values of T-Series AO/MDs in LDPE (unstabilised) in the absence and presence of CuCl with extruder (circulation mode) residence time of 0, 5 and 10 minutes

Sample Code/time 0,5,10 min	Sample values			Difference				MFI g/10min@190°C
	$L^*$	$a^*$	$b^*$	$\Delta L^*$	$\Delta a^*$	$\Delta b^*$	$\Delta E^*_{Lab}$	
Paper	87.67	2.61	-9.16					
T0A	32.02	-0.43	-0.61	-55.65	-3.04	8.55	56.39	1.40
T0A	34.38	-0.58	0.64	-53.39	-3.18	9.80	54.37	1.48
T0A	35.81	-0.87	1.73	-51.86	-3.48	10.90	53.11	1.70
Cu-T0A	33.04	-0.40	-0.29	-54.63	-3.00	8.87	55.43	1.64
Cu-T0A	28.50	-0.72	1.20	-59.17	-3.33	10.37	60.16	1.65
Cu-T0A	28.04	-0.81	2.12	-59.63	-3.41	11.29	60.79	1.74
T0	41.35	-0.43	-0.10	-46.32	-3.83	9.86	47.30	1.50
T0	35.45	0.13	4.35	-52.23	-2.48	13.52	54.00	1.50
T0	40.09	1.83	6.37	-47.58	-1.58	15.53	50.00	1.52
Cu-T0	39.18	-0.47	1.33	-48.49	-3.08	10.49	49.71	1.47
Cu-T0	32.99	0.97	7.39	-54.68	-1.64	16.55	57.16	1.50
Cu-T0	30.58	1.28	8.28	-57.09	-1.33	17.45	59.71	1.55
T1	37.99	-1.16	0.13	-49.68	-3.76	9.29	50.68	1.50
T1	42.13	-1.49	4.80	-45.54	-4.10	13.97	47.81	1.55
T1	40.52	-1.41	4.79	-47.15	-4.02	13.96	49.34	1.62
Cu-T1	40.39	-0.97	-0.81	-47.28	-3.58	8.35	48.15	1.50
Cu-T1	36.21	-1.17	3.30	-51.46	-3.77	12.46	53.00	1.55
Cu-T1	38.79	-1.24	6.64	-48.88	-3.84	15.81	51.52	1.64
T2	42.44	-0.85	1.57	-45.23	-3.45	10.73	46.61	1.45
T2	30.65	0.89	10.92	-57.02	-1.71	20.09	60.48	1.6
T2	27.98	2.81	13.69	-59.70	0.20	22.85	63.92	1.8
Cu-T2	40.57	-1.12	4.26	-47.10	-3.72	13.42	49.12	1.64
Cu-T2	29.78	1.83	8.42	-57.89	-0.77	17.59	60.51	1.66
Cu-T2	35.88	2.24	10.03	-51.80	-0.36	19.20	55.24	1.66
T3	37.59	-0.87	-0.50	-50.09	-3.48	8.67	50.95	1.55
T3	36.20	-0.34	5.24	-51.48	-2.95	14.40	53.53	1.55
T3	34.24	-0.52	6.81	-53.46	-3.12	15.97	55.89	1.60
Cu-T3	48.74	-0.90	1.41	-38.39	-3.50	10.57	40.49	1.36
Cu-T3	36.43	-1.66	6.50	-51.25	-4.27	15.67	53.76	1.55
Cu-T3	36.92	-0.85	10.85	-50.75	-3.45	20.01	54.67	1.57
T4	49.11	-1.20	-0.98	-38.56	-3.80	8.18	39.60	1.50
T4	41.72	-1.82	7.21	-45.95	-4.42	16.37	48.98	1.51
T4	37.09	-1.50	12.61	-50.58	-4.10	21.77	55.22	1.78
Cu-T4	42.14	-2.56	3.58	-45.53	-5.16	12.74	47.56	1.50
Cu-T4	48.96	-1.72	10.62	-38.71	-4.32	-19.78	-43.69	1.50
Cu-T4	45.67	-3.38	13.01	-42.01	-5.99	22.17	47.88	1.88

**Table A-7** MFI and Colour Index ( $L^*, a^*, b^*$ ) values of Commercial-Series AO/MDs in LDPE (unstabilised) in the absence of CuCl for multi-pass (normal mode) extrusion.

Sample Code	Sample values			Difference				MFI g/10min@190°C
	$L^*$	$a^*$	$b^*$	$\Delta L^*$	$\Delta a^*$	$\Delta b^*$	$\Delta E^*_{Lab}$	
LDPE-Pass 1	35.57	-0.37	-2.53	-52.10	-2.97	6.81	52.61	1.5
LDPE -Pass 3	33.88	-0.38	-2.15	-53.79	-2.99	7.01	54.33	1.35
LDPE -Pass 5	34.17	-0.37	-1.93	-53.50	-2.98	7.24	54.07	1.32
CaSt-Pass 1	34.92	-0.34	-2.30	-52.76	-2.95	6.86	53.28	1.56
CaSt -Pass 3	35.84	-0.31	-1.85	-51.83	-2.92	7.31	52.43	1.63
CaSt -Pass 5	39.19	-0.31	-1.74	-48.49	-2.91	7.43	49.14	1.70
ALKANOX®240-Pass 1	39.76	-0.32	-2.32	-47.91	-2.93	6.84	48.49	1.52
ALKANOX®240-Pass 3	39.45	-0.42	-2.04	-48.22	-3.03	7.12	48.84	1.60
ALKANOX®240-Pass 5	32.99	-0.49	-1.54	-54.68	-3.09	7.63	55.30	1.71
Base Stabiliser-Pass 1	42.79	-0.45	-1.57	-44.88	-3.05	7.59	45.62	1.37
Base Stabiliser-Pass 3	39.22	-0.55	-0.82	-48.45	-3.16	8.34	49.26	1.24
Base Stabiliser-Pass 5	36.68	-0.66	0.15	-50.99	-3.26	9.31	51.94	1.20
NAUGARD®XL-1-Pass 1	44.60	-0.31	-1.70	-42.99	-2.92	7.46	43.73	1.27
NAUGARD®XL-1-Pass 3	33.72	-0.52	-1.09	-53.95	-3.13	8.07	54.64	1.25
NAUGARD®XL-1-Pass 5	32.81	-0.59	-0.72	-54.86	-3.19	8.45	55.60	1.22
LOWINOX®MD24 -Pass 1	35.50	-0.28	-2.14	-52.18	-2.89	7.02	52.73	1.30
LOWINOX®MD24 -Pass 3	36.01	-0.29	-1.32	-51.67	-2.90	7.84	52.34	1.32
LOWINOX®MD24 -Pass 5	34.62	-0.32	-1.24	-53.05	-2.93	7.92	53.72	1.36

**Table A-8** MFI and Colour Index ( $L^*$ ,  $a^*$ ,  $b^*$ ) values of S-Series AO/MDs in LDPE (unstabilised) in the absence of CuCl for multi-pass (normal mode) extrusion.

Sample Code	Sample values			Difference				MFI g/10min@190°C
	$L^*$	$a^*$	$b^*$	$\Delta L^*$	$\Delta a^*$	$\Delta b^*$	$\Delta E^*_{Lab}$	
S0-Pass 1	35.96	-0.20	-1.96	-51.72	-2.80	7.20	52.29	1.22
S0-Pass 3	42.38	-0.42	-1.25	-45.29	-3.03	7.92	46.08	1.32
S0-Pass 5	41.12	-0.61	-0.59	-46.56	-3.22	8.57	47.45	1.33
S1-Pass 1	36.33	-0.58	-1.50	-51.34	-3.18	7.66	52.01	1.26
S1-Pass 3	36.48	-0.70	0.30	-51.20	-3.30	9.46	52.17	1.30
S1-Pass 5	37.80	-0.72	0.79	-49.87	-3.33	9.95	50.96	1.36
S2-Pass 1	34.94	-0.68	-0.42	-52.74	-3.29	8.74	53.56	1.24
S2-Pass 3	32.81	-0.87	1.50	-54.86	-3.48	10.66	56.00	1.34
S2-Pass 5	31.72	-0.83	2.39	-55.95	-3.44	11.55	57.24	1.43
S3-Pass 1	35.88	-0.69	1.11	-51.79	-3.29	10.27	52.90	1.31
S3-Pass 3	33.97	-0.85	2.06	-53.70	-3.45	11.23	54.97	1.40
S3-Pass 5	34.86	-0.74	2.06	-52.82	-3.34	11.23	54.10	1.50
S4-Pass 1	34.87	-0.56	-0.09	-52.80	-3.16	9.08	53.67	1.50
S4-Pass 3	36.07	-0.67	0.32	-51.60	-3.27	9.49	52.57	1.50
S4-Pass 5	33.23	-0.57	0.81	-54.44	-3.17	9.98	55.44	1.52
S5-Pass 1	35.19	-0.25	-1.87	-52.48	-2.86	7.29	53.07	1.33
S5-Pass 3	37.32	-0.29	-1.12	-50.36	-2.90	8.04	51.08	1.30
S5-Pass 5	37.49	-0.37	-0.24	-50.10	-2.98	8.93	51.06	1.33
S6-Pass 1	34.36	-0.21	-1.89	-53.31	-2.81	7.28	53.88	1.35
S6-Pass 3	35.32	-0.34	-1.13	-52.35	-2.94	8.03	53.05	1.43
S6-Pass 5	34.11	-0.21	-0.50	-53.56	-2.81	8.67	54.33	1.50
S7-Pass 1	36.29	-0.71	-0.74	-51.38	-3.31	8.42	52.17	1.35
S7-Pass 3	33.08	-0.86	-0.46	-54.59	-3.46	8.70	55.39	1.41
S7-Pass 5	34.92	-0.77	-0.24	-52.75	-3.37	8.92	53.61	1.50
S8-Pass 1	34.56	-0.52	-1.50	-53.12	-3.13	7.67	53.76	1.45
S8-Pass 3	36.24	-0.85	0.27	-51.43	-3.45	9.44	52.40	1.55
S8-Pass 5	35.12	-0.94	0.64	-52.56	-3.54	9.80	53.58	1.62

**Table A-9** MFI and Colour Index ( $L^*, a^*, b$ ) values of T-Series AO/MDs in LDPE (unstabilised) in the absence of CuCl for multi-pass (normal mode) extrusion.

Sample Code/time 0,5,10 min	Sample values			Difference				MFI g/10min@190°C
	$L^*$	$a^*$	$b^*$	$\Delta L^*$	$\Delta a^*$	$\Delta b^*$	$\Delta E^*_{Lab}$	
T0-Pass 1	36.41	-0.70	-0.91	-51.26	-3.30	8.26	52.02	1.50
T0-Pass 3	42.14	-0.74	0.05	-45.53	-3.35	9.22	46.57	1.50
T0-Pass 5	33.37	-0.94	0.75	-54.30	-3.54	9.91	55.31	1.50
T1-Pass 1	40.32	-0.42	-2.55	-47.35	-3.03	6.61	47.90	1.43
T1-Pass 3	40.07	-0.57	-1.36	-47.60	-3.18	7.80	48.34	1.48
T1-Pass 5	36.05	-0.65	-0.86	-51.63	-3.26	8.30	52.39	1.52
T2-Pass 1	37.67	-0.88	0.51	-50.00	-3.49	9.68	51.05	1.44
T2-Pass 3	36.08	-0.96	2.37	-51.59	-3.57	11.53	52.99	1.50
T2-Pass 5	35.00	-0.90	3.27	-52.67	-3.51	12.44	54.24	1.60
T3-Pass 1	34.39	-0.75	-0.87	-53.28	-3.36	8.30	54.03	1.46
T3-Pass 3	35.08	-1.00	-0.40	-52.59	-3.60	8.76	53.44	1.53
T3-Pass 5	35.95	-1.29	0.71	-51.72	-3.90	9.88	52.80	1.58
T4-Pass 1	36.29	-0.80	-0.24	-51.39	-3.40	8.39	52.27	1.5
T4-Pass 3	34.49	-1.00	0.09	-53.19	-3.60	9.25	54.11	1.52
T4-Pass 5	37.78	-1.01	1.22	-49.89	-3.61	10.38	51.09	1.53
T0A-Pass 1	47.23	-0.42	-1.43	-40.44	-3.02	7.74	41.28	1.5
T0A-Pass 3	37.53	-0.64	-1.19	-50.14	-3.25	7.98	50.88	1.62
T0A-Pass 5	34.77	-0.76	0.41	-52.90	-3.37	9.58	53.87	1.7

**Table A-10** MFI and Colour Index ( $L^*, a^*, b^*$ ) values of L-Series AO/MDs in LDPE (unstabilised) in the absence of CuCl for multi-pass (normal mode) extrusion.

Sample Code/time 0,5,10 min	Sample values			Difference				MFI g/10min@190°C
	$L^*$	$a^*$	$b^*$	$\Delta L^*$	$\Delta a^*$	$\Delta b^*$	$\Delta E^*_{Lab}$	
L1-Pass 1	35.62	-0.42	-0.71	-52.05	-3.02	8.45	52.82	1.5
L1-Pass 3	30.36	-0.46	0.18	-57.31	-3.06	9.35	58.15	1.6
L1-Pass 5	30.52	-0.45	1.37	-57.15	-3.05	10.53	58.20	1.65
L2-Pass 1	33.09	-0.33	-1.18	-54.58	-2.93	7.98	55.24	1.55
L2-Pass 3	33.42	-0.30	0.14	-54.25	-2.90	9.31	55.12	1.61
L2-Pass 5	38.23	-0.30	0.97	-49.44	-2.91	10.14	50.55	1.65
L3-Pass 1	33.42	-0.38	-0.98	-54.25	-2.99	8.18	54.95	1.6
L3-Pass 3	34.50	-0.41	-1.01	-53.17	-3.01	8.16	53.88	1.7
L3-Pass 5	30.86	-0.43	-0.13	-56.81	-3.04	9.04	57.61	1.8
L1A-Pass 1	36.23	-0.42	-1.46	-51.45	-3.03	7.71	52.11	1.56
L1A-Pass 3	35.72	-0.49	-0.32	-51.95	-3.09	8.85	52.79	1.60
L1A-Pass 5	32.42	-0.69	0.09	-55.25	-3.29	9.25	56.12	1.63
L2A-Pass 1	40.34	-0.36	-1.28	-47.34	-2.97	7.88	48.08	1.59
L2A-Pass 3	38.17	-0.42	-0.27	-49.51	-3.02	8.89	50.39	1.62
L2A-Pass 5	37.91	-0.56	0.01	-49.76	-3.17	9.17	50.70	1.66
L3A-Pass 1	33.17	-0.26	-0.99	-54.50	-2.87	8.17	55.19	1.63
L3A-Pass 3	40.57	-0.51	-1.29	-55.97	-3.16	8.76	56.74	1.64
L3A-Pass 5	40.29	-0.62	-0.16	-47.38	-3.23	9.00	48.34	1.67

Table A-11 Structure and Physical Properties of Commercial-Series AO/MDs

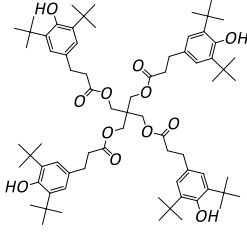
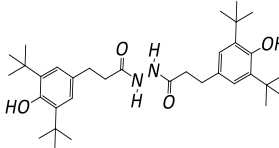
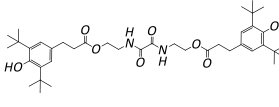
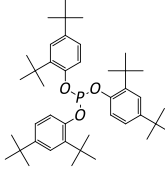
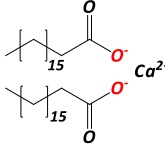
	Tradename/Code	Melting point range (°C)	Molar mass	Structure
	Name			
Hindered phenols	ANOX®20	110-125	1178	
	[3-[3-(3,5-ditert-butyl-4-hydroxy-phenyl)propanoyloxy]-2,2-bis[3-(3,5-ditert-butyl-4-hydroxy-phenyl)propanoyloxymethyl]propyl]3-(3,5-ditert-butyl-4-hydroxy-phenyl) propanoate			
Metal Deactivator	LOWINOX®MD24	221-232	553	
	3-(3,5-ditert-butyl-4-hydroxyphenyl)-N'-[3-(3,5-ditert-butyl-4-hydroxy phenyl)propanoyl]propanehydrazide			
Metal Deactivator	NAUGARD®XL-1	170-180	697	
	2-[[2-[2-[3-(3,5-ditert-butyl-4-hydroxyphenyl)propanoyloxy]ethylamino]-2-oxoacetyl]amino]ethyl 3-(3,5-ditert-butyl-4-hydroxyphenyl)propanoate			
Secondary Antioxidant	ALKANOX®240	180-186	646	
Tris (2,4-di-tert-butylphenyl) phosphite				
Acid Scavengers	CaSt	179	607	
Calcium Stearate				

Table A-12 Structure and Physical Properties of S-Series AO/MDs

Tradename/ Code	Melting range (°C)	point	Molar mass	Structure
S0	156-160	292	292	
S1	275-277	607	607	
S2	98-102	649	649	
S3	224	695	695	
S4	178	723	723	
S5	168	751	751	

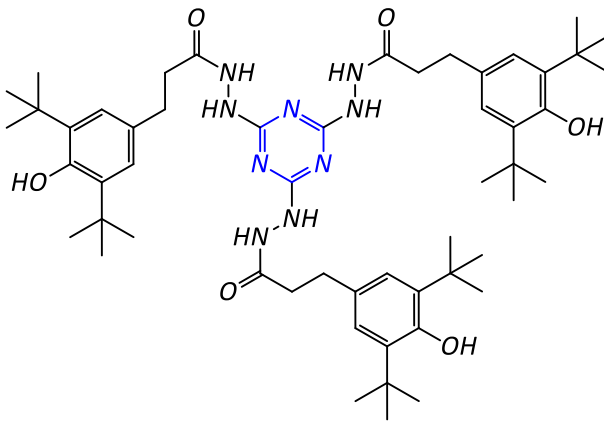
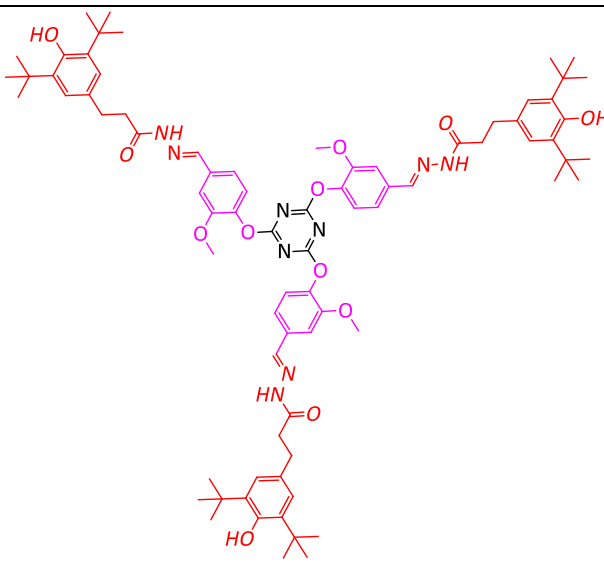
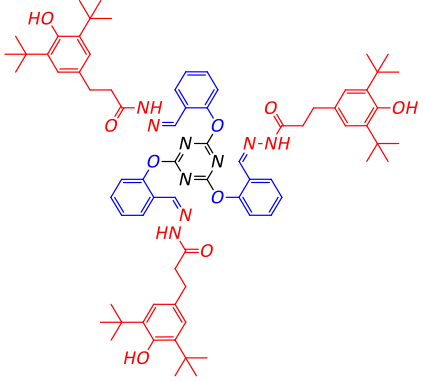
Tradename/Code	Melting point range (°C)	Molar mass	Structure
<b>Name</b>			
S6	179-183	952	 <p><i>N,N''</i>-(6-{2-[3-(3,5-di-tert-butyl-4-hydroxyphenyl)propanoyl]hydrazineylidene-1,6-dihydro-1,3,5-triazine-2,4-diyl}bis[3-(3,5-di-tert-butyl-4-hydroxyphenyl)propanehydrazide]</p>
S7	155-160	1355	 <p><i>N',N'',N'''</i>-(1,3,5-triazine-2,4,6-triyltris[oxy(3-methoxy-4,1-phenylene) (E) methanylylidene]} tris[3-(3,5-di-tert-butyl-4-hydroxyphenyl)propanehydrazide]</p>
S8	125-130	1265	 <p><i>N',N'',N'''</i>-(1,3,5-triazine-2,4,6-triyltris[oxy-2,1-phenylene(Z)methanylylidene]} tris[3-(3,5-di-tert-butyl-4-hydroxyphenyl)propanehydrazide]</p>

Table A-13 Structure and Physical Properties of L-Series AO/MDs

Tradename/ Code	Melting-point range (°C)	Molar mass	Structure
L1	245	819	<p><i>N',N''-bis[3-(3,5-di-tert-butyl-4-hydroxyphenyl)propanehydrazide]</i></p>
L2	208	847	<p><i>N',N''-(ethane-1,2-diylidene)bis[3-(3,5-di-tert-butyl-4-hydroxyphenyl)propane hydrazide]</i></p>
L3	248	875	<p><i>N',N''-{hexane-1,6-diylbis[oxy-2,1-phenylene(E)methanylylidene]}bis[3-(3,5-di-tert-butyl-4-hydroxyphenyl)propanehydrazide]</i></p>
L1A	149	879	<p><i>N',N''-bis[3-(3,5-di-tert-butyl-4-hydroxyphenyl)propanehydrazide]</i></p>
L2A	132	907	<p><i>N',N''-{butane-1,4-diylbis[oxy(3-methoxy-4,1-phenylene)(E)methanylylidene]}bis[3-(3,5-di-tert-butyl-4-hydroxyphenyl)propanehydrazide]</i></p>
L3A	143	935	<p><i>N',N''-{hexane-1,6-diylbis[oxy(3-methoxy-4,1-phenylene)(E)methanylylidene]}bis[3-(3,5-di-tert-butyl-4-hydroxyphenyl)propanehydrazide]</i></p>

Table A-14 Structure and Physical Properties of T-Series AO/MDs

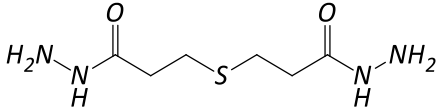
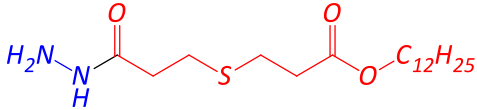
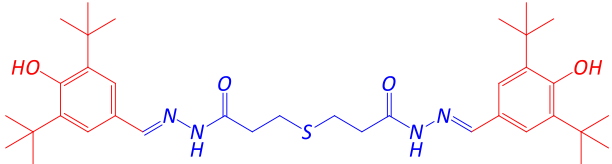
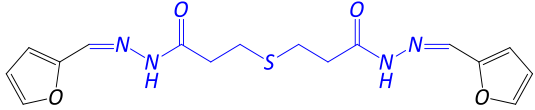
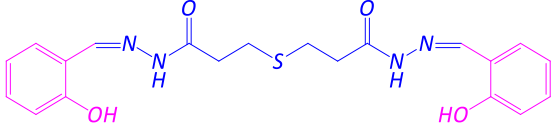
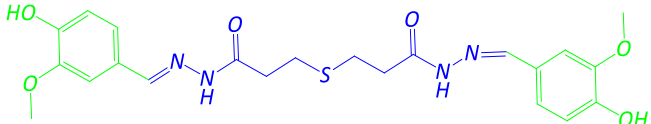
Tradename/Code	Melting point range (°C)	Molar mass	Structure
<b>Name</b>			
T0	148-155	206	
3,3'-thiodi(propanehydrazide)			
T0A	60-62	361	
3(2Hydrazinocarbonyl ethylsulfanyl)propionic acid dodecyl ester			
T1	250-255	639	
3,3'-sulfanediylbis{N'-[(E)-(3,5-di-tert-butyl-4-hydroxyphenyl)methylidene]propanehydrazide}			
T2	189-194	362	
3-[2-(Furan-2-ylmethylene-hydrazinocarbonyl)-ethylsulfanyl]-propionic acid furan-2-ylmethylene-hydrazide			
T3	245-250	414	
3-[2-(2-Hydroxy-benzylidene-hydrazinocarbonyl)-ethylsulfanyl]-propionic acid (2-hydroxy-benzylidene)-hydrazide			
T4	Not available	475	
N'-[(Z)-(4-hydroxy-3-methoxyphenyl)methylidene]-3-[(3-((2E)-2-[(4-hydroxy-3-methoxyphenyl)methylidene]hydrazinyl)-3-oxopropyl)sulfanyl]propanehydrazide			

Table A-15 Structure and Physical Properties of MD-Series AO/MDs

Tradename/Code	Melting point range (°C)	Molar masses	Structure
Name			
MD0 2,2'-(hydrazine-1,2-diylidenebis(methanylylidene))diphenol	215	240	
MD1 3-[2-(Furan-2-ylmethylene-hydrazinocarbonyl)-ethylsulfanyl]-propionic acid furan-2-ylmethylene-hydrazide	150	152	
MD1B (N',N'''E,N',N'''E)-N',N'''-(pentane-1,5-diylidene)bis(2-hydroxybenzohydrazide)	Not available	368	
MD1C (E)-2-hydroxy-N'-(4-hydroxy-3-methoxybenzylidene)benzohydrazide	212	286	

Trade name/C ode	Melting range (°C)	point	Molar mass	Structure
<i>Name</i>				
MD2A	220-225		294	
2,2'-((1E,1'E)-((2E,2'E)-ethane-1,2-diylidenebis(hydrazine-2,1-diylidene))bis(methanylylidene)) diphenol				
MD2B	155-160		242	
(1E,2E)-1,2-bis((E)-(furan-2-ylmethylene)hydrazono)ethane]				
MD4			428	
4,4'-(ethane-1,2-diylidenebis(azanylylidene)) bis(1,5-dimethyl-2-phenyl-1H-pyrazol-3(2H)-one)				
MD7	208-209		178	
2,3-Dihydroxybutanedihydrazide				
MD7A			386	
2,3-di bis(salicylidenehydrazono) hydroxybutanedioyl				